



Division of Drug Delivery and Tissue Engineering

School of Pharmacy

***In vitro* uptake studies of cell targeting agents and
nanoparticles**

Luana Sasso Bsc. Hons

Thesis submitted at the University of Nottingham for the degree of

Doctor of Philosophy

September 2014

Abstract

Recent progress in synthetic chemistry has enabled the preparation of new highly-defined polymers that exhibit changes in their structure in response to environmental changes. These responsive nanomaterials may be desirable as carriers of drugs to deliver at the cellular and sub-cellular level. However, the endocytic pathways used by these nanoparticles to access cells must be defined.

Carboxylated polystyrene beads (C-PB) of 50 and 100 nm size were chosen as 'model' nanomedicines and their route of uptake into cells characterised and compared to thermoresponsive PLGA-*b*-(PEGMA-co-PPGMA) and PLA-*b*-(DEGMA-co-OEGMA) block copolymers of 50-150 nm ('candidate' drug delivery systems) uptake. A number of protocols were optimised for endocytosis inhibition studies.

Results reported that the inhibition of clathrin mediated endocytosis (CME) with chlorpromazine (CPZ) was cell- and time-dependent. After the maximal effect of the inhibitor, the endocytosis of human transferrin (Htf), a marker of CME, recovered up to uninhibited levels in 3T3 and HCT116 cells. Furthermore, high passage number and ageing of cells showed a resistance towards the inhibition of the uptake of Htf with CPZ.

Both PLGA-*b*-(PEGMA-co-PPGMA) and PLA-*co*-(DEGMA-co-OEGMA) thermoresponsive block copolymers presented colloidal instability and aggregation that impeded further endocytic pathway internalization experiments. However, the results reported in this thesis question some of the interpretation in the literature of the susceptibility of cells to CPZ in the internalization of nanomaterials. New experimental settings for CPZ inhibition studies should be considered and protocols optimised in order to avoid incorrect and potentially misleading outcomes.

List of poster/presentations

Oral presentation

Gordon Research Seminar 'Lysosomes and Endocytosis', Andover, USA, 2014.

'In vitro uptake studies of cell targeting agents and nanoparticles'

Poster presentations

Gordon Research Seminar and Conference 'Lysosomes and Endocytosis', Andover, USA, 2014

'In vitro uptake studies of cell targeting agents and nanoparticles'

UKICRS Workshop and Symposium - Drug Delivery Uncorked, Cork, Ireland, 2014

'In vitro uptake studies of cell targeting agents and nanoparticles'

EMBO Conference 'Systems Dynamics in Endocytosis', Villars, Switzerland, 2013

'Optimization studies on the inhibition of endocytic pathways to investigate nanoengineered particles for drug delivery and their preferred route of uptake'

Papers in preparation

- Gallon, E., Sasso, L. et al. 'Delivery of nucleic acids and gene knockdown by responsive polymers'. To be submitted in October 2014.
- Sasso L. et al. 'Effects of endocytosis inhibitors on selected cell lines in vitro'.
- Sasso L. et al. 'Uptake, transport and intracellular processing of carboxylated polystyrene nanoparticles in selected cell lines'.

Acknowledgements

I would like to express my outmost gratitude to my supervisors Professor Cameron Alexander and Dr Anna Grabowska for their support during these 4 years of my PhD. Thanks for being always present at any time, day, night, weekends and whenever your support was needed. Thanks for sharing your views and guiding me in many crucial aspects of my work. I would also like to acknowledge Lee Moir, Nora Francini and Teresa Matini for providing polymers for my research and the EPSRC for supporting the studies described in this thesis.

I would like to recognise Professor David Bates for improving the organisation of the Cancer Biology laboratory in ways that boosted my research. I was also fortunate to work with Dr David Onion, who has been like a mentor in the early part of my studies. I would like to thank all the staff and colleagues of the Cancer Biology and Polymers Therapeutics groups, my laboratories, and especially Pam Collier for sharing her positive outlook on daily challenges in the lab, Dr Roya Babaei-Jadidi, Dr Maria Machado, Delyan Ivanov, Hiteshri Makwana, Xi Ye, Federica Lorenzi, Makhliyo Normatova, and Emenike Onyido for their kindness and outgoing way of being. My gratitude goes to Jane Wrigley and Dr Simon Jiang from Precos for repeatedly sharing equipment with me and to my former colleagues Dr Fernandes Trillo Francisco (Paco) and Dr Gokcen Yasayan for always sparing some of their time to discuss my scientific questions. Thanks to Amy Nairn, Sandra Lever, Carol Turrill, Gail Atkinson and Julia Crouch for their kind help with orders, meetings and conferences.

A special thanks goes to the cardiovascular unit of the QMC and flow cytometry facility. In particular to Jackie Glenn, Ann White, Jane May, Dr Sue Fox and Andrew Johnson for having been so kind and welcoming. From day one I never felt like a

stranger in your department. I wish to extend my thanks to Pete Stevens for his help with orders and early morning chats on sport, holidays and weather and to Seema Rajani, Professor Steve Atkinson, Tim Self and Denise Christie for their competent assistance with confocal microscopy and TEM.

It was an absolute pleasure to work with Musah-Eroje Ahmed and Tatiana Jamillo Forcada, they made the long hours in the lab light-hearted and cheery. I would like to acknowledge the staff of the Greenfield Medical Library and Hallward Library for the support with papers from around the world; in particular to the endless assistance of Sue Bingham at the interlibrary loans. I would also take the chance to thank two wonderful couples: Francesca Saini and Marco Muleri, and Federica Riu and Daniele Avitabile, you have made me feel at home during this chapter of my life in Nottingham.

I would finally express my sincere gratitude to the teachers and professors that I encountered during my academic studies and that have supported me through the years. Without Professors Mariella Giganti, Domenico D'Auria, Luciana Guazzoni and Jatinder Ahluwalia I would not be here.

Dulcis in fundo, as the Romans would say...My warmest and heartfelt love goes to my wonderful husband, Matteo. It is honestly impossible to express in words the infinite practical and emotional ways you have contributed to this achievement. I wish to thank you for just being you and may we always be this unique and exclusive thing that we are now.

My deepest love goes to my family: to my mum for her warm, protective and caring way of being a brilliant mum and to my lovely dad from whom I have taken the attitude of being a dreamer. My dearest love goes to the rest of my family and my extended family, in particular to my sister Loredana and to my grandma 'Nonna Maria'

for the wonderful memories that will always be with me. I feel blessed to have you both in my life.

Table of Contents

ABSTRACT	III
LIST OF POSTER/PRESENTATIONS	IV
PAPERS IN PREPARATION	IV
ACKNOWLEDGEMENTS.....	V
TABLE OF CONTENTS	VIII
LIST OF FIGURES	XIV
LIST OF TABLES	XVIII
LIST OF ABBREVIATIONS	XIX
LIST OF CELL LINES.....	XXII
1- CHAPTER 1	23
1.1 Barriers to drug delivery	24
1.2 Strategies for drug delivery.....	25
1.2.1 Nanomaterials in drug and gene delivery	25
1.3 Routes of cellular uptake	35
1.3.1 Endocytic compartments.....	36
1.3.2 Membrane domains	39

1.3.3 Phagocytosis	40
1.3.4 Clathrin-mediated endocytosis	42
1.3.5 Caveolae-dependent endocytosis	51
1.3.6 Non-clathrin, non-caveolae-mediated endocytosis	55
1.4 The biological environment and nanomaterials	58
1.4.1 Nanoparticles in the bloodstream	59
1.4.2 Extravasation of nanoparticles	62
1.4.3 Nanocarriers passage into body tissues and organs	63
1.4.4 Nanoparticles uptake into cells	63
1.5 Nanoparticles in the literature	67
1.5.1 Colloidal Gold Nanoparticles	67
1.5.2 Quantum dots (QDs)	68
1.5.3 Iron oxide nanoparticles	69
1.5.4 Polystyrene nanoparticles	69
1.6 Aims and thesis outline	73
1.7 Experimental Approach	75
2- CHAPTER 2	88
2.1 General Materials	89
2.1.1 Cell lines	89
2.1.2 Cell culture materials	89
2.1.3 Polymers studied	91

2.1.4 Materials for inhibition studies	92
2.2 General methods.....	93
2.2.1 General cell maintenance procedures.....	93
2.2.2 Dynamic Light Scattering (DLS)	95
2.2.3 Transmission Electron Microscopy (TEM) of C-PB.....	96
2.2.4 Zeta potential of C-PB.....	96
2.2.5 Toxicity Tests.....	97
2.2.6 Htf and LacCer Wash Efficiency Studies	102
2.2.7 Inhibition of Htf uptake with CPZ.....	106
2.2.8 Inhibition of Htf uptake with Pitstop 2	106
2.2.9 Inhibition of LacCer uptake with MBCD	107
2.2.10 Endocytosis inhibition in the presence of C-PB	108
2.2.11 Procedures for sterilization of coverslips for microscopy	108
2.2.12 Confocal microscopy live imaging methods.....	108
2.2.13 Immunofluorescence of clathrin and caveolin-1.....	109
3- CHAPTER 3	112
3.1 Introduction	113
3.2 Methods	114
3.2.1 C-PB size and charge characterization	114
3.2.2 Cell viability studies of C-PB, MBCD and CPZ.....	115

3.2.3 Immunofluorescence of clathrin heavy chain isoform α (CHC α) and caveolin-1 (cav-1) in 3T3, HCT116 and MGLVA-1	118
3.2.4 Wash efficiency studies for the removal of markers of endocytosis	120
3.3 Results	120
3.3.1 Size and Charge Characterization of 50 nm C-PB	120
3.3.2 Size and Charge Characterization of 100 nm C-PB	123
3.3.3 Cell viability studies of C-PB, CPZ and MBCD	125
3.3.4 C-PB cell viability studies	128
3.3.5 Characterization of the viability of cells treated with MBCD	130
3.3.6 Characterization of the effects on cells of CPZ.....	131
3.3.7 Clathrin and caveolin immunocytochemistry studies	132
3.3.8 Wash efficiency studies of endocytosis markers	136
3.4 Discussion.....	136
3.5 Conclusions.....	145
4- CHAPTER 4	150
4.1 Introduction	151
4.2 Methods	152
4.2.1 Optimization of the inhibition of Htf uptake	152
4.2.2 Optimization of the inhibition of LacCer uptake with MBCD.....	153
4.2.3 Inhibition of endocytosis of C-PB with CPZ and MBCD.....	153
4.2.4 Confocal microscopy live imaging	154

4.3 Results	155
4.3.1 Optimization of the inhibition of Htf uptake	155
4.3.2 Inhibition of the endocytosis of C-PB with CPZ and MBCD	166
4.3.3 Confocal microscopy live imaging studies	167
4.4 Discussion.....	189
4.5 Conclusions.....	201
5- CHAPTER 5	206
5.1 Introduction	207
5.2 Materials used for the studies.....	208
5.3 Methods	215
For a schematics of all the experiments carried out with polymers formulations 1-9, cell lines used, and aggregation state please refer to Table 5-3.	215
5.3.1 Cell viability studies.....	215
5.3.2 Cell uptake studies.....	216
5.3.3 Assessment of the uptake of polymer micelle-like nanoparticles 5	218
5.3.4 Assessment of the kinetics of endocytosis of formulation 6.....	218
5.3.5 Uptake studies for nanoparticle formulations 6 and 7.....	219
5.3.6 Uptake studies of the internalization of micelle 8.....	219
5.3.7 Uptake studies of the internalization of micelle-like nanoparticles 9	220
5.4 Results	221
5.4.1 Acute cell viability studies	221

5.4.2 Internalization studies of micelle-like structures from polymer 5.....	224
5.4.3 Micelle 6 and 7 live imaging studies.....	227
5.4.4 Live cell imaging of nanoparticles 8	234
5.4.5 Micelles 9 live imaging	247
5.5 Discussion.....	251
5.1 Conclusions.....	262
6- CHAPTER 6	266
7- APPENDIX I	279
8- APPENDIX II	284
9- APPENDIX III.....	289
10- APPENDIX IV	316

List of Figures

Figure 1-1 Different geometries in polymer structures..	26
Figure 1-2 Schematic representation of the hydration state changes in thermoresponsive polymers above a LCST..	28
Figure 1-3 Schematic representation of micelles and vesicles with their typical loads.....	30
Figure 1-4 Visual description of packing parameter, mean curvature and Gaussian curvature described in equation 1.....	32
Figure 1-5 Diagram for PEO-PBO block copolymers in relation to their concentration in water and their molecular weight..	34
Figure 1-6 Diagram showing the theoretical (a) and observed (b) shapes of PB-PEO block copolymers.....	34
Figure 1-7 Phagocytosis internalises different materials by different mechanisms of engulfment at the plasma membrane.....	41
Figure 1-8 Mechanisms of endocytosis.....	43
Figure 1-9 Schematic representation of the AP adaptor proteins.....	46
Figure 1-10 Schematic representation of the AP2 protein in its open state	46
Figure 2-1 Poly(lactide-co-glycolide)- <i>block</i> -poly(poly(ethylene glycol methyl ether methacrylate)-co-poly(propylene glycol methacrylate)) (PLGA- <i>b</i> -(PPGMA-co-PEGMA)) thermoresponsive polymers.....	91
Figure 2-2 Polylactide- <i>block</i> - poly(poly(diethylene glycol methacrylate)-co-poly(oligoethylene glycol methacrylate)) (PLA- <i>b</i> -(DEGMA-co-OEGMA)) thermoresponsive polymers.....	91
Figure 3-1 DLS characterization of 50 and 100 nm C-PB	122
Figure 3-2 TEM's plot of Feret's diameter for 50 and 100 nm C-PB.....	123
Figure 3-3 Double Gaussian distribution for 100 nm C-PB.....	123
Figure 3-4 TEM images of 50 nm (A) and 100 nm (B) C-PB	124
Figure 3-5 Titration curves of 3T3, HCT116 and MGLVA-1 cells at 4.5 h in HBSS/HEPES 20 mM with MTT (left) and Cell Titer Glo (right) at 4.5 h.....	126
Figure 3-6 MTT titration curves with 3T3, HCT116 and MGLVA-1 cells at 24 and 48 h.....	127
Figure 3-7 Biocompatibility studies of 50 and 100 nm C-PB at 4 h in 3T3, HCT116 and MGLVA-1 cells.....	129
Figure 3-8 MTT toxicity assay of 50 nm C-PB at 24 and 48 h incubation.	130
Figure 3-9 MBCD (left) and CPZ (right) toxicity studies at 4.5 h with MTT (black lines and squares), Cell Titer Glo (red lines and circles) and Apo I caspase 3/7 (green lines and diamonds) in 3T3, HCT116 and MGLVA-1 cells	131
Figure 3-10 CHC α and cav-1 flow cytometry immunofluorescence experiments...	133
Figure 3-11 Immunocytochemistry confocal microscopy experiments of 3T3, MRC-5, HCT116 and MGLVA-1 for CHC α	134

Figure 3-12 Immunocytochemistry confocal microscopy images of the staining of cav-1	135
Figure 3-13 Histograms of the fluorescence intensity for Clathrin mAb X22 and Caveolin-1 mAb clone 2297 immunolabelling	135
Figure 3-14 Flow cytometry results of 3 replicates experiments on the different efficiency of the removal of Htf and LacCer endocytic markers from the plasma membrane of cells for washes carried out on adherent cells (in T25 flasks) or in cell suspensions (Eppendorf tubes washes).	136
Figure 4-1 Flow cytometric analysis of the inhibition of the uptake of Htf with 80 μ M CPZ or 1.25 mM MBCD at 1,2,3 or 4 h in 3T3, HCT116 and MGLVA-1 cells.....	157
Figure 4-2 Flow cytometry histograms on the inhibition of Htf uptake with 80 μ M CPZ at different time points and cell lines. The X axes show the fluorescence intensity of Htf, the Y axes show the number of cells. The dark shadows show Htf uptake at basal, uninhibited levels while the light shadows show Htf uptake in the presence of 80 μ M CPZ	158
Figure 4-3 Effect of lower concentrations of CPZ on the inhibition of Htf uptake in 3T3 and HCT116 cells.....	160
Figure 4-4 Flow cytometry experiments incubated with different concentrations of CPZ in 3T3 and HCT116 cells in the absence of Ca^{2+} and Mg^{2+}	161
Figure 4-5 The effect of passage number and ageing of cells on the inhibition of CME with Htf 6.7 μ g/ml and 80 μ M CPZ at 1 and 2 h in 3T3 and HCT116 cells....	163
Figure 4-6 Htf inhibition of endocytosis with Pitstop 2 at 12.5, 18.75 and 25 μ M in HCT116 cells.....	164
Figure 4-7 Inhibition of LacCer uptake with 1.25 mM MBCD.....	165
Figure 4-8 Inhibition of the uptake of 50 nm and 100 nm C-PB with 80 μ M CPZ and 1.25 mM MBCD	167
Figure 4-9 Confocal live imaging studies of 3T3 cells treated with 50 μ g/ml 100 nm C-PB for a period of 60 min	169
Figure 4-10 Orthogonal projection of a 3D image of 3T3 cells treated with 50 μ g/ml 100 nm C-PB.....	170
Figure 4-11 3T3 fibroblasts treated with 100 nm C-PB	171
Figure 4-12 Zoom images of live experiments of 3T3 cells treated with 100 nm C-PB 50 μ g/ml for a period of 60 minutes	172
Figure 4-13 Analysis of the fluorescence of 3T3 cells treated with 50 μ g/ml 100 nm C-PB for a period of 60 min	172
Figure 4-14 Merge of fluorescence live images for HCT116 cells incubated with 50 μ g/ml of 50 nm C-PB for 60 minutes.....	176
Figure 4-15 Orthogonal projection of a 3D image obtained with HCT116 incubated with 50 nm C-PB	177
Figure 4-16 Images of the redistribution of the red CellMask membrane staining at 4 and 60 minutes in HCT116 cells	178
Figure 4-17 Details of the live imaging experiments of HCT116 cells incubated with 50 nm C-PB 50 μ g/ml for a period of 60 minutes	179

Figure 4-18 A. Spindle-like structures of HCT116 membrane of cells incubated for 4 minutes with 50 nm C-PB, demonstrating an intense activity of the membrane. B. Analysis of the green fluorescence of HCT116 cells incubated with 50 nm C-PB.	179
Figure 4-19 Confocal live studies of MGLVA-1 cells treated with 50 µg/ml 50 nm C-PB for a period of 60 minutes	181
Figure 4-20 Orthogonal projection of a 3D image taken from MGLVA-1 cells treated with 50 µg/ml 50 nm C-PB	182
Figure 4-21 MGLVA-1 cells treated with 50 µg/ml 50 nm C-PB for 60 minutes	183
Figure 4-22 Details of the live images studies of MGLVA-1 cells treated with 50 µg/ml 50 nm C-PB for a period of 60 minutes	184
Figure 4-23 Analysis of the fluorescence of MGLVA-1 cells treated with 50 nm C-PB for 60 minutes	184
Figure 4-24 MGLVA-1 gastric cancer cells treated with 100 nm C-PB for a period of 60 minutes	185
Figure 4-25 Orthogonal projection of a 3D image obtained from MGLVA-1 cells treated with 100 nm C-PB	186
Figure 4-26 Redistribution of the C-PB (Green) and CellMask membrane staining (Red) over time for MGLVA-1 cells treated with 50 µg/ml of 50 nm C-PB	187
Figure 4-27. A. Details of live images studies of the endocytosis of 100 nm C-PB in MGLVA-1 cells for a period of 60 minutes. B. Magnification of the regions enclosed in the squares of Figure 28A	188
Figure 4-28 Analysis of the fluorescence of MGLVA-1 cells treated with 100 nm C-PB for 60 minutes	189
Figure 5-1 Poly(lactide-co-glycolide)- <i>block</i> -poly(poly(ethylene glycol methyl ether methacrylate)- <i>co</i> -poly(propylene glycol methacrylate)) (PLGA- <i>b</i> -(PPGMA-co-PEGMA)) thermoresponsive polymers	209
Figure 5-2 Polylactide- <i>block</i> - poly(poly(diethylene glycol methacrylate)- <i>co</i> -poly(oligoethylene glycol methacrylate)) (PLA- <i>b</i> -(DEGMA- <i>co</i> -OEGMA)) thermoresponsive polymers	209
Figure 5-3 Manual method for the formation of micelle-like nanoparticles from amphiphilic polymers	217
Figure 5-4 Schematic representation of the mixing apparatus used for the production of polymer formulation 8 and 9	217
Figure 5-5 Assessment of cell activity interference of micelle-like formulation 1 (A), 2 (B), 3 (C) 4 (D) following incubation in 3T3, HCT116 and MGLVA-1 cells with an MTT acute test at 4 h	222
Figure 5-6 Assessment of cell activity of polymer micelles 6 on 3T3, HCT116 and MGLVA-1 cells with an MTT test	223
Figure 5-7 Micelle-like structures 5 incubated at 42°C (above TTT) for 8 h	226
Figure 5-8 Confocal live studies of the kinetics of uptake of micelle-like formulation 6 on 3T3 cells	228
Figure 5-9 Comparison of the fluorescence intensity of 3T3 cells before and after 1 h treatment with micelle-like formulation 6	229

Figure 5-10 3T3 cells treated with micelle-like formulation 6 for 2 h.....	232
Figure 5-11 3T3 cells treated with micelle-like nanoparticles 7 preincubated for 30 minutes at 37°C before application on cells for 2 h.....	232
Figure 5-12 Micelle-like nanoparticles 7 preincubated at 37°C for 30 minutes prior to the application on 3T3 cells for 2 h.....	233
Figure 5-13 Micelle-like formulation 6 preincubated at 37°C for 30 minutes and consequently applied to 3T3 cells for 17 h.....	233
Figure 5-14 Mann-Whitney t test of the fluorescence for the negative untreated cells and positive control cells treated with formulation 6.....	234
Figure 5-15 3T3, HCT116 and MGLVA-1 cells treated with different concentrations of formulation 8 for 24 h at 37°C.....	237
Figure 5-16 3T3, HCT116 and MGLVA-1 cells treated with 1000 µg/ml of formulation 8 for 24 h at 37°C.....	238
Figure 5-17 3T3, HCT116 and MGLVA-1 cells treated with 500 µg/ml of formulation 8 for 24 h at 37°C.....	239
Figure 5-18 3T3, HCT116 and MGLVA-1 cells treated with 250 µg/ml of formulation 8 for 24 h at 37°C.....	240
Figure 5-19 3T3, HCT116 and MGLVA-1 cells treated with 62.5 µg/ml of formulation 8 for 24 h at 37°C.....	241
Figure 5-20 3T3, HCT116 and MGLVA-1 cells treated with 31.25 µg/ml of formulation 8 for 24 h at 37°C.....	242
Figure 5-21 Evidence of aggregation over time of formulation 8 upon storage at -20°C.....	245
Figure 5-22 Flasks with or without HCT116 cells treated with formulation 8 at room temperature for 1 h, at 37°C overnight and before and after rinse.....	246
Figure 5-23 Formulation 9 incubated with HCT116 cells in different conditions.....	249
Figure 5-24 Internalization of 250 µg/ml of micelle suspension 9 after overnight incubation at 37°C.....	250
Figure 5-25 Orthogonal projection of a 3D image acquired on 3T3 (left) HCT116 cells (right) treated with 250 µg/ml of micelle suspension 9 overnight at 37°C.....	250

List of Tables

Table 1-1 Correlation between rearrangement of polymers in aqueous solutions and v , a , l , H and K parameters.....	33
Table 1-2 Summary of nanomedicines that have reached clinical trials or the market.....	73
Table 2-1 A summary of the cells lines used.....	90
Table 3-1 Statistical analysis of the Z factor and Signal Window at 4 h.....	127
Table 3-2 Statistical analysis for MTT assays at 24 and 48 h	128
Table 3-3 Reference values for Z factor and Signal Window provided according to ²⁵ (*) and ²⁶ (**)......	128
Table 3-4 Summary of the IC_{50} and 95% confidence intervals obtained in the tested cell lines with MTT and Cell Titer Glo at 4 h -24 and 48 h incubation of 50 nm C-PB.....	130
Table 3-5 IC_{50} and 95% confidence intervals of MTT, Cell Titer Glo and Apo I caspase 3/7 activity.	132
Table 4-1 Two-Way ANOVA statistical analysis of the inhibition of Htf uptake in the presence of CPZ and MBCD.	159
Table 4-2 Chlorpromazine (CPZ) chemical structure, chemical nomenclature and molecular weight.	189
Table 4-3 Pitstop chemical structure, nomenclature and molecular weight.	196
Table 5-1 Summary of the characteristics of the PLGA-b-(PPGMA-co-PEGMA) thermoresponsive polymers and micelle-like nanoparticles used for the study.	212
Table 5-2 Summary of the characteristics of PLA-b-(DEGMA-co-OEGMA) thermoresponsive micelle-like nanoparticles used in the study.....	213

List of Abbreviations

AAK1	Adaptor Associated Kinase 1	DMSO	Dimethylsulphoxide
ANOVA	Analysis of Variance	EDH2	EPS15 Homology Domain-containing protein 2
AP1	Assembly Polypeptide 1	EDTA	Ethylene Diamine Tetracetic Acid
AP2	Assembly Polypeptide 2	EE	Early Endosomes
AP3	Assembly Polypeptide 3	EEA-1	Early Endosome Antigen 1
AP4	Assembly Polypeptide 4	EGF	Epithelial Growth Factor
AP5	Assembly Polypeptide 5	eNOS	Endothelial Nitric Oxide Synthase
APC	Allophycocyanin	EPR	Enhanced Permeability and Retention
Apo I	Caspase 3/7 Apoptosis Assay	EPS15	Epithelial Growth Factor Receptor Pathway Substrate 15
Apo-Htf	Apo-transferrin	ErbB2	Epidermal Growth Factor (EGF) Receptor (EGFR) Tyrosine Kinases Family of Receptors
APP	Amyloid Precursor Protein	ESCRT	Endosomal Sorting Complex Required for Transport
ATCC	American Type Culture Collection	FAK	Focal Adhesion Kinase
A.U.	Arbitrary Units	F-BAR	Fer-CIP4 homology- Bin/amphiphysin/Rvs Protein
AuNP	Gold Nanoparticles	FBS	Foetal Bovine Serum
BAR	Bin/amphiphysin/Rvs protein	FCHo1/2	Fer/Cip4 homology domain-only (FCHO) protein 1 and 2
BSA	Bovine Serum Albumin	FDA	Food and Drug Administration
Cav-1	Caveolin-1	FI	Fluorescence Intensity
CD2AP	CD2 adaptor protein	FITC	Fluorescein Isothiocyanate
cdc42	Cell division control protein 42	GFP	Green Fluorescent Protein
CDE	Caveolae-Dependent Endocytosis	GI tract	Gastrointestinal tract
CHC α	Clathrin Heavy Chain α	GLUT4	Glucose Transporter 4
CIE	Clathrin-Independent Endocytosis	GMA	Glycidyl Methacrylate
CI-MPR	Cation-Independent Mannose 6-Phosphate Receptor	GPC	Gel Permeation Chromatography
CLIC-GEEC	Clathrin-Independent Carrier Glycosylphosphatidylinositol-Anchored Proteins Enriched Endocytic Compartment	GPI-APs	Glycosylphosphatidylinositol-Anchored Proteins
CMC	Critical Micellar Concentration	GRAF-1	Focal Adhesion Kinase-1
CME	Clathrin-Mediated Endocytosis	GULP	Engulfment Adaptor Protein
C-PB	Carboxylated Polystyrene Beads	HBSS	Hank's Balanced Salt Solution
CPP	Cell Penetrating Peptide	HDAC6	Histone Deacetylase 6
CPZ	Chlorpromazine	HEPES	2-[4-(2-hydroxyethyl)piperazin-1-yl]ethanesulfonic acid
CV	Coefficient of Variance	HIP1R	Huntingtin-binding Protein 1 Related
\bar{D}	Polydispersity	HIV-1	Human Immunodeficiency Virus Type 1
DAB2	Disabled Adaptor-2	HMEM	Hank's Minimum Essential Medium
DAPI	4',6-Diamino-2-Phenylindole, Dihydrochloride	Holo-Htf	Holo-transferrin
dBSA	Defatted Bovine Serum Albumin	Hsc70	Heat shock cognate protein 70
DEGMA	poly((diethylene glycol)methacrylate)		
DLS	Dynamic Light Scattering		
DMEM	Dulbecco Modified Eagle Medium		

HSP70	Heat Shock Protein 70 Family	PBS	Phosphate Buffered Saline
Hsp90	Heat shock protein 90	PDGF	Platelet-Derived Growth Factor
Htf	Human Transferrin	PEG	Polyethylene glycol
HUVEC	Human Umbilical Vascular Endotelium Cells	PEGMA	Poly((ethylene glycol) methacrylate)
IC ₅₀	Inhibitory Concentration (50%)	PEI	Polyethylenimine
ICOS	Interdisciplinary Computing and Complex Biosystems	PFA	Paraformaldehyde
IgG	Immunoglobulin G	PH domain	Pleckstrin Homology domain
IL2R β	Interleukin 2 Receptor β	PI(4,5)P2	Phosphatidylinositol 4,5 Bisphosphate
JACoP	Just Another Colocalization Plugin	PI3K	Phosphatidyl Inositol 3 Kinase
K _d	Apparent Dissociation Constant	PI3P	Phosphatidylinositol 3 Phosphate
LacCer	Lactosyl ceramide	PIC	Polyions Complexes
LAMP1/2	Lysosomes Associated Membrane Proteins 1 and 2	PICsomes	Polyion Complexes Vesicles
LC	Light Chain	PKN β	Protein Kinase N-construct β
LCST	Lower Critical Transition Temperature	PLA	Poly(lactic acid)
LDL	Low-Density Lipoproteins	PLGA	Poly(lactic-co-glycolic acid)
LE	Late Endosomes	PPGMA	Poly((propyleneglycol)methacrylate)
LSM	Laser Scanning Microscope	PSMA	Prostate Specific Membrane Antigen
mAb	Monoclonal Antibody	QD	Quantum Dots
MARCKS	Myristoylated Alanine-Rich C-Kinase Substrate protein	Rabs	Ras-like Small G Proteins
MBCD	Methyl- β -cyclodextrin	Rac1	Ras-related C3 Botulinum Toxin Substrate 1
MEM	Minimum Essential Medium Eagle	RAFT	Reversible Addition-Fragmentation Chain Transfer
MHC1	Histocompatibility Complex 1	Rho	Ras homolog oncogene
M _n	Molecular Weight	ROS	Radical Oxygen Species
MPRS	Mannose Phosphate Receptors	RPMI	Roswell Park Memorial Institute
M _r	Relative Molecular Weight	RT-PCR	Real Time Polymerase Chain Reaction
MRI	Magnetic Resonance Imaging	SAR	Structure-Activity Relationship
MSN	Mesoporous Silica Nanoparticles	SH3 domain	SRC- Sarcoma Oncogene Homology 3 Domain
MTT	(3-(4,5-Dimethylthiazol-2-yl)-2,5-Diphenyl-Tetrazolium Bromide)	SNAP	Synaptosome-Associated Protein
MVB	Multivesicular Bodies	SNAREs	Soluble N-ethylmaleimide-Sensitive Factor Attachment Protein Receptors
M _w	Weight Average Molecular Weight	SPION	Superparamagnetic Iron Oxide Nanoparticles
NEAA	Non-Essential Animo acids	SV40	Simian Virus 40
NLS	Nuclear Localization Sequence	TAT	HIV Tat-Protein Transduction Domain
ns	Non Significant	TEM	Transmission Electron Microscopy
OEGMA	Poly((oligoethylene glycol)methacrylate)	TR1	Transferrin receptor 1
PAA	Poly(acrylic acid)	TR2	Transferrin receptor 2
PAK 1 and 2	p21-Activated Kinase 1 and 2	t-SNARES	Target-bound Soluble N-ethylmaleimide-sensitive factor Attachment Protein Receptors
PAR1	Protease-Activated Receptor 1	TTT	Thermal Transition Temperature
PB	Polystyrene Beads	UCST	Upper Critical Solution Temperature
PB-PEO	Poly-Butadiene – Poly Ethylene Oxide		

UV	Ultra Violet	v-SNARES	Vesicle-bound Soluble N-ethylmaleimide-sensitive factor Attachment Protein Receptors
VAMP2	Vesicle-associated Membrane Protein 2	YO	Yellow-Orange
V-ATPases	vacuolar ATPases Membrane Proton Pumps	$\lambda_{\max, em}$	Maximal wavelength of emission
		$\lambda_{\max, ex}$	Maximal wavelength of excitation

List of Cell lines

3T3	Mouse Swiss Albino Embryo Fibroblasts
A549	Human Lung Carcinoma Cells
B16	Non-phagocytic Murine Melanoma Cells
ECV304	Endothelial Cell Line Derived from Human Bladder Cell Line T24
HCT116	Human Colon Cancer Cells
HeLa	Human Cervical Adenocarcinoma Cells
Hepa1-6	Murine Hepatoma
HepG2	Human Hepatocellular Carcinoma
KLN205	Murine Lung Squamous Cell Carcinoma
MGLVA-1	Human Ascites Gastric Cancer Cells
MKN45	Human Gastric Adenocarcinoma Cells
MKN45G	Human Gastrin Producing Gastric Cancer Cells
MRC-5	Human Foetal Lung Fibroblasts
THP1	Human Acute Monocytic Leukaemia Cell Line

1-Chapter 1

Nanomaterials and Endocytosis

1.1 Barriers to drug delivery

Many powerful drugs fail to reach the market because of delivery-related issues. Problems such as lack of absorption, poor solubility, poor biodistribution, metabolic modification with either rapid loss of therapeutic effect or increased toxicity, and undesirable clearance kinetics are all reasons why drugs fail to progress through clinical trials^{1,2}.

Physiological barriers to drug delivery depend on the route of administration and on the compartmentalization of the target organ³. For example, in oral administration, the low pH in the stomach and consequent adsorption through the gut are important barriers to overcome. Other examples of barriers to drug delivery are the blood brain barrier for central nervous system delivery of drugs, skin penetration for topical and transdermal applications, and mucus penetration for aerosol, gastric, ocular or vaginal administration⁴.

Drug delivery systems constitute a strategy for overcoming many of these barriers and are being actively studied in order to develop and optimise therapy with new drug compounds⁵⁻⁸. Amongst the classes of drug delivery systems are those classed as 'nanomedicines'. Materials with at least one dimension ranging between 1 and 100 nm have been defined as nanomaterials by the National Technology Initiative, the Food and Drug Administration (FDA) and American Society for Testing and Materials⁹. The advantages and applications of carrier systems with size ranges in the 'nanomaterial region' are numerous. Firstly, they can be easily internalised in cells with an inverse relationship between size and absorption; secondly they have a high surface to volume ratio that makes the surface chemistry of these materials highly represented and hence important for cell/nanoparticle interactions. Finally, the use of nanocarriers of drugs could make possible the delivery of nucleic acids for gene therapy which are otherwise

challenged by ubiquitous nucleases^{10,11}; they could be loaded with anticancer drugs and reduce their side effects and systemic exposure to the drug and toxicity. Moreover, they could be employed to increase the solubility of many drugs that are highly effective but their application is limited by their poor solubility by loading them in hydrophobic compartments of the carrier. Finally, not only therapy, but also diagnostics and probe technology, can benefit from these materials¹²⁻¹⁴. Examples are nanocarrier-mediated delivery of aptamers (small RNA, single stranded sequences of DNA or peptides with high affinity for one molecule or protein due to their specific 3D rearrangement)²¹⁰⁻²¹² for the diagnosis of cancer or gold nanoparticles for increased sensitivity in the detection of HIV-1 antigen^{15,16}.

1.2 Strategies for drug delivery

1.2.1 Nanomaterials in drug and gene delivery

A great variety of nanomaterials have been designed for use in drug delivery. Many of the investigated nanomaterials are based on polymers, usually with monomer components to confer surfactant or amphiphilic properties, i.e. with a hydrophobic region to interact with a hydrophobic drug compound and a hydrophilic component to enable dispersion in aqueous media or the bloodstream. To date, many combinations of different polymers have been investigated for drug and gene delivery¹⁷⁻¹⁹.

1.2.1.1 Block copolymers

When polymers are formed by two different monomers they are called copolymers; the two monomer constituents can be present randomly in the structure and in this case they are defined as statistical copolymers (Figure 1-1). When monomers of one type are grouped together and monomers of a second type are also attached to each other the resultant structure is defined as a block co-polymer. Depending on how many different monomer sequences and polymers are present, and consequently, how many

regions of the polymers can be distinguished, they are named diblock copolymers, triblock-copolymers and so on. Triblock copolymers can be classified as A+B+A or A+B+C depending on how many different polymers are included in the structure and how they are arranged with respect to each other²⁰. Hence, monomers can be covalently linked to each other²¹ and can be formed by homopolymer or more polymers with different characteristics and different patterns of assembly. Polymers can be linear, branched, or hyperbranched (grafted copolymers, dendrimers) and examples of branched and hyperbranched polymers can be viewed in Figure 1-1²¹.

Polymers can also be bound through electrostatic interactions. Examples are polyion complexes (PIC) which are formed by the interaction of two polymers with opposite charges or nucleic acid and a cationic polymer for gene delivery²².

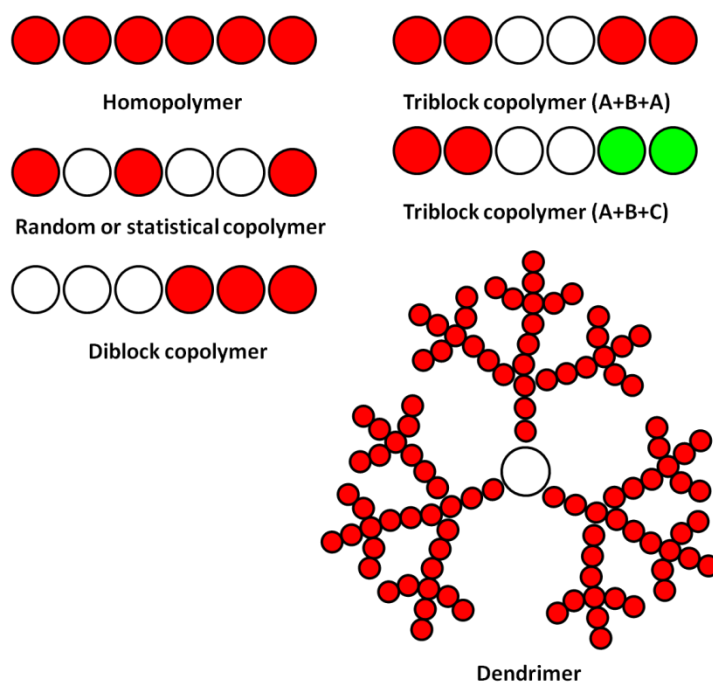


Figure 1-1 Examples of block copolymers. In this picture are shown the rearrangement of a linear homopolymer, a diblock, an A+B+A and A+B+C triblock copolymers, a random or statistical copolymer and a dendrimer. Polymers blocks with different polarities are shown in different colours.

Block copolymers can self-assemble into superstructures under certain conditions. The assembly can be spontaneous and irreversible or it can be triggered by a reversible stimulus.

1.2.1.2 Stimuli-responsive polymers

Many approaches have been investigated in order to obtain 'intelligent' or 'smart' materials that are able to release a loaded drug to a given target. Common examples are pH-sensitive, thermo-responsive, redox, light, ion, magnetic, ultrasound, enzymes-sensitive polymers and so on²²⁻²⁸.

Thermo-responsive polymers were the first 'intelligent systems' investigated and poly(N) isopropyl acrylamide was the first thermoresponsive polymer studied. Thermoresponsive polymers can be classified into two groups: polymers that present a Lower Critical Solution Temperature (LCST) and polymers that present an Upper Critical Solution Temperature (UCST). Thermoresponsive polymers below the LCST are soluble in appropriate solutions while above the LCST they lose their solubility (Figure 1-2). This effect is driven by the entropy of the system. Above a given temperature the most energetically convenient rearrangement of the polymer is out of solution. This is caused by the release of the water from the hydrophilic chains of the polymer that reduce the solubility of the polymer but also produces an increase of entropy which is energetically favourable. This effect is ruled by the Gibbs-Helmholtz equation²⁹:

$$\Delta G = H - T\Delta S$$

Where:

ΔG = free energy

H= enthalpy

T= temperature in Kelvin

ΔS = entropy

UCST polymers behave in an opposite way and are not solubilised below a given temperature while the solution results clear and homogeneous above an UCST. This effect is driven by the enthalpy of the system. Thermoresponsive carriers of drugs have been investigated for applications in inflammation sites where often a mild temperature gradient is present reaching a maximum temperature of 42°C or in conjunction with the external administration of mild hyperthermia by near infrared irradiation, ultrasound probes or microwave irradiation of the target body region.

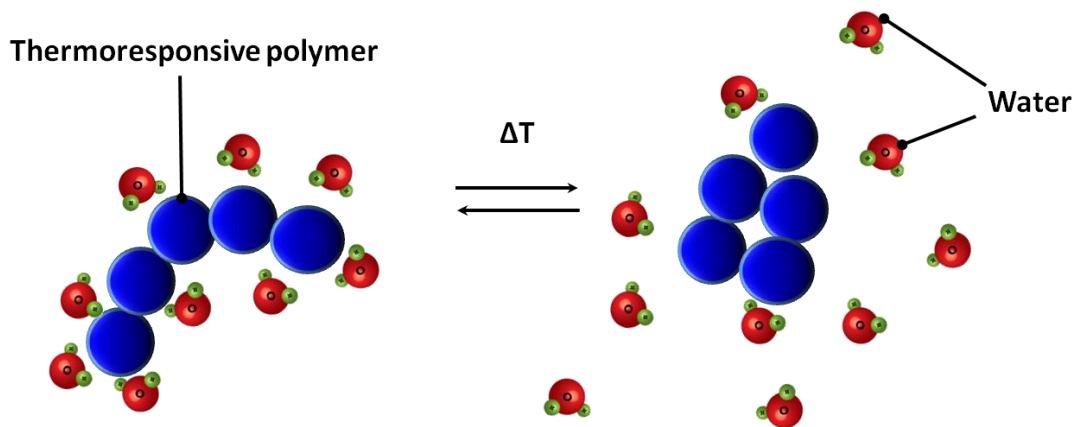


Figure 1-2 Schematic representation of the hydration state changes in thermoresponsive polymers above their LCST. Above the LCST the water molecules return to the solution and increase the entropy of the system and make this rearrangement energetically favourable.

pH-responsive systems are among the most studied and well-characterised polymers. Their solubility, volume, configuration or conformation can be reversibly manipulated by pH changes³⁰. Methacrylic acid and related co-polymers are examples of pH-responsive polymers. They are hydrophobic at low pHs and are deprotonated and hydrophilic with the increase of pH. Their use has been suggested in the gastrointestinal (GI) tract where a pH gradient is present within the stomach (pH ranges between 1 and 3) and the jejunum and ileum (pH between 6 and 7) where the pH

gradient can trigger the release of the loaded drug. Other applications are in cancerous tissues as they are acidic (pH ranges from 6 to 7.2) and at the subcellular level where the pH for endolysosome compartments has been reported between 4.5 and 6³¹.

Other stimuli-responsive systems are sensitive to the naturally reducing environment inside the cell (*redox polymers*). Disulfide groups are often used in these systems as, when they reach the inner cellular environment, they are easily targeted by glutathione activity and cleaved (Kim et al., 2010 as reported by³²). *Ion-sensitive polymers* have also been studied addressing the *salting in* and *salting out* properties of *chaotrope* (water structure breaker) and *kosmotrope* (water structure maker) ions²⁵. Many other smart polymers have been reported in the literature but a detailed overview of such systems is beyond the scope of this thesis.

Following stimulation, smart polymers produce a sharp conformational change that, in some cases, can be used to rapidly release the loaded drug. A recent new approach describes stimuli-responsive vesicles where only the permeability of such structures is increased instead of the arrangement being completely lost³³.

1.2.1.3 Micelles and vesicles

Covalently bound block copolymers can self assemble and produce micelles, which are formed by a hydrophilic shell and a hydrophobic core, or vesicles (also called polymersomes) with the creation of a hollow compartment surrounded by three layers: hydrophilic, hydrophobic and hydrophilic again, as depicted in Figure 1-3²⁰. Also non covalently bound electro-statically associated polyion complexes can produce micelles and vesicles (PICsomes)³⁴.

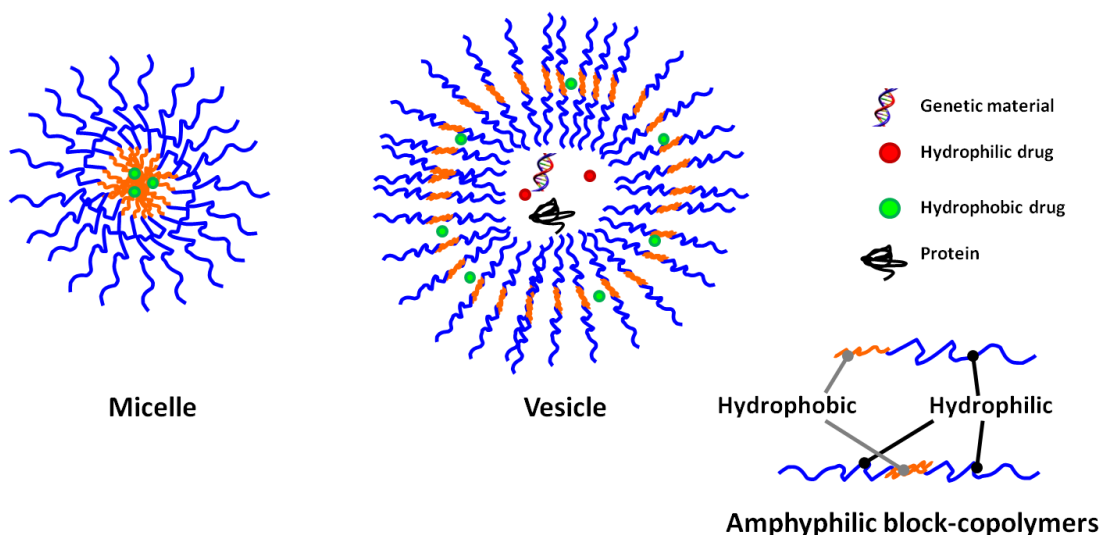


Figure 1-3 Schematic representation of micelles and vesicles with their typical loads. Hydrophobic regions are represented in orange, hydrophilic regions are represented in blue.

Hydrophobic drugs are usually loaded in the hydrophobic core of micelles or in the hydrophobic layer of polymersomes while hydrophilic drugs are usually encapsulated into the hydrophilic hollow compartment of polymersomes. Drugs can also be covalently linked to polymers. If the drug retains its activity when bound to the polymer the structure can be termed a polymer-drug. Here the drug can be directly bound to the polymer or can also be bound through a spacer. More often the drug must be released by the polymer to be active; in this case, the polymer-drug conjugate is called a macromolecular pro-drug. In macromolecular pro-drugs the spacer must be cleaved by hydrolytic, oxidative or enzymatic activity and, ideally, becoming susceptible to cleavage only when it has reached the target.

1.2.1.4 Formulation of copolymers into micelles, vesicles and nanoparticles

Single block copolymers formed by a hydrophobic block and a hydrophilic block are surfactants. In other terms they are surface active materials and rearrange at the solvent-air surface to reduce the contact of the water insoluble block of the polymer with an aqueous solvent. In this way they also reduce the surface tension of the solvent at the interphase. Amphyphilic block copolymers can self-assemble in aqueous solution

and produce micelles. This process occurs above a critical micellar concentration (CMC) that is dependent upon the temperature of the solution and the length of the carbon chain of the polymer. Above the CMC the polymers produce aggregates by a process called micellarization³⁶. These micelles can be spherical, rod-like (also called worms) or rearrange in flat membranes³⁷. However, for all the above-mentioned rearrangements, the hydrophobic portion of polymers reorganize orienting their structures so that they do not come into contact with the aqueous solution³⁸. The hydrophilic region of the polymer produces a corona around the hydrophobic region of the micelles minimising the contact area of the hydrophobic core with the incompatible solvent³⁹. The micellarization process is reversible and single block copolymers can be freed in solution below the CMC of the polymer and this aspect is important in drug delivery where the dilution of the micelles in the blood stream below the CMC might cause the micelles to disassemble before reaching the target⁴⁰.

Vesicles are formed in a two step self-assembly process:

- 1) The formation of a membrane;
- 2) The closure of the membrane into a vesicle⁴¹.

In the classical description, the shape of the vesicle is determined by equation 1²³(Figure 1-4):

$$\text{Equation 1} = p = \frac{v}{al} = 1 - Hl + \frac{Kl^2}{3}$$

Where:

p = surfactant packing parameter (Israeleachvili's parameter);

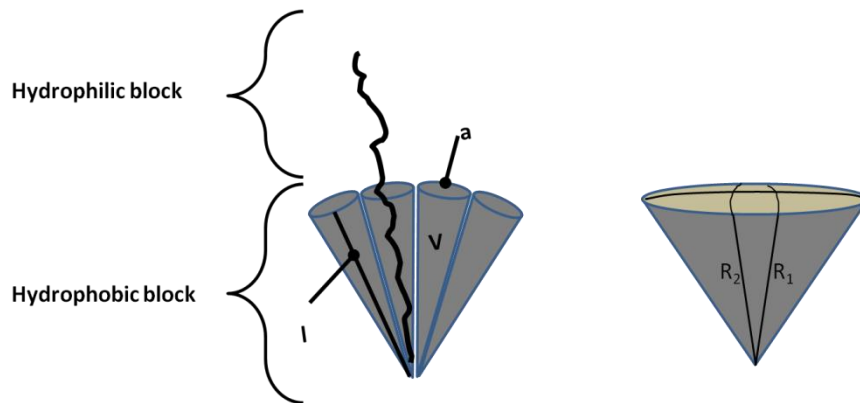
v = volume of the hydrophobic portion;

a = interfacial area;

l = the chain length normal to the interface of the hydrophobic portion;

H = mean curvature;

K = Gaussian curvature.



$$\text{Packing parameter} = \frac{v}{al}; \quad \text{Mean curvature} = H = \frac{1}{2} \left(\frac{1}{R_1} + \frac{1}{R_2} \right); \quad \text{Gaussian curvature} = K = \frac{1}{R_1 R_2}$$

Figure 1-4 Visual description of packing parameter, mean curvature and Gaussian curvature described in equation 1.

When the interfacial area increases in proportion to the hydrophilic block length, a reduction of the hydrophobic/hydrophilic ratio produces the shift from spherical to cylindrical micelles, to membranes and finally to vesicles (Table 1-1).

Shape	v/al	H	K
Sphere	1/3	1/R	1/R ²
Cylinder	1/2	1/(2R)	0
Bilayer	1	0	0

Table 1-1 Correlation between rearrangement of polymers in aqueous solutions and v , a , l , H and K parameters.

Other important parameters to consider are the entropy of the system or how stiff the block copolymer chain is, its degree of freedom and the level of interfacial energy. If the polymer is stiff, with low degree of freedom and entropy, membranes and vesicles are more probable. If the interfacial energy is high and the entropy loss is low, association thermodynamics are dominated by interfacial area energy minimization arrangements. Discher and Eisenberg suggested that a hydrophilic weight fraction of 35% \pm 10% is necessary in coil-coil block copolymers for vesicles formation^{23,42}. Stiffness of a block copolymer can be enhanced by complementarities within the block copolymer such as secondary interactions (H bonds, Van der Waals, electrostatic, π interactions and so on).

Vesicles easily form when the elasticity of the membrane is low and the surface tension is high. The surface tension increases when the concentration of block copolymers is low. When the concentration is high instead, the membrane chooses different rearrangements such as sheet-like micelles (Figure 1-5)^{24,41}.

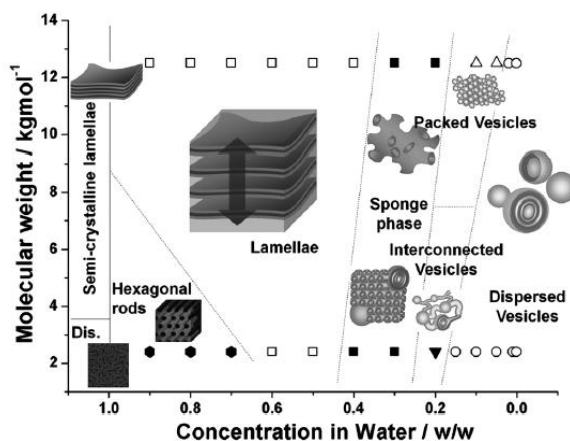


Figure 1-5 Diagram for PEO-PBO block copolymers rearrangements in solution in relation to their concentration in water and their molecular weight. (Diagram from²⁴). Reproduced by permission of the Royal Society of Chemistry.

Also ΔA , which is the difference between internal and external area of the polymer ($\Delta A = A_{in} - A_{ext}$) is another key parameter. A is proportional to the volume to area ratio $v = 6\pi^{1/2}VA^{-3/2}$ where V is the volume of the polymer. The following image describes the theoretical (a) and observed (b) changes in shape of poly-butadiene - polyethylene-oxide (PB-PEO) vesicles (Figure 1-6)⁴¹.

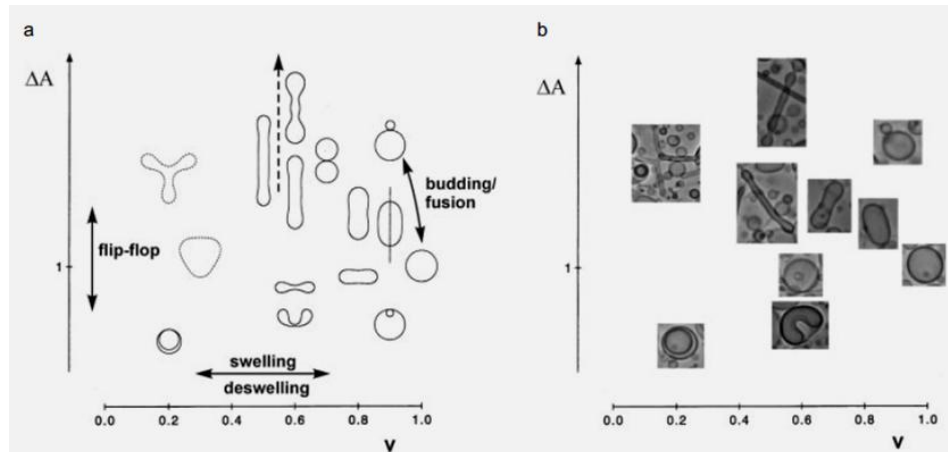


Figure 1-6 Diagram showing the theoretical (a) and observed (b) shapes of PB-PEO block copolymers in solution. (Diagram from⁴¹). Reproduced by permission of the Royal Society of Chemistry.

1.3 Routes of cellular uptake

The knowledge of the pathway used by nanocarriers to access cells is an important starting point to design efficient transporters of drugs and it is being intensely investigated for this purpose. For this reason the current state of understanding in cell uptake pathways, essential protein machinery and compartmentalization are considered below.

Eukaryotic cells use many different endocytotic mechanisms, some of which are still poorly understood. Endocytosis is an essential pathway for the uptake of nutrients and communication, and it is also used by toxins and viruses to enter cells⁴³. It can be divided into two main subgroups: phagocytosis and pinocytosis. The classic definitions of phagocytosis and pinocytosis are now widely accepted. Phagocytosis is the internalization of solid materials and it is usually carried out by specialised phagocytic cells such as macrophages, neutrophils, monocytes and dendritic cells⁴³. Pinocytosis is an ubiquitous process by which cells engulf liquids. Once internalised, cargoes undergo sorting towards different compartments and this often happens with the help of Ras-like small G proteins (Rabs). Rabs GTPases are the most prominent group of Rabs⁴⁴, they are a group of about 63 membrane proteins and control many processes such as endocytosis, trafficking, endosomes-membrane fusion and exocytosis^{45,46}. Examples of compartmentalization involving Rabs include endocytic vesicles and early endosomes (Rab5), late endosomes (Rab7), recycling endosomes (Rab4), the movement of vesicles from the trans-Golgi network to the plasma membrane (Rab11), endosomes directed to the Golgi (Rab9) and endoplasmic reticulum (Rab1 and 2)^{45,47}.

SNAREs (soluble N-ethylmaleimide-sensitive factor attachment protein receptors) are another important category of proteins. They are involved in membrane fusion of intracellular compartments and hence are a key class of proteins for endocytic

compartment maturation and in traffic⁴⁸. They bind SNAP (synaptosome-associated protein) receptors on the target membrane and can be localised in vesicles, and they are defined as v-SNAREs, or on the target (t-SNAREs). Their hallmark is a SNARE motif which is constituted by a sequence of 60-70 amino acids that is formed by a series of 7 amino acid repeat units (heptad repeat). Monomeric SNAREs are not organised in a defined structure, but, upon assembly organise in helices of high stability and produce a hydrophobic core where strongly conserved hydrophilic amino acids reside. Each SNARE bears one of these amino acids so that three SNARE proteins consist of glutamines (Q) and one of arginine (R). The respective SNARE proteins are named Qa, Qb, Qc and R-SNAREs^{46,49}.

1.3.1 Endocytic compartments

Upon endocytosis, the endocytic vesicle is directed towards the first cellular compartment: the Early Endosome (EE). EE is composed of a thin tubular extension of about 60nm and vesicular regions of about 400nm that present a multivesicular structure of an immature multivesicular body (MVB). These two morphologies of different regions of the same EE are believed to be essential for the subsequent processing and compartmentalization of the endocytosed cargo where, for example, recycling cargoes cluster around tubular membranes with a local pH of 6.5, while cargoes undergoing a degradative pathway cluster around MVB structures of the same compartment in which the pH of the lumen is more acidic (ranging between 6.2 and 5.5)⁵⁰. The acidification process occurs through vacuolar type H⁺ ATPases (V-ATPases) membrane proton pumps. EE are enriched in Rab5, in phosphatidylinositol 3 phosphate (PI3P), early endosome antigen 1 (EEA-1) and they interact with actin and microtubules tracts that confer motility to the compartment^{51,52}.

Another well-characterised subcellular compartment is the late endosome (LE). It is believed to be generated by maturation of EE where it becomes gradually enriched in

Rab7 and other proteins. This organelle is a pre-lysosomal compartment of about 100-600nm that the endocytosed cargo access roughly after 4-30 min from endocytosis in mammalian cells. It is more spherical with respect to EE and is formed by MVBs that are the hallmark of this compartment. LEs can in fact also be referred to as MVBs or multivesicular endosomes. They have intraluminal vesicles with an average size of about 50 nm and are formed by the action of endosomal sorting complex required for transport (ESCRT). The ESCRTs are a relatively recently discovered class of proteins required for the inward invagination of the endosomal membrane to produce intraluminal vesicles⁵³. LE are distinguished from the EE because they are more acidic (pH 5-5.5) and enriched in markers proteins such Rab7, and from the lysosomal compartments because they present mannose phosphate receptors (MPRs) that transport newly synthesised lysosomal protein from the Golgi complex. MVBs can mature to lysosomes or fuse to the plasma membrane and release intraluminal vesicles in the extracellular compartment in the form of exosomes^{49,54,55}.

Lysosomes are another compartment that endocytosed cargoes can be directed to. They are degradative compartments of less than 1µm in non specialised cells but can become larger in macrophages. They are enriched in hydrolases, and it is accepted that molecules smaller than 200Da can diffuse freely through their membrane. Lysosomes present about 20 different membrane transporters but to date only 3 have been fully characterised. They also present V-ATPases that acidify the pH of the lumen of the organelle to around 4.5. Lysosomes are defined as MPR negative and are positive for lysosomes associated membrane proteins 1 and 2 (LAMP1/2)⁵⁶. Occasionally lysosomes can present multilamellar structures in their lumen. However, these compartments are unrelated to multivesicular bodies (MVB). Lysosomal degradation products can be directed to the trans-Golgi-network or exocytosed⁵⁷.

Autophagosomes are other characteristic compartments that a cargo can be directed to by a process called autophagy that occurs during amino acid and nutrient starvation, oxidative stress and radical oxygen species production (ROS)⁵⁸. Autophagy is dependent on lysosomes and is used by cells for the degradation and recycling of intracellular components. There are 4 different categories of autophagy in mammals, classified as macroautophagy, microautophagy, chaperone-mediated autophagy and piecemeal microautophagy⁵⁹. Macroautophagy relies on the use of specialised vesicles localised in the cytosol that engulf a cytoplasmic components and that ultimately fuse with a lysosomes. Microautophagy relies on the production of invaginations directly on the membrane of the lysosomes that envelops parts of the cytoplasm that are for degradation; chaperone-mediated autophagy uses chaperones that unfold proteins that are then translocated into the lysosomes⁵⁹; piecemeal microautophagy has been observed in yeast and occurs by degradation of portions of the nucleus that are carried into a vacuole, where the vacuole is the yeast equivalent of lysosomes. The most common and best characterised process of autophagy is macroautophagy. It happens with a phagophore, also known as an isolation membrane, which has been suggested to originate from the point of contact of the endoplasmic reticulum and the mitochondria⁶⁰. This membrane elongates and envelopes around the cytoplasmic components that are intended for degradation and produces a compartment called autophagosome with a double membrane. This structure is then fused with different compartments of the endocytic process. An autophagosome shares the same machinery that is used for endocytosis and fuses with an EE, subsequently with a LE and finally a lysosome and produces a autolysosome, this process is called maturation of the autophagosome^{61,62}.

1.3.2 Membrane domains

Eukaryotic membranes possess a high variability in lipid composition and are formed by hundreds of different lipids. The membrane bilayer has evolved the ability to segregate its constituents laterally by dynamics of liquid-liquid lipids immiscibility. Different regions have been recognised on the plasma membrane, and can be seen as a mosaic of organised microdomains enriched in a few lipids that associate and are supplemented with specific plasma membrane proteins⁶³. This organization defines specialised subcompartments on the membrane that are used for endocytosis, signalling and trafficking. Lipid rafts are one of these domains. Lipid rafts are membrane microdomains of about 50 nm in diameter, with a membrane composition that differs from the adjacent areas and these are enriched in cholesterol, glycol-sphingo-lipids, sphingo-myelin, long and unsaturated phospholipids, proteins bound to glycosyl-phosphatidyl-inositol as well as some membrane spanning proteins^{64,65,66}. These structures are present as a metastable state that can be activated by specific lipid-lipid, lipid-protein and protein-protein interactions⁶⁶.

Another of the defined domains involved in endocytosis consists of clathrin-enriched large patches that have been described in both adherent and non adherent adipocytes. They present little lateral mobility and are also enriched with phosphatidylinositol 4,5 bisphosphate (PI(4,5)P2), cholesterol and receptors that are endocytosed by this pathway⁶⁷⁻⁷⁰. This structure also defines a membrane ruffling region where ruffling can be triggered by an unconventional myosin 1c expression. Ruffles are regions on the plasma membrane that arise when exocytosis is activated and actin polymerization pushes outward the membrane⁷¹. Myosin 1c expression is also responsible for exocytosis of GLUT4 (glucose transporter 4) vesicles in adipocytes and for E-cadherin-mediated cell-cell adhesion, both processes also rely on PI(4,5)P2 presence in the plasma membrane and also actin-enriched membrane projections⁷²⁻⁷⁵.

1.3.3 Phagocytosis

Phagocytosis (Figure 1-7) is carried out primarily by specialised phagocytes such as macrophages, monocytes, neutrophils and dendritic cells and it is a highly efficient process. Fibroblasts, epithelial cells and endothelial cells are also known as non-professional or paraprofessional phagocytes and can uptake particles via phagocytic mechanisms but to a lower extent with respect to phagocytic professional cells. Also many other cells have phagocytic capacities, for example thyroid and bladder cells phagocytose erythrocytes *in vivo* and other cells have been induced to phagocytose *in vitro*⁷⁶. The major differences between professional and non professional phagocytes are in the numbers of phagocytic receptors on their membrane; these receptors both speed up the process and allow a wider range of particles to be recognised and phagocytosed⁷⁶.

Even if every specialised cell has different fine tuning events in the phagocytic process three general steps can be distinguished:

a. *Opsonisation of the particle.* This usually occurs in the bloodstream and consists of tagging the target element with opsonins such as antibodies (especially IgG and IgM), complement elements C3, C4 and C5 (by complement activation via the classical, alternative or lectin pathway) and blood serum proteins such as laminin, fibronectin, C-reactive protein and type-I collagen and many others which opsonise foreign hydrophobic particles⁷⁷⁻⁷⁹.

b. *Recognition of the opsonised particle by the phagocytic cell.* Opsonised particles are recognised by specific receptors on the phagocytic cell such as Fc receptor for antibodies and complement receptors. Mannose/fructose and scavenger receptors can also be involved in phagocytic mechanisms while many other receptors (i.e. CD44 receptors) are still being discovered.

c. *Engulfment of the particle – Phagosome formation.* Opsonin–phagocytic cell interaction activates a transduction cascade via the Ras homolog oncogene (Rho) – family small GTPase that induces actin polymerization and activates the phagocytic process. The engulfment occurs via the formation of cytoplasmic protrusions or sinking for complement receptors-mediated endocytosis that finally enwrap the opsonised particle and translocate it into the cytoplasm (Figure 1-7)⁸⁰. During phagosome formation the actin filaments depolymerise and make the phagosome accessible by early endosomes that finally mature to late endosome and lysosomes and produce a phagolysosome. The compartment is acidified by proton pump ATPases located on the membrane and enriched with digestive enzymes such as esterases and cathepsins as well as chemical factors such as superoxides and hydrogen peroxide to degrade the phagocytic load.

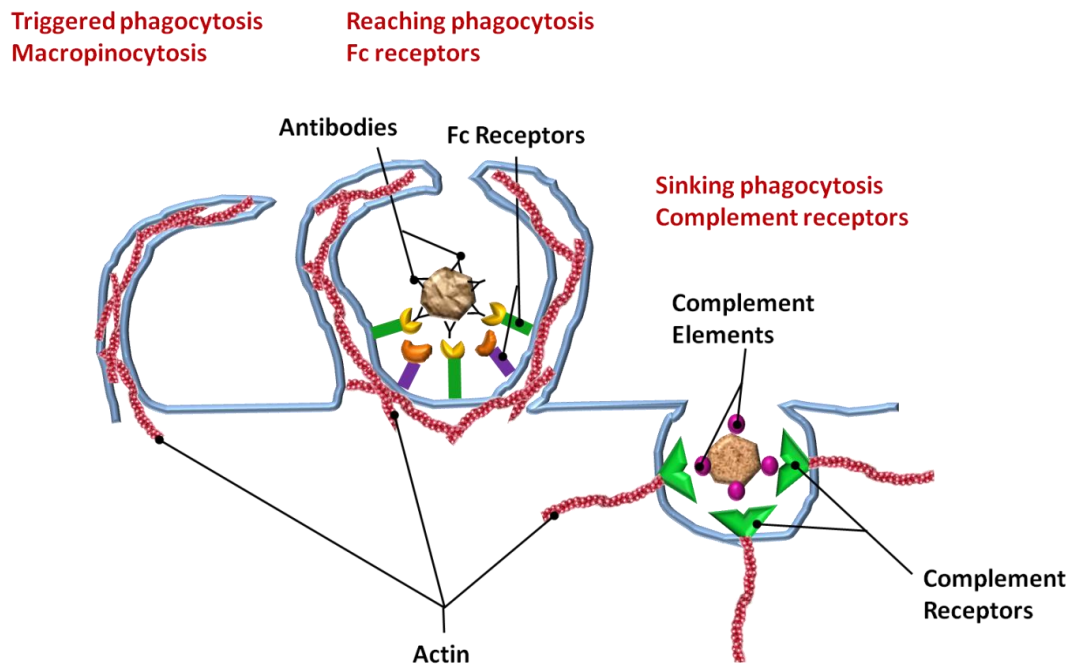


Figure 1-7 Phagocytosis internalises different materials by different mechanisms of engulfment at the plasma membrane.

1.3.4 Clathrin-mediated endocytosis

Clathrin-mediated endocytosis (CME, Figure 1-8) takes place for many essential events and well-studied examples are: low density lipoproteins (LDL) and transferrin receptor (TR) uptake. Other examples of receptor-mediated endocytosis though a clathrin-mediated mechanism are protease-activated receptor 1 (PAR1), the cation-independent mannose 6-phosphate receptor (CI-MPR). Also amyloid precursor protein (APP) and epithelial growth factor (EGF) access cells thorough CME. CME also has a key role in intracellular signalling and regulation of the expression of cell membrane receptors and ion channels, the movement of receptors in other compartments of the cell, synaptic transmission as well as uptake of toxins and viruses. It is also clathrin-mediated the 'zippering' of bacteria where the latter process is used by pathogens that express proteins on their plasma membrane that interact with host receptors and trigger internalization⁸¹⁻⁹⁰.

CME is the best-characterized endocytic process. The unravelling of its mechanism of action has taken place over the past 30 years. Crystal structures of components of the CME such as clathrin, adaptor proteins and the combination of these proteins in the presence and the absence of their substrates has provided evidence at the molecular level of the mechanisms of CME. The best characterized process in CME is the formation of the clathrin lattice at the plasma membrane. This paragraph, although not exhaustive of all the evidence present in the literature, gives an overview of the CME and it reveals the complexity of this endocytic process. This complexity is most likely to be applied to other endocytic pathways that are far less characterized at the present.

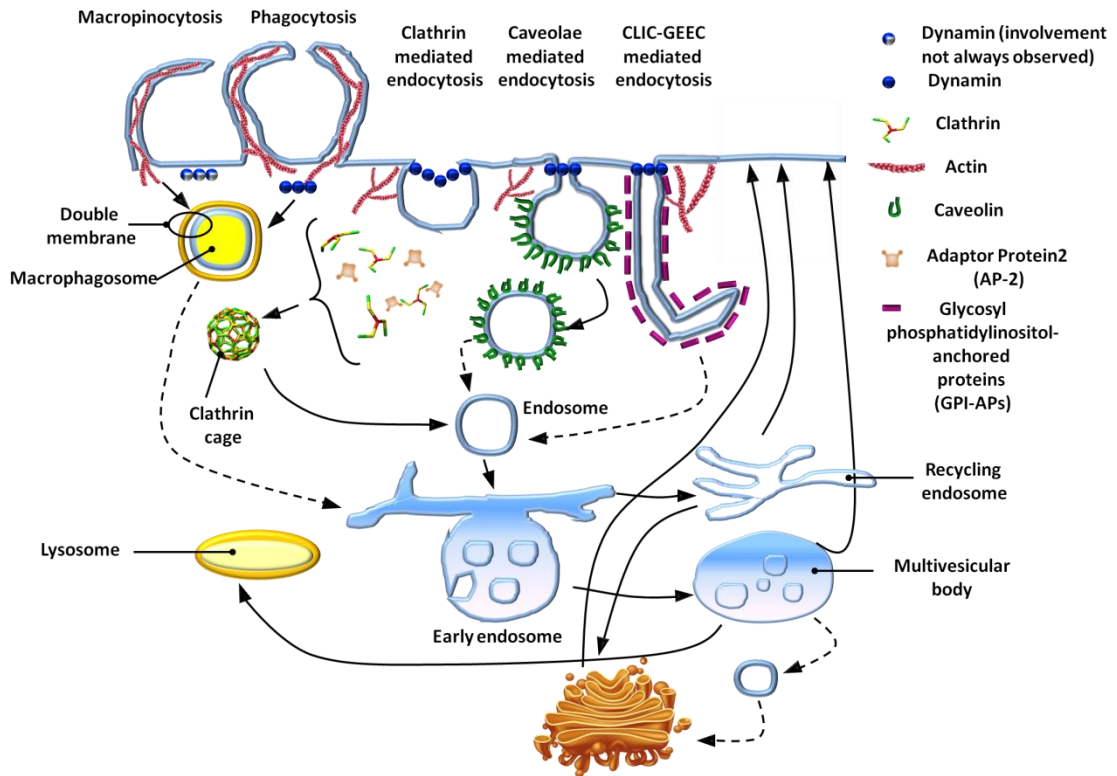


Figure 1-8 Mechanisms of endocytosis. In the schematics are shown macropinocytosis, phagocytosis, clathrin- and caveolin-mediated endocytosis and clathrin-independent carrier glycosylphosphatidylinositol anchored protein enriched endocytic compartments (CLIC-GEEC) endocytosis. The dotted lines show pathways that are not fully confirmed in the literature.

1.3.4.1 Clathrin, a brief introduction

Clathrin is a protein formed by three heavy chains of about 192kDa, each of which is bound to one of the two 30-kDa isoforms of the light chains: LCa and LCb. The 3 heavy chains produce a structure that is called triskelion or trimer. The heavy chain has an amino terminal β propeller domain and 7 WD40 β -sheet repeats followed by 42 α -helical zig-zags of about 30 amino acids, a longer final α -helix of 45 amino acids and a more flexible structure at the C-terminus of the protein⁹¹. The C-terminus contains a domain that is recognised by the heat shock protein family 70 (HSP70). This region is necessary for the disassembly of the clathrin cage after endocytosis and becomes accessible only upon assembly of the clathrin cage. The α -helix domain produces a

curved structure that is called 'leg'. From the vertex where all the 3 legs of clathrin converge, a single α -helix of clathrin light chain departs and connects on one heavy chain^{92,93}. The presence of the clathrin light chain does not seem to be necessary for the CME, however it has been suggested that this α -helical structure confers rigidity to the clathrin helping the CME process.

1.3.4.2 Assembly Peptide (AP) proteins family

Other essential components of the forming clathrin pit are the assembly polypeptides (APs). At the present 5 AP proteins are known, AP1, AP2, AP3, AP4 and AP5. Their schematic structure is shown in Figure 1-9. They are formed by 2 large L-shaped opposing regions that together form a squared 'bowl' structure⁹⁴. These two regions are called γ and β_1 in AP1, α and β_2 in AP2, δ and β_3 in AP3, ϵ and β_3 in AP4, ζ and β_5 in AP5. On the same AP protein also two small domains are present. They are called σ and μ and numbered from 1 to 5 depending on what AP protein they belong to; the σ regions interact with the two L shaped large regions at one point of contact while the μ domain is positioned over the angle of the L shaped β region (Figure 1-9)⁹⁵⁻⁹⁷. At the other point of contact of the large L shaped proteins two flexible domains called hinges are present, each one propelling from one of the L shaped regions, and each hinge connects to a small globular region forming a structure resembling antennae. In AP5 the described antennae region is not present. AP proteins are present in two conformations: 'open' and 'closed'. AP2 is responsible for the CME and it anchors the forming clathrin pit to the plasma membrane because clathrin itself does not contain any motifs for membrane binding (Figure 1-10). The other AP proteins are localised in different compartments of the cell and are responsible for clathrin-dependent cargo sorting to different intracellular compartments⁹⁷. When AP2 is in the closed conformation the protein is localised in the cytoplasm and the cargo binding sites are not accessible. When the AP2 changes conformation to an 'open' form (most probably

subsequently to phosphorylation by a AAK1, a kinase of the Prk/Ark serine/threonine kinase adaptor associated kinase family⁹⁵) its cargo binding site present on the μ_2 subunit becomes accessible and can recognise the Yxx Φ motif on the cytoplasmic region of trans-membrane proteins that can be endocytosis by CME⁸³ (Figure 1-9 and 1-10). The Yxx Φ motif is a linear sequence of amino acids that is widely used by cells in cargo sorting. It is a tyrosine-based sorting signal and the amino acid sequence is arranged as follows: Y is a tyrosine, x is any amino acid and Φ is a bulky hydrophobic amino acid (e.g. leucine, isoleucine, methionine, valine or phenylalanine)⁹⁸. The μ_2 subunit is also responsible for the binding of PI(4,5)P2 on the C-terminal domain producing a bridge between the plasma membrane and the forming clathrin lattice⁹⁵. On the α subunit, another common sorting motif recognition site becomes accessible in the 'open' conformation upon phosphorylation and it is the dileucine-based sequence [DE]xxx[L], where D represents an aspartic acid, E is a glutamic acid, L is a leucine and I is an isoleucine and x is any amino acid. The latter motif binds the nascent clathrin lattice interacting with EPS15 (epithelial growth factor receptor pathway substrate 15), amphiphysin and dynamin adaptor proteins. The hinge box of the β_2 subunit express a recognition site for clathrin called clathrin box that express an amino acid sequence as follows: L Φ x Φ D/E where x is any amino acid and Φ is a bulky hydrophobic amino acid and L is a leucine, D an aspartic acid and E a glutamic acid^{95,44,99-104}.

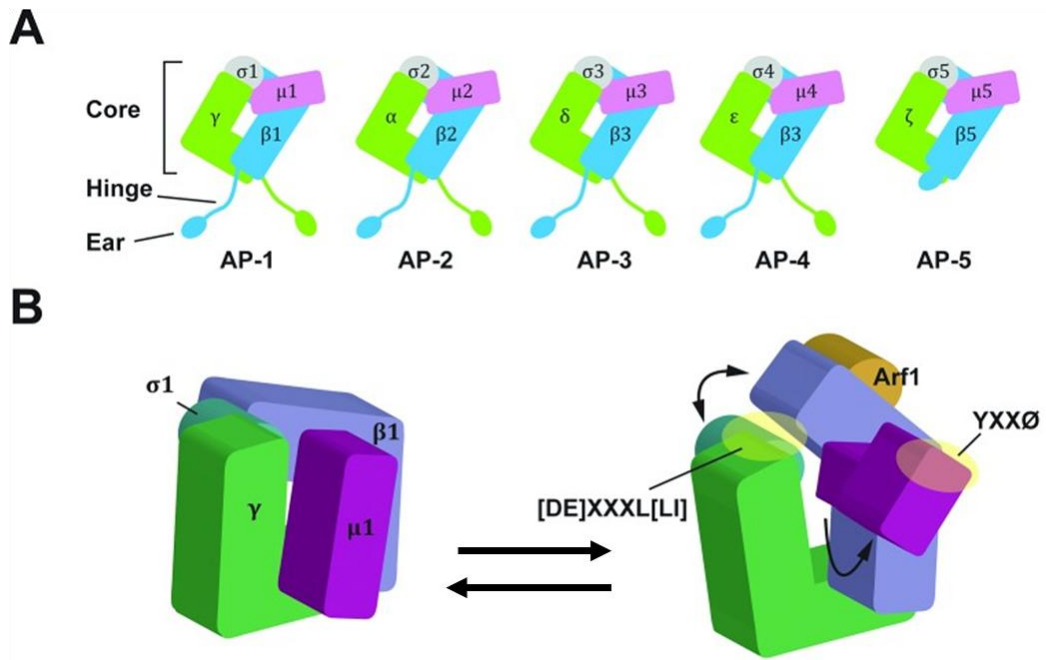


Figure 1-9 Schematic representation of the AP adaptor proteins. A. Schematic representation of all the AP proteins known in their close configuration. **B.** AP2 protein in its close (left) and open (right) configuration.(Readapted from⁹⁷).

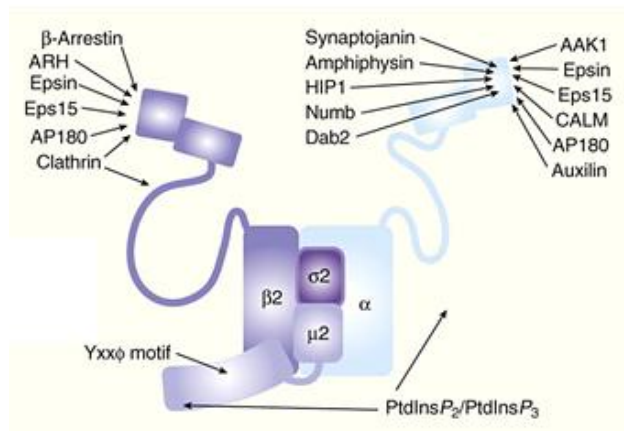


Figure 1-10 Schematic representation of the AP2 protein in its open state. The regions of the ‘ear’ (also called appendage from some authors) known interactions are described in this Figure. (Readapted from⁹⁵).

1.3.4.3 Clathrin nucleation at the plasma membrane and lattice assembly

There are at least two distinct mechanisms of endocytosis called canonical and non-canonical clathrin-mediated endocytosis. The canonical pathway is shared by LDL, EGF, transferrin and asialoorosomuroid and it is based on the evidence that all four clathrin-coated pits produced by the internalization of the above mentioned cargoes are identical. The non-canonical pathway is used by pathogens; requires clathrin and actin and follows a pathway and relies on accessory proteins that can differ from the canonical pathway^{88,93}.

1.3.4.4 The canonical clathrin pathway

Upon receptor binding, one clathrin triskelion arrives at the clathrin pit. Only one clathrin triskelion arrives in 70% of the cases; less frequently, there are 2 or 3 triskelions arriving at the same time. The clathrin triskelion arrives already bound to two AP2 proteins⁹⁹. AP2 has been proposed to work as a hub where clathrin and other adaptor proteins that are specific for one internalising receptor are associated. These adaptor proteins have binding motifs for the receptor and also bending activity. This implies the formation of specific clathrin pits depending on the membrane protein endocytosed and the sorting of the specific cargo starts already at the assembly of the coated pit¹⁰⁵. The F-BAR protein (Fer-CIP4 homology Bin/amphiphysin/Rvs protein) containing family FCHo1/2 (Fer/Cip4 homology domain-only (FCHo) protein 1 and 2) are not essential for the coated pit formation and have been suggested as part of a complex that stabilises the coated pit as 70% of the forming coated pits are not completing their process of endocytosis^{99,106}. The FCHo1/2 proteins bind to the coated pit at low curvatures of the membrane and enhance the curvature by a bending activity¹⁰⁵. Other members of this stabilising complex for the clathrin coated pit progression are epsin 1-2 and 3, EPS15, and intersectin^{99,107}. In these conditions the clathrin triskelion starts assembling in a process that is called nucleation; the

progression of the assembly of the clathrin lattice then occurs at increasingly accelerated rates. A mean of 4 legs from different clathrin triskelions overlap and produce a cage-like structure that is formed mainly by hexagons but also by heptagons and pentagons¹⁰⁸. Pentagons are essential to produce a curved cage where otherwise hexagons would produce a flat cage. The centre of the triskelion produces a tripod-like structure that is formed by the long terminal α -helix of 45 amino acids followed by the C-terminal domain. This region stabilises the forming clathrin cage interacting with distal clathrins⁹³. Actin involvement of CME has been questioned as the inhibition of actin polymerization does not reduce the levels of CME. However, microscopy has provided evidence of actin branched polymers at the endocytic site and around the neck of the forming endosomes^{109,110}. Kirchhausen and co-workers showed that the inhibition of actin polymerization did not inhibit the growth and un-coating of a clathrin pit but it interfered with the formation of new clathrin pits and large clusters of clathrin and AP2 proteins were observed¹¹¹. It has been proposed that actin is essential only when there is high membrane tension for example in adherent cells and when the cargo is unconventional and bulky (e.g. vesicular stomatitis virus, see also non-canonical clathrin pathway)⁸⁸. The last step of CME is the detachment of the clathrin vesicle from the plasma membrane. This process, also called membrane pinching, occurs through a large (100kDa) GTPase called dynamin¹¹². This protein exists as a tetramer and upon contact with a lipid bilayer can produce rings, spirals and helical tubes structures. It is believed to constrict the neck of the forming clathrin vesicle and it has been recently demonstrated that the numbers of dynamins bound to the neck of the clathrin vesicles vary between 26 (20% of pits), 26-52 (55%) and 52-70 (20%). Once the clathrin pit has pinched off the endocytic vesicle the clathrin cage starts a process of destabilization and uncoating that is rapid and leaves promptly the emerging endocytic vesicle. Upon detachment of the clathrin vesicle from the plasma membrane,

auxilin is recruited and arrives at the clathrin lattice. Auxilin binds by J-domains at the C-terminal domain of the clathrin at the vertex of the tripod structure described above. One auxilin binds to each clathrin, bringing up to 3 J-domains at the tripod, enlarging the funnel-like structure of the tripod and making it accessible to Hsc70 (heat shock cognate protein 70)¹¹³. The latter protein belongs to the HSP70 family and bears a ATPase domain which, upon contact of the Hsc70 with the J-domain of auxilin, hydrolyses the ATP and changes the conformation of the Hsc70 to a closed state where interacts with a HSP70 binding motif on the clathrin tripod at the C-terminal. This interaction deforms the clathrin and it has been proposed that the more these deformed conformations are present at the clathrin tripods of the clathrin lattice, the more the clathrin lattice is destabilised and the quicker the disassembly of the clathrin pit¹⁰⁸.

Vesicles are then sorted towards two different kinds of endosomes, fast maturing and slow maturing endosomes. Fast maturing endosomes are targeted with Rab5 and acquire Rab7 within 30 seconds; slow maturing endosomes present only Rab5 on their membrane and do not acquire Rab7 after 100 seconds but acquire Rab11, which is a target for a recycling pathway. LDL, influenza virus and EGF are targeted towards fast maturing and high mobility early endosomes that are also Rab5 and 7 positive or become Rab7 positive within 30 seconds, while transferrin can be targeted towards both sorts of fast or slow maturing early endosomes¹⁰¹.

1.3.4.5 The non-canonical clathrin pathway

Some pathogens have refined their machinery for host invasion and use the clathrin endocytic proteins that are hijacked for their invasion purposes. An example is the enteropathogenic *Escherichia coli*, a bacterium that adheres to the membrane of host cells but is not internalised. It recruits clathrin which is used as a signalling molecule and triggers actin polymerization, does not require AP2 but uses an alternative endocytic protein disabled adaptor-2 (DAB2) that has a PI(4,5)P2 binding motif and it

has been suggested to require PI(4,5)P2 for endocytosis¹¹⁴. However, as for clathrin endocytosis it also requires epsin 1, dynamin and EPS15. In this way the bacterium produces a sort of pedestal that is used to bind on the membrane of host cells⁸⁸. Another mechanism that is used by pathogens is the zippering which involves CME. Some pathogens, (e.g. *Listeria monocytogenes*, a bacterium that causes Listeria fever that can complicate to meningitis in immunodeficient subjects) express surface proteins that bind host cellular receptors and trigger clathrin-dependent internalization that only partially involves the machinery used in canonical clathrin endocytosis. As in the case of enteropathogenic *Escherichia coli*, *Listeria monocytogenes* needs clathrin, dynamin and DAB2 together with EPS15, cortactin and cortactin-interacting protein CD2AP (CD2 adaptor protein) and Huntingtin-binding protein 1 related (HIP1R). The latter protein is also involved in the binding of actin and clathrin at the endocytic clathrin pit. Neither pathogens require AP2 for exploiting their pathogenic action while phosphorylation of clathrin heavy chain also stabilises clathrin beneath the bacterium⁸⁸.

1.3.4.6 The endocytosis of transferrin

Transferrin endocytosis occurs through a receptor-mediated endocytosis of the transferrin receptor 1 that is localised on clathrin coated pits. When the transferrin receptor binds holo-transferrin, which is a form of transferrin binding 2 ions of iron, the CME is triggered and the internalization of the transferrin-receptor complex occurs. The endocytic vesicle soon fuses with sorting or early endosomes. The pH of the endocytic vesicle is acidified and the iron load is released. However, the transferrin stays tightly bound to the transferrin receptor until the complex is recycled on the plasma membrane where the neutral pH of the extracellular compartment releases the transferrin from the receptor¹¹⁵. The transferrin receptor has been monitored with real time fluorescent Rab cell imaging. This method has allowed the recognition of two populations of endosomes, one fast maturing that is tagged with Rab5 and within 30

seconds also conjugates with Rab7, and a slow maturing population of endosomes that does not conjugates with Rab7 after 100 seconds from the internalization of the transferrin¹¹⁶. The transferrin receptor and transferrin complex can both undergo quick recycling on the plasma membrane (this process occurs in about 4 minutes from the internalization) or can be directed towards a late endosomes and recycling compartment delaying the recycling of the receptor on the plasma membrane to 24 minutes⁴⁷. This process occurs with the association of the transferrin-receptor complex with Rab5 and EEA1 for early endosome localization. Then the vesicles become enriched with Rabenosin and Rab22a and these proteins are believed to define the fate of the transferrin-receptor complex towards a recycling fate¹¹⁷⁻¹¹⁹.

1.3.4.7 Involvement of clathrin with phagocytosis

Clathrin has been recently found to be involved in phagocytosis. A recent paper using micro RNAs shows that CHC α is involved in phagocytosis processes in shrimp hemocytes and murine macrophages RAW264.7¹²⁰. The same CHC has also been found involved in phagocytosis of apoptotic bodies by non-professional gliar cells during neuron differentiation and development. The paper showed a mechanism involving GULP, an adaptor protein involved in phagocytosis, associated with Jedi-1, a mammalian engulfment receptor also involved in phagocytosis. The phagocytic process was inhibited by the loss of interaction of a tyrosine phosphorylated form of CHC and GULP¹²¹.

1.3.5 Caveolae-dependent endocytosis

Caveolae-dependent endocytosis (CDE) is one of the best known uptake pathways after CME (Figure 1-8). Caveolae are flask-shaped invaginations of the cytoplasmic membrane that range between 50 and 100 nm in size in the wider part of the flask (typical values are 50-80nm). These invaginations are present in lipid rafts rich in caveolins, a family of cholesterol binding proteins and a membrane integral protein of

21kDa¹²², as well as cholesterol and glycolipids^{123,124}. They are highly stable and are produced spontaneously when caveolin-1 interacts with glycolipids of the membrane raft domains and disappear upon cholesterol depletion^{122,125}. Their stability is given by the interaction with the underlying actin cytoskeleton and only upon specific signals they are internalised in endocytic vesicles.

Endothelial cells are rich in caveolae that can constitute up to 10-20% of the cytoplasmic membrane. Abundance in caveolae has also been reported in smooth muscle cells, fibroblasts, skeletal muscle cells and adipocytes. The composition, function and appearance depend on the cell type. Caveolae in the endothelial cells are usually more narrowed at the neck of the flask shaped invagination and may have a diaphragm that reduces diffusion processes. Muscle cells present caveolae clusters of linear rows that produce the T-tubes while caveolae in epithelial tissues do not contain a diaphragm and are generally smaller¹²². Caveolae are formed by caveolin proteins, caveolin-1, caveolin-2, 3 and 4. Caveolin-1 and 2 are ubiquitous while caveolin-3 and 4 are present in the striated muscle of cells⁴³; caveolin-1 is essential for the formation of caveolae, together with cavin-1. Caveolin-1 is also present in bacteria where it triggers vesicles formation without cavin-1. However, in mammalian cells cavin-1 is essential for the formation of endocytic vesicles, while caveolin-1 is unstable and is quickly degraded in the absence of cavin-1¹²⁶. Caveolae components can be isolated as a single 80S complex and the stoichiometry of the proteins components of this complex appear to be 12 caveolin-1, 3 cavin-1 and 1 caveolin-2 or 3 implying that cavin-1 can form trimers¹²⁶. In the past two years two other proteins taking part in the caveolae-dependent endocytosis have been discovered. They are Pacsin 2 (also known as Sindapin 2) that presents a BAR sensing/binding motif that induces membrane curvature and is involved in caveolae morphogenesis and partially colocalize with caveolae¹²⁷⁻¹²⁹. The other protein is EPS15 homology domain-containing protein 2

(EDH2). It is an ATPase present in caveolae and its action is involved in actin binding and caveolae stabilization. Immuno-electron microscopy studies show that the protein is also localised at the neck of the caveolae^{127,130,131}. Caveolins have a specific orientation within the membrane as both the N and the C termini lie into the cytoplasm and are connected by a hydrophobic domain that is buried but does not span the membrane¹²². Furthermore, caveolins bind to palmitoyl acid on the C-terminus, to cholesterol and can be phosphorylated on tyrosine residues and aggregate and produce dimers or oligomers¹²². *Cavins* also are important coating proteins taking part in caveolae-mediated endocytosis. These proteins chaperone the formation of the membrane curvature but detailed mechanistic information on how these interact with caveolin and other caveolae components are not yet available¹³². Other components that play a role in the caveosome's subsequent fusion with the target compartment are vesicle associated membrane protein (VAMP2) and synaptosome associated protein (SNAP). Particles internalised by caveolae slide along the cell membrane until they reach a caveolae invagination⁷⁸. The particles are anchored to the membrane during the caveolae-mediated uptake, which has been reported as a slower process than the clathrin-mediated uptake. This event could occur via receptor-ligand interactions. The closure of the vesicle occurs via the dynamin GTPase action. The resulting vesicle has typical values of 60-70nm and does not have any specific enzymatic content or low pH environment although some authors have reported that unassembled caveolin can be directed towards degradative lysosomal compartments by ubiquitination and the help of ESCRT proteins¹³³.

Caveolae appear to be formed into the Golgi complex where they are associated with cholesterol, undergo partial oligomerization of caveolin-1 and become detergent resistant.

Often caveolae cargoes overlap with clathrin-independent carriers and a study has shown that caveolin-1 specifically binds to a guanine nucleotide dissociation inhibitor attached to cdc42 (cell division control protein 42) protein which is implicated in clathrin-independent carriers (GPI) – glycosylphosphatidylinositol anchored proteins enriched endocytic compartments (CLIC/GEEC) endocytosis¹³⁴. Furthermore, depletion in caveolin-1 has been reported to increase cdc42 activation at the plasma membrane.

The multi-functionality of caveolin-1 is also demonstrated by its interaction with endothelial nitric oxide synthase (eNOS). The binding of these two elements inhibits the enzymatic activity of eNOS while the disaggregation of the complex causes activation and production of nitric oxide and vessel dilation *in vivo*.

Other evidence suggests that caveolae-dependent and non-caveolar raft endocytosis may be connected⁶⁴. Nichols *et al* suggested that caveolin-mediated uptake may be effective in endothelial cells that express high rates of caveolins and caveolae while other mechanisms⁶⁴ could be activated in cells with lower concentrations of both caveolins and caveolae⁶⁴.

Caveolin has also been implicated in the down-regulation of platelet derived growth factor (PDGF) and EGF via the inhibition of their receptors that are present on caveolae. Over-expression of caveolin-1 inhibits such receptors. Na⁺/K⁺ATPase are also present in caveolae and appear to exert a regulatory function¹³⁵.

Caveolae-mediated receptor endocytosis has been reported for folic acid, albumin and cholesterol internalization as well as for viruses (SV40, virus-Simian Virus 40, and polyoma virus) and the prion protein. Also this pathway is sensitive to cholesterol depletion^{78,136} and, upon *cholesterol* depletion or oxidation, caveolae relocate to endosomes, Golgi complex or endoplasmic reticulum¹²².

1.3.6 Non-clathrin, non-caveolae-mediated endocytosis

Non-clathrin and non-caveolae-mediated endocytosis have not been extensively studied because of the lack of known specific cargoes that are endocytosed by one of these pathways. However, recently some markers of clathrin- and caveolin-independent endocytosis have been recognised. They are the major histocompatibility complex 1 (MHC1), interleukin 2 receptor β (IL2R β) and glycosylphosphatidylinositol-anchored proteins (GPI-APs) and some more information have started to emerge¹³⁷. However, data on these pathways are still fragmentary. For example, MHC I dependent endocytosis was found to necessitate of dynamin, tyrosine kinase and ubiquitin for correct endocytosis. IL2R β relies on actin though the regulation of PAK 1 and 2 (p21-activated kinase 1 and 2), Ras-related C3 botulinum toxin substrate 1 (Rac1), dynamin and phosphatidylinositol 3 kinase, (PI3K) that are also essential in macropinocytosis but a clear understanding of the mechanism is still not known¹³⁸⁻¹⁴⁰.

1.3.6.1 CLIC-GEEC endocytic pathway

The Clathrin-independent carrier/GPI-AP-enriched early endosomal compartments (CLIC-GEEC) pathway is an important uptake route of bulk fluid uptake in fibroblasts¹³⁷. The endocytic cargoes internalised by this pathway have a peculiar ring or tubular morphology¹⁴¹. The CD44 membrane glycoprotein receptor is internalised by this route and it has been used as marker of the pathway. The CD44 receptor is responsible for the uptake of hyaluronic acid and it is involved in cell-cell interaction, adhesion and migration. It localises with lipid rafts but upon stimulation and binding of its ligand ezrin, CD44 translocates to a different membrane region and partially colocalises with the transferrin receptor¹⁴². CLIC-GEEC endocytosis is regulated by the protein GTPase regulator associated with focal adhesion kinase-1 (GRAF-1) that possesses GAP activity and inhibits the activity of small GTPases by accelerating the hydrolysis of GTP to GDP¹⁴³. It has been shown to display such activity on the small GTPases RhoA, that

also displays actin cytoskeleton activity, and cdc42 through the interaction of FAK (focal adhesion kinase) and PKN β kinases (protein kinase N construct β)^{144,145}. GRAF-1 also presents a BAR domain for the membrane deformation activity necessary to form endocytic vesicles, a PH domain (Pleckstrin Homology domain, involved in cell signalling and trafficking) and a SH3 domain (SRC- sarcoma oncogene homology 3 domain) and a prolin rich region that is a SH3 binding domain as well¹⁴⁶. GRAF-1 BAR and PH appear to be important for the formation of tubular endocytic structures and the protein showed affinity for PI(4,5)P2 suggesting a PI(4,5)P2 mechanism for the anchoring of the protein to the plasma membrane. GRAF-1 needs dynamin for endocytosis, appears to colocalize with caveolin-rich domain of the plasma membrane but does not colocalize with clathrin¹⁴³.

1.3.6.2 Macropinocytosis

Macropinocytosis was the first endocytic process indentified by Lewis in 1931 as for¹⁴⁷. However, the lack of specific ligands that are internalized selectively by this mechanism makes the distinction of the macropinocytic pathway challenging with respect to other pathways. Macropinocytosis is a quiescent process that is constitutively activated only in some cell lines such as immature dendritic cells, macrophages and transformed cells¹⁴⁷. When not constitutively activated, it can be transiently triggered (5-10 min) by growth factors and tumour inducing factors such as Sonic hedgehog in neurons and epidermal growth factor in ephythelial cells^{148,149}. Many studies have associated macropinocytosis with the formation of actin rich extensions of the plasma membrane referred as planar and circular membrane ruffles but the formation of such structures does not appear necessary for macropinocytosis, as inhibition of ruffles does not inhibit macropinocytosis uptake¹⁵⁰. Macropinocytosis occurs at lipid rafts membrane subdomains, involves an actin-mediated membrane protrusions formation which than collapse and fuse back into the membrane or on themselves and generate large

pinocytic vesicles (~0.5-1µm) although vesicles of diameter up to 5 µm have been reported with the involvement of dynamin-2¹⁵¹. Once in the cytoplasm the vesicles usually acidify and shrink but the destiny of these compartments depends upon the cell type: examples of different fate for macropinocytosis include fusion with a lysosome or recycling of their load on the cellular surface. No specific coatings have been associated with this uptake pathway but it is often involved in nanocarrier uptake, the clearance of apoptotic bodies as well as some viruses (i.e. adenoviruses)^{78,136,152}.

Cholesterol, actin and PAK1 are essential for macropinocytosis. The latter kinase binds to Rho family GTP-binding protein rac1 and activates it. Also, PI3K, ras (another small GTPase family member), src protein tyrosine kinase, histone deacetylase 6 (HDAC6), heat shock protein 90 (hsp90) are involved in this uptake pathway but the extent and mechanisms are poorly understood. Macropinocytosis is involved in the internalization of viruses and bacteria as well as in the clearance of apoptotic bodies. This pathway has been reported as cholesterol-dependent. Virtually all cells can undergo macropinocytosis but some authors report that macrophages and micro-vessel endothelial cells do not adopt this pathway while others state that macrophages can also perform macropinocytosis. Macropinocytosis is considered a dynamin independent process although some specific types of macropinocytosis appear to be dynamin dependent. This specific way of internalization is called non-canonical macropinocytosis and it has been demonstrated to be involved with the uptake of the Ebola virus and quantum dots (QD)¹⁵³⁻¹⁵⁵.

1.3.6.3 Flotillin-mediated endocytosis

Flotillins are membrane bound proteins that are found almost ubiquitously in mammalian tissues. Flotillin microdomains are present in lipid rafts and are characterised by puncta on the plasma membrane. They are rich in flotillin which is formed by the oligomerization of flotillin 1 and 2¹⁵⁶ and possess membrane lateral

mobility that make them float and from this characteristic they derive their name. Although they do not share any homology with caveolin-1 they present some topology similarity such as the presence of both the N and C terminus in the cytoplasm and membrane domains that do not span the membrane¹⁵⁷. Flotillins are involved with endocytosis, membrane trafficking and signalling but it is not clear at the present if they constitute a separate endocytic pathway or if they induce endocytosis when the clathrin- and caveolin-dependent endocytosis is inhibited. Also, their endocytic machinery has not been defined at the present.

1.4 The biological environment and nanomaterials

Formulating new polymers for drug delivery is challenging as many different parameters such as particle charge, shape and size can affect the biodistribution and uptake of the delivery system. As bacteria, viruses and protozoa have hydrophobic surfaces, the human body has strategies to opsonise hydrophobic particulates, including synthetic hydrophobic nanoparticles^{77,79}. This occurs via interactions with serum proteins such as antibodies, complement factors (common examples are C3, C4 and C5) and blood serum proteins such as laminin, fibronectin, C-reactive protein, type I collagen and many others⁷⁷. These serum components facilitate the binding of nanoparticles with phagocytic cells such as macrophages, neutrophils, monocytes and dendritic cells that have a scavenger role⁷⁹. For this reason, hydrophobic polymers alone are not effective in drug delivery by intravenous routes. A well-known method to overcome such problems is the addition of a hydrophilic, protein-repelling polymer such as polyethylene glycol (PEG) to the drug delivery system. (please see below for a more extensive description of the process). On the other hand, positively charged polymers have shown higher toxicity profiles *in vitro*.

1.4.1 Nanoparticles in the bloodstream

Nanocarriers do not pass the intestinal epithelium¹⁵⁸ and only a slow absorption has been shown through Peyer's patches in the gut¹²; hence, they are often administered intravenously or subcutaneously, by inhalation through the lungs¹⁵⁹ or by intranasal adsorption¹⁶⁰.

Interaction of nanoparticles with blood components is an important aspect to take into account as it can change the biodistribution of the injected materials. Nanoparticles are known to bind serum proteins and molecules constituents. They can form a shield around the nanoparticles called corona within 30s¹⁶¹. The Dawson's group has introduced the concept of hard and soft corona^{162,163}. According to their description, the hard corona strongly interacts with the nanoparticles by electrostatic, Van Der Waals and hydrogen weak bonds and constitutes a hardly modifiable shield. A second layer that is bound less tightly to the hard corona is constituted by proteins and serum molecules that restore the original polarity of the nanoparticles, this compartment is more dynamic and interchanges more frequently with components of blood and constitutes the soft corona. The combination of soft and hard corona increases the overall size of the material. This idea of corona formation around the nanoparticles is not fully accepted and some authors question the existence of such distinct compartments around the nanoparticles and more generally refer to a unique corona of blood components that interchanges dynamically with blood constituents over time¹⁶⁴. Interactions of the nanocarriers with blood molecules can lead to formation of aggregates, might produce adducts with sizes bigger than capillaries and cause ischemia and blood clotting, which is potentially life-threatening. McGuinness and co-workers pointed out that amine and carboxyl derivatization of polystyrene and silica nanoparticles could produce aggregation of nanoparticles with platelets *in vitro*^{164,165}. Furthermore, the surface of blood vessels is negatively charged and it has been

reported that an ideal nanoparticle should have a neutral or slightly negative charge to avoid interaction with the vessel walls¹⁶⁶. However, it has also been proposed that negative charges reduce the extent of interactions of nanoparticles with cells membrane phospholipids that are negatively charged and, consequently, their access to intracellular compartments.

1.4.1.1 Opsonisation

One important aspect to evaluate in nanocarrier drug-delivery systems is the level of opsonisation of the particle in the bloodstream. Opsonisation reduces the concentration of particles in minutes with loss of their therapeutic effects. It occurs *in vivo* and it is carried out by the mononuclear phagocytic system, also known as reticulo-endothelial system⁷⁷. This process (described in §1.3.3) is the way the body scavenges foreign particles that are bigger than the renal threshold (typically around a molecular weight of 5,000 for linear polymers but up to 100,000 for branched or compacted polymers⁷⁷). Phagocytosed particles are readily accumulated into the spleen and liver, the main scavenger organs and, depending on the nature of the particle, can be either digested (biodegradable particles) or accumulated (non biodegradable particles) with high risk of toxicity⁷⁷.

The polarity of the surface of nanocarriers is an important aspect to evaluate when designing new drug delivery devices. As mentioned before, since bacteria, viruses and protozoa have hydrophobic surfaces, the human body has strategies to efficiently opsonise hydrophobic particulates^{77,79}. Hydrophobic particles are targets for serum proteins that adhere to the particles and tag them for rapid phagocytes recognition^{77,78}. On the other hand, nanoparticles with dense surface charge have also shown a high rate of opsonisation and scavenge rate including opsonisation by complement elements^{77,78}.

The process of adhesion of serum proteins to nanoparticles that produces a corona can give important information about both opsonisation and immunogenic reactions¹⁶⁷. Gold nanoparticle coronas coated with poly(acrylic acid) (PAA), for example, activate a cascade signal that leads to production of cytokines in human acute monocytic cell line THP1¹⁶⁸.

One strategy to reduce or block opsonisation consists of shielding the carrier with long hydrophilic but uncharged compounds that reduce non-specific protein binding such as polyethylene glycol⁷⁸. However, various shielding devices have been used for such a purpose: dextrans, alginates, cyclodextrins, hyaluronic acid, trehalose, polyacrylamide, poly-vinylalcohol, poly N vinyl pyrrolidone, poloxamines, and polysorbates^{77,169-171}.

1.4.1.2 Polyethylene glycol coating of nanocarriers

Among the above-listed shielding strategies, one of the most efficient is PEGylation. It can be carried out by surface adsorption but a clear drawback is represented by the easy desorption of the PEG which can lead to gaps in the shield and consequent opsonisation. Harper, Bazile and co-workers have shown that PEG covalent binding is more efficient with respect to surface adsorption^{172,173}. A classic view suggests that PEG chains of 2000Da or longer have reduced binding protein ability and hence are suggested for cargo shielding of drugs¹⁷⁴⁻¹⁷⁶. However, more recently it was shown that PEG chains of 400Da had reduced unfolding properties when incubated with bovine serum albumin (BSA) and lysozyme as measured by fluorescence spectroscopy emission of tryptophan. In the same study, longer chains were more disruptive on these proteins inducing a partial unfolding of the 3D structure¹⁷⁷. Also the unfolding ability towards proteins of a nanocarrier is an important parameter to take into consideration when evaluating its biocompatibility as this process can cause the exposure of antigenic domains to the immune system that can be buried in the 3D structure of a protein. Other important parameters for PEG coating are the surface

conformation of PEG and density. It has been reported that optimal PEG coating is obtained when PEG assumes a 'mushroom' conformation where PEG chains are both more flexible and generally closer to the carrier surface. However, a minimum concentration of PEG must be assured as low PEG concentration is not sufficient for an efficient coverage of the carrier. Also a too high concentration of the polymer is not desirable as it produces a PEG conformation denoted as semi-linear or 'brush' configuration which leads to a loss in flexibility and hindrance volume of the PEG chain and increased opsonisation. PEGylated particles are known to accumulate in the spleen upon opsonisation. Even if PEGylation is a key tool in reducing opsonisation, it has been often reported that PEG coated carriers show a reduced cell uptake, a phenomenon known as the PEG dilemma¹⁷⁸.

1.4.2 Extravasation of nanoparticles

Nanoparticles in the bloodstream must overcome the endothelial barrier in order to reach tissues and organs. The endothelium is typically formed by endothelial cells adhering to the each other through tight junctions and lying on a basement membrane. Tight junction gaps between cells have typical diameters of about 2nm; they are even smaller in the blood-brain barrier while the underlying basal membrane does not allow passage of materials bigger than 13-15nm⁷⁹. Some organs and tissues, depending on their physiological functions, allow the passage of larger particulates. For example, the liver has a fenestrated endothelium which increases the upper size limit to 100 nm while the discontinuous endothelium present in the spleen is even more accessible. However, in pathologic conditions such as inflammation and some kinds of cancers, the endothelium becomes leaky and allows the passage of particles of larger size. It has been reported that inflammation and tumors can cause an increase of fenestrae size up to 700nm in some capillaries¹⁷⁹. Inflammation is common in many pathologic events and, in cancer inflammation, is often associated with the loss of lymphatic

vessels that increases the retention of particulates in such tissues⁷⁹. The increased permeability of tumor sites is often referred as enhanced permeability and retention (EPR) effect¹⁸⁰. It is nevertheless true that the oncotic pressure is increased in extracellular compartments of cancerous tissues and the efficiency of drug delivery by this means is still a matter of debate.

1.4.3 Nanocarriers passage into body tissues and organs

Nanoparticles that overcome the endothelial barrier reach the extracellular matrix. The latter is composed by an aqueous solution of proteins (i.e. collagen), polysaccharides (i.e. hyaluronic acid) and glycoproteins (i.e. chondroitin sulphate). This environment impedes nanoparticle diffusion but the presence of aqueous channels makes this compartment still accessible^{12,181}.

1.4.4 Nanoparticles uptake into cells

Many efforts are being made to characterize the way that nanocarriers enter cells and draw some generalizations in order to understand further the process of uptake. However, at present, just a few concepts are clear^{182,183}.

1.4.4.1 Size, shape and charge of nanocarriers and endocytosis

1.4.4.1.1 Phagocytosis of nanomaterials

The size of nanocarriers, in the absence of any other changes in chemistry or surface properties, influences phagocytosis. Moghimi¹⁷⁹ reported that particles with size greater than 200nm were more promptly cleared from the bloodstream. Champion *et al* on the other hand, showed that the shape of the particle at the point of contact with macrophages determines the kinetics of uptake. In this study, polystyrene spheres were internalised promptly when in contact with alveolar macrophages while flat sides of rod-like polystyrene particles were internalised more slowly. A critical angle of 45° between the particle and the phagocytic membrane surface was calculated as the limit

for efficient phagocytosis where efficient uptake was obtained with lower angle values. This effect could be ascribed to the more complex actin structure to be realised in order to achieve phagocytosis. Surface charged nanoparticles are more readily taken up by macrophages.

1.4.4.1.2 Pinocytosis of nanomaterials and biodistribution

The characteristics of specific nanoparticles influence uptake by mechanisms other than phagocytosis in a more complicated and less evident way and it is thought that the degree of influence for such characteristics is dependent on to the cell type tested. Size, for instance, can limit internalization in some cells (i.e. Hepa 1-6 hepatoma, HepG2 and KLN 205) while it is reported not to influence uptake in HUVEC endothelial cells, ECV 304 bladder carcinoma cells and squamous carcinoma cell lines. Size can also influence the specific pathway of endocytosis⁷⁸. In melanoma B16 cells for instance small particles (<200nm) were taken up by a clathrin-mediated endocytic pathway while bigger particles showed a caveolae-mediated endocytic pathway. Other studies on HeLa cells reported that polystyrene particles of 40nm were internalised by clathrin-mediated endocytosis but particles smaller than 25nm were internalised by a non-clathrin-, non-caveolae-mediated endocytosis. Macropinocytosis, on the other hand, does not show size dependency and it has been reported to often occur together with other uptake pathways. Minchin studied the uptake of AuNP encapsulated in dendrimers of different charges and sizes and reported that distribution in some organs was dependent upon these properties. Studies of biodistribution in mice showed that small (5 nm) positive dendrimers were accumulated into the kidneys for days and mainly excreted through the urine; 5 nm neutral and negative particles were accumulated in spleen and liver. When the size of positive nanoparticles was increased to 22 nm they were not excreted by the kidneys but accumulated in lungs, liver and spleen¹⁸⁴.

Charged carriers can also influence cellular uptake. It has been reported that positively charged nanocarriers are promptly internalised by cells. This could be due, as reported before, to electrostatic interactions with the negatively-charged cell surface. Positively-charged nanoparticles have also been reported to produce defects on cell membrane in cell membrane models. Experiments on dendrimers and other amine containing polymers have been reported to strongly interact with lipid bilayers of membrane models^{9,185}. Such carriers produce membrane thinning at low concentrations and holes at higher concentrations⁹. Charged carriers have been classified in three categories:

- a. Charged particles that adhere closely to already present membrane defects but that cannot enhance these defects;
- b. Charged particles that cannot induce membrane defects but can increase them;
- c. Charged particles that can both start or increase membrane defects.

However, the membranes used to carry out these studies are not natural membranes. They are usually formed by a mixture of natural lipids that are often present in membranes but lack superficial and intercalating proteins and glycoproteins that can represent up to 50% of natural mammalian membranes and this should be taken into account when extrapolating to *in vivo* studies¹⁸⁶.

In the attempt to increase the efficiency of nanomedicines, and to enhance their uptake, nanoparticles have been conjugated with cell penetrating peptides (CPP). These peptides are short sequences that often resemble peptides that have been used by pathogens to access cells. They are rich in arginine and lysin that makes them positively charged or amphiphilic. Examples of CPP are TAT (HIV tat protein transduction domain) and penetratin (*Drosophila antennapedia* homeodomain)¹⁸⁷. Some of these materials have reached the market for topic applications.

Shape of nanoparticles in endocytosis has not been thoroughly investigated but it is known that some viruses (i.e. some strains of Ebola and H5N1) have filamentous shapes. When producing rod-like nanoparticles for drug delivery also the stability of the shape must be taken into consideration as it has been reported that rod-like micelles formed with PEG-*p*-PLA block copolymers were unstable and eventually shortened and produced spherical micelles¹⁸⁸. Other observations focusing on the increased penetration of worm-like micelles in gels suggested that rod-like micelles could have an enhanced penetration in tissues and organs which could be interesting to investigate to enhance oral adsorption of nanoparticles¹⁶⁶. However, depending on the length of nanoparticles, a rod-like shape might induce toxicity and inflammation and ROS production caused by phagocytic cells frustrated internalization as shown by asbestos and more recently by carbon nanotubes research¹⁸⁹.

From this brief overview it is possible to understand the complexity of the field. It is not trivial designing a new nanoparticle for drug or gene delivery and one approach can be a success or failure depending on the target.

However, some generalizations are possible. For example, the size and surface properties of nanoparticles size must be carefully controlled to avoid aggregation in the bloodstream, opsonization and reduced access in target cells. The ideal size range of drug delivery systems is likely to be similar of that of viruses, i.e. between 10 and 100 nm. The nanoparticle should not be strongly negatively or positively charged in order to prevent opsonisation, and respectively: low uptake or disruption of the plasma membrane of cells with consequent toxicity. Hence, the nanoparticle should ideally have a surface which is hydrophilic but not charged. The coating of drug delivery nanoparticles is intensely debated despite more than 30 years' literature on the subject. PEGylation of nanoparticles appears to delay the opsonisation but reduce the access

of the nanoparticle into cells and other coating materials are being investigated. Finally, rod like shape would be preferred as it increases the penetration of the nanoparticle into tissues and organs. However, possible side effects such as inflammation caused by a frustrated phagocytosis can also be triggered with detrimental effects for patients.

1.5 Nanoparticles in the literature

Nanoparticles such as polystyrene beads (PB), QD superparamagnetic iron oxide nanoparticles (SPION) and gold nanoparticles (AuNP) can be synthesised with a narrow size distribution and a controlled surface chemistry. For this reasons they are a useful tool in research, in diagnostics and in endocytosis studies and they have also been extensively used to understand the safety of nanomaterials¹⁹⁰⁻¹⁹³.

1.5.1 Colloidal Gold Nanoparticles

Nanoparticles derived from colloidal gold were the first colloidal nanoparticles synthesised. They present physiochemical characteristics that differ from metallic gold and are ruled by the Laws of Quantum Physics¹⁹⁴. The resulting nanoparticles in the range of 1-10nm present characteristics that are strictly dependent upon their size and do not resemble bulk metal or molecular characteristics of gold. They have a plasmon resonance band at around 530nm. The precise wavelength of that band depends on nanoparticle size and shape, and medium properties, and has found application in diagnostics¹⁹⁵. AuNP can be used in conjugation to polymers or proteins for drug delivery purposes¹⁹⁶. The gold core of such conjugates stabilises the geometry of the shell-like region around the nanoparticles and can be tailored to suit the most disparate applications. Sulphur-polymers anchored to AuNP for an easy release of the drug conjugate is an example, or polyethyleneimine (PEI) with a cyclodextrin-derivatised terminal co-polymers to enhance the hydrophobicity of the polymer terminal part for an enhanced DNA delivery¹⁹⁷. Furthermore, also their physical characteristics can be

exploited for therapeutic purposes. When the nanoparticles are hit by a light radiation in the range of 800-1200 nm they produce heating of the region and could be used in hyperthermia applications or, if conjugated with a thermoresponsive polymer could release the drug-load specifically at the intended target. From a recent review by Oh *et al.* it emerges that unconjugated AuNP of 50 nm were the most easily internalised nanoparticles while PEG coating reduced drastically internalization. Endocytosis of AuNP conjugated with cell penetrating peptide TAT and NLS (nuclear localization sequence) were enhanced. Unexpectedly, rod-like AuNP were more actively phagocytosed by macrophages than spherical nanoparticles^{183,198}.

1.5.2 Quantum dots (QDs)

QDs can be produced from many materials. Graphene, silica and hybrid CdSe or ZnS are the most common examples of such structures. They are semiconductor nanocrystals formed by a colloidal core and one or more layers to increase their water solubility¹⁹⁹. They are exceptionally bright with an intense and extremely stable fluorescence that finds many applications, from research in cell penetration studies, to cell imaging and cancer targeting. Uncoated CdSe core and CdS or ZnS coated QDs have been shown to access HEK (primary neonatal human epidermal keratinocytes). QD of 20 nm coated with COOH groups promptly accessed HEK cells with a caveolae-mediated internalization mechanism¹⁹⁹. It has been shown that the more the QDs are charged (both positive and negative charges) the more they are internalised by cells. Also 100 nm negatively charged nanoparticles are taken up more promptly than QDs of 28nm with the same charge according to Kelf *et al.*²⁰⁰. The same group also points out that the literature suggests a higher level of internalization with a clathrin-mediated mechanism of endocytosis for QDs of 50 nm.

1.5.3 Iron oxide nanoparticles

In the last decade iron oxide nanoparticles (especially maghemite, Fe_2O_3 , and magnetite, Fe_3O_4) have been studied for many applications. They are particularly interesting because of their biocompatibility and they have been approved by the FDA^{192,201}. As for AuNP, nanosized iron oxide nanoparticles present unique superparamagnetic and magnetic properties that do not resemble the atomic or the bulk material. They can produce hyperthermia in an alternating magnetic field and can be directed towards a specific tissue with a magnetic field²⁰². Unmodified SPIONs can precipitate in solution as they do not show water solubility and they must be coated to enhance their water compatibility for biological applications. Their most studied applications include cell labelling for cell separation, magnetic resonance imaging (MRI) and hyperthermia therapy. Recently, EGF-conjugated SPIONs have been tested in C6 glioma cells for the detection of early stage of cancer and so substitute gadolinium contrast agents²⁰³. Although SPION nanoparticles are not normally produced for internalization and many studies have shown that the nanoparticles are safe at concentrations up to 100 $\mu\text{g/ml}$, local accumulation of SPIONs can lead to toxicity²⁰². Colloidal iron can easily oxidise leading to the Fenton reaction that is extremely toxic for cells and it destabilises membranes, proteins and DNA. Their application is oriented towards the recognition of a specific tissue for diagnosis and therapy in conjunction with other therapeutics (e.i. thermoresponsive drug-carriers conjugates).

1.5.4 Polystyrene nanoparticles

There are many protocols to synthesise polystyrene beads (PB). One of the most common is with a dispersion polymerization method but other protocols are available in the literature (i.e. macro-raft agents and other techniques)²⁰⁴⁻²⁰⁷. The advantage in using polystyrene beads is that these materials can be easily synthesised in a relatively

economical way and produce materials with narrow distribution of sizes conveniently customized from the range of microns to about 20-25 nm. Furthermore, PB can easily be labelled with fluorescent or luminescent dyes for a detection with an array of techniques; they are visible in TEM without any labelling and can be readily modified to change the polarity of their surface or for derivatization with receptor proteins or vitamins²⁰⁸. For all these reasons they are a useful tool in research, in endocytosis studies and they have also been extensively used to understand the safety of nanomaterials¹⁹⁰. Many studies have been carried out on PB of the range of 50-100 nm. It has been shown that there is usually a good correlation between PB uptake and other nanomaterials despite differences in surface chemistry and composition²⁰⁹. However it appears that the pathway of internalization is strongly influenced by the cell lines used for the study and the same material can be susceptible to different inhibitors of endocytosis depending on the cell lines adopted for the study¹⁸².

In an attempt to enhance internalization of nanoparticles and specificity towards a target organ, many strategies have been adopted. For example, nanoparticles have been associated with cell targeting ligands such as proteins specific for cells membrane receptors, with antibodies and aptamers. Nanoparticles have been tagged with specific proteins to enhance their ability to accumulate in specific tissues. An example is prostate-specific membrane antigen (PSMA) that target prostate cancer cells and virtually all solid tumour neo-vasculature²¹³. Recently, nanoparticles composed of polylactic acid or polylactic-co-polyglycolic acid-PEG and tagged with PSMA were used to chemically entrap tamoxifen. This anticancer drug, has been approved for the treatment of many cancers including prostate, gastric, breast, lung, and head and neck, and has entered Phase I clinical trials with the identity name of BIND 014^{210,214} (Table 1-2). Transferrin protein is also commonly conjugated to

nanoparticles (Table 1-2). Transferrin binds to the transferrin receptor that is ubiquitously expressed in functional cells but it is modestly expressed in quiescent cells such as some endothelial, endocrine pancreas, breast, kidneys and liver cells¹¹⁶. The expression of transferrin receptor is dependent on the level of proliferation the cell is undergoing. For example, transferrin receptor is expressed in foetal cells and the extent of its expression can be modulated by the presence of iron in the diet. Transferrin receptor has also been found over-expressed in many cancers such as colon, pancreas, bladder and lung and for this reason has been used conjugated to nanoparticles in order to enhance specificity of the delivery of anticancer drugs. Another common strategy applies folate targeting to nanocarriers to enhance specificity towards a pathologic region. The concept behind this approach is that often folate receptors are over-expressed in ovarian, cervical, breast, brain, and lung cancer. Again, as for transferrin receptor, it is also expressed in healthy tissues such as lungs, kidneys and placenta. Folate is needed for DNA replication and many other cell functions and it acts binding to the folate receptor that is internalised by caveolae. This localization has made the functionalization of nanoparticles with this receptor highly appealing as there is little evidence in the literature that has observed caveolae-internalized materials being directed towards lysosomes and acidic degradation. The possibility of bypassing the lysosome compartment is a highly attractive feature in drug delivery. However, folate tagged nanomedicines have failed clinical trials so far and the latest example is Vintafolide, a vinblastine-folic acid conjugate that reached Phase III clinical trials for the treatment of platinum resistant ovarian cancers (the same compound is in Phase II trial for non-small cell lung cancer). Although there is increasing evidence of the efficacy of receptor protein conjugation approaches *in vitro* and in animal models, drugs that use these means to enhance specificity have failed in clinical trials to demonstrate the efficacy of such ligands. Furthermore, *in vitro* studies

show that the ligand internalization pathway is influenced by the presence of the conjugated nanoparticles. For example, CPP can be endocytosed by different machineries depending on the specific sequence and in the presence and absence of the intended cargo²¹⁵. Also, transferrin-conjugated nanoparticles studies suggest that transferrin-conjugated QDs are not internalised by the same route as transferrin alone¹⁵⁴. The same has also been confirmed for ricin and Shiga toxin-conjugated QDs and vitamin B12-conjugated polystyrene nanoparticles²⁰⁸. Also, it has been shown that using the same ligand protein (herceptin) specific for a membrane receptor (ErbB2) herceptin-conjugated AuNPs of 40 and 50 nm had the ability to change the internalization outcome, to modulate the expression of the receptor as well as inducing caspases and induce apoptosis with respect to the same nanoparticles of smaller or bigger sizes (size range 2-100 nm)²¹⁶. Finally it is known in the literature that nanocarriers in the blood stream can lose their specificity towards the target when in serum due to the formation of a corona of proteins enveloping the nanocarrier and shielding its functional molecules on their surface²¹⁷. There is a clear need for a better understanding of the nanoparticle characteristics that make cells activate a specific pathway. A recent publication has found a correlation between the specific serum proteins that bind the nanoparticles and the pathway of internalization which may provide a route forward for understanding this complex area²¹⁸.

Commercial name	Company	Formulation	Drug incorporated	Target	Pathology	Status
Nanomedicines without targeting ligands						
DaunoXome	Galen	Liposomes	Daunorubicin		Kaposi's sarcoma	Market
Miocet	Enzon	Liposomes	Doxorubicin		Combination therapy for, recurrent breast and ovarian cancers,	Market
Onco TCS	Inex Pharmaceuticals Corporation	Liposomes	vicristine		relapsed aggressive non-Hodgkin's lymphoma	Market
Depo-Cyt	Sigma-Tau	Liposomes	Cytarabine		Meningitis, leukaemia, glioblastoma	Market
Ambisome	Gilead	Liposomes	Amphotericin B		Fungal infection, cryptococcal meningitis	Market
Doxil-Caelyx	Janssen	PEG-Liposomes	doxorubicin		refractory Kaposi's sarcoma recurrent breast and ovarian cancers	Market
Lipoplatin	Regulon	PEG-Liposomes	Cisplatin		Various malignancies	Phase III
Thermodox	Celsion Corporation	Heat inactivated PEG-Liposomes	Doxorubicin		Hepatocellular carcinoma, recurrent chest wall breast cancer	Phase III
Abraxane	Astellas	Albumin bound-nanoparticle	Paclitaxel		Breast cancer	Market
Oncaspar	Sigma-Tau	PEG conjugated drug	L-asparaginase		Acute lymphoblastic leukemia	Market
Genexol-PM	Samyang	PLA-PEG micelles	paxlitaxel		metastatic breast cancer	Market
Abelcet	Sigma-Tau	Lipid-drug complex	Amphotericin B		Antimicrobial	Market
QD 800	Invitrogen	Streptavidin covalently bound QD			Imaging diagnostics detection of proteins and nucleic acids	Market
Resovist	Schering	SPION coated with carboxydextran			Hepatocellular carcinoma	Market
Feridex	AMAG Pharmaceuticals	Iron nanoparicles			Detection of liver lesions	Market
Nanomedicines with targeting ligands						
CALAA-01		Cyclodextrin-containing polymeric nanoparticles	siRNA	Transferrin	Solid tumors	Phase I
MBP-426		Liposome	Oxaliplatin	Transferrin	Gastric, oesophageal, gastric-oesophageal adenocarcinoma	Phase Ib/II
MCC-465		Liposome	Doxorubicin	F(ab)2 fragment of human antibody Ab GAH	Metastatic stomach cancer	Phase I (discontinued)
BIND-014		PLGA-PEG nanoparticles	Doxetaxel	PSMA peptide	Solid tumors	Phase I
SGT53-01		Liposome	P53 gene	Transferrin receptor specific-scAb	Solid tumors	Phase I

Table 1-2 Summary of nanomedicines that have reached clinical trials or the market^(219,210).

1.6 Aims and thesis outline

Despite numerous attempts to trigger the desired endocytic machinery for the uptake of nanomaterials, literature suggests that nanoparticles conjugated to a ligand specific for

a membrane receptor are internalised according to their physical characteristics rather than the conjugation ligand. Information on how these characteristics guide the internalization of nanoparticles through one pathway or the other is still limited, fragmentary and sometime contradictory. Also, results in the literature are challenged by the numerous variables that constitute the experimental environment of the *in vitro* studies and complicate the recognition of similarities and patterns of behaviour. However, this information is essential in order to develop nanocarriers of drugs with a desired internalization and hence, a more sophisticated control of nanomaterial interaction with cells.

The aim of this study was to investigate the pathway of internalization employed by carboxylated polystyrene nanoparticles of 50 and 100 nm as model particles to access a panel of both epithelial and fibroblastic cells. Firstly, the focus of the study revolved around understanding if there were any differences in the pathway involved in the uptake of carboxylated polystyrene nanoparticles based on differences in size. Secondly, an investigation was carried out on how different cell lines, such as fibroblasts and epithelial cancer cells could employ different mechanisms of internalization for the same material. The aim was to compare and contrast these findings with the uptake of thermoresponsive negatively charged PLGA-*b*-(PEGMA-*co*-PPGMA) and PLA-*b*-(DEGMA-*co*-OEGMA) polymeric micelles. These concepts are schematically summarised in Fig. 1-11. To pursue these objectives, inhibitors of endocytosis were employed to investigate the possible route of uptake of these materials. An assessment of the toxicity of both polystyrene nanoparticles, and inhibitors of endocytosis was carried out as well as optimization of the experimental settings for the endocytosis inhibition studies. These results are summarised in Chapter 3. Flow cytometry was used to investigate the inhibition of uptake of carboxylated polystyrene nanoparticles in the presence of inhibitors of endocytosis

while their internalization was detected by confocal live studies (Chapter 4). Finally, the results on the biocompatibility and internalization ability of thermoresponsive polymers are summarised in the last chapter of results (Chapter 5). Results are further commented on in a discussion chapter and some conclusions drawn (Chapter 6).

1.7 Experimental Approach

Two types of nanomaterials were used to study cellular uptake of nanoparticles. Carboxylated polystyrene nanoparticles, with sizes of 50 and 100nm, and a hydrophobic core and a hydrophilic coat were considered a valid model resembling research grade thermoresponsive polymers with the same size range and polarity distribution and were included in these studies. In addition, thermoresponsive PLGA-*b*-(PEGMA-co-PPGMA) and PLA-*b*-(DEGMA-co-OEGMA) block copolymers were used.

The investigation of different routes of uptake in different cell lines was carried out with human transferrin (Htf) and lactosylceramide (LacCer). These two molecules are routinely used and widely accepted markers of clathrin-dependent and -independent endocytosis. Chlorpromazine (CPZ) and methyl beta cyclodextrin (MBCD) have been extensively used as pharmacological inhibitors of clathrin-dependent and -independent endocytosis in the past 20 years. However, the lack of specificity of both CPZ and MBCD towards only one specific endocytic pathway is well documented in the literature and these experimental limitations were taken into account when drawing conclusions from results.

The choice of the cell lines for the study was based on evidence that many pathologies affect epithelial cells and for this reason are relevant for pharmaceutical investigations. Furthermore, increasingly significant data in the literature report of a role of mesenchymal cells in the instigation and progression of pathologies such as cancer and for this reason fibroblasts were included in the study. Immortalized cells were

preferred over primary cells because of the inherent genetic differences within primary cells from different patients. However, the limitations of this choice such as known differences between immortalized and normal cells, genetic instability are important and experimental limitations that should be devalued before drawing more general conclusions from the experimental results.

Further limitations in the above-mentioned experimental approach was due to the choice of *in vitro* settings over 3D or *in vivo* experiments that are known to resemble more closely the body environment and hence are physiologically more relevant. However, it is important to stress that much of the research field of endocytosis in mammalian cells at the moment is limited to more or less sophisticated 2D *in vitro* studies. The reason for such limitations is that 3D culture approaches are challenged by the level of perfusion of the more internal compartments of the 3D scaffolds. Another important limitation is provided by the level of detection of optical fluorescence techniques currently available and the level of penetration in thick specimens for the detection of fluorophores.

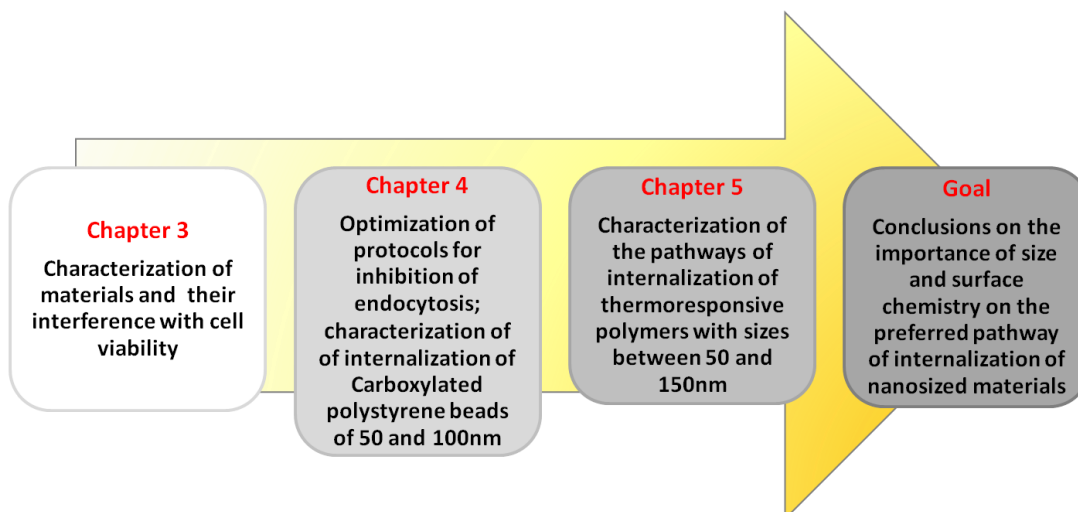


Figure 1-11 Flow chart showing the aims and experimental plans of this thesis.

References

- 1 Gaspar, R. & Duncan, R. Polymeric carriers: preclinical safety and the regulatory implications for design and development of polymer therapeutics. *Adv Drug Deliv Rev* **61**, 1220-1231 (2009).
- 2 Duncan, R. & Gaspar, R. Nanomedicine(s) under the Microscope. *Molecular Pharmaceutics* **8**, 2101-2141 (2011).
- 3 Alonso, M. J. Nanomedicines for overcoming biological barriers. *Biomed Pharmacother* **58**, 168-172, doi:10.1016/j.biopha.2004.01.007 (2004).
- 4 Schneider, M. *et al.* Crossing biological barriers for advanced drug delivery. *European Journal of Pharmaceutics and Biopharmaceutics* **84**, 239-241 (2013).
- 5 Thomsen, T. B., Li, L. & Howard, K. A. Mucus barrier-triggered disassembly of siRNA nanocarriers. *Nanoscale* (2014).
- 6 Lai, S. K., Wang Yy Fau - Hanes, J. & Hanes, J. Mucus-penetrating nanoparticles for drug and gene delivery to mucosal tissues. *Advanced Drug Delivery Reviews* **61**, 158-171 (2009).
- 7 Groo, A. C. & Lagarce, F. Mucus models to evaluate nanomedicines for diffusion. *Drug Discov Today* **19**, 1097-1108 (2014).
- 8 Bramini, M. *et al.* Imaging Approach to Mechanistic Study of Nanoparticle Interactions with the Blood–Brain Barrier. *ACS Nano* **8**, 4304-4312 (2014).
- 9 Leroueil, P. R. *et al.* Wide varieties of cationic nanoparticles induce defects in supported lipid bilayers. *Nano Letters* **8**, 420-424 (2008).
- 10 Yingyuad, P. *et al.* Enzyme-triggered PEGylated siRNA-nanoparticles for controlled release of siRNA. *Journal of RNAi and Gene Silencing* **28**, 490-499 (2014).
- 11 Cui, X. *et al.* Cationic Poly-L-Lysine-Fe₂O₃/SiO₂ nanoparticles loaded with small interference RNA: Application to silencing gene expression in primary rat neurons. *J Nanosci Nanotechnol* **14**, 2810-2815 (2014).
- 12 Wang, B., Siahaan, T. & Soltero, R. A. *Drug delivery Principles and applications*. 1st edition edn, (John Wiley&Sons, 2005).
- 13 Lin, K. Y., Kwong, G. A., Warren, A. D., Wood, D. K. & Bhatia, S. N. Nanoparticles that sense thrombin activity as synthetic urinary biomarkers of thrombosis. *ACS Nano* **7**, 9001-9009, doi:10.1021/nn403550c (2013).
- 14 Lu, W. *et al.* Facile synthesis and characterization of polyethylenimine-coated Fe(3)O(4) superparamagnetic nanoparticles for cancer cell separation. *Molecular Medicine Reports* **9**, 1080-1084 (2014).
- 15 Song, Y. *et al.* Point-of-care technologies for molecular diagnostics using a drop of blood. *Trends in Biotechnology* **32**, 132-139 (2014).
- 16 Xing, H., Hwang, K., Li, J., Torabi, S.-F. & Lu, Y. DNA aptamer technology for personalized medicine. *Current Opinion in Chemical Engineering* **4**, 79-87 (2014).
- 17 Zhou, Z., Li, L., Yang, Y., Xu, X. & Huang, Y. Tumor targeting by pH-sensitive, biodegradable, cross-linked N-(2-hydroxypropyl) methacrylamide copolymer micelles. *Biomaterials* **35**, 6622-6635 (2014).
- 18 MacEwan, S. R. & Chilkoti, A. Applications of elastin-like polypeptides in drug delivery. *Journal of Controlled Release* **190**, 314-330 (2014).
- 19 Potta, T. *et al.* Discovery of antibiotics-derived polymers for gene delivery using combinatorial synthesis and cheminformatics modeling. *Biomaterials* **35**, 1977-1988 (2014).
- 20 Qiu, L. Y. & Bae, Y. H. Polymer architecture and drug delivery. *Pharmaceutical Research* **23**, 1-30 (2006).
- 21 van Nostrum, C. F. Covalently cross-linked amphiphilic block copolymer micelles. *Soft Matter* **7**, 3246-3259 (2011).

- 22 Kanayama, N. *et al.* A PEG-based biocompatible block cationic polymer with high buffering capacity for the construction of polyplex micelles showing efficient gene transfer toward primary cells. *ChemMedChem* **1**, 439-444 (2006).
- 23 Le Meins, J. F., Sandre, O. & Lecommandoux, S. Recent trends in the tuning of polymersomes' membrane properties. *European Physical Journal E* **34** (2011).
- 24 LoPresti, C., Lomas, H., Massignani, M., Smart, T. & Battaglia, G. Polymersomes: nature inspired nanometer sized compartments. *Journal of Materials Chemistry* **19**, 3576-3590 (2009).
- 25 Magnusson, J. P. *et al.* Ion-sensitive "isothermal" responsive polymers prepared in water. *Journal of the American Chemical Society* **130**, 10852-10853 (2008).
- 26 Howard, K. A. *et al.* Nanocarrier stimuli-activated gene delivery. *Small* **3**, 54-57 (2007).
- 27 Thevenot, J., Oliveira, H., Sandre, O. & Lecommandoux, S. Magnetic responsive polymer composite materials. *Chemical Society Reviews* **42**, 7099-7116 (2013).
- 28 Huo, M., Yuan, J., Tao, L. & Wei, Y. Redox-responsive polymers for drug delivery: from molecular design to applications. *Polymer Chemistry* **5**, 1519-1528, doi:10.1039/c3py01192e (2014).
- 29 Ward, M. A. & Georgiou, T. K. Thermoresponsive Polymers for Biomedical Applications. *Polymers* **3**, 1215-1242 (2011).
- 30 Dai, S., Ravi, P. & Tam, K. C. Ph responsive polymers: synthesis, properties and applications. *Soft Matter* **4**, 435-449 (2008).
- 31 Gao, W. W., Chan, J. M. & Farokhzad, O. C. pH-responsive nanoparticles for drug delivery. *Molecular Pharmaceutics* **7**, 1913-1920 (2010).
- 32 Luo, Z. *et al.* Mesoporous Silica Nanoparticles End-Capped with Collagen: Redox-Responsive Nanoreservoirs for Targeted Drug Delivery. *Angewandte Chemie* **50**, 640-643 (2011).
- 33 Tamber H, Johansen P, Merkle H.P & B, G. Formulation aspects of biodegradable polymeric microspheres for antigen delivery. *Advanced Drug Delivery Reviews* **57**, 357-376 (2005).
- 34 Harada, A. & Kataoka, K. Formation of stable and monodisperse polyion complex micelles in aqueous medium from poly(L-lysine) and poly(ethylene glycol)-poly(aspartic acid) block copolymer. *Journal of Macromolecular Science* **34**, 21119-21133 (1997).
- 35 Branco, M. C. & Schneider, J. P. Self-assembling materials for therapeutic delivery. *Acta Biomaterialia* **5**, 817-831 (2009).
- 36 Holmberg, K., Jonsson, B., Kronberg, B. & Lindman, B. (John Wiley & Sons, Chichester, UK, 2002).
- 37 Warren, N. J. & Armes, S. P. Polymerization-Induced Self-Assembly of Block Copolymer Nano-objects via RAFT Aqueous Dispersion Polymerization. *Journal of the American Chemical Society* **136**, 10174-10185, doi:1 (2014).
- 38 Kabanov, A. V., Batrakova, E. V. & Alakhov, V. Y. Pluronic® block copolymers as novel polymer therapeutics for drug and gene delivery. *Journal of Controlled Release* **82**, 189-212 (2002).
- 39 Tyrrell, Z. L., Shen, Y. & Radosz, M. Fabrication of micellar nanoparticles for drug delivery through the self-assembly of block copolymers. *Progress in Polymer Science* **35**, 1128-1143 (2010).
- 40 Letchford, K. & Burt, H. A review of the formation and classification of amphiphilic block copolymer nanoparticulate structures: micelles, nanospheres, nanocapsules and polymersomes. *European Journal of Pharmaceutics and Biopharmaceutics* **65**, 259-269 (2007).
- 41 Antonietti, M. & Forster, S. Vesicles and liposomes: A self-assembly principle beyond lipids. *Advanced Materials* **15**, 1323-1333 (2003).
- 42 Discher, D. E. & Eisenberg, A. Polymer vesicles. *Science* **297**, 967-973 (2002).

- 43 Sahay, G., Alakhova, D. Y. & Kabanov, A. V. Endocytosis of nanomedicines. *Journal of Controlled Release* **145**, 182-195 (2010).
- 44 Zerial, M. & McBride, H. Rab proteins as membrane organizers. *Nat Rev Mol Cell Biol* **2**, 107-117 (2001).
- 45 Seachrist, J. L. & Ferguson, S. S. G. Regulation of G protein-coupled receptor endocytosis and trafficking by Rab GTPases. *Life Sciences* **74**, 225-235 (2003).
- 46 *Rab GTPases and Membrane Trafficking*. (Bentham Science Publishers, 2012).
- 47 Maxfield, F. R. & McGraw, T. E. Endocytic recycling. *Nat Rev Mol Cell Biol* **5**, 121 - 132 (2004).
- 48 Ungar, D. & Hughson, F. M. SNARE protein structure and function. *Annu Rev Cell Dev Biol* **19**, 493-517 (2003).
- 49 Piper, R. C. & Luzio, J. P. Late Endosomes: Sorting and Partitioning in Multivesicular Bodies. *Traffic* **2**, 612-621, doi:10.1034/j.1600-0854.2001.20904.x (2001).
- 50 Jovic, M., Sharma, M., Rahajeng, J. & Caplan, S. The early endosome: a busy sorting station for proteins at the crossroads. *Histol Histopathol* **25**, 99-112 (2010).
- 51 Bonifacino, J. S. Vesicular transport earns a Nobel. *Trends in Cell Biology* **24**, 3-5 (2014).
- 52 Recchi, C. & Chavrier, P. V-ATPase: a potential pH sensor. *Nat Cell Biol* **8**, 107-109 (2006).
- 53 Henne, W. M., Buchkovich, N. J. & Emr, S. D. The ESCRT pathway. *Dev Cell* **21**, 77-91, doi:10.1016/j.devcel.2011.05.015 (2011).
- 54 Killisch, I. *et al.* Characterization of early and late endocytic compartments of the transferrin cycle. Transferrin receptor antibody blocks erythroid differentiation by trapping the receptor in the early endosome. *J Cell Sci* **103 (Pt 1)**, 211-232 (1992).
- 55 Hanson, P. I. & Cashikar, A. Multivesicular body morphogenesis. *Annu Rev Cell Dev Biol* **28**, 337-362, doi:10.1146/annurev-cellbio-092910-154152 (2012).
- 56 Saftig, P. (ed Springer Science) (Landes Bioscience, New York, 2005).
- 57 Samie, M. A. & Xu, H. Lysosomal exocytosis and lipid storage disorders. *J Lipid Res* **55**, 995-1009 (2014).
- 58 Lamb, C. A., Dooley, H. C. & Tooze, S. A. Endocytosis and autophagy: Shared machinery for degradation. *Bioessays* **35**, 34-45 (2013).
- 59 Kunz, J. B., Schwarz, H. & Mayer, A. Determination of four sequential stages during microautophagy in vitro. *J Biol Chem* **279**, 9987-9996, doi:10.1074/jbc.M307905200 (2004).
- 60 Hamasaki, M. *et al.* Autophagosomes form at ER-mitochondria contact sites. *Nature* **495**, 389-393 (2013).
- 61 Xie, Z. & Klionsky, D. J. Autophagosome formation: core machinery and adaptations. *Nat Cell Biol* **9**, 1102-1109, doi:10.1038/ncb1007-1102 (2007).
- 62 Tooze, S. A. & Razi, M. The essential role of early endosomes in autophagy is revealed by loss of COPI function. *Autophagy* **5**, 874-875 (2009).
- 63 Edidin, M. Lipid microdomains in cell surface membranes. *Current Opinion in Structural Biology* **7**, 528-532 (1997).
- 64 Nichols, B. Caveosomes and endocytosis of lipid rafts. *Journal of Cell Science* **116**, 4707-4714 (2003).
- 65 Jacobson, K., Mouritsen, O. G. & Anderson, R. G. W. Lipid rafts: at a crossroad between cell biology and physics. *Nat Cell Biol* **9**, 7-14 (2007).
- 66 Simons, K. & Sampaio, J. L. Membrane Organization and Lipid Rafts. *Cold Spring Harbor Perspectives in Biology* **3** (2011).

- 67 Bellve, K. D. *et al.* Plasma Membrane Domains Specialized for Clathrin-mediated Endocytosis in Primary Cells. *Journal of Biological Chemistry* **281**, 16139-16146, doi:10.1074/jbc.M511370200 (2006).
- 68 Huang, S. *et al.* Phosphatidylinositol-4,5-bisphosphate-rich plasma membrane patches organize active zones of endocytosis and ruffling in cultured adipocytes. *Mol Cell Biol* **24**, 9102-9123 (2004).
- 69 Zhao, H. & Vaananen, H. K. Pharmacological sequestration of intracellular cholesterol in late endosomes disrupts ruffled border formation in osteoclasts. *J Bone Miner Res* **21**, 456-465 (2006).
- 70 Bose, A. *et al.* Unconventional myosin Myo1c promotes membrane fusion in a regulated exocytic pathway. *Mol Cell Biol* **24**, 5447-5458 (2004).
- 71 Bretscher, M. S. & Aguado-Velasco, C. EGF induces recycling membrane to form ruffles. *Current Biology* **8**, 721-S724 (1998).
- 72 Komaba, S. & Coluccio, L. M. Localization of myosin 1b to actin protrusions requires phosphoinositide binding. *J Biol Chem* **285**, 27686-27693 (2010).
- 73 Bose, A. *et al.* Glucose transporter recycling in response to insulin is facilitated by myosin Myo1c. *Nature* **420**, 821-824 (2002).
- 74 Tokuo, H. & Coluccio, L. M. Myosin-1c regulates the dynamic stability of E-cadherin-based cell-cell contacts in polarized Madin-Darby canine kidney cells. *Mol Biol Cell* **24**, 2820-2833 (2013).
- 75 Cocucci, E. & Meldolesi, J. (ed Landes Bioscience) (Madame Curie Bioscience Database Austin (TX), 2000).
- 76 Aderem, A. & Underhill, D. M. Mechanisms of phagocytosis in macrophages. *Annual Review of Immunology* **17**, 593-623 (1999).
- 77 Owens, D. E. & Peppas, N. A. Opsonisation, biodistribution and pharmacokinetics of polymeric nanoparticles. *International Journal of Pharmaceutics* **307**, 93-102 (2006).
- 78 Hillaireau, H. & Couvreur, P. Nanocarriers' entry into the cell: relevance to drug delivery. *Cellular and Molecular Life Sciences* **66**, 2873-2896 (2009).
- 79 Garnett, M. C. & Kallinteri, P. Nanomedicines and nanotoxicology: some physiological principles. *Occupational Medicine-Oxford* **56**, 307-311 (2006).
- 80 Underhill, D. M. & Goodridge, H. S. Information processing during phagocytosis. *Nat Rev Immunol* **12**, 492-502 (2012).
- 81 Kibbey, R. G., Rizo, J., Gierasch, L. M. & Anderson, R. G. The LDL receptor clustering motif interacts with the clathrin terminal domain in a reverse turn conformation. *J Cell Biol* **142**, 59-67 (1998).
- 82 Traub, L. M. Sorting it out: AP-2 and alternate clathrin adaptors in endocytic cargo selection. *J Cell Biol* **163**, 203-208, doi:10.1083/jcb.200309175 (2003).
- 83 Traub, L. M. & Bonifacino, J. S. Cargo Recognition in Clathrin-Mediated Endocytosis. *Cold Spring Harbor Perspectives in Biology* **5** (2013).
- 84 Le Roy, C. & Wrana, J. L. Clathrin- and non-clathrin-mediated endocytic regulation of cell signalling. *Nat Rev Mol Cell Biol* **6**, 112-126 (2005).
- 85 Zhang, Y. & Whittaker, G. R. Influenza entry pathways in polarized MDCK cells. *Biochem Biophys Res Commun* (2014).
- 86 Cossec, J. C. *et al.* Clathrin-dependent APP endocytosis and Abeta secretion are highly sensitive to the level of plasma membrane cholesterol. *Biochimica and Biophysica Acta* **1801**, 846-852 (2010).

- 87 Bhattacharyya, S., Ruthel, G., Bavari, S., Aman, M. J. & Hope, T. J. Ebola virus uses clathrin-mediated endocytosis as an entry pathway. *Virology* **401**, 18-28 (2010).
- 88 Humphries, A. C. & Way, M. The non-canonical roles of clathrin and actin in pathogen internalization, egress and spread. *Nat Rev Micro* **11**, 551-560 (2013).
- 89 Royle, S. J. *et al.* Non-canonical YXXGPhi endocytic motifs: recognition by AP2 and preferential utilization in P2X4 receptors. *J Cell Sci* **118**, 3073-3080 (2005).
- 90 Flores-Otero, J. *et al.* Ligand-specific endocytic dwell times control functional selectivity of the cannabinoid receptor 1. *Nat Commun* **5** (2014).
- 91 Xu, C. & Min, J. Structure and function of WD40 domain proteins.
- 92 Schmid, S. L. Clathrin-coated vesicle formation and protein sorting: An integrated process. *Annual Review of Biochemistry* **66**, 511-548 (1997).
- 93 Kirchhausen, T., Owen, D. & Harrison, S. C. Molecular structure, function, and dynamics of clathrin-mediated membrane traffic. *Cold Spring Harb Perspect Biol* **6**, a016725 (2014).
- 94 Jackson, L. P. *et al.* A Large-Scale Conformational Change Couples Membrane Recruitment to Cargo Binding in the AP2 Clathrin Adaptor Complex. *Cell* **141**, 1220-1229 (2010).
- 95 Ohno, H. Clathrin-associated adaptor protein complexes. *J Cell Sci* **119**, 3719-3721 (2006).
- 96 Owen, D. J., Collins, B. M. & Evans, P. R. Adaptors for clathrin coats: structure and function. *Annu Rev Cell Dev Biol* **20**, 153-191 (2004).
- 97 Park, S. Y. & Guo, X. Adaptor Protein Complexes and Intracellular Transport. *Biosci Rep* (2014).
- 98 Owen, D. J. & Evans, P. R. A structural explanation for the recognition of tyrosine-based endocytotic signals. *Science* **282**, 1327-1332 (1998).
- 99 Cocucci, E., Aguet, F., Boulant, S. & Kirchhausen, T. The First Five Seconds in the Life of a Clathrin-Coated Pit. *Cell* **150**, 495-507 (2012).
- 100 Kelly, B. T. *et al.* AP2 controls clathrin polymerization with a membrane-activated switch. *Science* **345**, 459-463 (2014).
- 101 Lakadamyali, M., Rust, M. J. & Zhuang, X. Ligands for Clathrin-Mediated Endocytosis Are Differentially Sorted into Distinct Populations of Early Endosomes. *Cell* **124**, 997-1009 (2006).
- 102 Vanlandingham, P. A. & Ceresa, B. P. Rab7 regulates late endocytic trafficking downstream of multivesicular body biogenesis and cargo sequestration. *J Biol Chem* **284**, 12110-12124 (2009).
- 103 Engedal, N. & Mills, I. G. in *Methods in Enzymology* Vol. 535 179-200 (2014).
- 104 Larson, B. T., Sochacki, K. A., Kindem, J. M. & Taraska, J. W. Systematic spatial mapping of proteins at exocytic and endocytic structures. *Mol Biol Cell* **25**, 2084-2093 (2014).
- 105 McMahon, H. T. & Boucrot, E. Molecular mechanism and physiological functions of clathrin-mediated endocytosis. *Nat Rev Mol Cell Biol* **12**, 517-533 (2011).
- 106 Henne, W. M. *et al.* FCHO Proteins Are Nucleators of Clathrin-Mediated Endocytosis. *Science* **328**, 1281-1284 (2010).
- 107 Kirchhausen, T., Owen, D. & Harrison, S. C. Molecular Structure, Function, and Dynamics of Clathrin-Mediated Membrane Traffic. *Cold Spring Harbor Perspectives in Biology* **6** (2014).
- 108 Bocking, T. *et al.* Key interactions for clathrin coat stability. *Structure* **22**, 819-829 (2014).
- 109 Taylor, M. J., Perrais, D. & Merrifield, C. J. A high precision survey of the molecular dynamics of mammalian clathrin-mediated endocytosis. *PLoS Biol* **9**, e1000604 (2011).
- 110 Collins, A., Warrington, A., Taylor, K. A. & Svitkina, T. Structural organization of the actin cytoskeleton at sites of clathrin-mediated endocytosis. *Curr Biol* **21**, 1167-1175 (2011).

- 111 Boucrot, E., Saffarian, S., Massol, R., Kirchhausen, T. & Ehrlich, M. Role of lipids and actin in the formation of clathrin-coated pits. *Experimental Cell Research* **312**, 4036-4048 (2006).
- 112 Hinshaw, J. in *Annual Reviews Collection* (Bethesda (MD), 2002).
- 113 Böcking, T., Aguet, F., Harrison, S. C. & Kirchhausen, T. Single-molecule analysis of a molecular disassemblase reveals the mechanism of Hsc70-driven clathrin uncoating. *Nat Struct Mol Biol* **18**, 295-301 (2011).
- 114 Maurer, M. E. & Cooper, J. A. The adaptor protein Dab2 sorts LDL receptors into coated pits independently of AP-2 and ARH. *Journal of Cell Science* **119**, 4235-4246 (2006).
- 115 Klauser, R. D., Ashwell, G., Van Renswoude, J., Harford, J. B. & Bridges, K. R. Binding of apotransferrin to K562 cells: Explanation of the transferrin cycle. *Proc Natl Acad Sci USA* **80**, 2263-2266 (1983).
- 116 Tortorella, S. & Karagiannis, T. C. Transferrin receptor-mediated endocytosis: a useful target for cancer therapy. *The Journal of Membrane Biology* **247**, 291-307 (2014).
- 117 van Dam, E. M., ten Broeke, T., Jansen, K., Spijkers, P. & Stoorvogel, W. Endocytosed Transferrin Receptors Recycle via Distinct Dynamin and Phosphatidylinositol 3-Kinase-dependent Pathways. *Journal of Biological Chemistry* **277**, 48876-48883 (2002).
- 118 Navaroli, D. M. *et al.* Rabenosyn-5 defines the fate of the transferrin receptor following clathrin-mediated endocytosis. *Proc Natl Acad Sci U S A* **109**, E471-480 (2012).
- 119 Magadan, J. G., Barbieri, M. A., Mesa, R., Stahl, P. D. & Mayorga, L. S. Rab22a regulates the sorting of transferrin to recycling endosomes. *Mol Cell Biol* **26**, 2595-2614 (2006).
- 120 Liu, C., Wang, J. & Zhang, X. The Involvement of MiR-1-Clathrin Pathway in the Regulation of Phagocytosis. *Plos One* **9**, e98747 (2014).
- 121 Sullivan, C. S. *et al.* The adaptor protein GULP promotes Jedi-1-mediated phagocytosis through a clathrin-dependent mechanism. *Molecular Biology of the Cell* (2014).
- 122 Pelkmans, L. & Helenius, A. Endocytosis via caveolae. *Traffic* **3**, 311-320 (2002).
- 123 Doherty, G. J. & McMahon, H. T. Mechanisms of endocytosis. *Annual Review of Biochemistry* **78**, 857-902 (2009).
- 124 Nichols, B. J. & Lippincott-Schwartz, J. Endocytosis without clathrin coats. *Trends in Cell Biology* **11**, 406-412 (2001).
- 125 Fra, A. M., Williamson, E., Simons, K. & Parton, R. G. De novo formation of caveolae in lymphocytes by expression of VIP21-caveolin. *Proc Natl Acad Sci U S A* **92**, 8655-8659 (1995).
- 126 Shvets, E., Ludwig, A. & Nichols, B. J. News from the caves: update on the structure and function of caveolae. *Current Opinion in Cell Biology* **29**, 99-106 (2014).
- 127 Hansen, C. G., Howard, G. & Nichols, B. J. Pacsin 2 is recruited to caveolae and functions in caveolar biogenesis. *Journal of Cell Science* **124**, 2777-2785 (2011).
- 128 Senju, Y., Itoh, Y., Takano, K., Hamada, S. & Suetsugu, S. Essential role of PACSIN2/syndapin-II in caveolae membrane sculpting. *Journal of Cell Science* **124**, 2032-2040 (2011).
- 129 Koch, D., Westermann, M., Kessels, M. M. & Qualmann, B. Ultrastructural freeze-fracture immunolabeling identifies plasma membrane-localized syndapin II as a crucial factor in shaping caveolae. *Histochemistry and Cell Biology* **138**, 215-230 (2012).
- 130 Moren, B. *et al.* EHD2 regulates caveolar dynamics via ATP-driven targeting and oligomerization. *Mol Biol Cell* **23**, 1316-1329, doi:10.1091/mbc.E11-09-0787 (2012).
- 131 Stoeber, M. *et al.* Oligomers of the ATPase EHD2 confine caveolae to the plasma membrane through association with actin. *EMBO Journal* **31**, 2350-2364 (2012).

- 132 Howes, M. T., Mayor, S. & Parton, R. G. Molecules, mechanisms, and cellular roles of clathrin-independent endocytosis. *Current Opinion in Cell Biology* **22**, 519-527, doi:10.1016/j.ceb.2010.04.001 (2010).
- 133 Hayer, A. *et al.* Caveolin-1 is ubiquitinated and targeted to intraluminal vesicles in endolysosomes for degradation. *J Cell Biol* **191**, 615-629 (2010).
- 134 Nevins, A. K. & Thurmond, D. C. Caveolin-1 functions as a novel Cdc42 guanine nucleotide dissociation inhibitor (GDI) in pancreatic beta cells. *Journal of Biological Chemistry* **281**, 18961-18972 (2006).
- 135 Xie, Z. J. & Askari, A. Na⁺/K⁺-ATPase as a signal transducer. *European Journal of Biochemistry* **269**, 2434-2439 (2002).
- 136 Belting, M., Sandgren, S. & Wittrup, A. Nuclear delivery of macromolecules: barriers and carriers. *Adv Drug Deliv Rev* **57**, 505-527 (2005).
- 137 Chaudhary, N. *et al.* Endocytic crosstalk: cavins, caveolins, and caveolae regulate clathrin-independent endocytosis. *PLoS Biol* **12**, e1001832 (2014).
- 138 Basquin, C. *et al.* The signalling factor PI3K is a specific regulator of the clathrin-independent dynamin-dependent endocytosis of IL-2 receptors. *J Cell Sci* **126**, 1099-1108 (2013).
- 139 Huang, T., Lehmann, M. J., Said, A., Ma, G. & Osterrieder, N. MHC class I downregulation induced by equine herpesvirus type 1 (EHV-1) pUL56 is through dynamin-dependent endocytosis. *J Virol* (2014).
- 140 Grassart, A., Dujeancourt, A., Lazarow, P. B., Dautry-Varsat, A. & Sauvonnnet, N. Clathrin-independent endocytosis used by the IL-2 receptor is regulated by Rac1, Pak1 and Pak2. *EMBO Rep* **9**, 356-362 (2008).
- 141 Howes, M. T. *et al.* Clathrin-independent carriers form a high capacity endocytic sorting system at the leading edge of migrating cells. *J Cell Biol* **190**, 675-691, doi:10.1083/jcb.201002119 (2010).
- 142 Donatello, S. *et al.* Lipid raft association restricts CD44-ezrin interaction and promotion of breast cancer cell migration. *Am J Pathol* **181**, 2172-2187 (2012).
- 143 Lundmark, R. *et al.* The GTPase-activating protein GRAF1 regulates the CLIC/GEEC endocytic pathway. *Curr Biol* **18**, 1802-1808 (2008).
- 144 Shibata, H. *et al.* PKNbeta interacts with the SH3 domains of Graf and a novel Graf related protein, Graf2, which are GTPase activating proteins for Rho family. *J Biochem* **130**, 23-31 (2001).
- 145 Taylor, J. M., Macklem, M. M. & Parsons, J. T. Cytoskeletal changes induced by GRAF, the GTPase regulator associated with focal adhesion kinase, are mediated by Rho. *J Cell Sci* **112** (Pt 2), 231-242 (1999).
- 146 Alexandropoulos, K., Cheng, G. & Baltimore, D. Proline-rich sequences that bind to Src homology 3 domains with individual specificities. *Proc Natl Acad Sci U S A* **92**, 3110-3114 (1995).
- 147 Amyere, M. *et al.* Origin, originality, functions, subversions and molecular signalling of macropinocytosis. *International Journal of Medical Microbiology* **291**, 487-494 (2001).
- 148 BoseDasgupta, S. & Pieters, J. How to clear a pathogen during inflammation: Switching from phagocytosis to macropinocytosis through coronin 1 phosphorylation. *Inflammation & Cell Signaling* **1**, 177-181 (2014).
- 149 Kolpak, A. L. *et al.* Negative guidance factor-induced macropinocytosis in the growth cone plays a critical role in repulsive axon turning. *J Neurosci* **29**, 10488-10498 (2009).
- 150 Kerr, M. C. & Teasdale, R. D. Defining macropinocytosis. *Traffic* **10**, 364-371 (2009).

- 151 Cao, H., Chen, J., Awoniyi, M., Henley, J. R. & McNiven, M. A. Dynamin 2 mediates fluid-phase micropinocytosis in epithelial cells. *J Cell Sci* **120**, 4167-4177 (2007).
- 152 Mercer, J. & Helenius, A. Virus entry by macropinocytosis. *Nat Cell Biol* **11**, 510-520 (2009).
- 153 Mulherkar, N., Raaben, M., de la Torre, J. C., Whelan, S. P. & Chandran, K. The Ebola virus glycoprotein mediates entry via a non-classical dynamin-dependent macropinocytic pathway. *Virology* **419**, 72-83 (2011).
- 154 Tekle, C., Deurs, B. v., Sandvig, K. & Iversen, T.-G. Cellular Trafficking of Quantum Dot-Ligand Bioconjugates and Their Induction of Changes in Normal Routing of Unconjugated Ligands. *Nano Letters* **8**, 1858-1865, doi:10.1021/nl0803848 (2008).
- 155 Iversen, T. G., Frerker, N. & Sandvig, K. Uptake of ricinB-quantum dot nanoparticles by a macropinocytosis-like mechanism. *J Nanobiotechnology* **10**, 33 (2012).
- 156 Howes, P. & Green, M. Colloidal and optical stability of PEG-capped and phospholipid-encapsulated semiconducting polymer nanospheres in different aqueous media. *Photochemical & Photobiological Sciences* **9**, 1159-1166 (2010).
- 157 Otto, G. P. & Nichols, B. J. The roles of flotillin microdomains--endocytosis and beyond. *J Cell Sci* **124**, 3933-3940 (2011).
- 158 Rausch, K., Reuter, A., Fisher, K. & Schmidt, M. Evaluation of nanoparticles aggregation in human blood serum *Biomacromolecules* **11**, 2836-2839 (2010).
- 159 Chen, L. *et al.* Nanoparticle-mediated delivery of pitavastatin into lungs ameliorates the development and induces regression of monocrotaline-induced pulmonary artery hypertension. *Hypertension (Baltimore)* **57**, 343 (2011).
- 160 Xu, J. H. *et al.* Intranasal vaccination with chitosan-DNA nanoparticles expressing pneumococcal surface antigen A protects mice against nasopharyngeal colonization by streptococcus pneumoniae. *Clinical and Vaccine Immunology* **18**, 75-81 (2011).
- 161 Lundqvist, M. Nanoparticles: Tracking protein corona over time. *Nat Nano* **8**, 701-702 (2013).
- 162 Lundqvist, M. *et al.* Nanoparticle size and surface properties determine the protein corona with possible implications for biological impacts. *Proceedings of the National Academy of Sciences* **105**, 14265-14270 (2008).
- 163 Milani, S., Baldelli Bombelli, F., Pitek, A. S., Dawson, K. A. & Rädler, J. Reversible versus Irreversible Binding of Transferrin to Polystyrene Nanoparticles: Soft and Hard Corona. *ACS Nano* **6**, 2532-2541 (2012).
- 164 Tenzer, S. *et al.* Rapid formation of plasma protein corona critically affects nanoparticle pathophysiology. *Nat Nano* **8**, 772-781 (2013).
- 165 McGuinness, C. *et al.* Surface derivatization state of polystyrene latex nanoparticles determines both their potency and their mechanism of causing human platelet aggregation in vitro. *Toxicological Sciences* **119**, 359-368 (2011).
- 166 Cabral, H. & Kataoka, K. Multifunctional nanoassemblies of block copolymers for future cancer therapy. *Science and Technology of Advanced Materials* **11** (2010).
- 167 Monopoli, M. P., Bombelli, F. B. & Dawson, K. A. Nanobiotechnology: Nanoparticle coronas take shape. *Nature Nanotechnology* **6**, 11-12 (2011).
- 168 Deng, Z. J., Liang, M. T., Monteiro, M., Toth, I. & Minchin, R. F. Nanoparticle-induced unfolding of fibrinogen promotes Mac-1 receptor activation and inflammation. *Nature Nanotechnology* **6**, 39-44 (2011).
- 169 Li, J. Self assembled supramolecular hydrogels based on polymer-cyclodextrin inclusion complexes for drug delivery. *Nature Asia-Pacific –Asia Materials* **2**, 112-118 (2010).
- 170 Dubruel, P. & Schacht, E. Vinyl polymers as non-viral gene delivery carriers: current status and prospects. *Macromolecular Bioscience* **6**, 789-810 (2006).

- 171 Wong, S. Y., Pelet, J. M. & Putnam, D. Polymer systems for gene delivery-past, present, and future. *Progress in Polymer Science* **32**, 799-837 (2007).
- 172 Harper, G. R. *et al.* Steric stabilization of microspheres with grafted polyethylene oxide reduces phagocytosis by rat Kupffer cell-in vitro. *Biomaterials* **12**, 695-700 (1991).
- 173 Bazile, D. *et al.* PEG-PLA nanoparticles avoid uptake by the mononuclear phagocytes system. *Journal of Pharmaceutical Science* **84**, 493-498 (1995).
- 174 Gref, R. *et al.* 'Stealth' corona-core nanoparticles surface modified by polyethylene glycol (PEG): influences of the corona (PEG chain length and surface density) and of the core composition on phagocytic uptake and plasma protein adsorption. *Colloids Surf B Biointerfaces* **18**, 301 - 313 (2000).
- 175 Peracchia, M. T. *et al.* Stealth PEGylated polycyanoacrylate nanoparticles for intravenous administration and splenic targeting. *J Control Release* **60**, 121-128 (1999).
- 176 Pozzi, D. *et al.* Effect of polyethyleneglycol (PEG) chain length on the bio-nano-interactions between PEGylated lipid nanoparticles and biological fluids: from nanostructure to uptake in cancer cells. *Nanoscale* **6**, 2782-2792 (2014).
- 177 Wu, J. *et al.* Binding characteristics between polyethylene glycol (PEG) and proteins in aqueous solution. *Journal of Materials Chemistry B* **2**, 2983-2992 (2014).
- 178 Lai, T. C., Bae, Y., Yoshida, T., Kataoka, K. & Kwon, G. S. pH-sensitive multi-PEGylated block copolymer as a bioresponsive pDNA delivery vector. *Pharmaceutical Research* **27**, 2260-2273 (2010).
- 179 Moghimi, S. M., Hedeman, H., Muir, I. S., Illum, L. & Davis, S. S. An Investigation of the filtration capacity and the fate of large filtered sterically-stabilized microspheres in rat spleen. *Biochimica Et Biophysica Acta* **1157**, 233-240 (1993).
- 180 Kobayashi, H., Watanabe, R. & Choyke, P. L. Improving conventional enhanced permeability and retention (EPR) effects; what is the appropriate target? *Theranostics* **4**, 81-89, doi:10.7150/thno.7193 (2013).
- 181 Pegoraro, C. *et al.* Translocation of flexible polymersomes across pores at the nanoscale. *Biomaterials Science* **2**, 680-692 (2014).
- 182 dos Santos, T., Varela, J., Lynch, I., Salvati, A. & Dawson, K. A. Effects of transport inhibitors on the cellular uptake of carboxylated polystyrene nanoparticles in different cell lines. *Plos One* **6**, e24438 (2011).
- 183 Oh, N. & Park, J. H. Endocytosis and exocytosis of nanoparticles in mammalian cells. *Int J Nanomedicine* **9 Suppl 1**, 51-63 (2014).
- 184 Minchin, R. Sizing up targets with nanoparticles. *Nature Nanotechnology* **3**, 12-13 (2008).
- 185 Hong, S. P. *et al.* Interaction of polycationic polymers with supported lipid bilayers and cells: Nanoscale hole formation and enhanced membrane permeability. *Bioconjugate Chemistry* **17**, 728-734 (2006).
- 186 Mercke, A. *et al.* Lipid bilayer disruption by polycation polymers: the roles of size and chemical functional groups. *Langmuir* **21**, 10348-10354 (2005).
- 187 Zorko, M. & Langel, U. Cell-penetrating peptides: mechanism and kinetics of cargo delivery. *Advanced Drug Delivery Reviews* **57**, 529-545, doi:10.1016/j.addr.2004.10.010 (2005).
- 188 Geng, Y. & Discher, E. D. Hydrolytic degradation of poly(ethylene oxide)-blockpolycaprolactone worm micelles. *Journal of American Chemical Society* **127**, 12780-12781 (2005).
- 189 Foldbjerg, R. *et al.* The toxic effects of single-walled carbon nanotubes are linked to the phagocytic ability of cells. *Toxicology Research* **3**, 228-241 (2014).

- 190 Johnston, H. J. *et al.* Evaluating the uptake and intracellular fate of polystyrene nanoparticles by primary and hepatocyte cell lines in vitro. *Toxicol Appl Pharmacol* **242**, 66-78 (2010).
- 191 Pellach, M., Grinberg, I. & Margel, S. Near IR fluorescent polystyrene/albumin core/shell nanoparticles for specific targeting of colonic neoplasms. *Macromol Biosci* **12**, 1472-1479 (2012).
- 192 Gupta, A. K. & Gupta, M. Synthesis and surface engineering of iron oxide nanoparticles for biomedical applications. *Biomaterials* **26**, 3995-4021 (2005).
- 193 Iversen, T.-G., Frerker, N. & Sandvig, K. Quantum dot bioconjugates: uptake into cells and induction of changes in normal cellular transport. *Proc. SPIE* **7189** (2009).
- 194 Daniel, M. C. & Astruc, D. Gold nanoparticles: assembly, supramolecular chemistry, quantum-size-related properties, and applications toward biology, catalysis, and nanotechnology. *Chem Rev* **104**, 293-346 (2004).
- 195 Alkilany, A. M. & Murphy, C. J. Toxicity and cellular uptake of gold nanoparticles: what we have learned so far? *J Nanopart Res* **12**, 2313-2333 (2010).
- 196 Aubin-Tam, M. E. Conjugation of nanoparticles to proteins. *Methods Mol Biol* **1025**, 19-27 (2013).
- 197 Ghosh, P., Han, G., De, M., Kim, C. K. & Rotello, V. M. Gold nanoparticles in delivery applications. *Advanced Drug Delivery Reviews* **60**, 1307-1315 (2008).
- 198 Chithrani, D. B. *et al.* Gold nanoparticles as radiation sensitizers in cancer therapy. *Radiat Res* **173**, 719-728 (2010).
- 199 Zhang, L. W. & Monteiro-Riviere, N. A. Mechanisms of Quantum Dot Nanoparticle Cellular Uptake. *Toxicological Sciences* **110**, 138-155 (2009).
- 200 Kelf, T. A. *et al.* Non-specific cellular uptake of surface-functionalized quantum dots. *Nanotechnology* **21**, 285105 (2010).
- 201 Khandhar, A. P., Ferguson, R. M. & Krishnan, K. M. Monodispersed magnetite nanoparticles optimized for magnetic fluid hyperthermia: Implications in biological systems. *J Appl Phys* **109**, 7B310-317B3103 (2011).
- 202 Singh, N., Jenkins, G. J., Asadi, R. & Doak, S. H. Potential toxicity of superparamagnetic iron oxide nanoparticles (SPION). *Nano Rev* **1** (2010).
- 203 Shevtsov, M. A. *et al.* Superparamagnetic iron oxide nanoparticles conjugated with epidermal growth factor (SPION-EGF) for targeting brain tumors. *Int J Nanomedicine* **9**, 273-287 (2014).
- 204 Yeole, N., Hundiwale, D. & Jana, T. Synthesis of core-shell polystyrene nanoparticles by surfactant free emulsion polymerization using macro-RAFT agent. *J Colloid Interface Sci* **354**, 506-510 (2011).
- 205 Milošević, I. *et al.* Synthesis and size control of polystyrene nanoparticles via “liquid crystalline” nanoemulsion. *Microporous and Mesoporous Materials* **120**, 7-11 (2009).
- 206 Jinhua, L. & Guangyuan, Z. *Polystyrene Microbeads by Dispersion Polymerization: Effect of Solvent on Particle Morphology*. Vol. 2014 (2014).
- 207 Im, S. H. *et al.* Synthesis of polystyrene beads loaded with dual luminophors for self-referenced oxygen sensing. *Talanta* **67**, 492-497 (2005).
- 208 Fowler, R. *et al.* Nanoparticle Transport in Epithelial Cells: Pathway Switching Through Bioconjugation. *Small*, n/a-n/a (2013).
- 209 Zauner, W., Farrow, N. A. & Haines, A. M. R. In vitro uptake of polystyrene microspheres: effect of particle size, cell line and cell density. *Journal of Controlled Release* **71**, 39-51 (2001).
- 210 Yeo, Y. *Nanoparticulate Drug Delivery : Systems Strategies, Technologies, and Applications*. (John Wiley & Sons, 2013).

- 211 Leśniewska, K., Warbrick, E. & Ohkura, H. Peptide aptamers define distinct EB1- and EB3-binding motifs and interfere with microtubule dynamics. *Molecular Biology of the Cell* **25**, 1025-1036 (2014).
- 212 Pei, X., Zhang, J. & Liu, J. Clinical applications of nucleic acid aptamers in cancer. *Mol Clin Oncol* **2**, 341-348 (2014).
- 213 Hrkach, J. *et al.* Preclinical Development and Clinical Translation of a PSMA-Targeted Docetaxel Nanoparticle with a Differentiated Pharmacological Profile. *Science Translational Medicine* **4**, 128ra139 (2012).
- 214 Kamaly, N., Xiao, Z., Valencia, P. M., Radovic-Moreno, A. F. & Farokhzad, O. C. Targeted polymeric therapeutic nanoparticles: design, development and clinical translation. *Chem Soc Rev* **41**, 2971-3010 (2012).
- 215 Johnson, R., Harrison, S. & Maclean, D. in *Cell-Penetrating Peptides* Vol. 683 *Methods in Molecular Biology* (ed Úlo Langel) Ch. 38, 535-551 (Humana Press, 2011).
- 216 Jiang, W., KimBetty, Y. S., Rutka, J. T. & ChanWarren, C. W. Nanoparticle-mediated cellular response is size-dependent. *Nat Nano* **3**, 145-150 (2008).
- 217 Salvati, A. *et al.* Transferrin-functionalized nanoparticles lose their targeting capabilities when a biomolecule corona adsorbs on the surface. *Nat Nanotechnol* **8**, 137-143 (2013).
- 218 Walkey, C. D. *et al.* Protein Corona Fingerprinting Predicts the Cellular Interaction of Gold and Silver Nanoparticles. *ACS Nano* **8**, 2439-2455 (2014).
- 219 Yu, M. K., Park, J. & Jon, S. Targeting strategies for multifunctional nanoparticles in cancer imaging and therapy. *Theranostics* **2**, 3-44 (2012).

2-Chapter 2

General Materials and Methods

2.1 General Materials

2.1.1 Cell lines

HCT116 human colon cancer cells¹, MGLVA-1 ascites gastric cancer cells² - ascites of a variant of MKN45 human gastric adenocarcinoma cells³, gastrin producing (MKN45G) generated in our laboratories -, 3T3-Swiss albino mouse embryo fibroblasts⁴ and MRC-5 human foetal lung fibroblasts⁵ were purchased from the American Type Culture Collection (ATCC) and LGC Standards, Teddington, UK and from the Health Science Research Resource Bank, (Osaka, Japan). Cells were harvested in Roswell Park Memorial Institute (RPMI) medium or Dulbecco Modified Eagle Medium (DMEM) supplemented with 10% v/v heat inactivated Foetal Bovine Serum (FBS), 2 mM L-glutamine (Sigma-Aldrich, Dorset, UK) and in minimum essential medium Eagle (MEM) 10% v/v FBS, 2 mM L-glutamine, 1% v/v non essential amino acids (NEAA) according to ATCC and Cell Bank specifications. HCT116 cells were grown from passage 4 to 50, MGLVA-1 for passage 5 to 50, 3T3 from passage 21 to 60, MRC-5 from passage 34 to passage 50. All the cell lines used were adherent. A summary of the characteristics of the cells can be viewed in Table 2-1.

2.1.2 Cell culture materials

Trypan blue (0.4% w/v), porcine trypsin (0.5 g/l)/Ethylenediaminetetracetic acid (EDTA, 0.2 g/l) and dimethylsulfoxide (DMSO) were purchased from Sigma-Aldrich, Dorset, UK. Phosphate buffered saline (PBS) was purchased from Oxoid (Thermo Scientific, Basingstoke, UK), 96 wells clear bottom and clear or black wall plates, clear 24 and 6 well plates, 75 and 25cm² tissue culture vented flasks, 2 ml cryovials, 0.6-1.7 ml Eppendorf tubes were obtained from Corning Life Sciences (Amsterdam, The Netherlands; Tultidan, Mexico). 10 and 1000 µl pipettes tips from Starlab, Milton

General Materials and Methods

Keynes, UK; 200 µl tips from Sarstedt, Leicester, UK; Minisart filters for tissue culture 0.1 and 0.2 µm pore size were purchased from Sartorius, Stonehouse, UK. Needles 0.8x40 mm were purchased from BD Microlance, syringes from BD Plastipactm, Oxford, UK.

Cell lines	3T3	HCT116	MGLVA-1	MRC-5
Description	3T3-Swiss albino mouse	HCT116 human colon cancer	MGLVA-1 human gastric cancer ascites	MRC-5 human foetal lung fibroblasts
Media	DMEM 10% FBS 1% L-Glutamine	RPMI 10% FBS 1% L-Glutamine	RPMI 10% FBS 1% L-Glutamine	MEM 10% FBS 1% L Glutamine 1% NEAA
Tissue or origin	Embryo / normal	Colonrectal carcinoma	MKN45G gastric adenocarcinoma cells ascites – gastrin producing	14 weeks foetus lungs/ normal
Species	<i>Mus Musculus</i>	<i>Homo Sapiens</i>	<i>Homo Sapiens</i>	<i>Homo Sapiens</i>
Genetic modifications	Hypertriploid, modal chromosome number = 68 (30%) Polyploids (2.4%)	mutation in codon 13 of the ras proto-oncogene – diploid, modal number = 45 (62%), polyploids (6.8%)	Diploid modal number = 40-44(50%)	Normal diploid (monal number = 46 (70%), XY karyotype – polyploids (3.6%) normal X and Y chromosomes
Type	Fibroblasts	Epithelial	Epithelial	Fibroblasts
Immortalization procedure	Spontaneous	Spontaneous	Already established	SV40

Table 2-1 A summary of the cells lines used in this study with their most important characteristics such as tissue of origin, species, genetic modifications and immortalization procedure as well as the growth media employed. All the cell lines employed in these studies were adherent.

2.1.3 Polymers studied

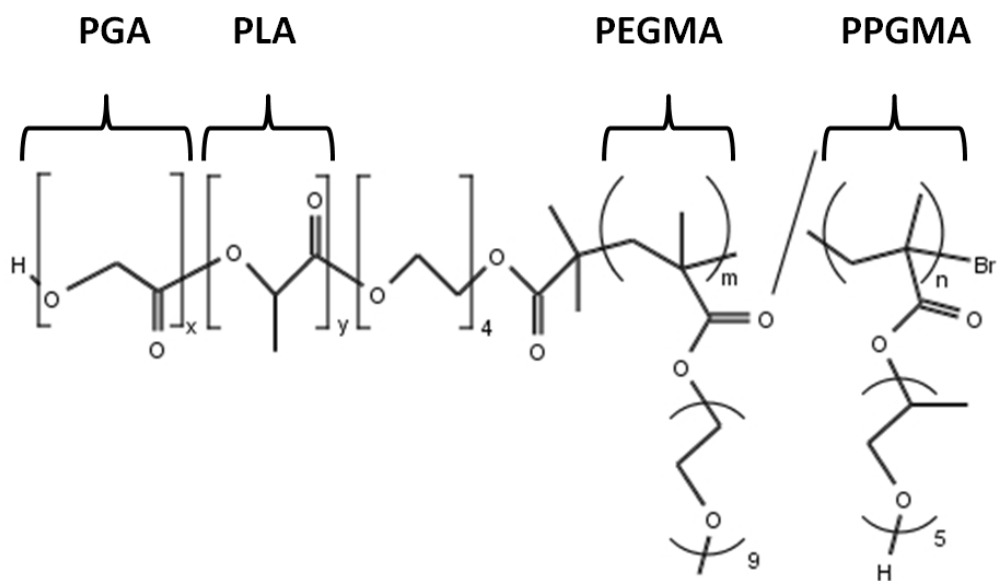


Figure 2-1 Poly(lactide-*co*-glycolide)-*block*-poly(poly(ethylene glycol methyl ether methacrylate)-*co*-poly(propylene glycol methacrylate)) (PLGA-*b*-(PPGMA-*co*-PEGMA)) thermoresponsive polymers.

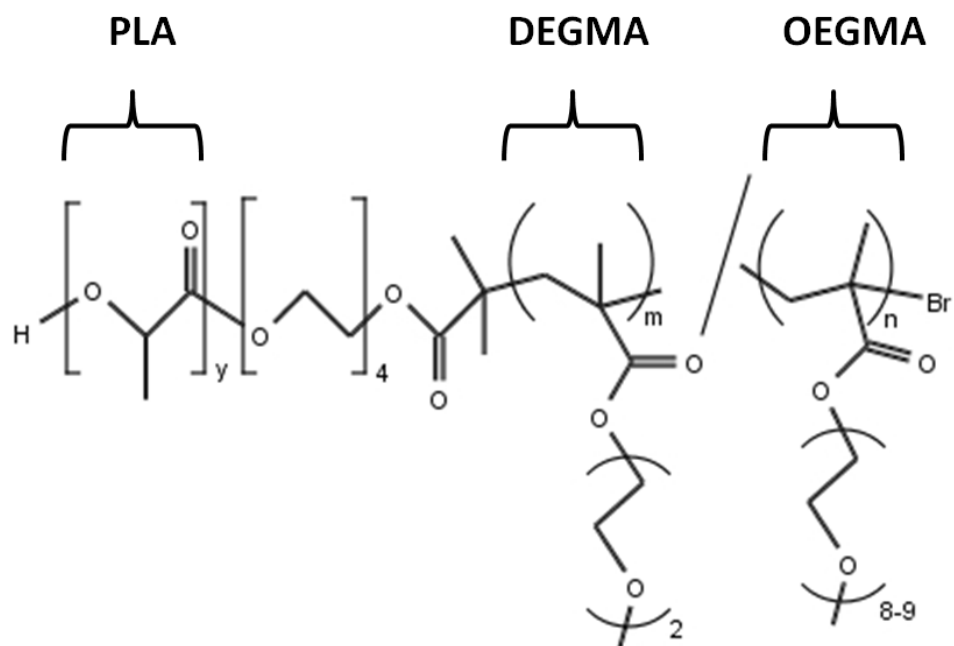


Figure 2-2 Polylactide- *block*- poly(poly(diethylene glycol methacrylate)-*co*-poly(oligoethylene glycol methacrylate)) (PLA-*b*-(DEGMA-*co*-OEGMA)) thermoresponsive polymers.

Thermoresponsive polymers used in these studies were based on previous work from Abulateefeh *et al* and they were synthesised by Lee Moir (School of Pharmacy, University of Nottingham, UK)⁶. Their chemical names are poly(lactide-*co*-glycolide)-*block*-poly(poly(ethylene glycol methyl ether methacrylate)-*co*-poly(propylene glycol methacrylate)) and its abbreviation is PLGA-*b*-(PPGMA-*co*-PEGMA) (Figure 2-1) and poly(lactide- *block*- poly(poly(diethylene glycol methacrylate)-*co*-poly(oligoethylene glycol methacrylate)) and its abbreviation is PLA-*b*-(DEGMA-*co*-OEGMA). (Figure 2-2). In these polymers the PLGA/PLA region formed the hydrophobic solid core of the micelle while the PPGMA/PEGMA or DEGMA/OEGMA formed the hydrophilic region of the polymer.

2.1.3.1 Polystyrene nanoparticles

Polystyrene Fluoresbrite Yellow-Orange carboxylated polystyrene beads (C-PB) of 50 nm (catalogue number 19775) and 100 nm (catalogue number 18791), $\lambda_{\text{max ex}} 529\text{nm}$ – $\lambda_{\text{max em}} 546\text{nm}$, were purchased from Polysciences, Heppenheim, Germany.

2.1.4 Materials for inhibition studies

LacCer complexed with Bovine Serum Albumin (BSA), transferrin from human serum, conjugated with Alexafluor 633 (Htf), and 2-[4-(2-hydroxyethyl)piperazin-1-yl] ethanesulfonic acid (HEPES) buffer were purchased from Fisher Scientific, Loughborough, UK. Chlorpromazine (CPZ), methyl- β -cyclodextrin (MBCD) and any other material not specified in this list was purchased from Sigma (Sigma-Aldrich, Dorset, UK). Methanol free paraformalehyde (PFA) was purchased from Electron Microscopy Science, Sunnyvale, CA, Alexafluor 488 and 594 secondary antibodies were purchased from Molecular Probes, Paisley, UK, anti-clathrin heavy chain monoclonal antibody (mAb) (clone X22) was purchased from Merk Biosciences, Feltham, UK and anti-caveolin-1 mAb (clone 2297) from BD Transduction

Laboratories, Lexington, KY, defatted albumin (dBSA) was purchased from Sigma-Aldrich, Dorset, UK.

2.2 General methods

2.2.1 General cell maintenance procedures

2.2.1.1 Routine tissue culture procedures

Cells were routinely grown in 75cm² vented cap flasks in tissue culture incubators at controlled CO₂ atmosphere (5% v/v), 37°C and 95% v/v humidity. Routine cell maintenance was carried out 3 times per week. Cells were checked under a reverse microscope to verify health, lack of contamination and confluence. For cell splitting procedures, cells were grown to reach 80% confluence. EDTA and trypsin/EDTA were pre-warmed to 37°C in a tissue culture water bath before use. After checking cells at the microscope they were treated as follows: MGLVA-1, and MRC-5 were washed with 5 ml EDTA before applying trypsin/EDTA 8ml (MGLVA-1) and 4ml respectively (MRC-5). HCT116 and 3T3 cells were treated with 4ml trypsin/EDTA only. Upon detachment of cells, cell suspensions were collected in a sterile vial and the culture flask rinsed with 6 or 12ml of the appropriate cell culture media. Cell suspensions were centrifuged at 200g for 5 minutes, the supernatant was removed by aspiration and cells were re-suspended in 10 ml appropriate media. Cells were seeded depending on the desired numbers for setting up purposes or 1/10 of cell suspension re-cultured in a 75cm² sterile flask for cell line routine maintenance according to ATCC and Japanese Cell Bank protocols. For MRC-5 only the splitting ratio was kept to 1/3.

2.2.1.2 General procedures for cell counting and experiments setup

Cells detached as described above and re-suspended in their own media were mixed with the aid of a vortex (3T3, MRC-5) or passed through a 0.8 mm needle to get rid of

General Materials and Methods

clumps of cells and to ease the counting process (HCT116 and MGLVA-1). Subsequently, four aliquots of 50 µl of cells were added to 50 µl trypan blue and cells counted on a Neubauer haemocytometer counting chamber (Hawksley, Cambridge, UK) with a manual counter (ENM, Chicago, USA). The count averaged according to the following formula:

$$\left[\frac{(\text{count 1}) + (\text{count 2}) + (\text{count 3}) + (\text{count 4})}{4} \right] \times 2 \times 10^4 = \text{numbers of cells/ml}$$

The number of dead cells was also annotated on a lab-book and experiments were not set up if the number of dead/trypan blue positive cells was more than 5% for each count. MGLVA-1 and HCT116 cells prepared for experiments were passed through a needle as described above before an aliquot of the appropriate volume of cells was diluted to the appropriate number of cells/ml for experiments setup.

2.2.1.3 Preparation of frozen stocks of cells

Confluent cells were detached from cell culture flasks with trypsin/EDTA as described above and centrifuged at 200 g for 5 minutes. Supernatant was aspirated off and the pellet re-suspended with the aid of a vortex. Fresh culture media supplemented with 10% v/v dimethyl sulfoxide (DMSO, Sigma-Aldrich, Dorset, UK) suitable for cell culture was applied to re-suspended cells and the mixture quickly transferred to a sterile labelled cryovial where the cell line, passage number, date and name of the owner was annotated for future reference. The cryovial was placed in a Mr Frosty (Thermo Scientific, Loughborough, UK) at -80°C for 24 h and to a storage box in a -80°C freezer for up to 6 months or to a -150°C freezer for long storage and maintenance of cells stocks.

2.2.1.4 Cell revival from -150°C freezer

Prior to defrosting the desired cell line, a 75 cm² flask containing 15 ml of the appropriate media was prepared and left to equilibrate in a tissue culture incubator at 37°C and 5% CO₂ 95% humidity for 30 minutes. Cryovials of the desired cell lines were removed from the freezer, moved quickly to 37°C water-bath and swirled until defrosted. Subsequently, the cryovial content was moved with the aid of sterile 5 ml pipette into the pre-warmed flask and cells left to recover for 24 h or until completely adherent to the bottom of the flask. Finally, the media was replaced with fresh warm media to remove the DMSO present in the freezing media. A buffer period of 7-10 days was applied before using the defrosted cells for experiments.

2.2.2 Dynamic Light Scattering (DLS)

DLS is a technique used to measure the hydrodynamic radius of particles in solution. During the measurement, the solution is irradiated by coherent laser light, and a detector measures the scattered light from the particles. Fluctuations in scattering intensities are fitted to a correlation function to determine the diffusion of particles in solution. From the estimated diffusion coefficient, the hydrodynamic radius of the nanoparticles is derived by the Stoke- Einstein equation:

$$R_H = \frac{kT}{6\pi\eta D}$$

where R_H is the hydrodynamic radius, k is the Boltzmann constant, T the absolute temperature and η is the viscosity of the solvent and D is the translational diffusion (also known as Brownian motion) coefficient. The particles are assumed spherical and non-interacting. A Malvern Instruments Viscotek802 DLS (Malvern, UK) was used for all the measurements. The light source for the instrument is a diode laser, 830nm wavelength, 50 mW internal laser, 90° angle of detection. All measurements were carried out at 20°C.

50 nm C-PB were diluted in PBS buffer at a concentration of 200 µg/ml and 100 nm C-PB were prepared at a concentration of 50 µg/ml according to Malvern support suggestions. The solution was diluted to the desired concentration in PBS filtered with a 0.2 µm filter and vortexed for 1 minute to remove any C-PB aggregates before each measurement. Each reading was the result of averages of 10 readings carried out for 10 s each. 3 readings for each polystyrene bead were made and the 3 readings were averaged and data plotted in GraphPad Prism.

2.2.3 Transmission Electron Microscopy (TEM) of C-PB

TEM images were obtained with a Tecnai G12 Bio Twin Digital Transmission Electron Microscope System.

Stock solutions of 50 and 100 nm C-PB were diluted to 25 and 26.5 µg/ml in filtered PBS as described above, the prepared solution was mixed with a vortex for one minute to get rid of any aggregates and applied on a Formvar/Carbon support film 300 mesh copper grids and allowed to dry overnight. A minimum of 12 images for each size of polystyrene nanoparticles were taken for a minimum count of 250 particles for each size of C-PB. Images were analysed with ImageJ software and the Feret diameter (the larger diameter of a particle not assumed to be spherical) plotted in GraphPad Prism.

2.2.4 Zeta potential of C-PB

Electrokinetic potential or zeta potential is the description of the charge of particles in suspension. Particle suspensions are loaded onto a special chamber that is provided with two electrodes. The electrophoretic mobility of the particles is measured and the measurement converted to zeta potential through the following equation:

$$\zeta = 1.328x \left[\frac{\eta \cdot \mu_E}{\epsilon_r \cdot f(K_a)} \right]$$

where η is the viscosity of the solution, μ_E is the measured electrophoretic mobility, ϵ_r is the solution dielectric constant and $f(K_a)$ is a constant calculated on the basis of experiments conditions such as ionic strength and temperature.

Zetasizer measurements were acquired with a Malvern Zetasizer Nano, Malvern, UK. The particles suspensions were prepared in HEPES buffer 1 mM, Ph 7.4 at a concentration of 200 $\mu\text{g/ml}$. The values obtained were the result of 12 measurement replicates. All measurements were carried out at 20°C.

2.2.5 Toxicity Tests

2.2.5.1 MTT (3-(4,5-Dimethylthiazol-2-yl)-2,5-diphenyl-tetrazolium bromide) assay

The MTT assay is a colorimetric assay used to determine metabolic activity of cells. Upon application of the yellow MTT solution, the MTT is converted by the functional mitochondrial and cytoplasmic succinate dehydrogenase activity of viable cells to a purple, water insoluble formazan. The absorbance of the solubilised purple formazan can be quantified at a wavelength of 550 nm by a spectrophotometer.

The optimal concentration of cells for toxicity tests was verified by a titration curve prior the test of drugs/nanoparticles. The titration curve was obtained by serial 1 to 2 dilutions of cells from a maximum of 312000 to the limit of the detection of cells for the assay. 100 μl of cells dilutions were seeded in triplicates in the middle wells of a clear 96 well plate and extra triplicate wells for media only were left for the blank. The edges of the wells used for the titration curve were filled with 200 μl media to avoid excessive evaporation of media from assay wells.

For toxicity assays, 100 μl of cells were seeded into the middle 60 wells of a clear 96 well plate at a density of 31200 cells/cm², allowed to attach to the well overnight and successively treated for 4.5 h with chemical inhibitors of endocytic pathways or for 4-

General Materials and Methods

24 and 48 h with nanoparticles. Each inhibitor was applied in triplicates and both inhibitors, C-PB and polymers were prepared in HBSS supplemented with HEPES buffer 20 mM. Serial dilutions were prepared at a 1/2 ratio for CPZ, MBCD and thermoresponsive polymers or 1/10 for C-PB. CPZ and MBCD toxicity were tested every time a new stock solution was prepared to avoid weighing errors. Both CPZ, MBCD and nanoparticle toxicity tests were carried out with a reference positive and negative control consisting of PEI 0.5 mg/ml and HBSS/HEPES 20 mM respectively. A blank consisting of the same C-PB serial dilutions triplicates used in toxicity tests applied to wells without cells was also analysed in C-PB toxicity studies and the absorbance values of the blank subtracted accordingly. Upon completion of the incubation time at 37°C and 5% CO₂, MTT (50 µl of 1 mg/ml solution) was applied and cells supplemented with MTT incubated for further 4 h. Upon completion of the MTT incubation time the solution was aspirated and 75 µl of DMSO applied to solubilise the purple water-insoluble crystals formed by the functional mitochondrial and cytoplasmic succinate dehydrogenase activity of viable cells. Blanks plates of C-PB were processed as the other tested samples (same time of incubation, same volume of MTT added, same incubation time of MTT, MTT aspirated off and DMSO applied). Absorbance readings were recorded at 550 nm on a MRX revelation microplate reader, Thermo Lab Systems, Altrincham, UK. The results were plotted in GraphPad Prism and normalised against the untreated controls.

2.2.5.2 Apo I (caspase 3/7) apoptosis assay

Caspase 3 and 7 are members of cysteine aspartic acid-specific protease (caspase) family and they are synthesized during apoptosis. Apo I caspase 3/7 detection kit (Promega, Southampton, UK) consists of profluorescent substrate formed by a peptidic region conjugated to a fluorescent dye (Rhodamine 110). In the presence of caspase 3/7 the peptidic region of the substrate is specifically cleaved by caspases 3

General Materials and Methods

and 7 and releases the fluorescent dye that is detected at 535nm. The fluorescence detected is therefore proportional to the number of apoptotic cells.

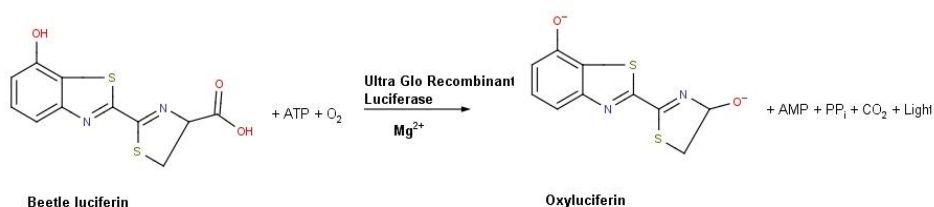
25 µl of HCT116, MGLVA-1 and 3T3 cell suspensions were seeded into the middle 240 wells of a 384 clear bottom black well plate at a density of 31200 cells/cm² in full growth media and left to attach to the bottom of the wells overnight. Two rows of wells at the edges of the 384 wells plate were filled with 50 µl of growth media to provide moisture and help to avoid excessive evaporation of media from the wells overnight. The day after, the medium was carefully aspirated off with a pipette tip and replaced with 25 µl of HBSS/HEPES 20 mM for negative control, PEI 0.5 mg/ml and CPZ dilutions of 320-240-160-80 and 40 µM obtained in HBSS/HEPES 20 mM. Quintuplicate wells devoid of cells were replaced with HBSS/HEPES 20 mM for a blank reading. CPZ and control wells were applied in quintuplicate and 3 independent experiments repeated for each cell line. CPZ was incubated for 4.5 h. When the incubation time was over 25 µl of Apo I reagents mix was prepared according to manufacturer specifications and added to each well. Briefly, Apo I reagents were thawed and equilibrated to room temperature and Apo I substrate diluted 1/100 with Apo I buffer and added to assay wells to lyse the cells and start the conversion of the substrate to the fluorescent product by caspase 3 and 7 enzymatic activity of apoptotic cells. The plate was placed on an orbital plate shaker for 30 minutes and plate read on a spectrofluorometer (Flex Station II 384 microplate reader, Molecular Devices, Wokingham, UK). The excitation was set at 485nm, emission at 535 nm, 495 nm cutoff.

2.2.5.3 Cell Titer Glo viability assay

Cell Titer Glo viability assay is based on the activity of ultra glo recombinant luciferase, a mono-oxygenase enzyme that converts luciferin substrates to oxyluciferin. Oxyluciferin emits a luminescence signal and the quantity of oxyluciferin

General Materials and Methods

produced is dependent on ATP that is provided by the cells in the tested sample. Hence, the amount of conversion and luminescence signal is directly proportional to the ATP content in the tested sample and the ATP levels are directly proportional to the metabolic activity and numbers of cells. The luciferase reaction is shown below:



The luminescence signal can be quantified by a luminometer.

The optimal concentration of cells for toxicity tests was verified by a titration curve prior to the testing of drugs and nanoparticles. The titration curve was obtained in HBSS/HEPES 20 mM by 10 serial 1 to 2 dilutions of cells from a maximum of 312000 to a minimum of 635 cells/cm². 100 μ l of cells dilutions were seeded in triplicates in the middle 36 wells of a 96 well plates and extra triplicate wells for media only were left for the blank. The edges of the wells used for the titration curve were filled with 200 μ l media to avoid excessive evaporation of assay media.

For the Cell Titer Glo assay, cells at a density 31200 cells/cm² were seeded in the middle 60 wells of a clear bottom, black well plate and allowed to attach to the bottom of the wells overnight. The day after, the media of cells was aspirated off and 100 μ l of the material of interest was applied in HBSS/HEPES 20 mM in triplicates. Two or three independent experiments were carried out. C-PB of 50 and 100 nm were tested at concentrations ranging between 1000 μ g/ml and 1 and dilutions of 1/10. CPZ tested concentrations ranged between 320 and 10 μ M with dilutions 1/2. For each experiment a positive and negative control were also used consisting of PEI 0.5

mg/ml and HBSS/HEPES 20 mM respectively and a blank consisting of HBSS/HEPES 20 mM without cells. C-PB were incubated at 37°C and 5% CO₂ for 4 h. Endocytosis inhibitors were incubated 4.5 h. 15 minutes before the incubation time was over, the cells were removed from the incubator and left to equilibrate to room temperature according to manufacturer specification. Subsequently, Cell Titer Glo mix 100 µl was applied and plates loaded on an orbital mixer for 2 minutes to allow cell lysis. The plate was further incubated at room temperature for 10 minutes to allow the luminescence signal to stabilize. For C-PB toxicity studies only, prior to the application of the Cell Titer Glo mix, the wells content was removed with a pipette tip and 100 µl of HBSS/HEPES 20 mM applied. This procedure was carried out to prevent or reduce the interaction of the nanoparticles with the Cell Titer Glo recombinant proteic enzyme and potentially reduce its activity. The luminescence signal was read for 1 second per well according to manufacturer specifications and recorded with a FluoStar Optima microplate reader (BMG LABTECH GmbH, Ortenberg, Germany).

2.2.5.4 Statistical Analysis

For all toxicity tests the Z factor and Signal Window were calculated according to the formulas below:

$$Z \text{ Factor} = 1 - \left(\frac{(3xSDp.c. + 3xSDn.c.)}{|Mp.c. - Mn.c. |} \right)$$

(7)

$$\text{Signal Window} = \left(\frac{[Mn.c. - Mp.c. - 3x(SDp.c. + SDn.c.)]}{SDn.c.} \right)$$

(8)

Where:

SDp.c = Standard Deviation of the positive control

SDn.c = Standard Deviation of the negative control

Mp.c = Mean of the positive control

Mn.c. = Mean of the negative control

These two parameters were calculated to confirm that there was sufficient separation of the signals obtained from the negative and positive control at the chosen concentration of cells for cell activity studies and hence the studies carried out were producing good quality and reliable cell activity data.

2.2.6 Htf and LacCer Wash Efficiency Studies

Detection methods such as flow cytometry or plate reading of the signal of fluorescent markers of endocytosis cannot distinguish between the fluorescence signal from the membrane or internalised markers of endocytosis. For this reason, both Htf and LacCer washes are routine procedures for efficient removal of the endocytic marker from the plasma membrane in endocytosis inhibition studies. The following procedures were carried out to verify the efficiency of the wash of Htf and LacCer from the membrane of cells. In these experiments the buffers of the washes suggested from the literature were not altered. However, two different procedures were attempted:

- Cells treated with markers of endocytosis were washed in flasks with standard buffers before being removed with trypsin and fixed for flow cytometry.
- Cells treated with markers of endocytosis were removed from flasks with trypsin, collected in Eppendorf tubes and cells washed with standard buffers on cells suspensions. Each wash step was followed by a centrifugation step at 2000 g for 5 minutes at 4°C.

General Materials and Methods

2.2.6.1 Htf and LacCer removal from the cell membrane with washes on cells suspensions

Cells were seeded at a density of 31200 cells/cm² in 25 cm² flasks and allowed to attach to the bottom of the flask overnight. Subsequently, cells were detached from flasks with trypsin, collected in Eppendorf tubes and centrifuged at 2000 g for 5 min at 4°C. The supernatant was aspirated off with a pipette tip and Eppendorf tubes placed on ice and left to equilibrate for one minute. Subsequently, cells were re-suspended in ice cold HBSS /HEPES 20 mM (negative control) or ice cold Htf 6.7 µg/ml in HBSS/HEPES 20 mM in or LacCer 0.81 µM in HBSS/HEPES 20 mM in duplicate Eppendorf tubes. The 2 Eppendorf tubes treated with Htf 6.7 µg/ml or LacCer 0.81 µM in HBSS/HEPES 20 mM consisted of one positive control not treated with consequent washing steps and used as a reference control of the membrane bound marker of endocytosis, and one positive control treated with washes on cells suspensions. The Eppendorf tubes were incubated for 5 minutes on ice to allow the binding of the marker of endocytosis on the cell membrane without internalization. Hence, cells were washed with the buffers and procedures described below.

The buffers used to remove membrane bound Htf consisted of 2 rinses with ice cold HMEM-G+I, on ice (Hank's Minimum Essential Medium (HMEM) without glucose - Gibco, Paisley, UK - supplemented with 10 mM HEPES and 5 mM sodium azide, NaN₃, to inhibit metabolic activity) followed by 1 minute ice cold wash with 0.2 mM acetic acid 0.2 mM NaCl buffer pH 4.6⁹. The acidic wash was then rinsed on ice with 2 cold washes of HMEM-G+I.

The buffers used to remove membrane bound LacCer consisted of two ice cold washes with HMEM-G+I followed by 6 rinses (10 minutes each, on ice) of HMEM-G+I supplemented with 5% w/v dBSA (back exchange method)¹⁰.

General Materials and Methods

The washes described above were carried out on cell suspensions and each wash was followed by 5 minutes centrifugation at 2000 g at 4°C. The last wash step was then followed by centrifugation at 2000 g for 5 minutes at 4°C and cells re-suspended in PFA 4% v/v PBS and fluorescence of cells analysed by flow cytometry with a Becton-Dickinson (BD) LSR II flow cytometer, Oxford, UK and detected with optical filters (FITC 530/30 bandpass filter for LacCer detection or an APC channel, 660/20 optical bandpass filter for the detection of Htf). Data were analysed with Weasel software, normalised against the positive and negative controls assumed being 100% and 0% uptake of the markers of endocytosis and plotted in GraphPad Prism.

2.2.6.2 Htf and LacCer removal from the cell membrane with washes on adherent cells

Cells were seeded at a density of 31200 cells/cm² in 25 cm² flasks and allowed to attach to the bottom of the flask overnight. The day after, cells were placed on ice and left to equilibrate for 10 minutes. Subsequently, full growth media was aspirated off and cells treated with ice cold HBSS/HEPES 20 mM for the negative control or ice cold Htf 6.7 µg/ml or LacCer 0.81 µM in HBSS/HEPES 20 mM in duplicate flasks. The 2 additional flasks for each marker of endocytosis consisted of one positive control not treated with consequent washing steps and used as a reference control of the membrane bound marker of endocytosis, and a positive control subsequently treated with flask washes. The flasks were incubated for 5 minutes on ice to allow the binding of the Htf or LacCer on the cell membrane without internalization. Hence, cells were washed on ice with the buffers and procedures described below.

The buffers used to remove membrane bound Htf consisted of 2 rinses with ice cold HMEM-G+I, on ice followed by 1 minute ice cold wash with 0.2 mM acetic acid 0.2 mM NaCl buffer pH 4.6⁹. The acidic wash was then followed by 2 cold washes of

General Materials and Methods

HMEM-G+I on ice, cells were trypsinised, centrifuged at 2000 g for 5 minutes at 4°C and fixed in PFA 4% v/v PBS.

The buffers used to remove membrane bound LacCer consisted of two ice cold washes with HMEM-G+I followed by 6 rinses (10 minutes each, on ice) of HMEM-G+I supplemented with 5% w/v dBSA (back exchange method)¹⁰. Cells were then trypsinised, centrifuged at 2000 g for 5 minutes at 4°C and fixed in PFA 4% v/v PBS and analysed by flow cytometry with a Becton-Dickinson (BD) LSR II flow cytometer, Oxford, UK and detected with optical filters (FITC 530/30 bandpass filter for LacCer detection or an APC channel, 660/20 optical bandpass filter for the detection of Htf). Data were analysed with Weasel software, normalised against the positive and negative controls that were assumed being 100% and 0% uptake of the endocytosis markers and plotted in GraphPad Prism.

Inhibitors of endocytosis	Mechanism of action	Pathways' interference
CPZ	Direct binding to calmodulin leading to plasma membrane depletion of free phosphatidyl-inositol 4,5 biphosphate	<ul style="list-style-type: none"> •Clathrin mediated endocytosis •Phagocytosis •Macropinocytosis
Pitstop 2	Direct antagonist of Clathrin mediated endocytosis	<ul style="list-style-type: none"> •Clathrin mediated endocytosis •Phagocytosis
MBCD	Plasma membrane depletion of cholesterol	<ul style="list-style-type: none"> •Caveolae mediated endocytosis •Clathrin mediated endocytosis •Non caveolae non clathrin mediated endocytosis

Table 2-2 Summary of the inhibitors of endocytosis used in this study

2.2.7 Inhibition of Htf uptake with CPZ

Cells were seeded in 25 cm² vented caps flasks at a density of 31200 cells/cm² and allowed to attach to the bottom of the flasks overnight. Subsequently, full media was replaced with HBSS supplemented with 20 mM HEPES with or without chemical inhibitors of endocytic pathways for 30 minutes and then replaced with HBSS/HEPES 20 mM with or without LacCer 0.81 µM or Htf 6.7 µg/ml and chemical inhibitors. Chemical inhibitors working concentrations were selected as 1.25 mM MBCD and 40, 60 and 80 µM CPZ (Table 2-2). Upon completion of the incubation time, cells were washed as described above, detached from flasks with trypsin-EDTA or EDTA alone, centrifuged at 2000 g for 5 minutes and re-suspended in a fixation buffer consisting of PFA 4% v/v in PBS. Cells were then analysed with a BD LSR II flow cytometer (APC 660/20 bandpass filter). Briefly, Htf acidic wash consisted of two cold washes with HMEM-G+I followed by 1 minute ice cold wash with 0.2 mM acetic acid 0.2 mM NaCl buffer⁹. The acidic wash was then rinsed out with 2 cold washes of HMEM-G+I. The Htf washes were carried out in 25 cm² flasks. A variant of this protocol included the used of HBSS devoid of Ca²⁺ and Mg²⁺ supplemented with 20 mM HEPES instead of standard HBSS. This protocol was aiming at depleting cells of Ca²⁺ and consequently of ATP and overall energy.

2.2.8 Inhibition of Htf uptake with Pitstop 2

Cells were seeded at a density of 31200 cells/cm² in 25 cm² vented cap flasks and allowed to attach to the bottom of the flask overnight. Subsequently, full media was replaced with HBSS supplemented with HEPES 20 mM with or without Pitstop 2 (abCam, Cambridge, UK, Table 2-2) for 15 minutes and then replaced with HBSS/HEPES 20 mM with or without Htf 6.7 µg/ml and chemical inhibitor. Working concentrations of Pitstop 2 were selected as 12.5, 18.75 and 25 µM and incubation times set at 1 or 2 h. Upon completion of the incubation time, cells were washed as

described above, detached from flasks with trypsin-EDTA or EDTA alone, centrifuged at 2000 g for 5 minutes and re-suspended in a fixation buffer consisting of PFA 4% in PBS. Cells were then analysed with a BD LSR II flow cytometer (APC 660/20 bandpass filter). Briefly, Htf acidic wash consisted of two cold washes with HMEM-G+I followed by 1 minute ice cold wash with 0.2 mM acetic acid 0.2 mM NaCl buffer⁹. The acidic wash was then rinsed with 2 cold washes of HMEM-G+I. The acidic washes were carried out in flasks.

2.2.9 Inhibition of LacCer uptake with MBCD

Cells were seeded at a density of 31200 cells/cm² and allowed to attach to the 25 cm² flasks overnight. Subsequently, full media was replaced with HBSS supplemented with 20 mM HEPES with or without chemical inhibitors of endocytosis for 30 minutes and subsequently replaced with HBSS/HEPES 20 mM alone (negative control), LacCer 0.81 µM (positive controls) or with LacCer 0.81 µM in the presence of 80 µM CPZ or 1.25 mM MBCD (Table 2-2). The incubation times were 1-2-3 and 4 h for all cell lines. Chemical inhibitors working concentrations were selected as the lowest affective inhibiting concentration of the chemical inhibitors. Upon completion of the incubation time cells were washed as described above and subsequently detached from flasks with trypsin-EDTA. Detached cells were centrifuged at 2000 g for 5 minutes and re-suspended in a fixation buffer consisting of PFA 4% v/v in PBS. Cells were then analysed with a BD LSR II flow cytometer and detected with optical filters (FITC 530/30 bandpass filter).

Briefly, LacCer wash consisted of two ice cold washes with HMEM-G+I followed by 6 rinses (10 minutes each) of HMEM-G+I supplemented with 5% w/v dBSA (back exchange method)¹⁰.

2.2.10 Endocytosis inhibition in the presence of C-PB

Cells were seeded at a density of 31200 cells/cm² and allowed to attach to the 25 cm² flasks overnight. Subsequently, full media was replaced with HBSS supplemented with 20 mM HEPES with or without chemical inhibitors of endocytosis for 30 minutes. The buffer was subsequently replaced with HBSS/HEPES 20 mM alone (negative control), 50 nm C-PB 100 µg/ml or 100 nm C-PB 100 µg/ml (positive controls), or with 50 or 100 nm C-PB 100 µg/ml in the presence of 80 µM CPZ or 1.25 mM MBCD. C-PB and inhibitors were further incubated for 1-2 or 4 h. Subsequently, cells were washed twice with HBSS/HEPES 20 mM and EDTA, detached from flasks with trypsin/EDTA, centrifuged at 2000 g for 5 minutes and re-suspended in PFA 4% v/v PBS. Cells were then analysed with a BD LSR II flow cytometer and detected with optical filters (FITC 530/30 bandpass filter).

2.2.11 Procedures for sterilization of coverslips for microscopy

Round 22x1.5 mm glass coverslips (SLS, Nottingham, UK) were handled in a Class II cabinet. They were picked up with autoclaved tweezers and immersed in absolute ethanol (Sigma, Dorset, UK) for 5 minute. The coverslips were then removed from ethanol and left to dry to the air of the class II cabinet in a sterile six well plate before use.

2.2.12 Confocal microscopy live imaging methods

Cells were seeded in full media to a final density of 31200 cells/cm² in 6 well plates in the presence of sterile rounded 22x1.5 mm glass coverslips (SLS, Nottingham, UK). Cells were left to attach to the glass coverslips overnight. On the next day the cells were stained with Hoechst 33342 (Thermo Scientific, Rockford, USA) 1 µg/ml and Cell Mask deep red cell membrane stain 1 µg/ml for 30 minutes (Molecular Probes, Paisley, UK). The media was then replaced with HBSS/HEPES 20 mM for live imaging. Confocal equipment consisted of a Zeiss Laser Scanning Microscope (LSM)

710, Jena, Germany. This was supplied with a heated chamber at 37°C that was switched on and equilibrated to temperature overnight. Glass rounded coverslips were mounted on a coverslip holder that had been previously sterilised and equilibrated at 37°C overnight. Images of stained cells in buffer were taken prior to the exposure of cells to C-PB. The C-PB solution was then added to the buffer solution at a ratio 1:1 to obtain a final concentration of C-PB of 50 µg/ml. Images of the 4 regions of interests were acquired at 4-10-20-30-40-50 and 60 minutes on a 40x water objective.

2.2.13 Immunofluorescence of clathrin and caveolin-1

Cells were seeded at a density of 31200 cells/cm² and allowed to attach to squared 22x22x1.5 mm glass coverslips (SLS, Nottingham, UK) or 25 cm² flasks overnight. The day after cells were washed and fixed for 30 minutes at room temperature with PFA 4% v/v for immunofluorescence or trypsinized and pelleted at 2000 g for 5 minutes before fixation for flow cytometry. Cells on coverslips were washed 3 times for 5 minutes in PBS while trypsinized cells suspensions for flow cytometry were washed in PBS once for 5 minutes on a rocker. Subsequently, PBS, 0.3% v/v Triton X-100, 5% v/v goat serum blocking buffer was applied for 1.5 h. When the incubation time was over, the blocking buffer was gently removed with a pipette tip and the chosen antibody applied according to manufacturer specifications. Anti-clathrin heavy chain mouse IgG1mAb (clone X22) prepared in PBS, 1% w/v BSA, 0.3% v/v Triton X-100 was used at a concentrations of 0.12 µg/ml and anti-caveolin-1 mouse IgG1mAb (clone 2297), prepared in PBS, 1% w/v BSA, 0.3% v/v Triton X-100, was applied at a concentration of 0.83 µg/ml for all cell lines. Mouse IgG1 was utilised as a negative control at concentrations of 0.12 µg/ml for clathrin IgG1 negative control and 0.83 µg/ml for caveolin-1 IgG1 negative control. An additional negative control consisting in cells treated with secondary antibody were incubated with PBS, 1% w/v BSA, 0.3%

General Materials and Methods

v/v Triton X-100. All cells were incubated for 1.5h; subsequently, cells on coverslips were washed 3 times for 5 minutes in PBS while cell suspensions were washed once on a rocker for 5 minutes, and goat anti-mouse (H+L) IgG1 AlexaFluor 488 nm or 594 nm secondary antibody (Molecular Probes, Paisley, UK) in PBS, 1% w/v BSA and 0.3% v/v Triton X-100 was applied overnight at 4°C. The secondary antibody was diluted to 5 µg/ml for both clathrin and caveolin staining. The following day, the secondary antibody was aspirated off and cells washed 3 times for 5 minutes with PBS. Cells prepared for microscopy were removed from the wells with the aid of a needle and tweezers, further stained with Prolong Gold Antifade DAPI mounting media (Invitrogen, Paisley, UK) applied on glass slides and left to dry at room temperature in the dark overnight. The following day, coverslips edges were sealed with nail polish to the glass slides and stored at 4°C until used on a Zeiss LSM700 confocal microscope, Jena, Germany. Cells prepared for flow cytometry were resuspended in PBS. Flow cytometry data were acquired with a BD LSR II flow cytometer (FITC 530/30 bandpass filter for AlexaFluor488 secondary antibody) and analysed with Weasel software.

References

- 1 Brattain, M. G. *et al.* Heterogeneity of malignant cells from a human colonic carcinoma. *Cancer Research* **41**, 1751-1756 (1981).
- 2 Watson, S. A., Durrant, L.G., Morris, D.L. The effect of the E2 prostaglandine enprostil, and the somatostatin analogues SMS 201 995, on the growth of a human gastric cell line, MKN45G. *International Journal of Cancer* **45**, 90-94 (1990).
- 3 Hojo, J. Establishment of cultured cell lines of human stomach cancerorigin and their morphological characteristics. *Niigata Igakukai Zasshi* **91**, 737 (1977).
- 4 Todaro, G. J. & Green, H. Quantitative studies of the growth of mouse embryo cells in culture and their development into established lines. *J Cell Biol* **17**, 299-313 (1963).
- 5 Jacobs, J. P., Jones, C. M. & Baille, J. P. Characteristics of a human diploid cell designated MRC-5. *Nature* **227**, 168-170 (1970).
- 6 Abulateefeh, S. R. *et al.* Facile synthesis of responsive nanoparticles with reversible, tunable and rapid thermal transitions from biocompatible constituents. *Chemical Communications*, 6068-6070 (2009).

General Materials and Methods

- 7 Zhang, J. H., Chung, T. D. F. A. U. O. & Oldenburg, K. R. A Simple Statistical Parameter for Use in Evaluation and Validation of High Throughput Screening Assays. *Journal of Biomolecular Screening* **4**, 67-73 (1999).
- 8 Iversen, P. W., B.J., E., Sittampalam, G. S. & Cox, K. L. A comparison of assay performance measures in screening assays: signal window, Z' factor, and assay variability ratio. *Journal of Biomolecular Screening* **11**, 247-252 (2006).
- 9 van Renswoude, J., Bridges, K. R., Harford, J. B. & Klausner, R. D. Receptor-mediated endocytosis of transferrin and the uptake of Fe in K562 cells: identification of a nonlysosomal acidic compartment. *Proceedings of the National Academy of Sciences* **79**, 6186-6190 (1982).
- 10 Pagano, O. C. M. a. R. E. Internalization and sorting of a fluorescent analogue of glucosylceramide to the Golgi apparatus of human skin fibroblasts: utilization of endocytic and nonendocytic transport mechanisms. *J Cell Biol* **125**, 769-781 (1994).

3-Chapter 3

Characterisation of Materials and Cell Lines

3.1 Introduction

Synthetic and natural polymers are being extensively studied as carriers of drugs^{1,2}. The ability of some polymers to self-assemble, creating protected compartments for the transport of drugs, together with the possibility to respond to external stimuli by conformational rearrangement and release of the drug load, are appealing characteristics for biomedical use. However, chemical and physical characteristics of these polymers such as size and superficial charge can modulate the extent of their internalization in cells as well as influencing their pathway of uptake³⁻⁶. A better understanding of how these characteristics can change cellular processing of these materials in different cell lines will help the design of more reliable carriers of drugs. For this reason, commercially available Polysciences Carboxylated Yellow-Orange Polystyrene Beads (C-PB) of well defined size charge and shape were used as a model for polymeric nanomaterials with a hydrophobic bulk and slightly negative surface charge. The C-PBs were characterized in the intended buffer for the endocytosis experiments by ζ potential measurements and their sizes determined by both DLS and TEM. The effects of these materials on cell viability were also characterized by MTT and Cell Titer Glo ATPase assays.

The choice of the cell lines for the study was made on the basis of evidence that many pathologies affect epithelial cells⁷⁻⁹. However, literature reports an increasing role of mesenchymal cells in the instigation and progression of pathologies such as cancer. Here, myofibroblasts are heavily involved in the production and preservation of the tumor microenvironment; the so called 'niche' or stroma where myofibroblasts and epithelial cell signalling and cross-talk promotes changes in epithelial cells towards more aggressive cancers^{10,11}. Moreover, fibroblasts are also involved in other pathologies such as fibrosis, inflammation and arthritis which make their activity also

a potential target for new therapeutics. For all these reasons, two epithelial cancer cells, HCT116 and MGLVA-1 and one fibroblastic cell line, Swiss Albino 3T3 fibroblasts, were chosen for the study and characterized for the presence of clathrin and caveolin that are involved in the two best characterized endocytic pathways.

In this chapter a series of experiments were carried out to define the experimental settings for the studies of endocytosis inhibition. The investigation of different routes of uptake in different cell lines was carried out with human transferrin (Htf) and lactosylceramide (LacCer). These two molecules are widely accepted markers of clathrin-dependent and -independent endocytosis¹². Chlorpromazine (CPZ) and methyl beta cyclodextrin (MBCD) have been widely used as pharmacological inhibitors of clathrin-dependent and -independent endocytosis^{13,14}. As the specificity of both CPZ and MBCD have been questioned in the past, the inhibition experiments with each marker of endocytosis were carried out in the presence of both pharmacological inhibitors to spot any non-specific inhibition of endocytosis¹³⁻¹⁵. The extent of inhibition was measured by flow cytometry as this technique gives a better snapshot of the rate of internalization of markers of endocytosis at the single cell level and can detect also small shifts in inhibition of endocytosis in a statistically robust way. Finally, as both CPZ and MBCD have been reported as cytotoxic, a thorough characterization of their cell activity was carried out¹⁶⁻²⁴. The effects of MBCD on cell activity was tested with both MTT and Cell Titer Glo while CPZ was investigated with MTT, Cell Titer Glo and Apo I assays.

3.2 Methods

3.2.1 C-PB size and charge characterization

Detailed information on the DLS and TEM methods used to characterize 50 and 100 nm C-PB can be found in the materials and methods §§ 2.2.2 and 2.2.3. Briefly, for

Results - Characterization of Materials and Cell lines

DLS studies, 50 and 100 nm C-PB were diluted to 200 µg/ml and 50 µg/ml in filtered PBS buffer, vortexed for 1 minute to remove aggregates of nanoparticles and 10 µl of the nanoparticles suspension loaded into a quartz micro-cuvette in a DLS reader previously equilibrated to 20°C. The DLS equation settings were updated for the PBS buffer, and the mean size of nanoparticles was given by 10 replicates measurements. These measurements were repeated 3 times, averaged and plotted in GraphPad Prism.

For TEM, the nanoparticles were diluted to 25 or 26.5 µg/ml in PBS, loaded on a copper grid and allowed to dry overnight. The day after, a minimum of 12 TEM images were collected for a minimum of 250 nanoparticles counts. Nanoparticle sizes were measured from images with ImageJ software and data plotted in GraphPad Prism. The coefficient of variance for the TEM and DLS measured size was calculated as follows:

$$CV\% = \left(\frac{\sigma}{M}\right) \cdot 100$$

Were CV% = coefficient of variance %

σ = STDEV

M = mean size of the nanoparticles

ζ potential measurements were carried out in HEPES buffer 1 mM, Ph 7.4 at 20°C at concentrations of C-PB of 200 µg/ml. The results are reported as the mean of 12 measurement replicates.

3.2.2 Cell viability studies of C-PB, MBCD and CPZ

3.2.2.1 Cell viability assays titration curves and statistical analysis

The seeding density of cells to obtain a linear relationship between numbers of cells and viability signal was investigated by a titration curve for MTT and Cell Titer Glo

Results - Characterization of Materials and Cell lines

prior to toxicity tests. Different titration curves were run for different time of incubations. For a more detailed description of the procedures used to obtain the titration curves please refer to §§ 2.2.5.1 and 2.2.5.3. Briefly, cells were counted and seeded at densities ranging from 312000 to 1985 cells/cm² and incubated overnight. The day after, the media was aspirated off and HBSS/HEPES 20 mM added to cells for the desired time-length. Upon completion of the incubation time, the cells were treated according to the standard assay protocol and colorimetric or luminescence signals recorded.

For all toxicity tests the Z factor and Signal Window were calculated according to the formulae below:

$$Z \text{ Factor} = 1 - \left(\frac{(3xSD_{p.c.} + 3xSD_{n.c.})}{|Mp.c. - Mn.c. |} \right)$$

(25)

$$\text{Signal Window} = \left(\frac{[Mn.c. - Mp.c. - 3x(SD_{p.c.} + SD_{n.c.})]}{SD_{n.c.}} \right)$$

(26)

Where:

SD_{p.c.} = Standard Deviation of the positive control

SD_{n.c.} = Standard Deviation of the negative control

M_{p.c.} = Mean of the positive control

M_{n.c.} = Mean of the negative control

These two parameters were calculated to confirm that there was sufficient separation from the signal between negative and positive control at the chosen concentration of

Results - Characterization of Materials and Cell lines

cells for cell viability studies and hence the studies carried out were producing good quality and reliable cell viability data.

3.2.2.2 Metabolic activity (viability) of cells in the presence of C-PB

Studies at 4 h of C-PB of 50 and 100 nm in cells were carried out in triplicate wells in 3 independent experiments. Effects of C-PB were investigated by MTT and Cell Titer Glo assays. Only one replicate for MTT viability tests at 24 and 48 h were carried out with 50 nm C-PB in triplicate wells. For a thorough description of the methods used please refer to §§ 2.2.5.1 and 2.2.5.3. Briefly cells at a density of 31200 cells/cm² were seeded in a 96 well plate and allowed to attach to the wells overnight. The day after the media was replaced with serial dilutions of C-PB in HBSS/HEPES 20 mM, for C-PB concentrations ranging from 1 to 1000 µg/ml and a negative control consisting of assay media (HBSS/HEPES 20 mM) or PEI 0.5 mg/ml positive control, in triplicate wells. The same serial dilutions were placed on 96 well plates without cells for a blank reading for both the MTT and the Cell Titer Glo assays and blank values subtracted from the absorbance/luminescence readings on the C-PB with cells. C-PB of 50 and 100 nm were incubated for 4 h, 50 nm C-PB were also tested with an MTT at 24 and 48 h. Upon completion of the incubation time MTT or Cell Titer Glo were applied according to standard protocols. Acquired absorbance and luminescence measurements were normalised against the negative control that was assumed being the 100% viability of cells.

3.2.2.3 Studies on the effects of MBCD on cell viability

The effects of MBCD on cells were carried out in triplicate wells for a minimum 3 independent experiments using the MTT and Cell Titer Glo assays. For a more complete description of the methods used refer to §§ 2.2.5.1 and 2.2.5.3. Briefly, cells at a density of 31200 cells/cm² were seeded in a 96 well plate and allowed to attach

to the wells overnight. The day after the media was replaced with serial dilutions of MBCD in HBSS/HEPES 20 mM, for concentrations ranging from 0.33 to 10 mM. Each assay presented also a positive control consisting of PEI 0.5 mg/ml, a negative control of cells in HBSS/HEPES 20 mM only and a blank reading in HBSS/HEPES 20 mM assay media devoid of cells. MBCD was incubated for 4.5 h and upon completion of the incubation time MTT or Cell Titer Glo were applied according to manufacturer protocols. Acquired colorimetric and luminescence measurements were normalised against the negative control that was assumed being the 100% viability of cells.

3.2.2.4 Effects of CPZ on cell viability

A thorough investigation of the effects of CPZ was carried out using MTT, Cell Titer Glo and Apo I caspase 3/7 viability assays. Studies using CPZ were carried out in triplicate wells in 3 independent experiments. Cells were seeded in 96 well plates for MTT and Cell Titer Glo and on 384 well plate for Apo I caspase 3/7 assay. For a thorough description of the methods used please refer to § 2.2.5.1 for the MTT, § 2.2.5.3 for Cell Titer Glo and § 2.2.5.2 for Apo I. Briefly cells at a density of 31200 cells/cm² were allowed to attach to the wells overnight. The day after the media was replaced with serial dilutions of CPZ in HBSS/HEPES 20 mM, for concentrations ranging from 10 to 457 µM and incubated for 4.5 h. Upon completion of the incubation time, MTT, Cell Titer Glo and Apo I caspase 3/7 were applied according to standard protocols.

3.2.3 Immunofluorescence of clathrin heavy chain isoform α (CHC α) and caveolin-1 (cav-1) in 3T3, HCT116 and MGLVA-1

A more extensive description of these methods can be found at § 2.2.13. Here, 3T3 mouse fibroblasts, MRC-5 human fibroblasts, HCT116 human colon cancer and MGLVA-1 human gastric cancer cells were seeded at a density of 31200 cells/cm² and allowed to attach to glass coverslips or 25 cm² flasks overnight. The day after,

Results - Characterization of Materials and Cell lines

cells were washed and fixed for 30 min at room temperature with PFA 4% v/v for confocal microscopy or trypsinized and pelleted at 2000 g for 5 min before fixation for flow cytometry. Rinsed cells were treated with PBS, 0.3% v/v Triton, 5% v/v goat serum blocking buffer for 1.5h. Subsequently, the blocking buffer was gently removed with a pipette tip, and anti-CHC α mouse IgG1mAb (Immunoglobulin G1 monoclonal antibody, clone X22) 0.12 μ g/ml and anti-caveolin-1 isoform α mouse IgG1mAb (clone 2297) 0.83 μ g/ml incubated for further 1.5 h. Mouse IgG1 was utilised as a negative control at concentrations of 0.12 μ g/ml for clathrin IgG1 negative control and 0.83 μ g/ml for cav-1 IgG1 negative control. An additional negative control consisting of cells treated only with secondary antibody were incubated with PBS, 1% w/v BSA, 0.3% v/v Triton. Upon completion of the incubation time, cells were rinsed and treated with goat anti-mouse (H+L) IgG1 AlexaFluor 488 nm or 594 secondary antibody overnight at 4°C. The following day, the secondary antibody was removed and cells washed with PBS. Cells prepared for microscopy were removed from the wells with the aid of a needle and tweezers, further stained with Prolong Gold Antifade DAPI mounting media, applied on glass slides and left to dry at room temperature in the dark overnight. The following day, coverslips edges were sealed to the glass slides with nail polish and stored at 4°C until use on a Zeiss LSM 700 confocal microscope. Cells prepared for flow cytometry were resuspended in PBS. Flow cytometry data were acquired with a BD LSR II flow cytometer with a FITC 530/30 bandpass optical filter and analysed with Weasel software and plotted in GraphPad Prism.

To verify that the binding affinity of the mAb was comparable between human and murine proteins, CHC α and cav-1 protein 3D rearrangement were compared to the human sequences with ICOS protein 3D simulator software, where a score ranging between 0 and 4 was given for the amino acids (aa) more or less exposed to the surface of the protein and external environment.

3.2.4 Wash efficiency studies for the removal of markers of endocytosis

A detailed description of the methods carried out in these experiments can be found in the general materials and methods section at § 2.2.6.

Briefly, two wash procedures were attempted to verify the removal of membrane bound endocytic markers: one with adherent cells in 25 cm² flasks and another in Eppendorf tubes and cell suspensions. The wash solutions used for both Htf and LacCer removal were the traditional buffers reported in the literature^{27,28}. The buffer wash procedures used to remove membrane bound Htf consisted of 2 rinses with ice cold HMEM-G+I, on ice (HMEM without glucose supplemented with 10 mM HEPES and 5 mM sodium azide to inhibit metabolic activity) followed by 1 minute ice cold wash with 0.2 mM acetic acid 0.2 mM NaCl buffer pH 4.6²⁷. The acidic wash was then followed by 2 cold washes of HMEM-G/HEPES/NaN₃ on ice.

The buffer wash methods for removal of membrane bound LacCer consisted of two ice cold washes with HMEM-G+I followed by 6 rinses (10 minutes each, on ice) of HMEM-G+I supplemented with 5% w/v BSA (back exchange method)²⁸.

3.3 Results

3.3.1 Size and Charge Characterization of 50 nm C-PB

Polysciences described C-PB as in the size range of 50 nm ±15% coefficient of variance. DLS studies of the 50 nm C-PB showed that the measured sizes of the materials were in general agreement with the sizes stated by the manufacturer (Figure 3-1A). DLS intensity, mass and number distribution ranges of the diameter of the nanoparticles reported a mean size of 57 nm. However, the coefficient of variance for intensity, mass and number distributions were higher than those stated and equal to ±39.7%. TEM measurements (Figure 3-2A) indicated a mean diameter of 30 nm

Results - Characterization of Materials and Cell lines

and a coefficient of variance of $\pm 29\%$. Figure 3-4A shows a TEM picture of 50 nm C-PB. From TEM data the diameters of C-PB ranging between 20 and 40nm accounts for 286 events while the edges of the Gaussian distribution (from 5 -19 to 41 – 70 nm) account for 51 events.

Z potential measurements revealed a charge of -37.7 mV.

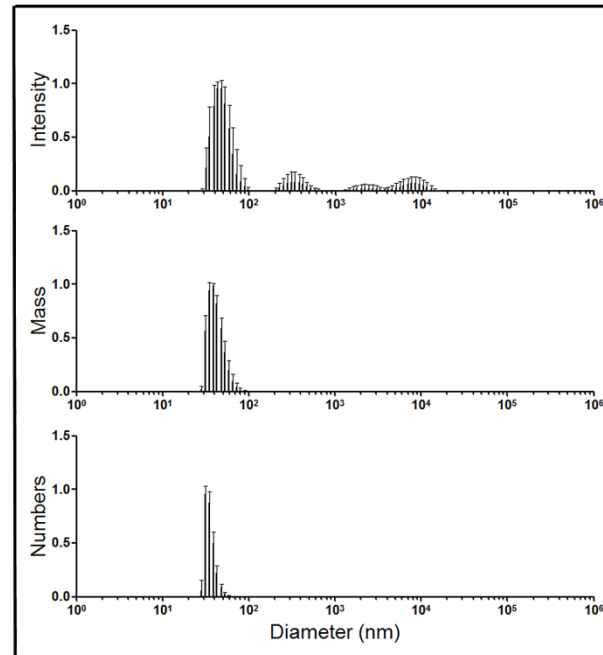
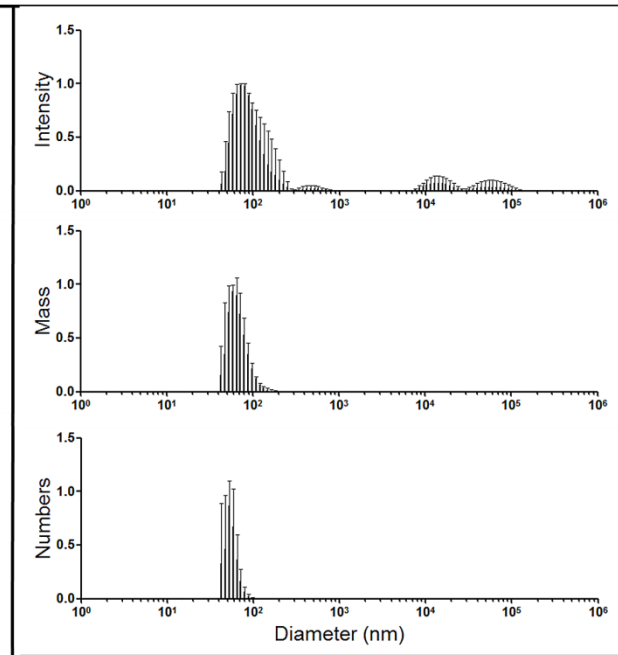
A. 50nm C-PB**B. 100nm C-PB**

Figure 3-1 DLS characterization of 50 and 100 nm C-PB shown as intensity, mass and number plots (A and B). 100 nm CPB intensity peak is broad and the data fit a double Gaussian distribution. 50 and 100 nm C-PB were diluted to 200 $\mu\text{g/ml}$ and 50 $\mu\text{g/ml}$ in filtered PBS buffer, vortexed for 1 minute and loaded into a quartz micro-cuvette in a Malvern Instruments Viscotek 802 DLS reader previously equilibrated to 20°C. The DLS equation settings were updated for the PBS buffer, and the mean size of nanoparticles was given by 10 replicates measurements. This procedure was repeated 3 times and data plotted in GrapPad Prism. Intensity, mass and number distributions of the 50 nm C-PB report a peak diameter of 57nm. Intensity measurements for 100 nm C-PB shows a broader peak that corresponds to a double population of nanoparticles. Peak diameter is at 108 nm for intensity, 71 nm for mass and 67 nm for number distributions.

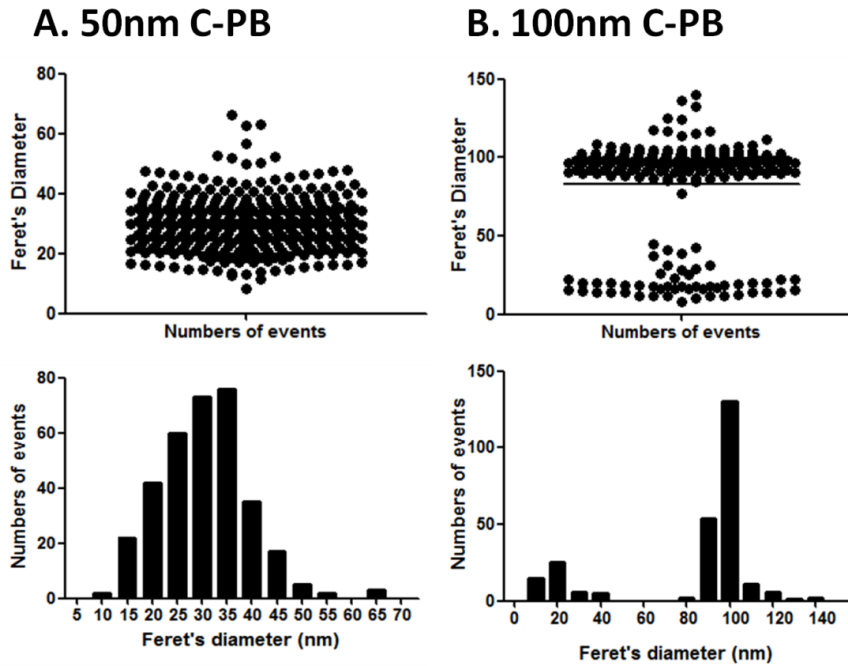


Figure 3-2 TEM's plot of Feret's diameter measurements confirming the presence of a second population of smaller nanoparticles for 100 nm C-PB. The measurements were obtained from 12 images and a minimum of 250 nanoparticles for 50 and 100 nm C-PB. C-PB were diluted to 25 $\mu\text{g}/\text{ml}$ and 26.5 $\mu\text{g}/\text{ml}$ in PBS, loaded on a copper grid and allowed to dry overnight. The day after, a minimum of 12 TEM images were collected for a minimum of 250 nanoparticles counts. Nanoparticle sizes were measured with ImageJ software and data plotted in GraphPad Prism. TEM data confirm the DLS findings: 50 nm C-PB present a single but slightly broad size distribution with a maximal peak at 30 nm while 100 nm C-PB showed two main populations at 20 and 100 nm.

3.3.2 Size and Charge Characterization of 100 nm C-PB

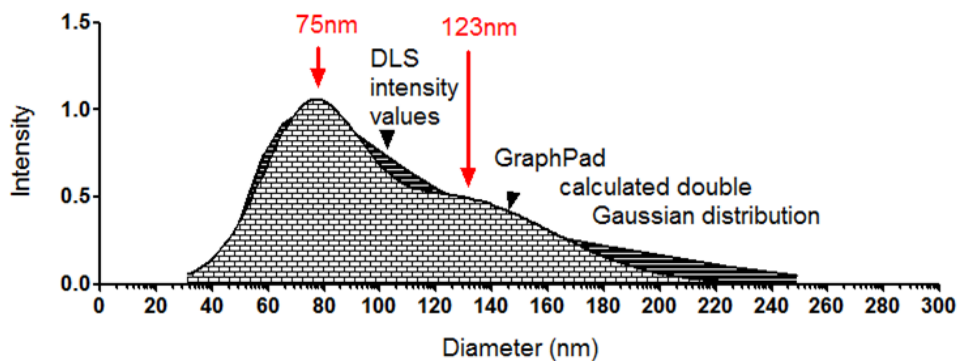
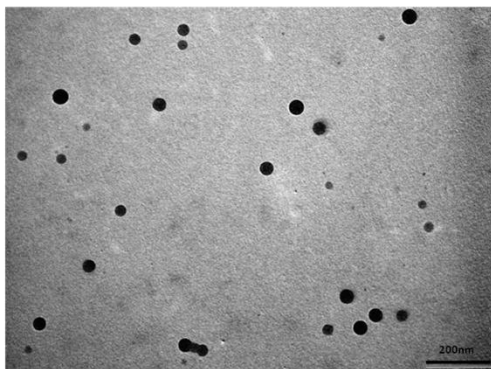


Figure 3-3 Intensity DLS data for 100 nm C-PB fit a double Gaussian distribution. The double Gaussian distribution was calculated by GraphPad Prism. Here, two sizes of nanoparticles are measured with peak diameters at 75 nm and 123 nm (red arrows).

A. 50nm C-PB



B. 100nm C-PB

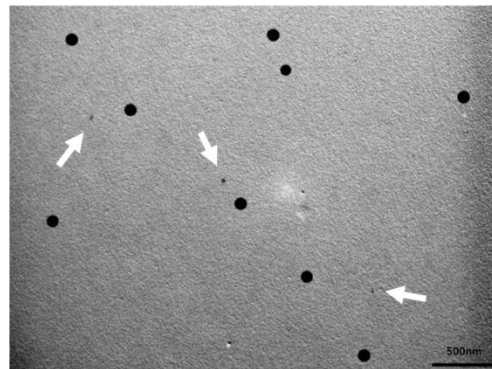


Figure 3-4 TEM images of 50 nm (A) and 100 nm (B) C-PB. The arrows on picture B point to the smaller particles sizes detected also by DLS. TEM measurements report a size of around 20 nm for the second population of nanoparticles (about 5% of the total population of cells). Scale bar for 50 nm C-PB: 200nm; Scale bar for 100 nm C-PB: 500 nm.

Polysciences described the C-PB as 100 nm \pm 10% coefficient of variance. DLS data (Figure 3-1B) reported a mean of 108 nm and coefficient of variance of 45% for the intensity values, a mean of 71 nm and \pm 93% variance for the mass and a mean of 67 nm and \pm 80% variance for the number distributions. Furthermore, the analysis of the DLS intensity values revealed a double Gaussian distribution with mean diameter values at 75 and 123 nm (Figure 3-3). TEM data (Figure 3-2B) reported a mean value of 83 nm and a coefficient of variance of \pm 39% for the main peak of nanoparticles. The size range 90-110 nm accounts for 195 events with 11 off peak events in total for nanoparticles size of 80-89 nm and 111-140 nm. However, a second peak of materials was detected around 20 nm. The size distribution of this peak ranged between 10 and 40 nm for a total of 51 events (5% of the total) and was also confirmed in TEM data where two size populations were visible at 20 and 100 nm diameters. Picture 3-4B shows the smaller population of nanoparticles (arrows). Z potential measurements revealed a charge of -34.2 mV.

3.3.3 Cell viability studies of C-PB, CPZ and MBCD

3.3.3.1 Cell viability assays titration curves and statistical analysis

Titration curves obtained with MTT and Cell Titer Glo at 4.5h are shown in Figure 3-5, titration curves with MTT at 24 and 48 h are shown in Figure 3-6. The titration curves show that the density used in toxicity assays of 31200 cells/cm² is within the linear correlation range between number of cells and detection signal. To further confirm these results, statistical measurements of the Z factor and Signal Window measured for negative and positive controls were also calculated for MTT, Apo I and Cell Titer Glo assays and are shown in Table 3-1. The statistical analysis confirms that the concentration of cells used for all endocytosis experiments was also suitable for toxicity studies. The Z factor and Signal Window calculated for the MTT tests at 24 and 48 h are reported in Table 3-2. The Z factor values range between 0.9 and 0.6, which correspond to excellent assays according to Zhang's classification while Signal Window values range between 1.4 and 34 corresponding to ideal and acceptable assays according to Iversen's classification (Table 3-1,3-2 and 3-3)^{25,26}

Results - Characterization of Materials and Cell lines

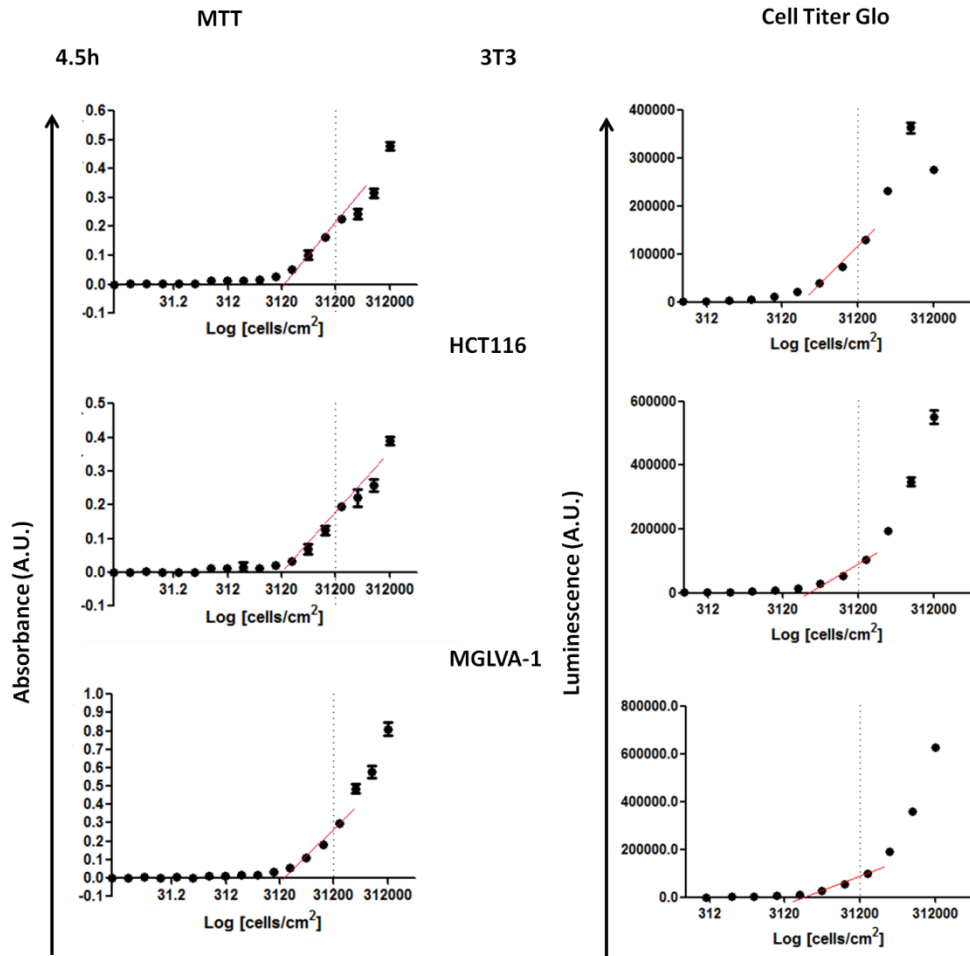


Figure 3-5 MTT and Cell Titer Glo titration curves for 3T3, HCT116 and MGLVA-1 cells showing a linear correlation between numbers of cells and signal from viable cells at the concentration used for toxicity tests and inhibition studies (red dotted lines). The readings were obtained at 4.5 h in HBSS/HEPES 20 mM for both MTT (left) and Cell Titer Glo (right). The upper density of cells for both assays was set to 312000 cells/cm² and was diluted 2-fold to achieve the minimum detection limit for the assay. Cell viability assays should be set within this linear detection region in order to obtain a linear correlation between signal and number of cells. Error bars represent the standard deviation of the mean (n=3).

Results - Characterization of Materials and Cell lines

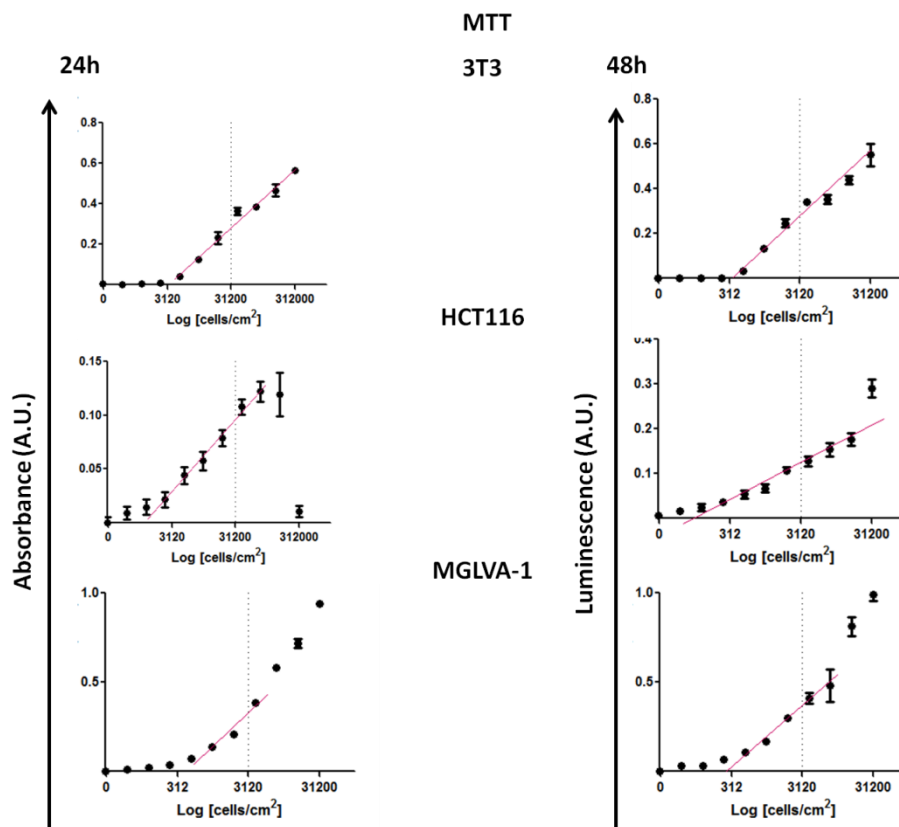


Figure 3-6 MTT titration curves for 3T3, HCT116 and MGLVA-1 cells at 24 and 48 h showing a linear correlation between number of cells and signal from viable cells at the concentrations of cells used for toxicity and inhibition studies (dotted lines). Error bars represent the standard deviation of the mean (n=3).

	Toxicity assay					
	MTT		Cell Titer Glo		Apo I	
Statistical analysis	Z factor [*]	Signal Window ^{**}	Z factor [*]	Signal Window ^{**}	Z factor [*]	Signal Window ^{**}
3T3	0.8	8	0.7	9.9	0.7	26.5
HCT116	0.6	1.9	0.6	16	0.7	8
MGLVA-1	0.6	1.4	0.5	2.8	0.9	12

Table 3-1 Statistical analysis to confirm that the cell density of 31200cells/cm² was suitable for cell viability studies. For MTT, Cell Titer Glo and Apo I toxicity assays, the Z factor and Signal Window in the 3 cell lines used was calculated against the positive and negative control signal values for each test according to equations described in the material and methods. (*²⁵, **²⁶).

Results - Characterization of Materials and Cell lines

	MTT			
	24h		48h	
Statistical analysis	Z factor*	Signal Window**	Z factor*	Signal Window**
<i>3T3</i>	0.9	34	0.7	8
<i>HCT116</i>	0.9	11	0.8	12
<i>MGLVA-1</i>	0.9	28	0.6	5

Table 3-2 Statistical analysis to confirm that the cell density used for MTT assays at 24 and 48 h was giving a good separation between negative and positive control according to ²⁵(*) and ²⁶(**).

Reference values *,**			
Z Factor*		Signal window**	
range	comments	range	comments
Z=1	Ideal*	SW>2	Recommended **
1>Z≥0.5	Excellent *	1>SW>2	Acceptable**

Table 3-3 Reference values for Z factor and Signal Window provided according to ²⁵ (*) and ²⁶ (**).

3.3.4 C-PB cell viability studies

Cell viability studies at 4 h incubation were mainly in agreement for the effects of 100 nm C-PB and generally showed very little toxicity of the nanoparticles with broad IC₅₀ values due to low toxicity.

In contrast, 50 nm C-PB were found to be more detrimental for cell viability in both tests, with the largest effects shown in the MTT assay. The IC₅₀ values of 50 nm C-PB were cell dependent and the IC₅₀ and 95% confidence interval at 4 h for 50 nm C-PB with an MTT and Cell Titer Glo tests are summarised in Table 3-4. No signs of cell toxicity were detected by the visual examination of cells treated with both 50 and 100 nm C-PB under a reverse microscope for concentrations up to 100 µg/ml.

Results - Characterization of Materials and Cell lines

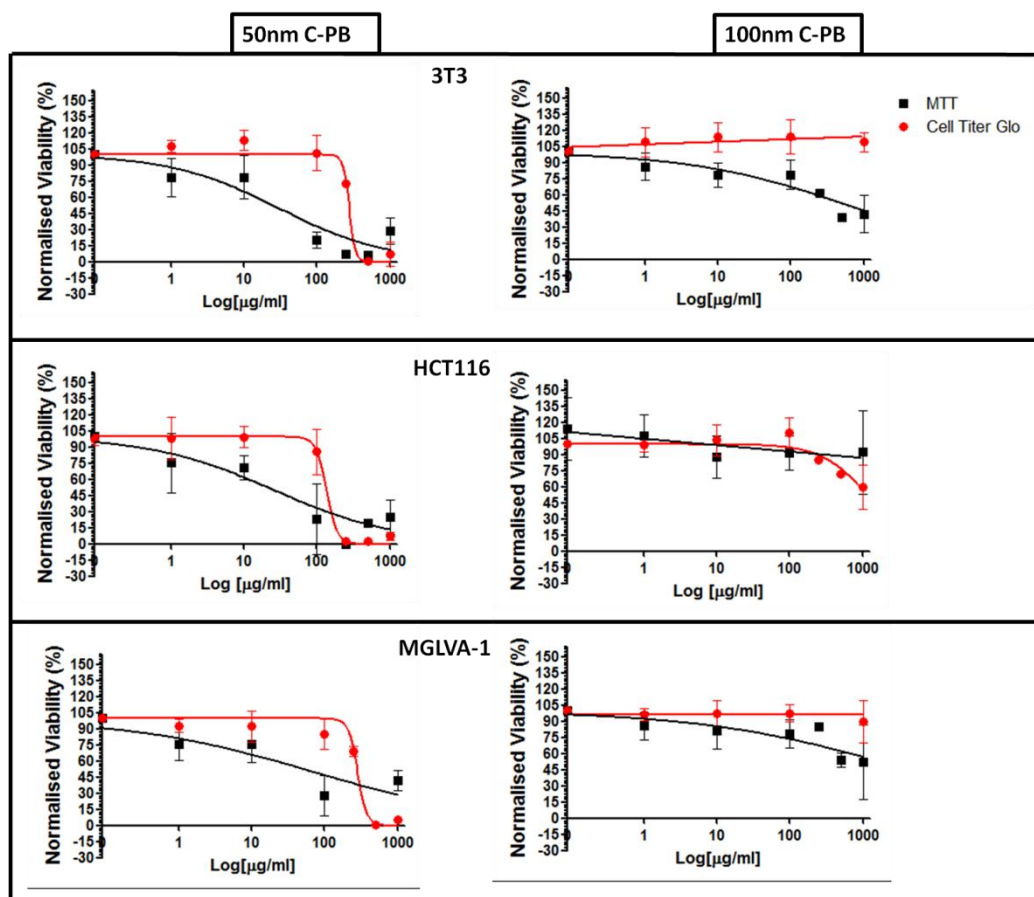


Figure 3-7 Biocompatibility studies of 50 and 100 nm C-PB at 4 h in 3T3, HCT116 and MGLVA-1 cells. Metabolic activity as a proxy for toxicity was detected with MTT (black lines and squares in the graphs) and Cell Titer Glo assays (red lines and circles in the graphs). Error bars represent the standard deviation of the mean (n=3).

As a consequence, a preliminary screening with an MTT of 50 nm C-PB was also run at 24 and 48 h (Figure 3-8 and Table 3-4). Results are based on one experiment only and show that the MTT assay does not report the same low viability for 50 nm C-PB. The IC_{50} and 95% confidence intervals at 24 and 48 h incubation of 50 nm C-PB are summarised in Table 3-4. Z factor and Signal Windows for 3T3 cells at 24 h were equal to 0.8 and 12.2 respectively and 0.9 and 34 at 48 h corresponding to an excellent assay for the Z factor values and a recommended value for the Signal Window according to Zhang's and Iversen's classification. Z factor for HCT116 at 24 h was equal to 0.6 and a Signal Window of 5, Z factor of 0.8 and Signal Window of 11 at 48 h. In MGLVA-1 cells the Z factor at 24 h was equal to 0.7 and Signal Window of 8 and 0.9 and 28 for the Z factor and Signal Window at 48 h. the reported Z factor

Results - Characterization of Materials and Cell lines

values correspond to an excellent assay, Signal Windows values correspond to a recommended assay. The IC₅₀ results reported above refer to one single experiment replicate for 50 nm C-PB incubated at 24 and 48 h¹.

	50nm C-PB							
	4h				24h		48h	
	MTT		Cell Titer Glo		MTT		MTT	
	IC50	95% CI	IC50	95% CI	IC50	95% CI	IC50	95% CI
3T3	30	12-71	276	72-1056	309	213-450	312	213-450
HCT116	27	8-81	135	70-261	271	196-373	341	251-463
MGLVA-1	72	19-337	283	237-337	197	134-284	338	246-465

Table 3-4 Summary of the IC₅₀ and 95% confidence intervals obtained with MTT and Cell Titer Glo triplicate experiments at 4 h incubation of 50 nm C-PB and preliminary results from one experiments only with an MTT assays at 24 and 48 h incubation. The values are expressed in µg/ml of C-PB.

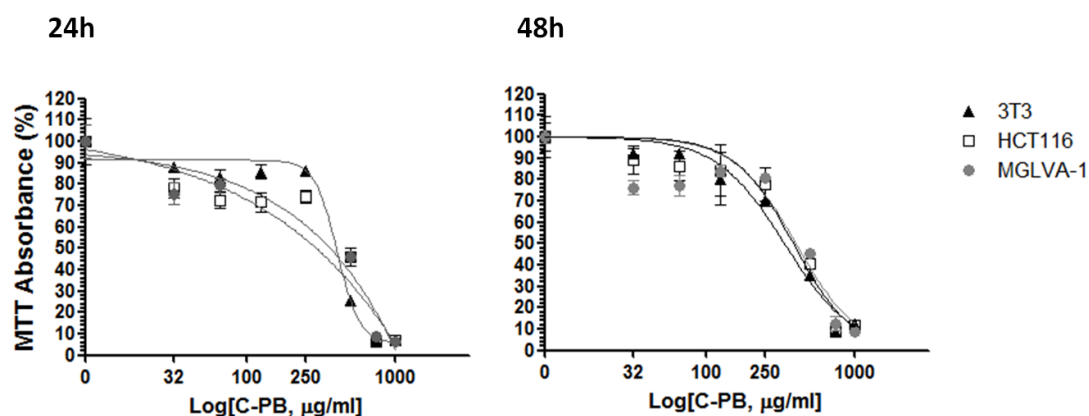


Figure 3-8 MTT toxicity assay of 50 nm C-PB at 24 and 48 h incubation in HBSS/HEPES 20 mM in 3T3 (black triangles and connecting line), HCT116 (white squares and black connecting line) and MGLVA-1 cells (grey circles and connecting lines). The results report the mean and standard deviation of a pilot study experiment obtained from triplicate wells. The experiments were not repeated due to lack of time. Error bars represent the standard deviation of the mean of triplicate wells (n=1).

3.3.5 Characterization of the viability of cells treated with MBCD

MBCD reduction of viability of cells was tested with both MTT and Cell Titer Glo toxicity studies of MBCD reported no toxicity for MBCD at concentrations up to 10 mM (Figure 3-9A, B and C). Although the toxicity of this drug was low, from the MTT inhibition curves it was possible to measure IC₅₀ values. MBCD in 3T3 cells had an

¹ The experiments were not repeated because of lack of time.

Results - Characterization of Materials and Cell lines

IC₅₀ value of 140.8 mM; in HCT116 the IC₅₀ was 15.5 mM while MGLVA-1 presented an IC₅₀ of 10.6 mM. However, the IC₅₀ 95% confidence intervals (IC50_{95%}) were very broad limiting the reliability of such values. As both toxicity tests were in agreement no further tests on the effects of MBCD on cells were carried out.

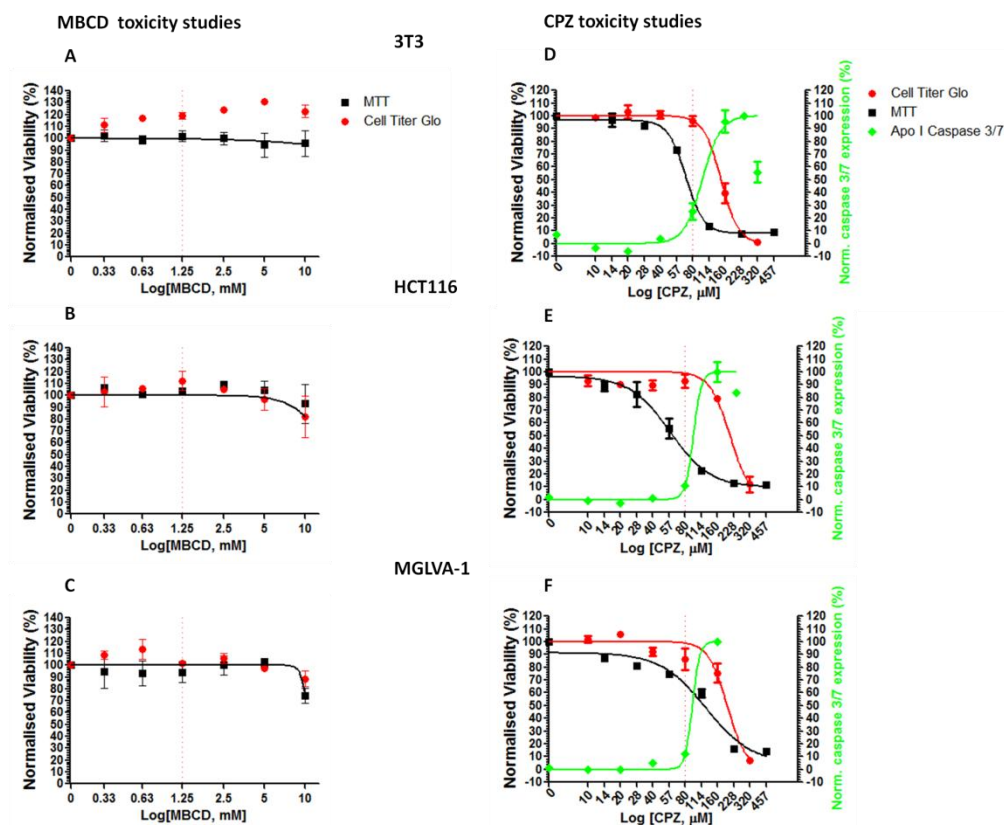


Figure 3-9 MBCD (left) and CPZ (right) toxicity studies at 4.5 h with MTT (black lines and squares), Cell Titer Glo (red lines and circles) and Apo I caspase 3/7 (green lines and diamonds) in 3T3, HCT116 and MGLVA-1 cells. From graphs A, B and C it is possible to appreciate the low toxicity of MBCD at the concentration used in endocytosis inhibition studies of 1.25 mM (red dotted line in the graph) and the marked difference in cell viability of cells treated with CPZ reported in 3 different assays at 80 µM (red dotted line in the graph). 80 µM was the highest concentration used for endocytosis inhibition studies. Cells were seeded in triplicate wells and treated with different concentrations of inhibitors of endocytosis for 4.5 h. After the incubation time cells were processed as from standard protocol for each test and data recorded and normalised against the positive control assumed to be 100% viability or 0% caspase 3/7 expression. Error bars represent the standard deviation of the mean (n=3).

3.3.6 Characterization of the effects on cells of CPZ

The effects of CPZ (Figure 3-9, D, E and F, Table 3-5) was analysed by the 3 different viability tests: MTT Cell Titer Glo, and Apo I caspase 3/7, which quantifies

Results - Characterization of Materials and Cell lines

the presence of apoptotic caspase 3/7 enzyme activity. MTT, Cell Titer Glo and Caspase 3/7 IC₅₀ ± CI_{95%} of CPZ are reported in Table 3-5. No visible signs of cell toxicity were detected after examination under a reverse microscope for concentrations of CPZ up to 80 µM.

	CPZ 4.5h					
	MTT		Cell Titer Glo		Apo I	
	IC50	95% CI	IC50	95% CI	IC50	95% CI
3T3	73	68-77	147	143-151	96	86-107
HCT116	64	54-75	211	200-223	147	144-151
MGLVA-1	112	102-123	197	187-209	93	64-134

Table 3-5 IC₅₀ and 95% confidence intervals calculated with 3 different cell viability tests: MTT, Cell Titer Glo and Apo I caspase 3/7 activity at 4.5 h. Results are expressed in µM.

3.3.7 Clathrin and caveolin immunocytochemistry studies

The qualitative and quantitative characterization of CHCα and cav-1 proteins in the cell lines intended for endocytosis inhibition studies was carried out by both confocal microscopy and flow cytometry. Flow cytometry (Figure 3-10) and fluorescence microscopy data (Figures 3-11 and 3-12) show that HCT116 cells expressed high levels of CHCα, while MGLVA-1 cells expressed high levels of cav-1. Furthermore, 3T3 murine fibroblastic cells presented a low fluorescence for CHCα and cav-1 and these results were reproducible over triplicate experiments. To confirm that the levels of immunostaining were comparable to the levels in human mesenchymal cells, expression of caveolin-1 was characterised by flow cytometry and confocal microscopy experiments using MRC-5 human fibroblasts (Figures 3-10, 3-12). The data report consistently similar levels of the immunostaining of the protein in the human and mouse cell lines.

Results - Characterization of Materials and Cell lines

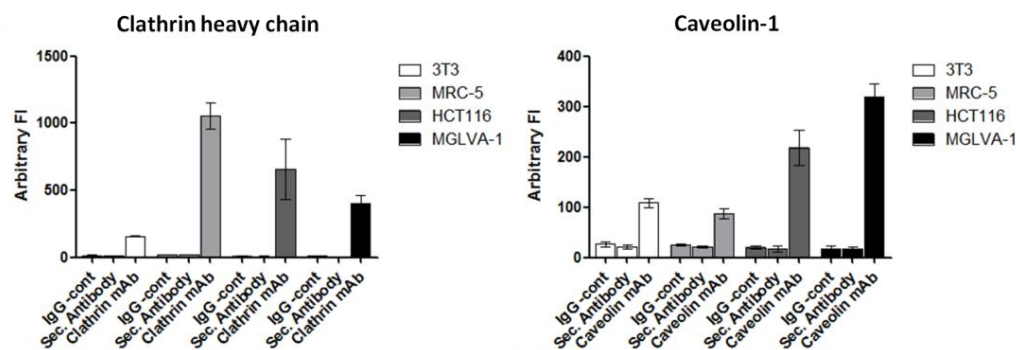


Figure 3-10 CHC α and cav-1 flow cytometry immunofluorescence quantification. The plot shows a merge of 3 independent replicates of immunocytochemistry experiments. Here, the expression of CHC α and cav-1 were investigated in the 3 cell lines used for endocytosis studies (3T3, HCT116 and MGLVA-1). An additional human mesenchymal cell line was characterised and used to compare the expression of the 2 endocytic proteins in human and mouse fibroblasts. Error bars represent the standard deviation of the mean (n=3).

The same approach was undertaken to confirm the reliability of immunofluorescence experiments with CHC α in mouse 3T3 cells. However, immunocytochemistry experiments showed that human CHC α levels in MRC-5 were high and this contrasted with the level of CHC α found in 3T3 cells. To further probe that there were unlikely to be any differences in binding of anti-human antibody to human and murine cav-1, murine cav-1 was compared to the human sequence with ICOS protein 3D simulator software where a score ranging between 0 and 4 was given for the amino acids (aa) more or less interacting in the 3D structure of the protein and/or exposed to the external environment. The simulation reported a different score for murine and human antibody epitope regions of cav-1 both when analysing only the exposure to the solvent of the epitope region and when analysing the total 2D and 3D rearrangements of the protein. This suggested that the murine protein rearranged in a 3D structure that did not resemble the human cav-1 in the epitope region and subsequently the mAb could potentially bind to the two regions with different strength and affinity (Appendices I and II)²⁹⁻³¹.

Results - Characterization of Materials and Cell lines

To verify that the binding affinity of the mAb was comparable between human and murine proteins, mouse CHC α protein 3D rearrangement was compared with the human sequences with ICOS protein 3D simulator software. The prediction suggested that the 2 point mutations were sufficient to modify the 3D structure and the exposure to the solvent of the epitope region recognised by the mAb. In other terms, the aa in the epitope region did not present the same 3D architecture and exposure to the solvent in human CHC α and murine CHC α according to the simulation (Appendices III and IV). From these data it is possible to suggest that the low expression of CHC α in 3T3 cells might not be genuinely due to the level expression of cav-1 and CHC α .

Finally, cav-1 levels in the epithelial cells tested were represented by a broad peak or dot plot suggesting that within the same cell line some cells might have expressed more cav-1 than others (Figure 3-13).

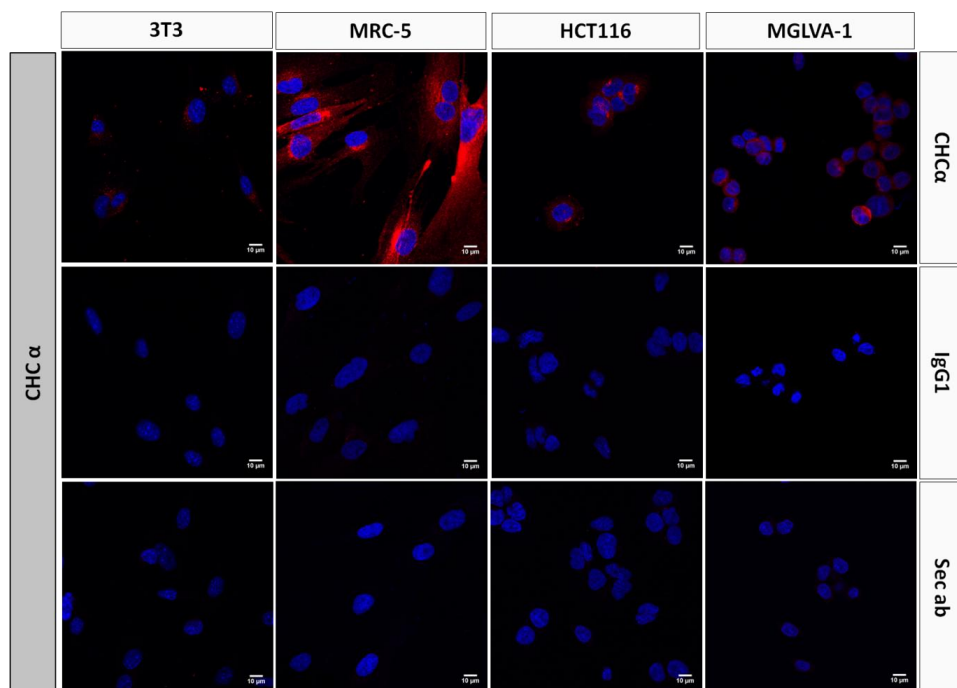


Figure 3-11 Qualitative immunocytochemistry confocal microscopy experiments for the detection of CHC α in 3T3, MRC-5, HCT116 and MGLVA-1. Here two negative controls were used: IgG1 and the secondary antibody. Blue fluorescence: nuclei (Dapi), Red fluorescence: CHC α , IgG1 or Secondary antibody (Sec. Ab.). Scale bars represent 10 μ m.

Results - Characterization of Materials and Cell lines

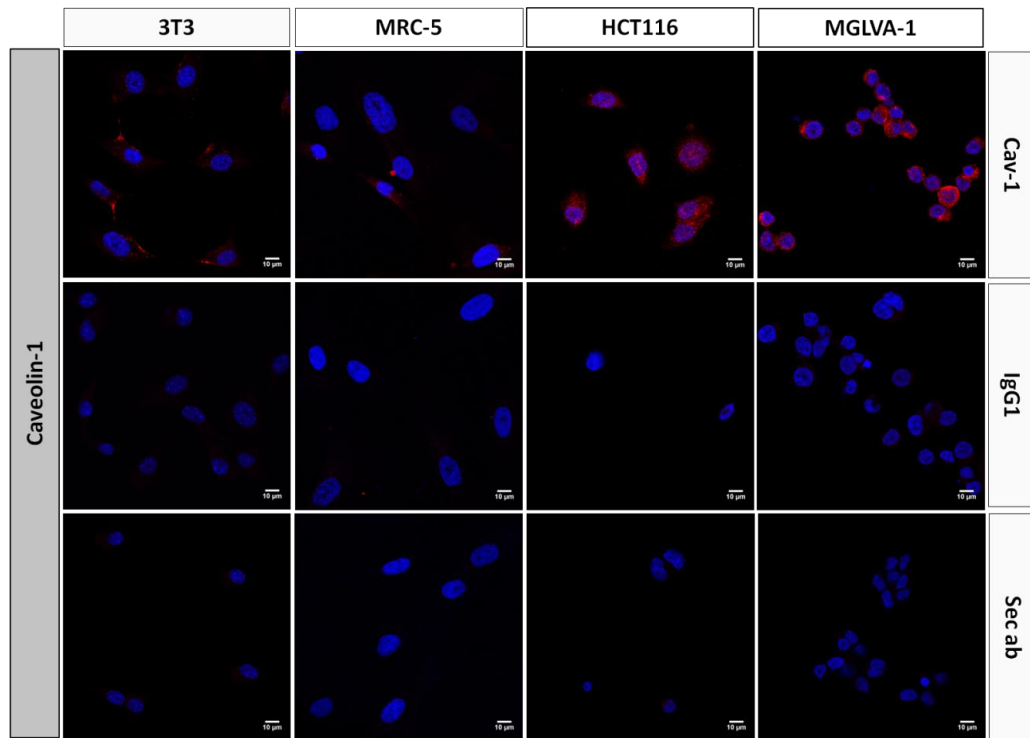


Figure 3-12 Immunocytochemistry confocal microscopy images of the staining of cav-1 in 3T3, MRC-5, HCT116 and MGLVA-1 cells. The above pictures show the blue fluorescence of the nuclei (Dapi) and the red fluorescence of cav-1 (first row of pictures), IgG1 and secondary antibody (Sec ab.) negative controls (second and third row of pictures). Scale bars represent 10 μm.

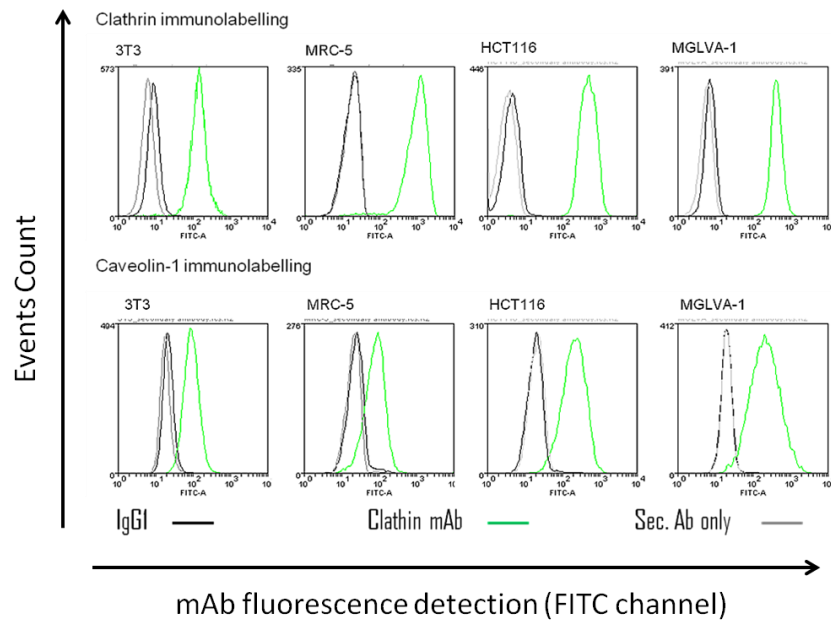


Figure 3-13 Histograms of the fluorescence intensity for Clathrin mAb X22 / Caveolin-1 mAb clone 2297 immunolabelling (Green), IgG1 (Black) and AlexaFluor 488 secondary antibody (Grey) negative controls in 3T3 murine fibroblasts, MRC-5 human lung fibroblasts, HCT116 human colon carcinoma and MGLVA-1 human gastric cancer cells.

3.3.8 Wash efficiency studies of endocytosis markers

Experiments were designed to verify that the surface-bound ligands used as markers of endocytosis were efficiently removed to ensure that only the fluorescence of internalised markers was detected. Results of the wash efficiency studies are shown in Figure 3-14. These set of experiments show wash efficiency differences between Htf and LacCer. Here two different experimental setups were investigated: the washes were carried out both on cell suspensions in Eppendorf tubes on ice and were compared to the same buffer combination on 25 cm² flasks on ice and adherent cells. Results show that a more efficient removal of Htf was obtained when the washes occurred in Eppendorf tubes, on trypsinized cell suspensions. The opposite was true for LacCer where the most efficient removal of the surface-bound marker of endocytosis occurred in 25 cm² flasks on ice.

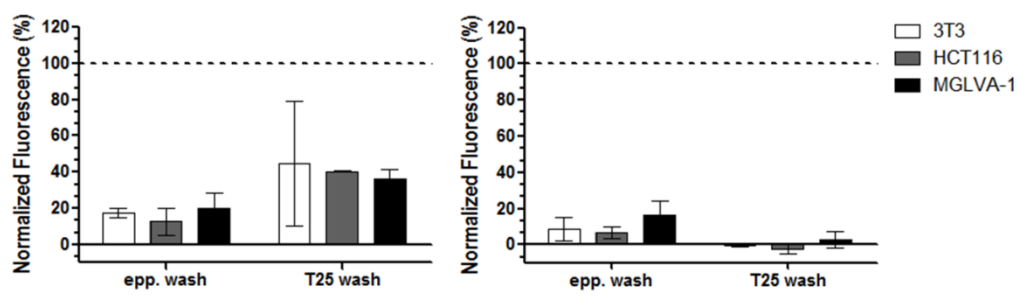


Figure 3-14 Flow cytometry results of 3 replicates experiments on the different efficiency of the removal of Htf and LacCer endocytic markers from the plasma membrane of cells. The washes were carried out on adherent cells (in 25 cm² flasks (T25)) or in cell suspensions (Eppendorf tubes washes (Epp wash)). The dotted line represents the fluorescence of the unwashed plasma membrane of cells calculated for positive controls and normalised to 100%. Error bars represent the standard deviation of the mean (n=3).

3.4 Discussion

C-PB of 50 and 100 nm diameter were characterized for effects on cell viability, size and charge; the concentration-dependent effects of endocytosis inhibitors were also evaluated and the presence of CHC isoform α and cav-1 in the cell lines designated

Results - Characterization of Materials and Cell lines

for endocytosis studies was determined by immunofluorescence. Finally, surface bound markers of endocytosis washing efficiency was also investigated with two different experimental procedures.

Size and charge characterization showed that C-PB of 50 nm displayed a broad size distribution with particle diameters ranging between 10 and 65 nm from TEM images and 28 and 97 nm from DLS measurements. The mean diameter was 30 nm from TEM and 57 nm from DLS studies. The fact that TEM results reported a smaller size than the one stated from the manufacturer is expected as TEM is a technique that measures the size of materials in dry conditions. Accordingly, the hydration diameter due to the solvent is not taken into consideration in TEM, although this is likely to be low for surface-carboxylated PS particles in aqueous media. However, DLS measurements reported a size of 57 nm which is closer to 50 nm of the manufacturer's report. The broad distribution of sizes, confirmed by both TEM and DLS, was an unexpected result and it is essential information to take into consideration when studying endocytosis as it has been extensively reported in literature that the size of the nanomaterials endocytosed can heavily affect the route of uptake³²⁻³⁴.

Characterization of 100 nm C-PB reported a double Gaussian distribution of sizes by both TEM and DLS studies. TEM data showed particles in two size ranges of 20 and 100 nm in diameter. The double Gaussian distribution in the DLS data did not allow distinction between the two populations of sizes, and the intensity measurements reported sizes ranging from 43 to 249 nm. DLS intensity data fitted a double Gaussian correlation as derived using GraphPad Prism with two major peaks apparent at 75 and 123 nm. The diameter of these materials as denoted in DLS was bigger than the TEM diameter for the two populations. This again might be due to the hydration diameter measured by DLS that is not measured in dry TEM conditions.

Results - Characterization of Materials and Cell lines

Another explanation might be that the two overlapping Gaussian distribution of sizes are too close for a precise discrimination of the size of the two populations of particles by DLS. TEM images of 50 and 100 nm C-PB show nanoparticles that are mainly separated and not aggregated on the grid which means that the sample preparation technique was appropriate for size characterization studies. The same images show that some nanoparticles are also less electron-dense with a lower extent of staining. This may have been due to heterogeneous composition of the material (for example as a result of uneven cross-linking during the polymer synthesis process) and suggests that these materials might not behave as one component during subsequent cell trafficking assays.

Zeta potential measurements of C-PB of 50 and 100 nm showed a negative charge that is slightly above the 30 mV threshold that is considered an approximate limit for colloidal stability³⁵. This meant that the nanoparticles used in this study were expected to be relatively stable to aggregation.

Preliminary studies using viability tests, statistical analysis and titration curves showed that it was possible to test for cell viability at the same cell numbers and concentrations consistent with endocytic pathway inhibition studies. Indeed, it has previously been reported that increasing the concentration of cells in toxicity tests changes the susceptibility of cells to toxic materials³⁶. The aim in these preliminary studies was to obtain accurate measures of any toxicity of materials under conditions analogous to those used in inhibition experiments.

C-PB viability studies were carried out with Cell Titer Glo and MTT assays. Both assays are routinely used to study the effects of nanoparticles on cell metabolic activity³⁷⁻⁴⁰. Both MTT and Cell Titer Glo are in agreement and report a low interference of such nanoparticles with the dehydrogenase activity of the MTT test and high levels of ATP in cells treated with 100 nm C-PB. These results suggest low

Results - Characterization of Materials and Cell lines

interference of these nanoparticles with the physiological functions of the tested cells. However, a big discrepancy between the results of the two tests was observed in regards to IC_{50} of 50 nm C-PB in MTT and Cell Titer Glo experiments. For this reason, a preliminary screening of cell viability for cells treated with 50 nm C-PB at 24 and 48 h was attempted with an MTT assay in order to confirm the toxicity of the materials. Cell viability profiles of the same 50 nm C-PB incubated for longer times with the cells showed IC_{50} values markedly higher than the ones reported for 4 h incubation. This result was not expected as toxicity is believed to be proportional to the extent of time that the toxic material is in contact to the cell line. Another group of researchers showed that MTT tests overestimate the toxicity of amine modified mesoporous silica nanoparticles (MSN). This effect is due to an increase of the exocytosis of the formazan crystals forming by the dehydrogenases of living cells, and that this is affected by the presence of MSN⁴¹. It is likely that this effect might not be only limited to positively charged MSN but also to other synthetic materials. Cell activity interference of 50 nm C-PB at 4, 24 and 48 h with an MTT test also accredits the hypothesis that MTT test should not be used with materials that interfere with endocytic processes as it is more extensively discussed below.

CPZ and MBCD were chosen as pharmacological inhibitors of endocytosis. As these materials have been repeatedly reported as toxic, the effects of CPZ and MBCD were characterised by two assays: MTT and Cell Titer Glo. An additional toxicity test was also used for CPZ and consisted of an Apo I caspase 3/7 assay^{13,42-44}.

MBCD toxicity was found to be low at the concentrations tested (up to 10 mM) in 3T3, HCT116 and MGLVA-1 cells. The Cell Titer Glo assay reported an increase of ATP content in 3T3 cells treated with increasingly high concentrations of MBCD when compared to ATP content of negative control cells. A possible explanation of this phenomenon might be that an increase in MBCD concentration might cause a

Results - Characterization of Materials and Cell lines

progressive increase in inhibition of endocytosis. It has been shown that endocytosis, which is a constant and energy demanding process, necessitates actin rearrangements, with energy required for cytoskeleton movements as well as for small GTPase intervention in the endocytic process (dynamin, Rab GTPases). As a consequence, inhibition of endocytic pathways might lead to a general increase of ATP and energy levels as ATP normally produced by cells for endocytic processes is not being used at the typical physiological rate⁴⁵⁻⁴⁸. The above mentioned hypothesis might also explain why Cell Titer Glo usually underestimated toxicity profiles in CPZ studies (please see below).

CPZ has also been extensively reported as toxic in prior literature. The drug affects mitochondria at concentrations lower than 10 μM causing rounding, swelling and migration to the periphery of the nucleus of these organelles^{21,49}. At concentrations of 20-30 μM it interferes with the cytoskeleton and blocks cell cycle in G2-M phase²⁰ while at concentrations of 50-100 μM it binds to calmodulin. Calmodulin regulates the recruitment of myristoylated alanine rich C kinase substrates (MARCKS) that sequester phosphatidylinositol 4,5-bisphosphate (PI(4,5)P₂). Consequently, CPZ inhibits CME by stopping the interaction of the AP-2 adaptor complex with membrane bound PI(4,5)P₂^{19,50}. For all these reasons, a full evaluation of its effects in the used cell lines was necessary.

It has been suggested that, since the MTT assay relies on endocytosis for the test compound to access healthy cells, and thus convert MTT to purple formazan, conducting an MTT assay in the presence of endocytosis inhibitors is inherently flawed⁵¹⁻⁵³. For all these reasons it was necessary to run further tests. Because of the high ATP levels in tested cells reported by Cell Titer Glo assay, it was hypothesized that if CPZ were to be toxic, the overall effect would lead to apoptosis. As a consequence, the presence of apoptotic cells was investigated through an Apo I

Results - Characterization of Materials and Cell lines

Caspase 3/7 kit. For 3T3 cells, IC_{50} and confidence intervals of the three tests suggested that the real IC_{50} values of CPZ ranged between 68 and 151 μ M for 3T3 and 64 and 209 μ M for MGLVA-1 cells. For HCT116 cells the three toxicity assays gave broader IC_{50} values ranging from 54 to 223 μ M. The Cell Titer Glo assay reported the highest IC_{50} values in the range, suggesting the effects of CPZ on ATP levels in all cell lines were lower than its effects on other metabolic pathways. MTT and Apo I assays were in partial agreement, suggesting that there was toxicity associated with the use of the drug at 4.5 h. However, the MTT test reported the highest effects on cell viability compared to Apo I and Cell Titer Glo. This might have been due to the effect of CPZ on mitochondria, where dehydrogenases that are partially involved in the conversion of the MTT to formazan reside. More specifically, CPZ has been reported to inhibit mitochondrial complex I activity that has been also reported to be involved in the reduction of the MTT to purple formazan in *in vitro* isolated mitochondria^{49,51}. If this hypothesis were to be true the MTT assay might be the most sensitive and reliable toxicity assay of the three reported in this chapter. However, even though reduction of activity of mitochondrial complex I is an excellent indication of cell viability given that the complex is involved in the oxidative phosphorylation and ATP production, CPZ is inhibiting a rather energy demanding process and for this reason ATP levels stay high. Hence, in these conditions, it is not clear if cells are really less viable or if there is a fine balance between the reduction of ATP production and ATP usage that enables cells to carry on with their physiological activities at low CPZ concentrations. Another point must be stressed: if the MTT assay relies also on an energy-dependent pathway for the MTT dye to enter cells rather than passive diffusion, a lack of purple formazan dye detected in the assay may have been due to lack of MTT uptake rather than loss of cell viability. These considerations might explain another anomaly: i.e. why did the Apo I caspase 3/7

Results - Characterization of Materials and Cell lines

assay do not indicate toxicity until CPZ concentrations reached higher levels than those in the MTT assay where viability decreased. Another possible way to explain such an anomaly might be that caspase 3/7 enzymes are produced at a rather late stage of the cell death process and thus would not have been activated at time points by which cell viability (as shown by MTT) had already decreased. However, evidence in the literature suggests that apoptosis is a rather rapid process that occurs within 5-15 minutes. In these papers, evidence of apoptosis activation was detected as a sharp increase of caspase 3 activity^{54,55}.

Immunofluorescence confocal and flow cytometry studies with anti human CHC isoform α clone X22 and cav-1 clone 2297 revealed that HCT116 cells expressed high levels of CHC α . MGLVA-1, on the other hand, presented high levels of cav-1 expression and this was an interesting result *per se* because the literature reports that *in vitro* cell lines often lack caveolae⁵⁶. Finally, cav-1 and CHC α expression was relatively low in 3T3 fibroblasts compared to the other cell lines. However, given that 3T3 fibroblasts were the only non human cell lines tested, a legitimate doubt was that the antibody used for immunofluorescence was less active against murine CHC α and cav-1. Cav-1 is a protein with 178aa and the mAb clone 2297 anti cav-1 recognises a region between aa 61 and 71⁵⁷. This region is conserved in both human and mouse according to FASTA database but murine and human cav-1 are not identical. They present 9 point mutations, two before the mAb target region (aa 36-37) and 7 after and corresponding to aa 106-107, 154, 163, 170 and 173-174. CHC α (1675aa) of mouse and human are better conserved with respect of cav-1, and mouse CHC α presents 2 point mutations only at aa 1146 and 1406 respectively. These mutations are after the mAb clone X22 epitope region 1109-1128⁵⁸. To investigate whether the immunocytochemistry results in murine 3T3 cells could be correlated to those in human cells, an additional human fibroblastic cell line, MRC-5 lung derived, was also

Results - Characterization of Materials and Cell lines

used. Concentrations of cav-1 expression in MRC-5 was also found to be low. For CHC α levels, on the other hand, 3T3 immunofluorescence data was at variance with MRC-5 clathrin expression levels. These differences brought to the decision to investigate further the reliability of the immunofluorescence data with ICOS 3D prediction software. Results from the analysis of the 3D rearrangement of the proteins and their exposure to the solvent showed that both cav-1 and CHC α 3D architecture of the epitopes recognised by the two mAb were different. For these reasons it is not possible to conclude that CHC α and cav-1 quantification in 3T3 cells with immunofluorescence experiments can be compared to human expression of the same proteins as the mAb used are likely to have different levels of activity against human and mouse proteins.

The last experiments in this series were for the determination of the most efficient procedures for the removal of endocytic markers from the plasma membrane. Here two techniques were investigated:

- flask wash procedures using traditional buffers for the removal of endocytic markers from the plasma membrane of cells were applied on adherent cells before trypsinization, or
- cells were trypsinized and wash steps carried out on suspensions of cells.

When comparing washes in cell suspensions to washes on adherent cells of Htf it was evident that the best way to remove the Htf marker was with washes of suspensions of cells in Eppendorf tubes. The contrasting settings (in flasks) were better for the removal of LacCer from the plasma membrane. Three possible explanations can be hypothesised here for the more efficient removal of Htf in Eppendorf tubes. It is known in the literature that trypsin cleaves the membrane localised Htf receptor⁵⁹. This is only a partial pool of the overall transferrin receptors

Results - Characterization of Materials and Cell lines

that are also present in the cytoplasm of cells, but the cleavage nevertheless neutralizes part of this pool and continuing these washes on ice might slow down and stop any further recycling on the plasma membrane. Trypsinization might have removed both the free receptor and the receptor bound to Htf. By doing so the application of trypsin might have aided the effects of the wash by contributing to the removal of membrane- and receptor-bound Htf. Trypsin cleavage of Htf receptor free from Htf might also have limited any unwanted interaction of the Htf that was being removed from the membrane and freed into solution with the Htf receptor. The detachment of the Htf from the receptor occurs during the last 2 steps of washes and after the acid wash. The acid wash ($\text{pH} \leq 5$) reduces and removes the iron from the holo-Htf producing an apo-Htf^{59,60}. Apo-Htf remains tightly bound to its receptor at acid pH (apparent dissociation constant, $K_d = 13 \times 10^{-9} \text{M}$,⁶¹). When the complex is then exposed again to neutral pH the apo-Htf is released. Apo-Htf has a binding affinity to the receptor at neutral pH that is 3 orders of magnitude lower than holo-Htf but still can bind the receptor, especially when the concentration of holo-Htf ($K_d = 7 \times 10^{-9} \text{M}$) is low in solution and it is not competing for its binding. Also, the media used for washes has $0.1 \mu\text{g/ml}$ of ferric nitrate $\text{Fe}(\text{NO}_3)_3 \cdot 9\text{H}_2\text{O}$ which means that potentially the apo-Htf can bind to the iron in the media and produce a new holo-Htf for high affinity receptor binding. Finally, another practical consideration might contribute towards the efficiency of the washes in Eppendorf tubes. When Eppendorf tubes are on ice it is easier to control the temperature compared to the analogous experiments with larger 25cm^2 flasks on ice, as uneven distribution of the ice might create local gradients of temperatures making possible the internalization of Htf, which is a high speed process with recycling of the receptor back to the plasma membrane in as little as 4 minutes^{62,63}.

Removal of LacCer from the plasma membrane was more efficient in flasks than in Eppendorf tubes. A possible explanation is that the diffusion of the buffer components used for the washes was less efficient in Eppendorf tubes with respect to flask washes. Here, interaction of defatted albumin with the plasma membrane is essential for the displacement of LacCer from the membrane of cells and it is possible that a major exposure of the cells' surface to the buffer in adherent cells on flasks might aid the process. Also, defatted albumin buffers are usually applied for 10 minutes and it might happen that the natural sedimentation of suspensions of cells might interfere with the process. Finally, another hypothesis might explain why the surface of trypsinized cells is less accessible to the wash buffer and albumin. Cells presenting hydrophobic LacCer on their membrane might more promptly aggregate and consequently make the access of defatted albumin to the adherent portions of the two plasma membranes virtually impossible and by doing so reduce the overall efficiency of the wash processes.

3.5 Conclusions

In this set of experiments the conditions for the inhibition studies of endocytic pathways with pharmacological inhibitors were delineated. It was established that the C-PB chosen for the experiments were negatively charged as expected and that they were more colloidally stable than assumed. However, they also presented a broader range of size variation than expected, which was an unwanted characteristic for these materials in the intended experiments. Also, the bi-modal size distributions of 100 nm C-PB, although affecting only 5% of the population of such materials, was also an undesirable characteristic to take into consideration in inhibition studies. The effects of 50 nm C-PB on cell viability were shown to be low for Cell Titer Glo while a high toxicity profile was obtained for MTT in HCT116 and MGLVA-1 cells. These findings

Results - Characterization of Materials and Cell lines

suggested setting the concentration of nanoparticles for endocytosis inhibition to 100 µg/ml and microscopy studies to 50 µg/ml. The intended concentration of MBCD of 1.25 mM for inhibition studies was found to be appropriate as MBCD was virtually non toxic at this concentration in all cell lines. However, the intended concentration of CPZ for inhibition studies (80 µM) was accompanied by some toxicity. Although a final IC₅₀ for the drug was not measured univocally by three separate tests, Apo I and MTT assays suggested that the dose of CPZ suitable for inhibition studies (80 µM) might be close to a toxic level. For this reason, it was decided to carry out inhibition studies also with 40 and 60 µM CPZ. Immunocytochemistry experiments delineated the experimental conditions in terms of quantity of endocytic proteins such as clathrin and caveolin in the cell lines used. The final experiments of this set on the efficiency of the removal of Htf and LacCer from the plasma membrane gave evidence that the best procedure for the washes utilized small scale Eppendorf tube washes and cells suspensions for Htf stripping from the membrane and on adherent cells and flasks for LacCer removal.

References

- 1 McMillan, J., Batrakova, E. & Gendelman, H. E. Cell delivery of therapeutic nanoparticles. *Prog Mol Biol Transl Sci* **104**, 563-601 (2011).
- 2 Raemdonck, K., Martens, T. F., Braeckmans, K., Demeester, J. & De Smedt, S. C. Polysaccharide-based nucleic acid nanoformulations. *Adv Drug Deliv Rev* **65**, 1123-1147 (2013).
- 3 Champion, J. A., Katare, Y. K. & Mitragotri, S. Particle shape: a new design parameter for micro- and nanoscale drug delivery carriers. *J Control Release* **121**, 3-9 (2007).
- 4 Saha, K. *et al.* Surface functionality of nanoparticles determines cellular uptake mechanisms in mammalian cells. *Small* **9**, 300-305, doi:10.1002/smll.201201129 (2013).
- 5 Elder, A., Vidyasagar, S. & DeLouise, L. Physicochemical factors that affect metal and metal oxide nanoparticle passage across epithelial barriers. *Wiley Interdiscip Rev Nanomed Nanobiotechnol* **1**, 434-450 (2009).
- 6 Dirisala, A. *et al.* Optimized rod length of polyplex micelles for maximizing transfection efficiency and their performance in systemic gene therapy against stroma-rich pancreatic tumors. *Biomaterials* **35**, 5359-5368 (2014).

Results - Characterization of Materials and Cell lines

- 7 Koch, S. & Nusrat, A. The life and death of epithelia during inflammation: lessons learned from the gut. *Annu Rev Pathol* **7**, 35-60 (2012).
- 8 Schlage, W. K. *et al.* In vitro systems toxicology approach to investigate the effects of repeated cigarette smoke exposure on human buccal and gingival organotypic epithelial tissue cultures. *Toxicol Mech Methods*, 1-37 (2014).
- 9 Frede, J., Adams, D. J. & Jones, P. H. Mutation, clonal fitness and field change in epithelial carcinogenesis. *J Pathol* (2014).
- 10 Kharraishvili, G. *et al.* The role of cancer-associated fibroblasts, solid stress and other microenvironmental factors in tumor progression and therapy resistance. *Cancer Cell International* (2014).
- 11 Sotgia, F. *et al.* Understanding the Warburg effect and the prognostic value of stromal caveolin-1 as a marker of a lethal tumor microenvironment. *Breast Cancer Research* **13**, 213 (2011).
- 12 Sahay, G., Alakhova, D. Y. & Kabanov, A. V. Endocytosis of nanomedicines. *Journal of Controlled Release* **145**, 182-195 (2010).
- 13 Vercauteren, D. *et al.* The Use of Inhibitors to Study Endocytic Pathways of Gene Carriers: Optimization and Pitfalls. *Mol Ther* **18**, 561-569 (2010).
- 14 Lamaze, C. & Schmid, S. L. The emergence of clathrin-independent pinocytic pathways. *Current Opinion in Cell Biology* **7**, 573-580 (1995).
- 15 Ivanov, A. I. Pharmacological inhibition of endocytic pathways: is it specific enough to be useful? *Methods in molecular biology* **440**, 15-36 (2008).
- 16 Stuart, A. D. & Brown, T. D. Entry of feline calicivirus is dependent on clathrin-mediated endocytosis and acidification in endosomes. *J Virol* **80**, 7500-7509 (2006).
- 17 Holmsen, H. & Rygh, T. Chlorpromazine makes the platelet plasma membrane permeable for low-molecular weight substances and reduces ATP production. *Biochemical Pharmacology* **40**, 373-376 (1990).
- 18 Francesco, C. D. & Bickel, M. H. Membrane lipids as intracellular binders of chlorpromazine and related drugs. *Chem Biol Interact* **16**, 335-346 (1977).
- 19 Eisenberg, S., Giehl, K., Henis, Y. I. & Ehrlich, M. Differential Interference of Chlorpromazine with the Membrane Interactions of Oncogenic K-Ras and Its Effects on Cell Growth. *Journal of Biological Chemistry* **283**, 27279-27288 (2008).
- 20 Lee, M. S. *et al.* The Novel Combination of Chlorpromazine and Pentamidine Exerts Synergistic Antiproliferative Effects through Dual Mitotic Action. *Cancer Research* **67**, 11359-11367 (2007).
- 21 Dudani, A. K. & Gupta, R. S. Effect of chlorpromazine and trifluoperazine on cytoskeletal components and mitochondria in cultured mammalian cells. *Tissue and Cell* **19**, 183-196 (1987).
- 22 Maurer, I. & Möller, H.-J. Inhibition of complex I by neuroleptics in normal human brain cortex parallels the extrapyramidal toxicity of neuroleptics. *Mol Cell Biochem* **174**, 255-259 (1997).
- 23 Ulloth, J. E. *et al.* Characterization of methyl-beta-cyclodextrin toxicity in NGF-differentiated PC12 cell death. *Neurotoxicology* **28**, 613-621, doi:D - nlm: nihms25952
- 24 Ulloth, J. E. *et al.* Characterization of methyl-beta-cyclodextrin toxicity in NGF-differentiated PC12 cell death. *Neurotoxicology* **28**, 613-621 (2007).
- 25 Zhang, J. H., Chung, T. D. F. A. U. O. & Oldenburg, K. R. A Simple Statistical Parameter for Use in Evaluation and Validation of High Throughput Screening Assays. *Journal of Biomolecular Screening* **4**, 67-73 (1999).

Results - Characterization of Materials and Cell lines

- 26 Iversen, P. W., B.J., E., Sittampalam, G. S. & Cox, K. L. A comparison of assay performance measures in screening assays: signal window, Z' factor, and assay variability ratio. *Journal of Biomolecular Screening* **11**, 247-252 (2006).
- 27 van Renswoude, J., Bridges, K. R., Harford, J. B. & Klausner, R. D. Receptor-mediated endocytosis of transferrin and the uptake of Fe in K562 cells: identification of a nonlysosomal acidic compartment. *Proceedings of the National Academy of Sciences* **79**, 6186-6190 (1982).
- 28 Pagano, O. C. M. a. R. E. Internalization and sorting of a fluorescent analogue of glucosylceramide to the Golgi apparatus of human skin fibroblasts: utilization of endocytic and nonendocytic transport mechanisms. *J Cell Biol* **125**, 769-781 (1994).
- 29 Stout, M., Bacardit, J., Hirst, J., Smith, R. & Krasnogor, N. Prediction of topological contacts in proteins using learning classifier systems. *Soft Computing* **13**, 245-258 (2009).
- 30 Bacardit, J., Stout, M., Krasnogor, N., Hirst, J. D. & Blazewicz, J. in *Proceedings of the 8th annual conference on Genetic and evolutionary computation* 247-254 (ACM, Seattle, Washington, USA, 2006).
- 31 Stout, M., Bacardit, J., Hirst, J. D. & Krasnogor, N. Prediction of recursive convex hull class assignments for protein residues. *Bioinformatics* **24**, 916-923 (2008).
- 32 Frohlich, E. *et al.* Action of polystyrene nanoparticles of different sizes on lysosomal function and integrity. *Particle and Fibre Toxicology* **9**, 26 (2012).
- 33 Canton, I. & Battaglia, G. Endocytosis at the nanoscale. *Chemical Society Reviews* **41**, 2718-2739 (2012).
- 34 Rejman, J., Oberle, V., Zuhorn, I. S. & Hoekstra, D. Size-dependent internalization of particles via the pathways of clathrin- and caveolae-mediated endocytosis. *Biochem J* **377**, 159-169 (2004).
- 35 Xu, R. (Kluwer, Dordrecht, Netherland, 2001).
- 36 Freshney, R. I. (Alan R. Liss, Inc., New York, 1987).
- 37 Wang, F. *et al.* Time resolved study of cell death mechanisms induced by amine-modified polystyrene nanoparticles. *Nanoscale* (2013).
- 38 Lesniak, A. *et al.* Effects of the Presence or Absence of a Protein Corona on Silica Nanoparticle Uptake and Impact on Cells. *ACS Nano* **6**, 5845-5857 (2012).
- 39 Vetten, M. *et al.* Label-free in vitro toxicity and uptake assessment of citrate stabilised gold nanoparticles in three cell lines. *Particle and Fibre Toxicology* **10**, 50 (2013).
- 40 Frohlich, E. *et al.* Action of polystyrene nanoparticles of different sizes on lysosomal function and integrity. *Part Fibre Toxicol* **9**, 26, doi:10.1186/1743-8977-9-26 (2012).
- 41 Fisichella, M. *et al.* Mesoporous silica nanoparticles enhance MTT formazan exocytosis in HeLa cells and astrocytes. *Toxicology in Vitro* **23**, 697-703 (2009).
- 42 Sun, X., Yau, V. K., Briggs, B. J. & Whittaker, G. R. Role of clathrin-mediated endocytosis during vesicular stomatitis virus entry into host cells. *Virology* **338**, 53-60 (2005).
- 43 Cantín, C., Holguera, J., Ferreira, L., Villar, E. & Muñoz-Barroso, I. Newcastle disease virus may enter cells by caveolae-mediated endocytosis. *Journal of General Virology* **88**, 559-569 (2007).
- 44 Kiss, T. *et al.* Evaluation of the cytotoxicity of beta-cyclodextrin derivatives: evidence for the role of cholesterol extraction. *Eur J Pharm Sci* **40**, 376-380 (2010).
- 45 Schmid, S. L. & Carter, L. L. ATP is required for receptor-mediated endocytosis in intact cells. *J Cell Biol* **111**, 2307-2318 (1990).
- 46 Hutagalung, A. H. & Novick, P. J. Role of Rab GTPases in membrane traffic and cell physiology. *Physiological Reviews* **91**, 119-149 (2011).

Results - Characterization of Materials and Cell lines

- 47 Samuel C Silverstein, Ralph M Steinman & Cohn, Z. A. ENDOCYTOSIS. *Ann Rev Biochem* **46**, 669-722 (1977).
- 48 Schmid, S., Carter, L. & Smythe, E. in *Endocytosis* Vol. 62 *NATO ASI Series* (ed PierreJ Courtney) Ch. 13, 105-111 (Springer Berlin Heidelberg, 1992).
- 49 Hroudova, J. & Fisar, Z. In vitro inhibition of mitochondrial respiratory rate by antidepressants. *Toxicol Lett* **213**, 345-352 (2012).
- 50 Levin, R. M. & Weiss, B. Mechanism by Which Psychotropic Drugs Inhibit Adenosine Cyclic 3',5'-Monophosphate Phosphodiesterase of Brain. *Molecular Pharmacology* **12**, 581-589 (1976).
- 51 Liu, Y., Peterson, D. A., Kimura, H. & Schubert, D. Mechanism of Cellular 3-(4,5-Dimethylthiazol-2-yl)-2,5-Diphenyltetrazolium Bromide (MTT) Reduction. *Journal of Neurochemistry* **69**, 581-593 (1997).
- 52 Liu, Y. & Schubert, D. Cytotoxic Amyloid Peptides Inhibit Cellular 3-(4,5-Dimethylthiazol-2-yl)-2,5-Diphenyltetrazolium Bromide (MTT) Reduction by Enhancing MTT Formazan Exocytosis. *Journal of Neurochemistry* **69**, 2285-2293 (1997).
- 53 Ahmad, S., Ahmad, A., Schneider, K. B. & White, C. W. Cholesterol interferes with the MTT assay in human epithelial-like (A549) and endothelial (HLMVE and HCAE) cells. *Int J Toxicol* **25**, 17-23 (2006).
- 54 Tyas, L., Brophy, V. A., Pope, A., Rivett, A. J. & Tavaré, J. M. Rapid caspase-3 activation during apoptosis revealed using fluorescence-resonance energy transfer. *EMBO Rep* **1**, 266-270 (2000).
- 55 Rehm, M. *et al.* Single-cell fluorescence resonance energy transfer analysis demonstrates that caspase activation during apoptosis is a rapid process. Role of caspase-3. *J Biol Chem* **277**, 24506-24514 (2002).
- 56 D'Alessio, A., Al-Lamki, R. S., Bradley, J. R. & Pober, J. S. Caveolae Participate in Tumor Necrosis Factor Receptor 1 Signaling and Internalization in a Human Endothelial Cell Line. *The American Journal of Pathology* **166**, 1273-1282 (2005).
- 57 Scherer, P. E. *et al.* Caveolin isoforms differ in their N-terminal protein sequence and subcellular distribution. Identification and epitope mapping of an isoform-specific monoclonal antibody probe. *J Biol Chem* **270**, 16395-16401 (1995).
- 58 Liu, S.-H., Wong, M. L., Craik, C. S. & Brodsky, F. M. Regulation of Clathrin Assembly and Trimerization Defined Using Recombinant Triskelion Hubs. *Cell* **83**, 257-267 (1995).
- 59 Dautry, A., Ciechanover, A., Lodish, C. & Lodish, F. H. Ph and the recycling of transferrin during receptor-mediated endocytosis. *Proc Natl Acad Sci U S A* **80**, 2258-2262 (1983).
- 60 Klauser, R. D., Ashwell, G., Van Renswoude, J., Harford, J. B. & Bridges, K. R. Binding of apotransferrin to K562 cells: Explanation of the transferrin cycle. *Proc Natl Acad Sci USA* **80**, 2263-2266 (1983).
- 61 Maxfield, F. R. & McGraw, T. E. Endocytic recycling. *Nat Rev Mol Cell Biol* **5**, 121 - 132 (2004).
- 62 Presley, J. F., Mayor, S., McGraw, T. E., Dunn, K. W. & Maxfield, F. R. Bafilomycin A1 treatment retards transferrin receptor recycling more than bulk membrane recycling. *J Biol Chem* **272**, 13929-13936 (1997).

4-Chapter 4

Inhibition of endocytosis and microscopy studies

4.1 Introduction

Endocytosis is a highly regulated and efficient process that takes place in all cells. This process is used to introduce nutrients and growth factors by receptor-mediated pathways and the same route is also used for signalling^{1,2}. Furthermore, some pathogens such as viruses have evolved mechanisms to enter cells by endocytosis³⁻⁹. An increasingly high proportion of the literature reports that synthetic nanomaterials can access cells through endocytosis^{8,10-13}.

In this chapter are reported and discussed the results on the optimization of inhibition studies with both LacCer and Htf, markers of clathrin-dependent endocytosis (CME) and clathrin-independent endocytosis (CIE), and CPZ and MBCD, inhibitors of CME-phagocytosis/macropinocytosis and CIE. MBCD was tested at 1.25 mM and CPZ at 80 μ M; these quantities were chosen from a preliminary screening as the lowest concentrations of inhibitors that efficiently inhibited CME and CIE. From viability results shown in chapter 3, MBCD did not produce any toxic effects at 1.25 mM, and for this reason this concentration only was tested in inhibition studies. However, as viability and a toxicity assay reported IC₅₀ values close to 80 μ M for CPZ, experiments with 40 and 60 μ M CPZ were also carried out. The results of the cell entry inhibition assays with low concentrations of CPZ were compared to the results obtained with 80 μ M CPZ to detect any effects on endocytosis that the higher and supposedly toxic concentration was having on the uptake of Htf. To further probe that the effects obtained with 80 μ M CPZ were not due to general toxicity of the drug on cells, experiments in the absence of Ca²⁺ and Mg²⁺ were also performed. Finally, from the data obtained, the effect of the passage number of cells on inhibition studies was also investigated. CME inhibition was also studied with Pitstop 2, a relatively new molecule that binds the amino-terminal domain of CHC that is involved in the

interaction of clathrin with the adaptor proteins that help the formation of the clathrin lattice¹⁴. Finally, C-PB of 50 and 100 nm were chosen as a model of negatively charged nanocarriers of drugs and their route of uptake inhibited with CPZ 80 μ M and MBCD 1.25 mM in 3T3, HCT116 and MGLVA-1 cells. Confocal microscopy was carried out on live cells treated with C-PB of 50 and 100 nm that were shown from inhibition studies to access cells through specific pathways. The aim of these experiments was to verify that the C-PB accessed cells and to characterize the specific route of uptake by any differences in compartmentalization.

4.2 Methods

4.2.1 Optimization of the inhibition of Htf uptake

4.2.1.1 Inhibition of Htf uptake with CPZ

For a more complete description of the methods used in these experiments please refer to §2.2.7 of the materials and methods. Here, cells were seeded at a density of 31200 cells/cm² and allowed to attach to the bottom of the 25 cm² flasks overnight. Subsequently, full media was replaced with HBSS supplemented with 20 mM HEPES with or without 40-60 or 80 μ M CPZ and 1.25 mM MBCD for 30 minutes and then replaced with HBSS/HEPES 20 mM with or without Htf 0.81 μ M and 40-60 and 80 μ M CPZ or 1.25 mM MBCD. Upon completion of the incubation time, cells were washed, detached from flasks and then analysed with a BD LSR II flow cytometer. The acid wash was carried out on 25 cm² flasks on ice.

4.2.1.2 Inhibition of Htf uptake with Pitstop 2

HCT116 cells were seeded at a density of 31200 cells/cm² and allowed to attach to the bottom of 25 cm² flasks overnight (§2.2.8). Subsequently, full media was replaced with HBSS supplemented with 20 mM HEPES with or without Pitstop 2 for 15 minutes and then replaced with HBSS/HEPES 20 mM with or without Htf 6.7 μ g/ml and

chemical inhibitor for 1 or 2 h. Pitstop working concentrations were selected as 12.5, 18.75 and 25 μM . Upon completion of the incubation time, cells were washed, detached from flasks and then analysed with a BD LSR II flow cytometer. The results are shown as the mean of 2 independent experiments. Htf was removed by an acid wash as reported in the literature¹⁶ and in methods described above and §2.2.6.

4.2.2 Optimization of the inhibition of LacCer uptake with MBCD

Cells were seeded at a density of 31200 cells/cm² and allowed to attach to 25 cm² flasks overnight. Subsequently, full media was replaced with HBSS supplemented with 20 mM HEPES with or without chemical inhibitors of endocytosis for 30 minutes and subsequently replaced with HBSS/HEPES 20 mM alone (negative control), LacCer 0.81 μM (positive controls) or with LacCer 0.81 μM in the presence of 80 μM CPZ or 1.25 mM MBCD. The incubation times were 1-2-3 and 4 h for all cell lines. Upon completion of the incubation time, cells were washed with the back exchange method and subsequently detached from flasks and then analysed with a BD LSR II flow cytometer and detected on a FITC channel, 530/30 optical bandpass filter¹⁷. The results were normalised against the positive and negative controls¹⁵. The LacCer washes were carried out in 25 cm² flasks on ice to inhibit endocytosis.

4.2.3 Inhibition of endocytosis of C-PB with CPZ and MBCD

Inhibition of endocytosis in the presence of 50 and 100 nm C-PB was carried out according to the protocols described in the materials and methods section §2.2.10. Cells were seeded at a density of 31200 cells/cm² and allowed to attach to 25cm² flasks overnight. Subsequently, full media was replaced with HBSS supplemented with 20 mM HEPES with or without 80 μM CPZ and 1.25 mM MBCD for 30 minutes. The buffer was then replaced with HBSS/HEPES 20 mM alone (negative control), 50 nm or 100 nm C-PB 100 $\mu\text{g/ml}$, (positive controls) or with 50 or 100 nm C-PB 100 $\mu\text{g/ml}$ in the presence of 80 μM CPZ or 1.25 mM MBCD. C-PB and inhibitors were

further incubated for 1 and 2 h with 3T3 and HCT116 cells and for 2 and 4 h with MGLVA-1 cells. Subsequently, cells were washed twice with HBSS/HEPES 20 mM and EDTA, detached from flasks with trypsin/EDTA, centrifuged at 2000 g for 5 minutes and re-suspended in PFA 4% v/v in PBS. 10000 gated cells were then analysed with a BD LSR II flow cytometer and detected on a FITC channel, 530/30 optical bandpass filter. The results were normalised against the positive and negative controls¹⁵.

4.2.4 Confocal microscopy live imaging

Cells that showed sensitivity to CPZ and MBCD for the internalization of 50 and 100 nm C-PB were also investigated by live cell confocal microscopy studies. Endocytosis of 100 nm C-PB was investigated in 3T3 cells, endocytosis of 50 nm C-PB was studied in HCT116 cells and endocytosis of 50 and 100 nm C-PB were examined in MGLVA-1 cells. The confocal microscopy experiments were run on live cells for a period of 1 h. For a more detailed description of the materials and methods of this section please refer to §2.2.12. Briefly, cells were seeded in full media to a final density of 31200 cells/cm² in 6 well plates on sterile rounded 22x1.5 mm glass coverslips. Cells were left to attach to the glass coverslips overnight. The day after, cells were stained with Hoechst 33342 (1 µg/ml) and CellMask deep red cell membrane dye (1 µg/ml) for 30 minutes at 37°C. The cells were then rinsed with HBSS/HEPES and the media replaced with HBSS/HEPES 20 mM for live imaging. Live images of 4 regions of interest were acquired at 4-10-20-30-40-50 and 60 minutes on a 40x water objective.

The measurements of the integrated fluorescence density of the C-PB for each cell and time point were processed with ImageJ software and subtracted from the integrated background from a region adjacent to each cell taken into the analysis as for the equation below:

$$(\int_{\text{Fluor}})_{\text{Corr}} = \int_{\text{Fluor}} - (A_{\text{cell}} \times M_{\text{Fluor bkd}})$$

Where:

$(\int_{\text{Fluor}})_{\text{Corr}}$ = Correct integrated fluorescence density

\int_{Fluor} = Integrated fluorescence density of the cell of interest (IntDen in ImageJ)

A_{cell} = area of the cell (Area in ImageJ)

$M_{\text{Fluor bkd}}$ = mean fluorescence of the background (Mean in ImageJ)

Analysis of the integrated fluorescence density was derived from measuring a minimum of 30 cells for each time-point and plots showing the mean and the standard deviation.

Co-localization of the C-PB with Hoechst and CellMask was determined by calculation of the Pearson's correlation coefficient with a JACoP plugin of ImageJ. The Pearson's coefficient obtained for each picture and the time-point was averaged and the mean and the standard deviation are shown in the results. For each experiment, one z stack was also obtained to acquire a 3D image of the distribution of C-PB in cells.

4.3 Results

4.3.1 Optimization of the inhibition of Htf uptake

4.3.1.1 Optimization of the inhibition of Htf uptake with CPZ

In these experiments, CPZ at a concentration of 80 μM was used to inhibit the uptake of Htf in 3T3, HCT116 and MGLVA-1 cells. Endocytosis was also inhibited with 40 μM CPZ in 3T3 fibroblasts while additional inhibition studies in HCT116 cells were carried out with 40 and 60 μM CPZ. For each experiment and time-point 1.25 mM MBCD was used as a control to evaluate if any interference on CME by MBCD occurred. All

Results - Inhibition of Endocytosis and Microscopy Studies

these experiments were run for 1, 2, 3 or 4 h and results at each time-point compared. The experimental results shown below are the combination of 2 independent experiments for concentrations of CPZ of 40 and 60 μ M and up to 6 independent experiments for 80 μ M CPZ.

Inhibition of Htf uptake with CPZ was temporary and occurred over an incubation time that was cell-dependent (Figure 4-1 and 4-2, Table 4-1). The maximum inhibition of Htf uptake was obtained at 2 h for 3T3 fibroblasts, 1 h for HCT116 cells and 4 h for MGLVA-1. After that maximal inhibition, the uptake of Htf recovered to normal non-inhibited levels in 3T3 and HCT116 cells at 4 h. The extent of inhibition was affected by the concentration of CPZ used, with low inhibition of the uptake of Htf at lower concentrations of CPZ (Figure 4-3). However, the pattern of inhibition at different time points also remained unchanged at lower concentrations of CPZ and was time-dependent, with an optimal incubation time at 2 h for 3T3 and 1 h for HCT116. After maximal inhibition at that time-point, the uptake of Htf was restored in 3T3 and HCT116 cells. The extent of the recovery was dependent on the concentration of CPZ used with longer recovery times for higher concentrations of CPZ.

Results - Inhibition of Endocytosis and Microscopy Studies

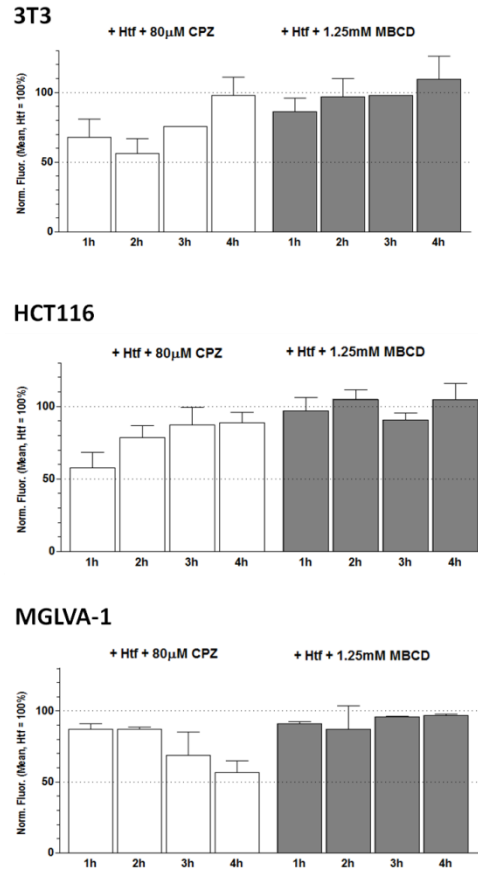


Figure 4-1 Flow cytometry results showing the time and cell dependence of the inhibition of the uptake of Htf with 80 μ M CPZ in 3T3, HCT116 and MGLVA-1 cells. Cells were preincubated with one inhibitor of endocytosis or HBSS/HEPES 20 mM for negative and positive control for 30 minutes. After that period of incubation the buffer was aspirated and replaced with HBSS/HEPES 20 mM for the negative control or Htf 0.81 μ M in HBSS/HEPES with or without inhibitors of endocytosis and further incubated for 1, 2, 3 or 4 h. The results are the combination of up to 6 independent experiments. They are shown as the mean and standard deviation of the fluorescence of 10000-20000 gated cells for each experiment and are normalised against the Htf treated positive control that was considered as 100% uptake. The dotted lines refer to 50 and 100% uptake of Htf.

Results - Inhibition of Endocytosis and Microscopy Studies

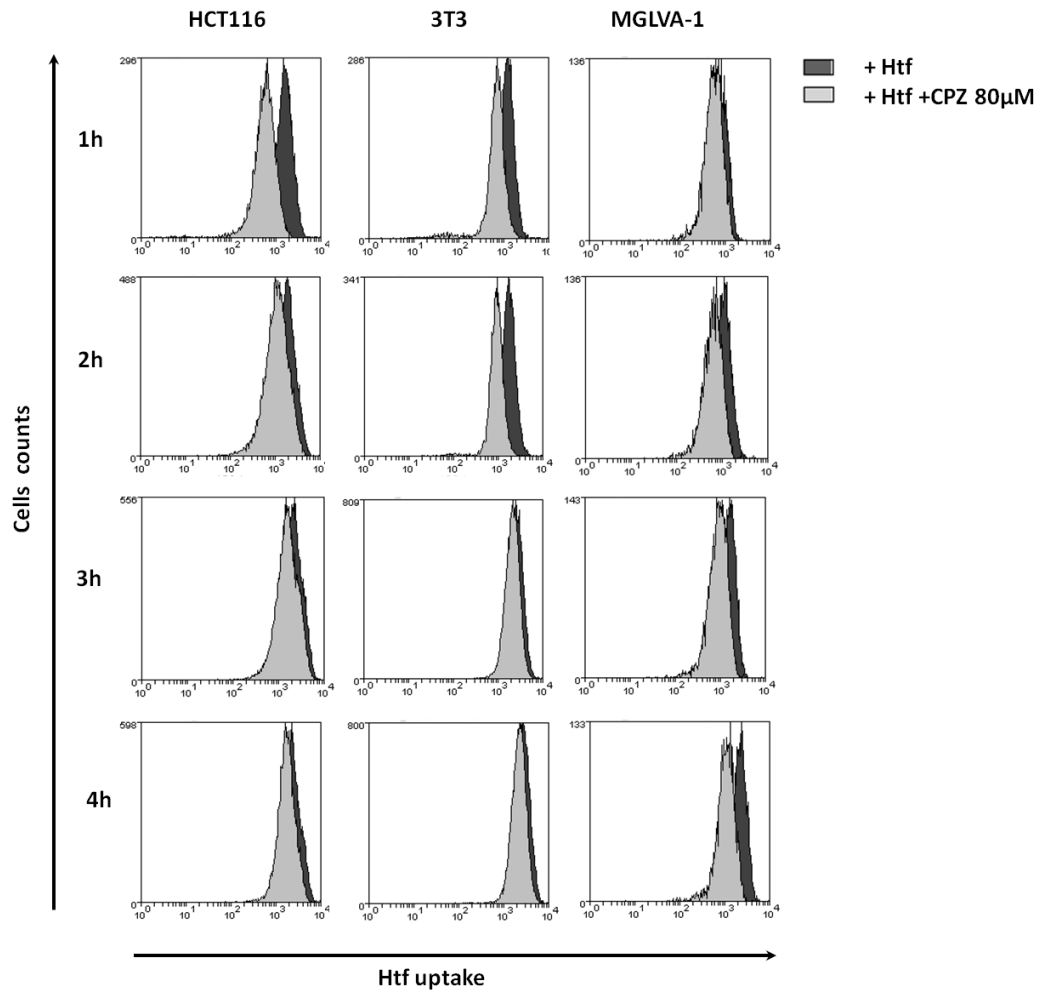


Figure 4-2 Flow cytometry histograms on the inhibition of Htf uptake with 80 μM CPZ at different time points and cell lines. The X axes show the fluorescence intensity of Htf, the Y axes show the number of cells. The dark shadows show Htf uptake at basal, uninhibited levels while the light shadows show Htf uptake in the presence of 80 μM CPZ.

Results - Inhibition of Endocytosis and Microscopy Studies

Statistical analysis of inhibition of Htf endocytosis with CPZ and MBCD			
Two-Way ANOVA	3T3	Htf vs CPZ	Htf vs MBCD
3T3	1h	***	ns
	2h	***	ns
	3h	*	ns
	4h	ns	ns
HCT116	1h	***	ns
	2h	**	ns
	3h	ns	ns
	4h	ns	ns
MGLVA-1	1h	ns	ns
	2h	ns	ns
	3h	**	ns
	4h	***	ns

Table 4-1 Two-Way ANOVA and Bonferroni post-analysis test of the inhibition of Htf uptake in the presence of CPZ and MBCD. Htf uptake of untreated cells was compared with the uptake of Htf in the presence of CPZ and MBCD. The results above show that there is a significant inhibition in the uptake of Htf in the presence of CPZ and the significance is time dependent and depend on the cell line. MBCD inhibition of endocytosis of the uptake of Htf on the other hand, does not show statistical significance. (ns: non significant, $P>0.05$; *: $P<0.05$; **: $P<0.01$; ***: $P<0.001$).

Inhibition of CME was also obtained with 1.25 mM MBCD and the extent of inhibition was time-dependent, affecting up to 15% of Htf uptake in 3T3 cell lines at 1 h incubation, 10% of Htf uptake in HCT116 cells at 4 h, and 13% at 2 h with MGLVA-1 (Figure 4-1). However a two-way ANOVA statistical analysis showed that the inhibition of internalization of Htf by the action of MBCD was not statistically significant (Table 4-1).

Results - Inhibition of Endocytosis and Microscopy Studies

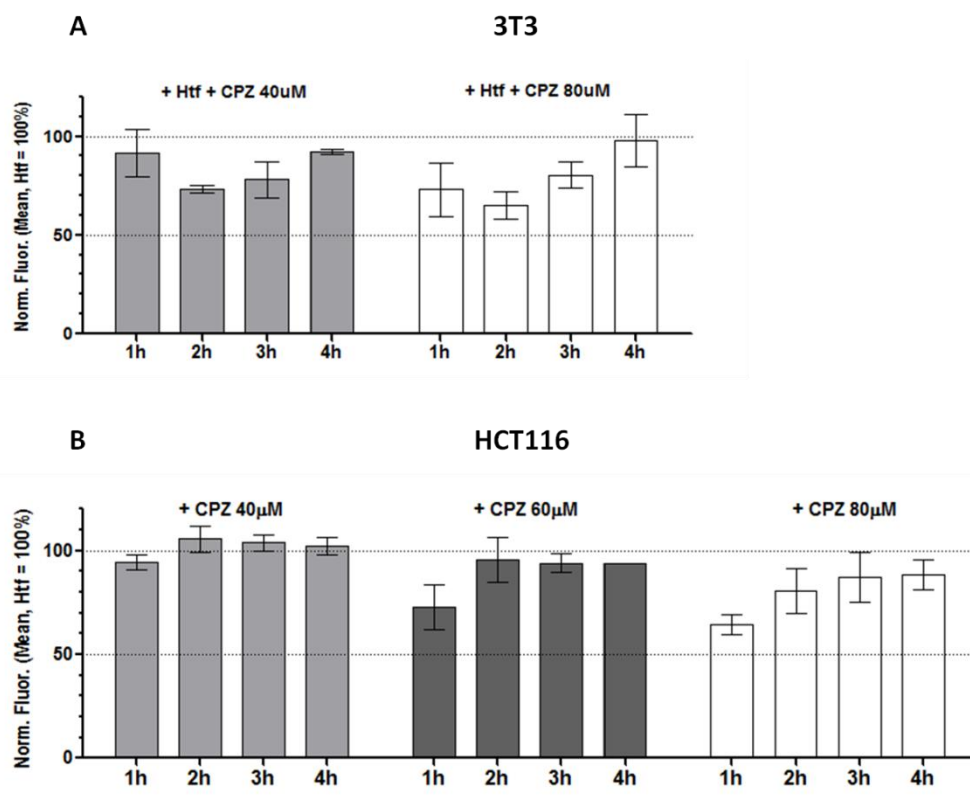


Figure 4-3 Lower concentrations of CPZ reduce the extent of inhibition of Htf uptake in 3T3 and HCT116 cells. The flow cytometry results are normalised against the fluorescence of Htf positive control and expressed at the mean and standard deviation of a minimum of 10000 gated cells for each experiment (n=2). Cells were preincubated with HBSS/HEPES 20 mM with or without inhibitor for 30 minutes. Subsequently the pretreatment buffer was aspirated and 3T3 cells were treated with 40 and 80 µM CPZ for up to 4 h and HCT116 with 40, 60 and 80 µM of CPZ for up to 4 h. The dotted lines refer to 50 and 100% uptake of Htf.

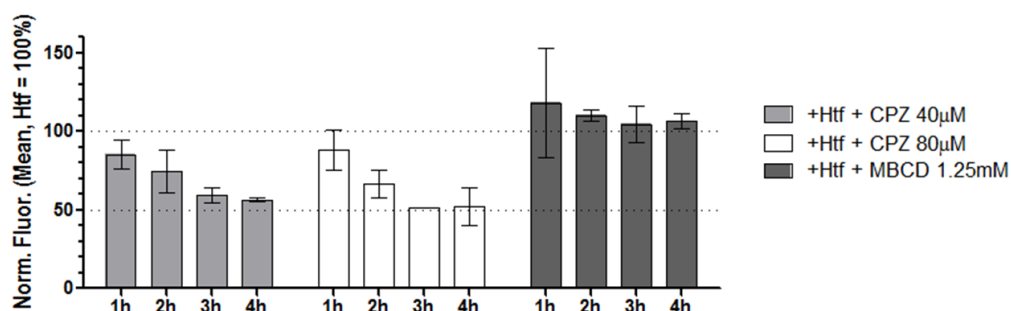
In addition, to assess the consequences on cell viability induced by energy depletion resulting from endocytosis, CPZ stock solutions of 40 and 80 µM were prepared with HBSS without Ca²⁺ and Mg²⁺ (instead of the standard HBSS with supplements of the two ions), complemented with HEPES 20 mM and applied on 3T3 and HCT116 cells as for standard protocol for a period of up to 4 h. The results are given by the combination of 2 independent experiments for 3T3 fibroblasts while only one experiment was attempted for HCT116 cells².

² The experiment was not repeated due to lack of time.

Results - Inhibition of Endocytosis and Microscopy Studies

Inhibition studies with HBSS without Ca^{2+} and Mg^{2+} (Figure 4-4) in 3T3 cells showed that the effects on cell viability and induction of apoptosis by media depletion of essential ions was not sufficient to produce a recovery of the internalization of Htf. This suggested that the recovery of uptake of Htf is an energy dependent process that happens in viable cells but not in energy-depleted and stressed cells.

3T3 with HBSS no Ca^{2+} no Mg^{2+}



HCT116 with HBSS no Ca^{2+} no Mg^{2+}

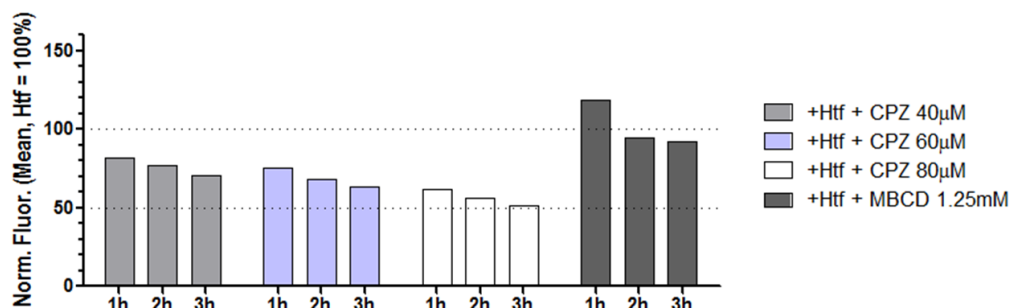


Figure 4-4 Effects of the absence of Ca^{2+} and Mg^{2+} from the assay media on the inhibition and recovery of the uptake of Htf with CPZ. The results shown are represented as the mean and standard deviation of 2 independent experiments in 3T3 cells and only one pilot study experiment in HCT116 cells. The results are normalised against the Htf positive control and show the mean and the standard deviation of 10000 gated cells. Cells were preincubated with HBSS/HEPES 20 mM devoid of Ca^{2+} and Mg^{2+} with or without inhibitor for 30 minutes. Subsequently the pretreatment buffer was aspirated and replaced with fresh solutions of HBSS/HEPES 20 mM devoid of Ca^{2+} and Mg^{2+} with or without Htf 6.7 $\mu\text{g}/\text{ml}$, different concentrations of CPZ ranging from 40 to 80 μM and MBCD 1.25 mM. The cells were further incubated for 1, 2, 3 or 4 h for 3T3 cells and 1, 2 and 3 h for HCT116 cells. The dotted lines refer to 50% and 100% uptake of Htf. Error bars represent the standard deviation of the mean of duplicate experiments, n=2 (3T3 cells).

Results - Inhibition of Endocytosis and Microscopy Studies

Finally, the effect of passage number on the extent of the inhibition of endocytosis was investigated in 3T3 and HCT116 cells. Endocytosis was inhibited on 3T3 fibroblasts at passage number ranging between 28 and 53 and HCT116 at passage number 18-44. The experiments were run as from standard protocol for 1 h and 2 h. Each set of experiments was run in duplicates independent experiments and the results merged and averaged.

The inhibition of endocytosis with CPZ was affected by the passage number of the cells used for inhibition studies, with higher passage numbers being more resistant to the inhibition of Htf uptake (Figure 4-5 graph B for 3T3 cells and E for HCT116 cells). The maximal incubation time did not change at low passage numbers but was gradually lost in aged cells. When 3T3 fibroblasts at passage number 53 and 55 were inhibited with 80 μ M CPZ at 1 and 2 h, the inhibition was reduced and also the pattern of inhibition of endocytosis of Htf changed, as shown in graph C in Figure 4-5 with a comparable extent of inhibition at 1 and 2 h.

Results - Inhibition of Endocytosis and Microscopy Studies

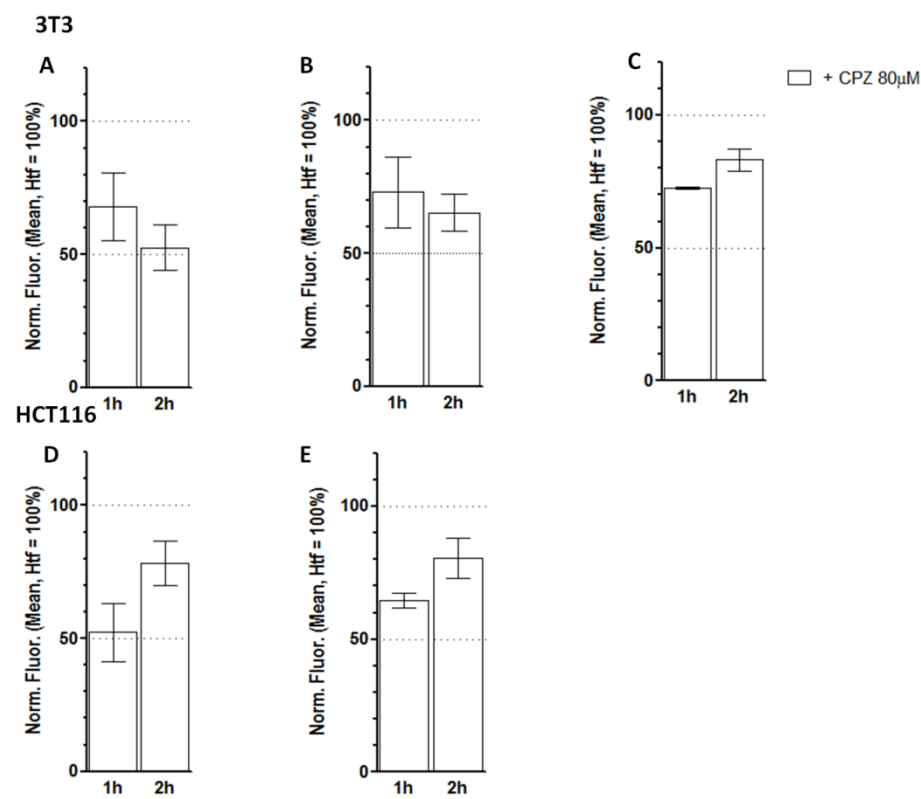


Figure 4-5 Passage number and ageing of cells affects the extent of inhibition of Htf uptake with CPZ. Cells at different passage numbers were incubated with Htf 6.7 μg/ml and 80 μM CPZ at 1 and 2 h in 3T3 and HCT116 cells. Graph A shows the inhibition obtained with 80 μM CPZ in 3T3 cells at passage number 28 and 30, graphs B and C show the inhibition obtained by the same inhibitor and cell line at passage number 39-41 and 53-55 respectively. Graphs D and E show the extent of the inhibition obtained with 80 μM CPZ in HCT116 cells at passage number 18-20 (graph D) and passage number 42-44 (graph E). Cells were treated as in previous experiments with 30 min preincubation of CPZ or HBSS/HEPES that was replaced by HBSS/HEPES 20 mM buffer supplemented of Htf for the positive control or 80 μM CPZ and Htf, and further incubated for 1 or 2 h. The dotted lines refer to 50 and 100% uptake of Htf. The results show the mean and standard deviation of a minimum of 10000 gated cells for each experiment (n=2).

4.3.1.2 Optimization of the inhibition of Htf uptake with Pitstop 2

HCT116 cells incubated with Pitstop 2 12.25 μM did not show any significant inhibition of endocytosis for a period of up to 2 h (Figure 4-6). When the concentration was raised to 18.75 and 25 μM, Pitstop 2 reduced endocytosis to a consistent level and the extent of such inhibition was dependent on the concentration of the inhibitor. The recovery of the Htf uptake was not observed here at the incubation times and

Results - Inhibition of Endocytosis and Microscopy Studies

concentrations used. Finally, indications of toxicity were detected at concentrations of Pitstop 2 of 18.75 and 25 μM , with cells appearing rounded and unhealthy.

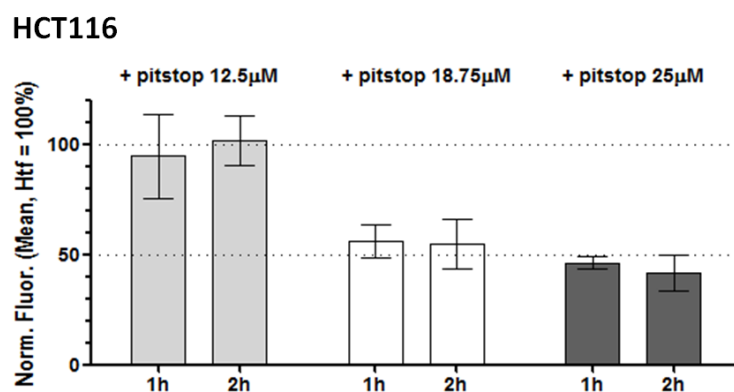


Figure 4-6 Effects of the inhibition of Htf endocytosis with Pitstop 2 at 12.5, 18.75 and 25 μM in HCT116 cells. The results represent the combination of 2 independent experiments and show the mean fluorescence of Htf uptake of 20000 gated cells per experiment and the standard deviation of the mean of replicate experiments (n=2). The dotted lines refer to 50 and 100% uptake of Htf.

4.3.1.3 Optimization of the inhibition of LacCer uptake with MBCD

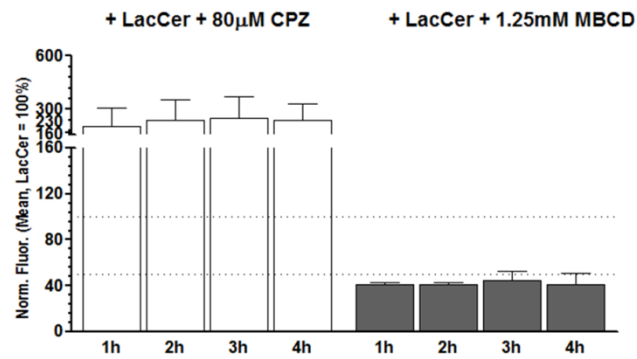
In these experiments, MBCD 1.25 mM was used as an inhibitor of CIE. The effect of the inhibitor on the uptake of LacCer, a marker of CIE, was studied at 1,2,3 and 4 h on 3T3, HCT116 and MGLVA-1 cells. As a further control, the specificity of CPZ on the inhibition of CME at each time point was also investigated with LacCer incubated in the presence of 80 μM CPZ.

LacCer uptake inhibition with MBCD was easier to obtain, compared to the Htf inhibition with CPZ, as the inhibition was strong and steady for a period of up to 4 h (Figure 4-7). The effect of MBCD inhibition on LacCer uptake was less cell-dependent and a concentration 1.25 mM of MBCD produced a potent inhibition of endocytosis for all cell lines tested. A 1 h incubation period of the drug was sufficient to obtain maximal inhibition of endocytosis in 3T3 and HCT116, whereas 2 h were necessary for MGLVA-1 cells. Also, when CPZ was used as a control for specific clathrin-mediated endocytosis (CME), CPZ showed no ability to inhibit clathrin-

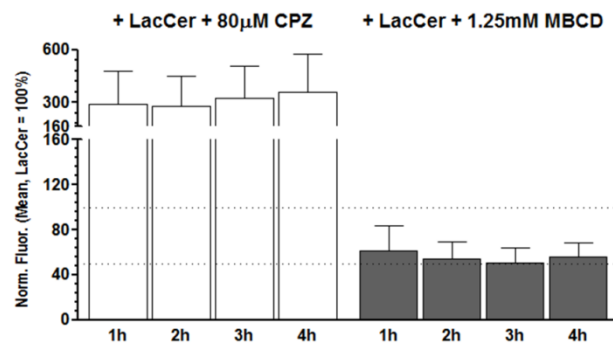
Results - Inhibition of Endocytosis and Microscopy Studies

independent endocytosis (CIE). Instead, treatment with CPZ resulted in substantial increase of endocytosis of LacCer in all cells tested, enhancing the uptake of LacCer to 3 times higher levels than those observed in the positive control.

3T3



HCT116



MGLVA-1

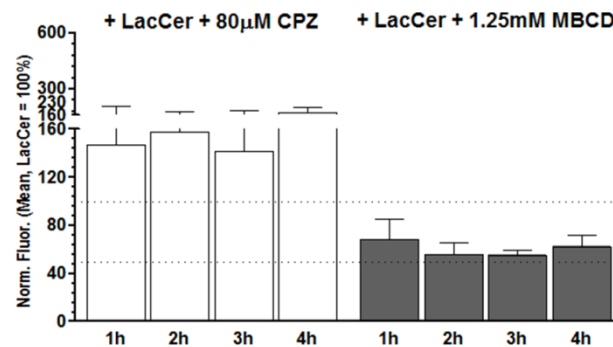


Figure 4-7 Effect of the inhibition of LacCer uptake with 1.25 mM MBCD. Cells were treated as described before. A preincubation step of 30 min was carried out in the presence and in the absence of endocytosis inhibitors. Upon completion of the preincubation time the media was aspirated and replaced with LacCer 0.81 µM in the presence of in the absence of inhibitors of endocytosis. Cells were incubated for a maximum of 4 h and the results are the combination of 2 independent experiments (n=2), the error bars represent the standard deviation of the mean of a minimum of 20000 gated cells per experiment. The dotted lines refer to 50 and 100% uptake of LacCer.

4.3.2 Inhibition of the endocytosis of C-PB with CPZ and MBCD

The optimized protocol for the inhibition of Htf and LacCer uptake with CPZ and MBCD was applied for the inhibition of the endocytosis of 50 and 100 nm C-PB.

Results (Figure 4-8) show that the inhibition of 50 nm C-PB uptake was obtained with 80 μ M CPZ in both epithelial cells investigated, HCT116 and MGLVA-1. The reduction of the uptake of 50 nm C-PB in HCT116 cells was strong already at 1 h incubation of the inhibitor and the inhibition obtained was steady and uptake did not recover by 2 h. Reduction in the uptake of 50 nm C-PB with CPZ in MGLVA-1 cells was already evident at 2 h with approximately 35% reduction of endocytosis. However, the maximum effect of CPZ was obtained at 4 h with 60% inhibition of 50 nm C-PB uptake with respect to the positive control. The incubation of 50 nm C-PB with CPZ and MBCD in 3T3 fibroblasts produced an activation of the endocytosis of C-PB as for CPZ in LacCer inhibition studies. The same effect was observed in HCT116 and MGLVA-1 cells for 50 nm C-PB incubated with MBCD where an activation of endocytosis at 1-2 h in HCT116 and 2-4 h in MGLVA-1 cells were obtained. The activation was stronger in MGLVA-1 cells than HCT116 cells. No inhibition of endocytosis of 50 nm C-PB was obtained with CPZ and MBCD incubated for 1 and 2 h in 3T3 cells but the endocytosis was up-regulated by both inhibitors.

Endocytosis of 100 nm C-PB was sensitive to CPZ in 3T3 cells and sensitive to MBCD in MGLVA-1 cells. 100 nm C-PB nanoparticles were endocytosed by a non-CPZ non-MBCD sensitive pathway in HCT116 cells. Here, both CPZ and MBCD up-regulated the endocytosis of 100 nm C-PB.

Inhibition of 100 nm C-PB with CPZ in 3T3 cells was obtained at 1 h incubation and the endocytosis recovered almost completely at 2 h. The endocytosis of the same nanoparticles was only partially inhibited with MBCD at 2 h incubation in MGLVA-1

cells, and subsequently completely recovered, showing a modest up-regulation after 4 h.

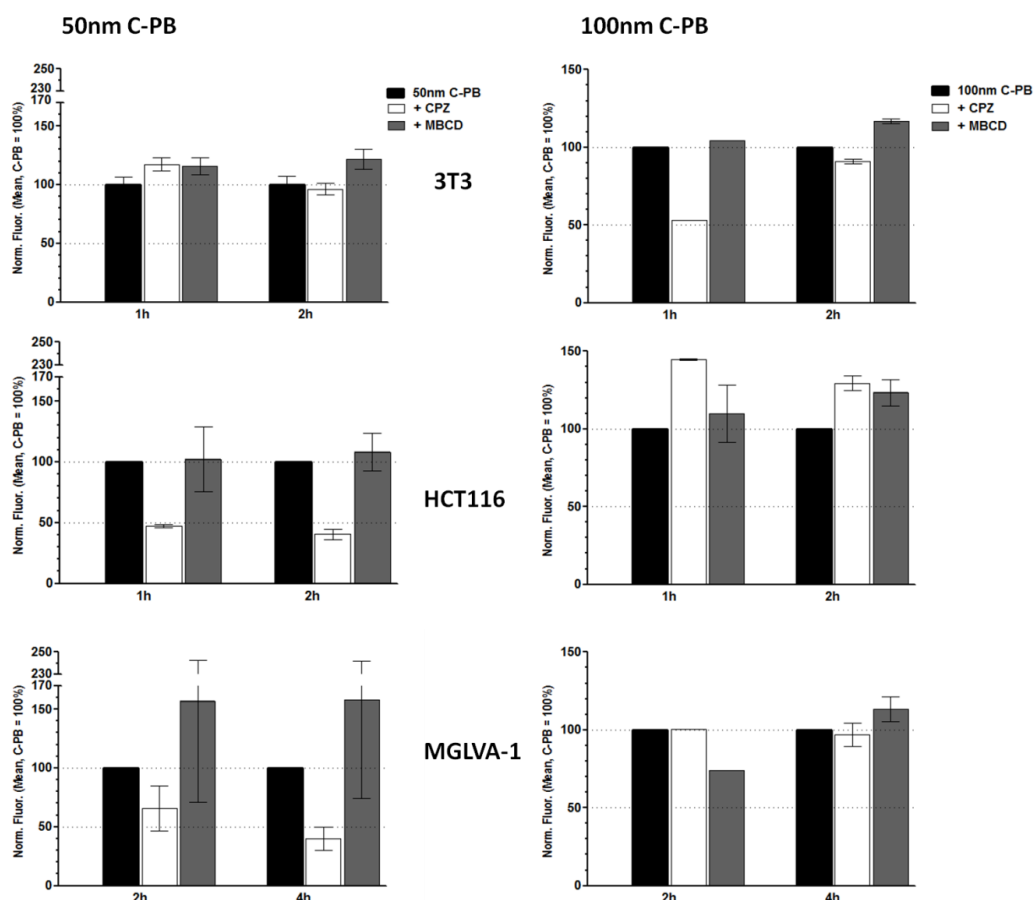


Figure 4-8 Inhibition of the uptake of 50 nm and 100 nm C-PB with 80 μ M CPZ and 1.25 mM MBCD. 3T3 and HCT116 inhibition of the uptake of C-PB was monitored for 1 and 2 h while MGLVA-1 inhibition of the uptake was examined at 2 and 4 h. The results are shown as the mean and standard deviation of 2 independent flow cytometry experiments obtained on 10000 gated cells (n=2). The dotted lines refer to 50 and 100% uptake of C-PB.

4.3.3 Confocal microscopy live imaging studies

Cell lines that showed sensitivity to endocytic inhibitors in the presence of 50 or 100 nm C-PB were further investigated with confocal microscopy live imaging with the aim of confirming endocytosis and localization of the nanoparticles within the cell membrane boundaries. The internalization was not verified in flow cytometry experiments as the technique does not distinguish between membrane-bound and internalized signal from cells. As some cell lines incubated with C-PB showed

Results - Inhibition of Endocytosis and Microscopy Studies

different susceptibility to inhibitors of endocytosis, live images of cells in the presence of C-PB were also carried out to study any pattern in compartmentalization of C-PB sensitive to different inhibitors of endocytosis.

Cells incubated with 50 and 100 nm C-PB showed a rapid uptake of nanoparticles. Endocytosis could already be detected at 4 minutes incubation in all cell lines studied (Figures 4-9, 4-14, 4-19 and 4-24). The Pearson's coefficient of co-localization for each time-point did not show any significant increase of co-localization of C-PB and Hoechst with time suggesting that the nanoparticles did not access nuclei under the experimental conditions used and time-points investigated (Figures 4-13, 4-18B, 4-23 and 4-28). Only a minor, non-statistically significant increase of colocalization of green fluorescence from the nanoparticles and blue fluorescence from the nuclei was detected in HCT116 that might be attributed to a possible effect of proximity with the nuclei of the nanoparticles localized to a perinuclear region resembling the endoplasmic reticulum (ER).

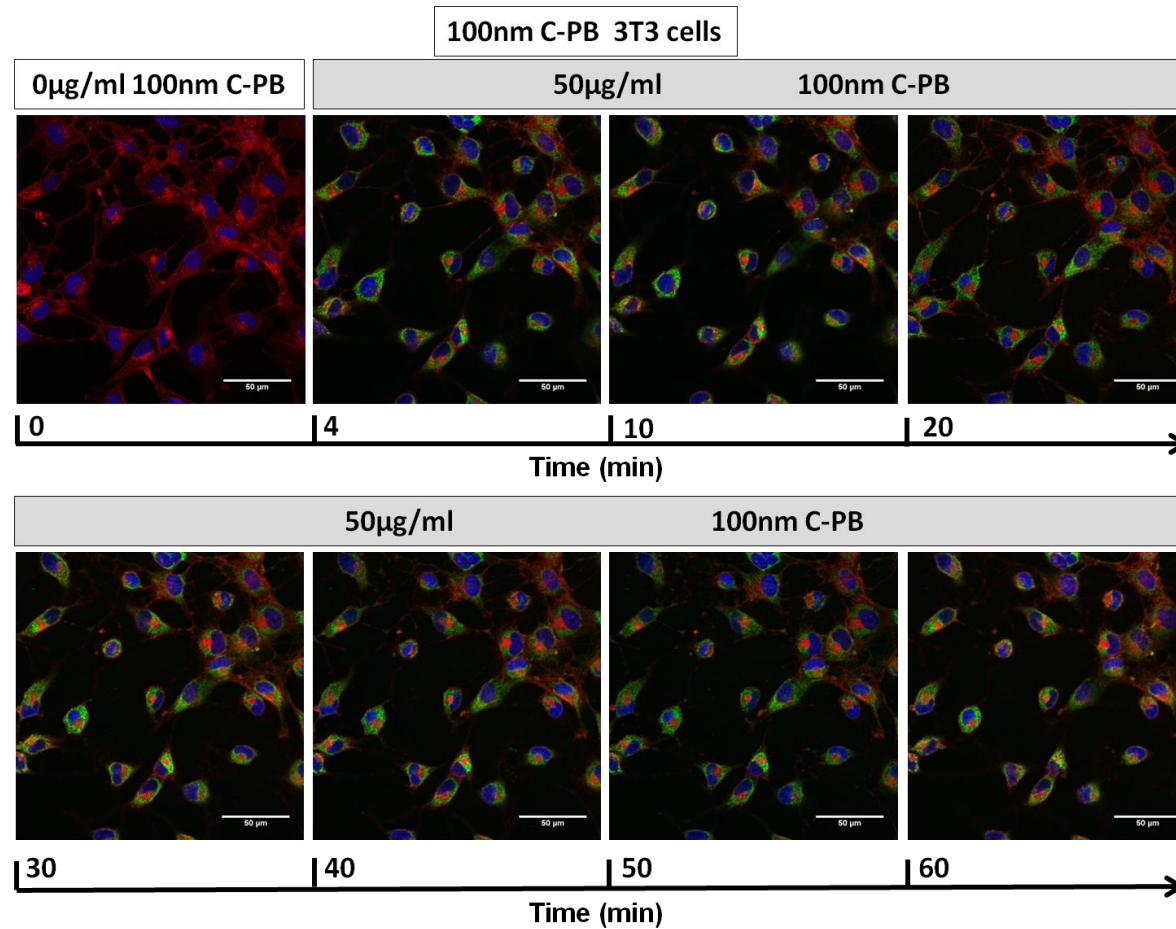


Figure 4-9 Confocal live imaging studies of 3T3 cells treated with 50 µg/ml 100 nm C-PB for a period of 60 min. Red fluorescence: CellMask deep membrane staining, Green: C-PB, Blue: Hoechst nuclei staining. Time 0 refers to cells before application of the C-PB. Pictures were then acquired at 4 and at 10, 20, 30, 40, 50 and 60 minutes from the application of the C-PB. The red intracellular structures stained by CellMask are believed to be the ER. Scale bars represent 50 µm.

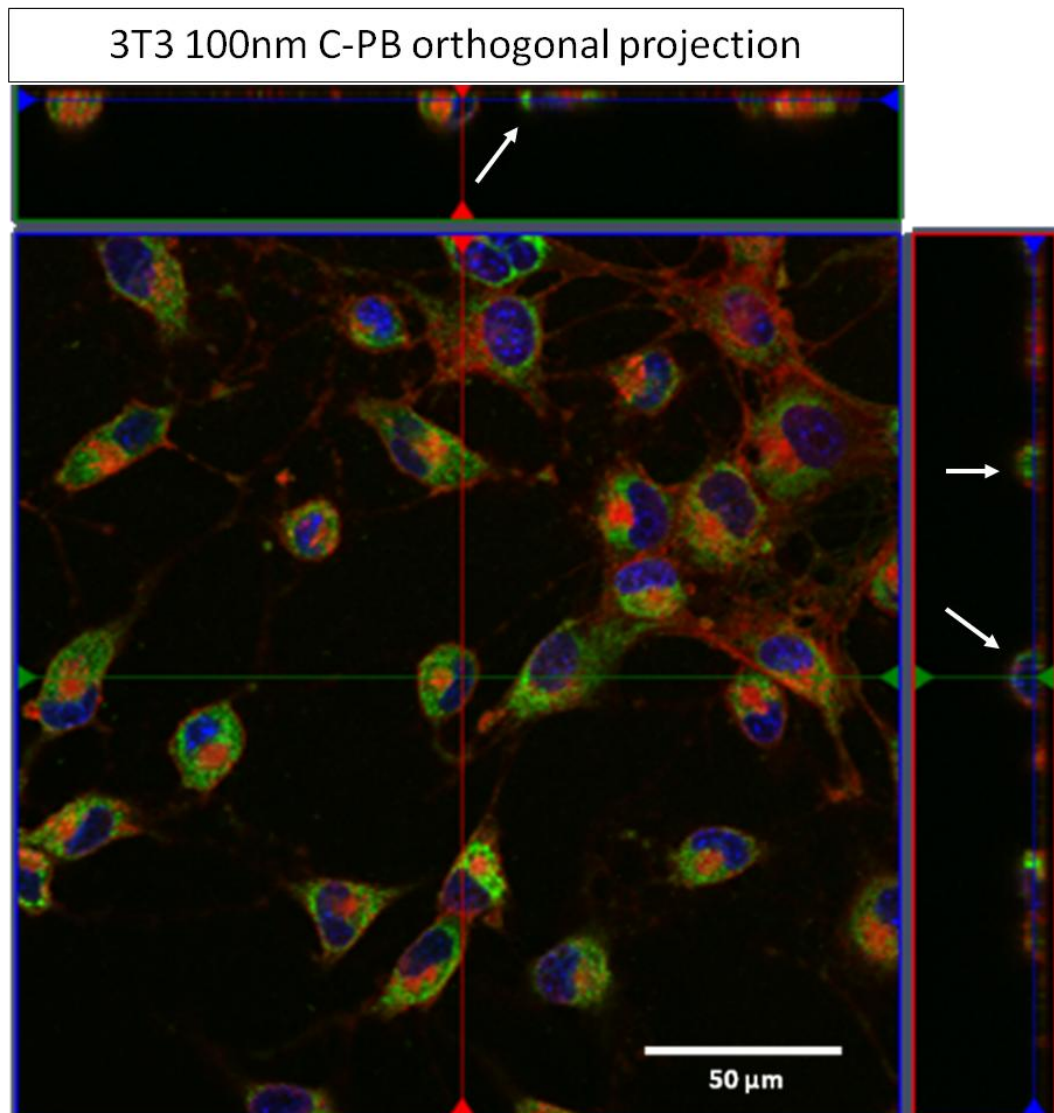


Figure 4-10 Orthogonal projection of a 3D image of 3T3 cells treated with 50 μg/ml 100 nm C-PB showing internalised green nanoparticles (arrows) that can be seen inside the red membrane limit of the cells. Green: C-PB, Red: CellMask deep red membrane dye, Blue: Hoechst nuclei staining. The Cell Mask deep red membrane dye is staining a perinuclear intracellular compartment believed to be the ER. Scale bar represents 50 μm.

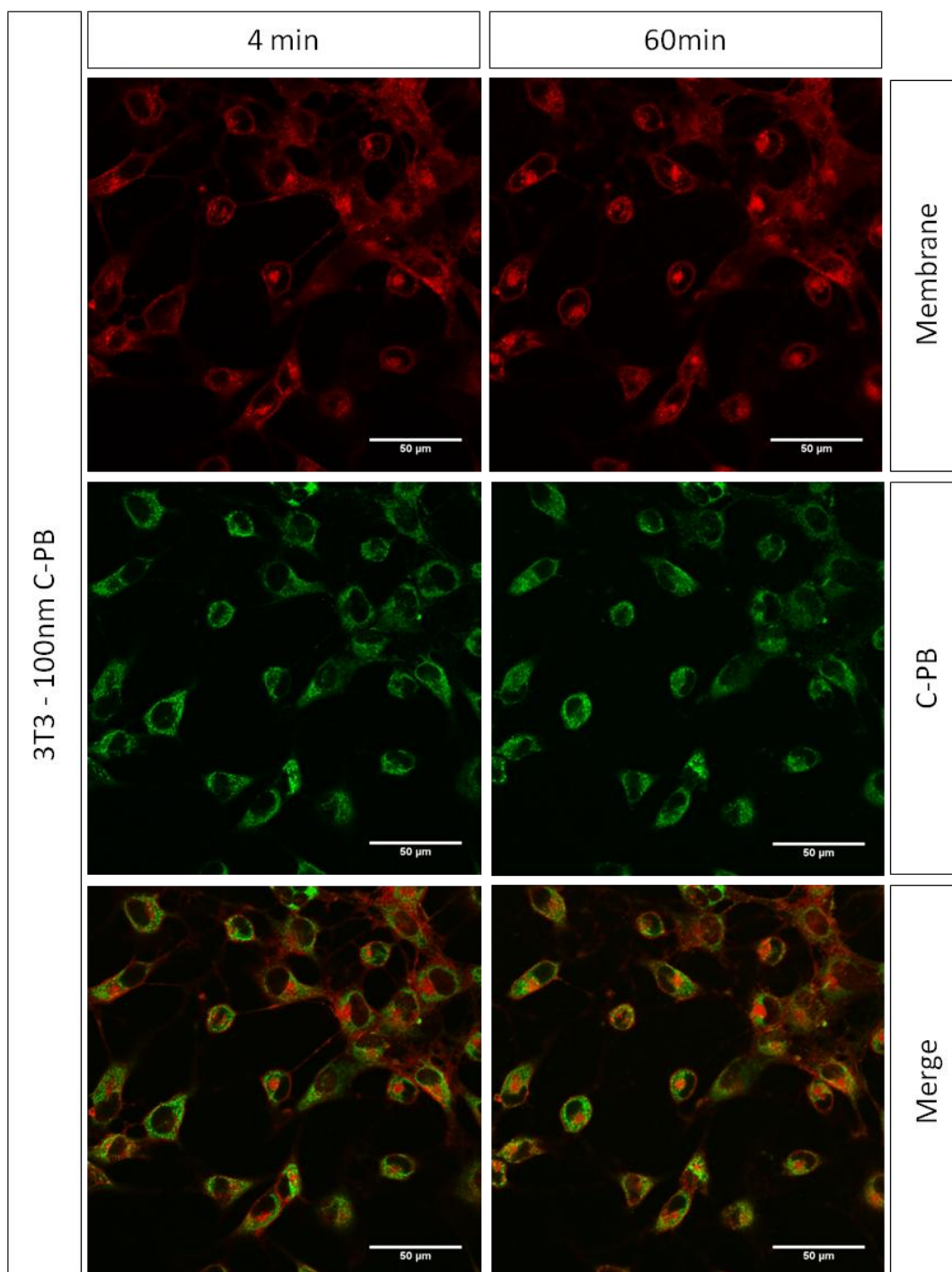


Figure 4-11 This picture shows the differences in the redistribution of CellMask red plasma membrane staining at 4 and 60 minutes in 3T3 fibroblasts treated with 100 nm C-PB. Less confluent cells appear to redistribute the dye more quickly to the plasma membrane of cells, while more confluent cells show the dye in the cytoplasmic region of cells also after 60 minutes incubation of cells in the presence of C-PB. The redistribution of C-PB from a perinuclear region to a cytoplasmic region is not evident from these pictures. Scale bar represents 50 µm. Green: 100 nm C-PB; Red: CellMask deep red membrane staining.

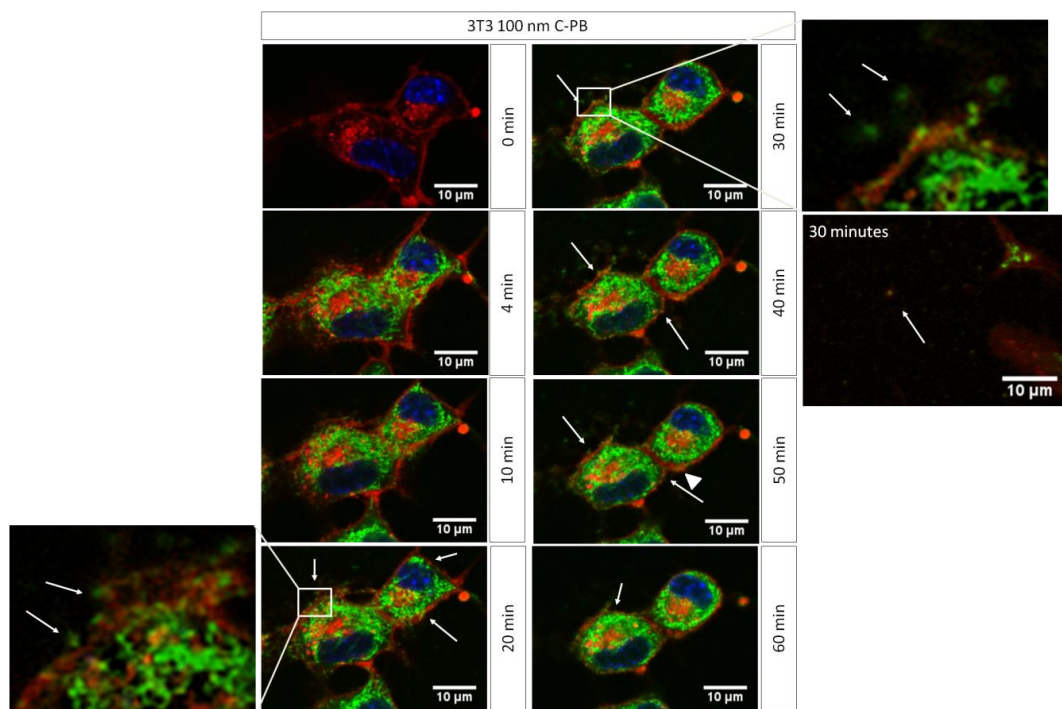


Figure 4-12 Zoom images of live experiments shown in Figure 4-9 – 4-11 of 3T3 cells treated with 100 nm C-PB 50 µg/ml for a period of 60 minutes. The arrows show aggregates of nanoparticles that detach from the membrane (details pictures). The arrow heads point to the membrane ruffling on the plasma membrane of 3T3 cells. Scale bars represent 10 µm. Green: C-PB; Red: CellMask membrane staining; Blue: Nuclei.

3T3 100nm

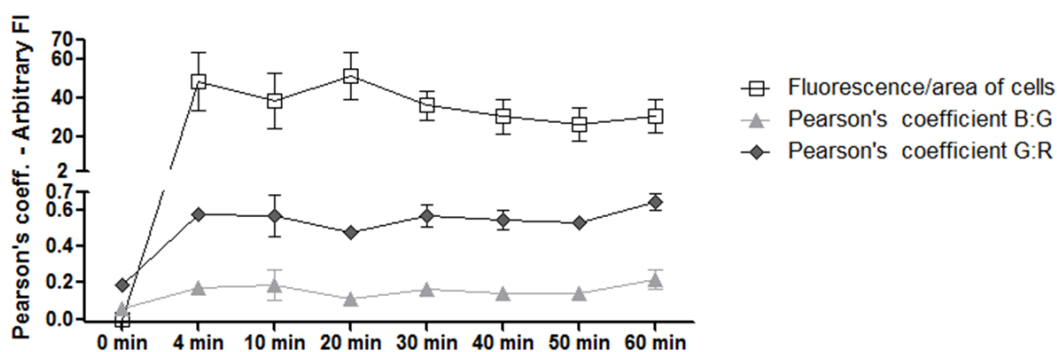


Figure 4-13 Analysis of the fluorescence of 3T3 cells treated with 50 µg/ml 100 nm C-PB for a period of 60 min. G: Green fluorescence of 100 nm C-PB; R: Red fluorescence of the CellMask deep red membrane staining; B: Hoechst nuclei staining. Here the green fluorescence normalised per area of cells and subtracted of the background of a region adjacent to the cells taken into the analysis is measured at different time points. From the graph it is possible to visualize an increase of the green fluorescence up to 20 minutes with a subsequent relative non statistically significant drop in the fluorescence of the C-PB. The Pearson's coefficient analysis, obtained with a JACoP plugging of ImageJ, shows there is little co-localization of the nanoparticles with the nuclei and a partial co-localization of the CellMask deep red membrane staining and the C-PB. Error bars represent the standard deviation of the mean (n>20).

Results – Inhibition of Endocytosis and Microscopy Studies

All cell lines showed some extent of internalization of the CellMask with a different degree of internalization depending on the cell line (Figures 4-11, 4-16, 4-21 and 4-26). The extent of internalization was higher in 3T3 and HCT116 cells with respect to MGLVA-1 cells.

CellMask stained the intracellular compartments of 3T3 cells more promptly than the plasma membrane where only weak staining was obtained (Figure 4-11), while a strong and stable staining of the cell membrane for up to 60 minutes was obtained with the dye in HCT116 cells (Figure 4-16). The same dye predominantly labeled the plasma membrane of MGLVA-1 cells, with moderate staining of intracellular compartments (Figure 4-21 and 4-26).

Furthermore, CellMask appeared to redistribute after application of the C-PB on cells with a stronger staining of the plasma membrane after application of 50 nm C-PB on HCT116 cells (Figures 4-14 and 4-16). A similar pattern was observed in 3T3 cells (Figures 4-9 and 4-11). However, here different confluence of cells also showed a different pattern of redistribution of CellMask where more confluent cells redistributed CellMask more slowly from the cytoplasm to the plasma membrane, while cells in less confluent regions looked more rounded and lost their elongated features (typical for this cell line) and presented a lower level of CellMask staining into the cytoplasm. The redistribution of CellMask in MGLVA-1 cells was less obvious after application of 50 and 100 nm C-PB (Figures 4-19, 4-21, 4-24 and 4-26). Uptake of C-PB was already evident at 4 minutes from their application in all cell lines.

Green fluorescence from C-PB in 3T3 cells (normalized per area of cells) increased immediately after application of 100 nm C-PB for up to 20 minutes, with a slight reduction of fluorescence at 10 minutes. However, after 20 minutes the green fluorescence due to the C-PB began to decrease with time. Here, the difference in the green fluorescence at different time points was not statistically significant with a t

Results – Inhibition of Endocytosis and Microscopy Studies

test (Figure 4-13). Figure 4-12 at 20 and 30 minutes gives evidence of the presence of aggregates of nanoparticles adjacent to the plasma membrane at 20 minutes from the application of the 100 nm C-PB. These structures were also detected at other time-points (arrows) suggesting a rather active process taking place. Zoom images at 20 and 30 minutes in Figure 4-12 suggest that the process occurring might be exocytosis. Here, it is possible to see that 2 out of 3 C-PB aggregates present on the plasma membrane at 20 minutes (arrows) are detached and in the extracellular compartment at 30 minutes. The measured size of these aggregates was between 500-700 nm and lower than 1 μ m as measured by ImageJ. Also, at 30 minutes incubation (see expanded image) vesicle-like structures loaded with nanoparticles were detected in the extracellular compartment, with ImageJ measured size of about 1 μ m. The white arrowheads in the same set of pictures show ruffling of the plasma membrane that is symptomatic of exocytic, macropinocytic or phagocytic processes taking place. Co-localization studies of CellMask and C-PB show that 100 nm C-PB presented a partial degree of co-localization that was steady over time (Figure 4-13). Finally, the green fluorescence of the 100 nm C-PB in 3T3 cells did not appear to redistribute towards different regions of the cells over a 1 h period (Figure 4-11).

HCT116 cells incubated with 50 nm C-PB showed a rapid uptake of the nanoparticles at 4 minutes and localization of the nanoparticles in the cytoplasm of cells and adjacent to the peripheral region of nuclei (Figures 4-14, 4-16). The presence of the nanoparticles in this region was also suggested by a slight, albeit statistically non significant according to a t test, increase of the colocalization obtained by the green and blue channels of the C-PB and the nuclei at 4 and 10 minutes that was reduced upon translocation of the nanoparticles towards more peripheral regions of the cell (Figure 4-18B); this result is likely to be due to an effect of proximity of the nanoparticles with the nuclei. The analysis of fluorescence in cells showed that the

Results – Inhibition of Endocytosis and Microscopy Studies

emission from 50 nm C-PB was steady and not increasing for up to 20 minutes (Figure 4-18B). Over time, the fluorescence of the cells increased slightly but in a non-statistically significant way. From 30 minutes, it was possible to appreciate the presence of C-PB on the cell membrane of HCT116 cells (Figure 4-14, 4-16 and 4-17). Nanoparticles appeared to redistribute from the perinuclear region towards the periphery of the cells and the membrane (Figure 4-16) where the cytoplasmic membrane, stained in red at 4 minutes, turned orange at 60 minutes incubation suggesting co-localization of green nanoparticles and red membrane staining. This effect was also suggested by a small increase of co-localization at 40, 50 and 60 minutes of incubation (Figure 4-18B). From the higher magnification images in Figure 4-17 the redistribution of the CellMask membrane dye from time 0 can be seen. Cells appeared more rounded and the membrane more clearly defined after application of the C-PB. Cells internalized quickly the C-PB in the cytoplasm of cells. However, cells gradually moved the C-PB towards the membrane (white arrows), where they became increasingly more concentrated on the edges of cells, immediately above the CellMask membrane staining towards the extracellular compartment at 50 and 60 minutes (yellow arrows and zoom at 60 minutes of the same Figure). Furthermore, aggregates of nanoparticles of about 500 nm in diameter were present in proximity of the plasma membrane from 30 minutes (zoom at 30 minutes on the same Figure). The intense activity of the membrane of cells was also demonstrated by the spindle-like structures (Figure 4-18A) that were already visible at 4 minutes incubation of the nanoparticles with cells and from membrane ruffling in Figure 4-17 as indicated by the arrowheads.

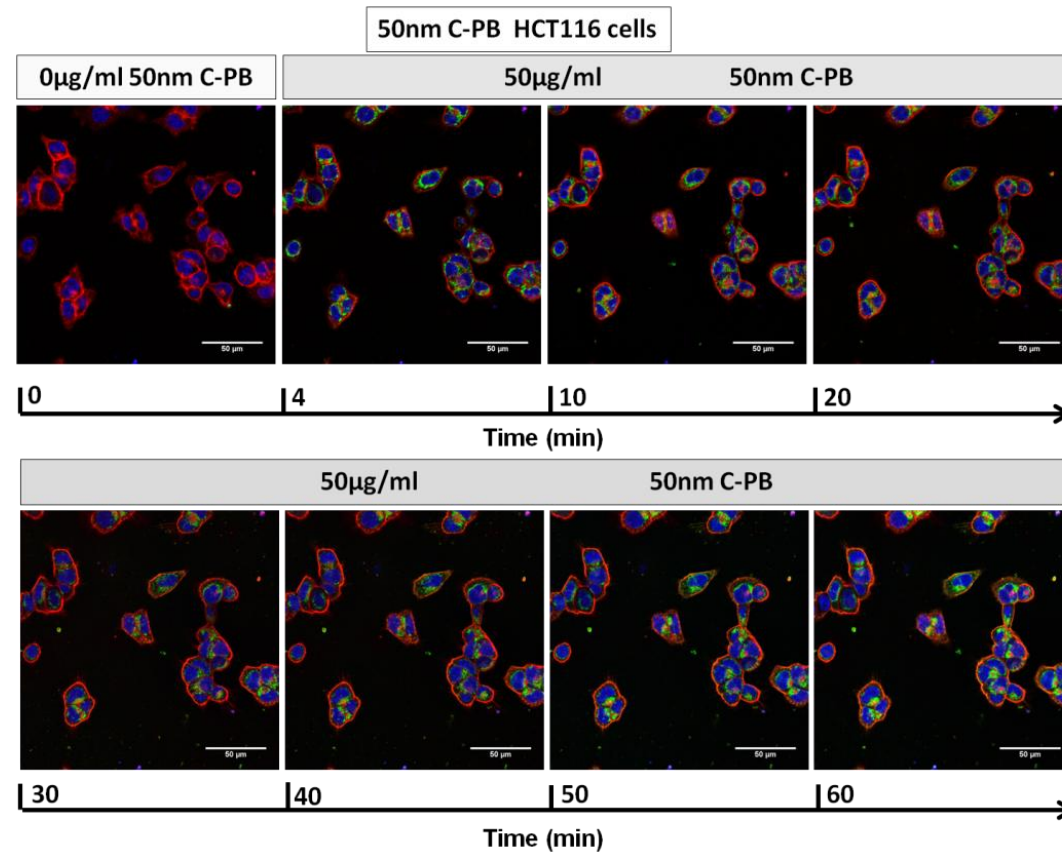


Figure 4-14 Merge of fluorescence live images for HCT116 cells incubated with 50 µg/ml of 50 nm C-PB for 60 minutes. Red: CellMask deep membrane staining, Green: C-PB, Blue: Hoechst nuclei staining. Scale bars represent 50 µm This set of pictures was obtained at time 0, before applying the solution of C-PB and at 4, 10, 20, 30, 40, 50 and 60 minutes after the application of the solution of C-PB. From the images it is possible to observe a quick uptake of the nanoparticles that were already internalised and localizing in a perinuclear region 4 minutes after their application on cells.

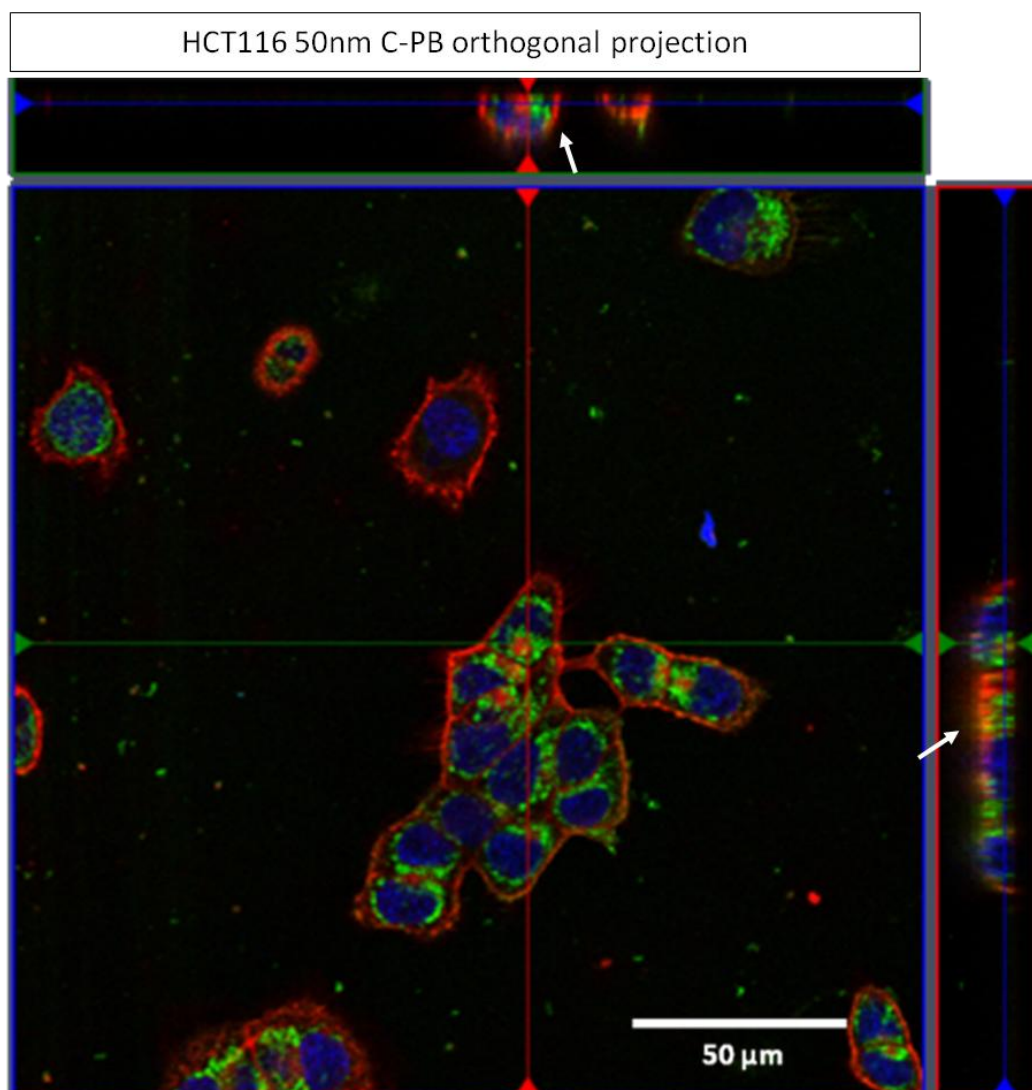


Figure 4-15 Orthogonal projection of a 3D image obtained with HCT116 incubated with 50 nm C-PB. This picture shows that the nanoparticles are localized inside cells (arrows). Scale bar represents 50 μm. Green: C-PB; Red: Membrane staining; Blue: Nuclei.

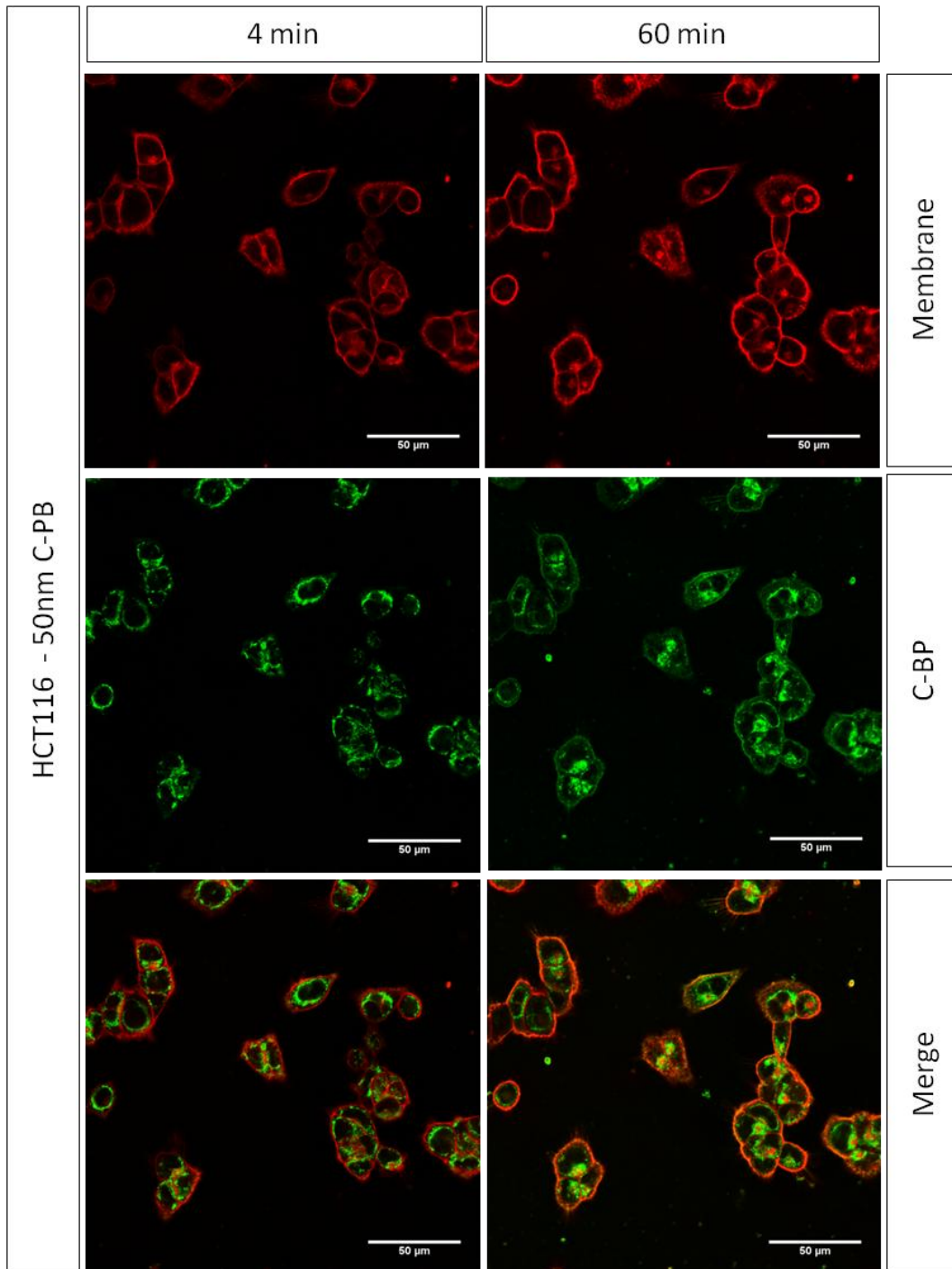


Figure 4-16 Images of the redistribution of the red CellMask membrane staining at 4 and 60 minutes in HCT116 cells. Also the 50 nm C-PB redistribute from a perinuclear region towards the membrane of HCT116 cells at 60 minutes incubation. Scale bar represents 50 μm . Red: Membrane staining; Green: C-PB.

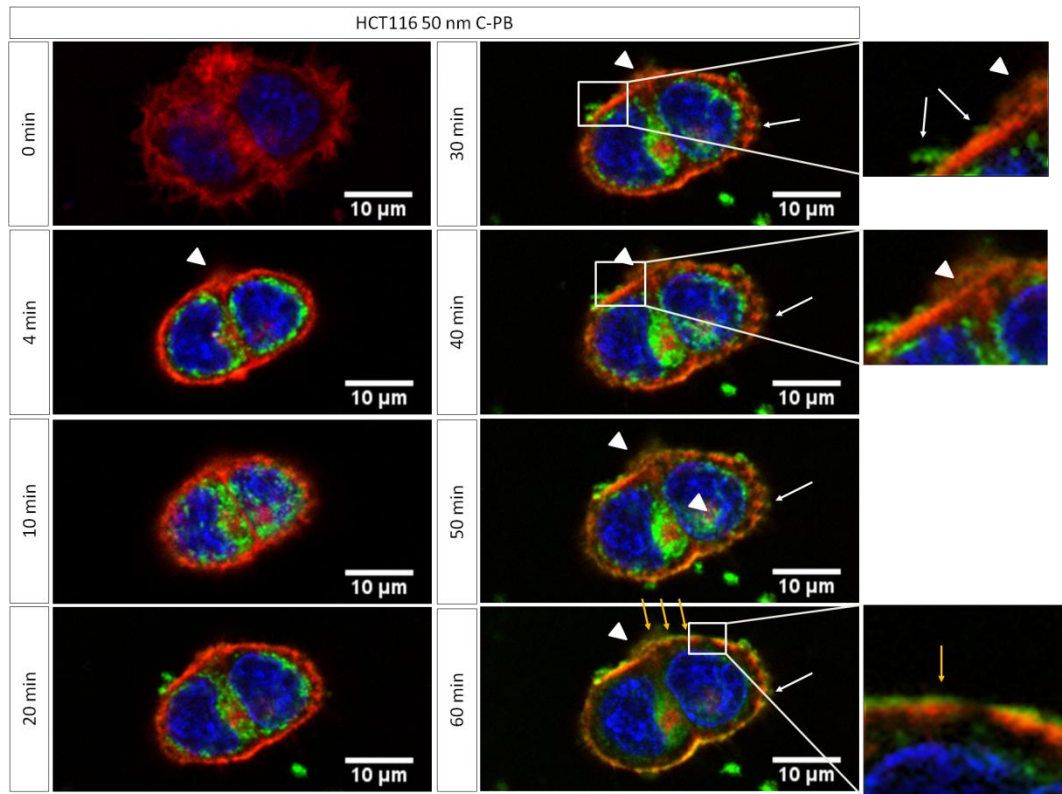


Figure 4-17 Details of the live imaging pictures shown in Figure 4-14 – 4-16 with HCT116 cells incubated with 50 nm C-PB 50 $\mu\text{g}/\text{ml}$ for a period of 60 minutes. The white arrows point to aggregates of nanoparticles on the cell surface of HCT116 cells, the yellow arrows point to the layer of C-PB in the cell membrane at 60 minutes (the same aspect is also reproduced in detail in the adjacent magnification image). The arrowheads point to membrane ruffling. Scale bars represent 10 μm . Green: C-PB; Red: Membrane staining; Blue: Nuclei.

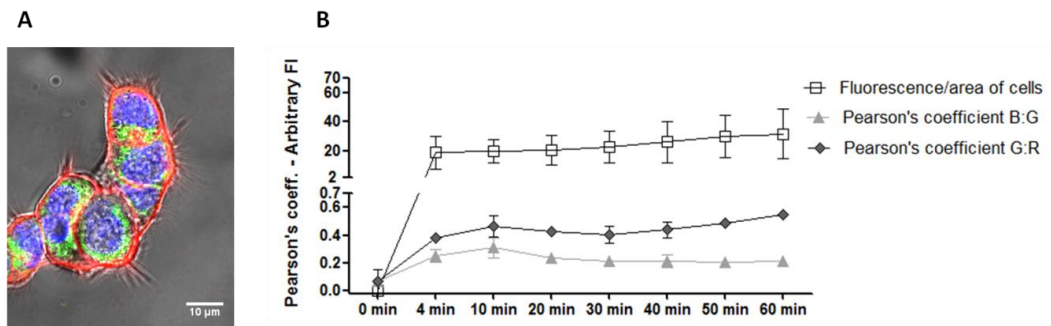


Figure 4-18 A. Spindle-like structures of HCT116 membrane of cells incubated for 4 minutes with 50 nm C-PB, demonstrating an intense activity of the membrane. Blue: Nuclei; Green: C-PB; Red: Membrane staining. Scale bars represent 10 μm . **B.** Analysis of the green fluorescence of HCT116 cells incubated with 50 nm C-PB (white squares and black connecting line) and of the Pearson's coefficient measuring the co-localization of the green fluorescence of the C-PB and the red membrane staining (light grey triangle and connecting line) and the green and the blue staining of the nuclei (dark grey diamonds and black connecting line). Error bars represent the standard deviation of the mean ($n > 20$).

Results – Inhibition of Endocytosis and Microscopy Studies

From confocal live cell imaging studies (Figures 4-19, 4-21, 4-24 and 4-26) on MGLVA-1 cells incubated with 50 µg/ml of 50 and 100 nm C-PB it was not possible to detect any distinct difference in the compartmentalization of the 2 nanoparticles (according to inhibition studies, the two nanoparticles were endocytosed by two discrete CPZ and MBCD sensitive pathways). The 50 and 100 nm C-PB nanoparticles showed little co-localization with CellMask, which mainly stained the plasma membrane of these cells (Figures 4-21 and 4-26). The normalized fluorescence per cell area was constant over the 60 minutes time-lapse of the experiment suggesting that the cells were balancing the ingress of nanoparticles with membrane localization or particle exocytosis. Evidence of accumulation of aggregates of nanoparticles on the plasma membrane is provided by images shown in Figure 4-22 for 50 nm C-PB and in Figure 4-27 for 100 nm C-PB (zoom at 10 and 20 minutes incubation for 50 nm C-PB and 20 and 30 minutes incubation for 100 nm C-PB). From zoom images at 10 and 20 minutes obtained for MGLVA-1 cells incubated with 50 nm C-PB (Figure 4-22) it is not possible to define any likely direction of the movement of the aggregates of nanoparticles and for this reason it is not possible to suggest any specific exocytic or endocytic process. For MGLVA-1 cells treated with 100 nm nanoparticles (Figure 4-27), zoom images at 20 and 30 minutes show a movement towards the plasma membrane of aggregates of nanoparticles of 700 nm according to ImageJ measurements suggesting an exocytic process taking place (arrows). Finally, evidence of membrane ruffling is shown by the arrow heads in both MGLVA-1 cells incubated with 50 nm (Figure 4-22) and 100 nm C-PB (Figure 4-27).

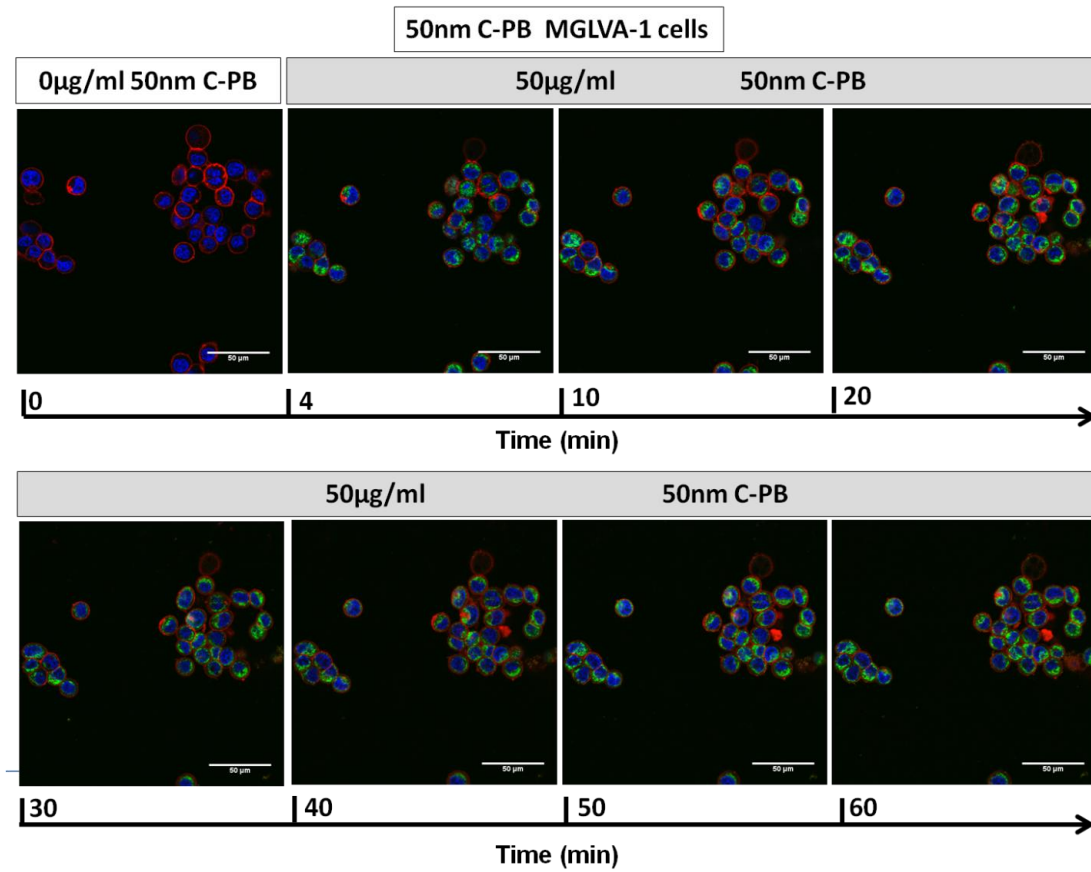


Figure 4-19 Confocal live studies of MGLVA-1 cells treated with 50 µg/ml 50 nm C-PB for a period of 60 minutes. Pictures were taken before applying the C-PB (time 0) and after 4, 10, 20, 30, 40, 50 and 60 minutes from the application of the C-PB. Green fluorescence: C-PB, Red: CellMask deep membrane staining and blue: Hoechst nuclei dye. Scale bars represent 50 µm.

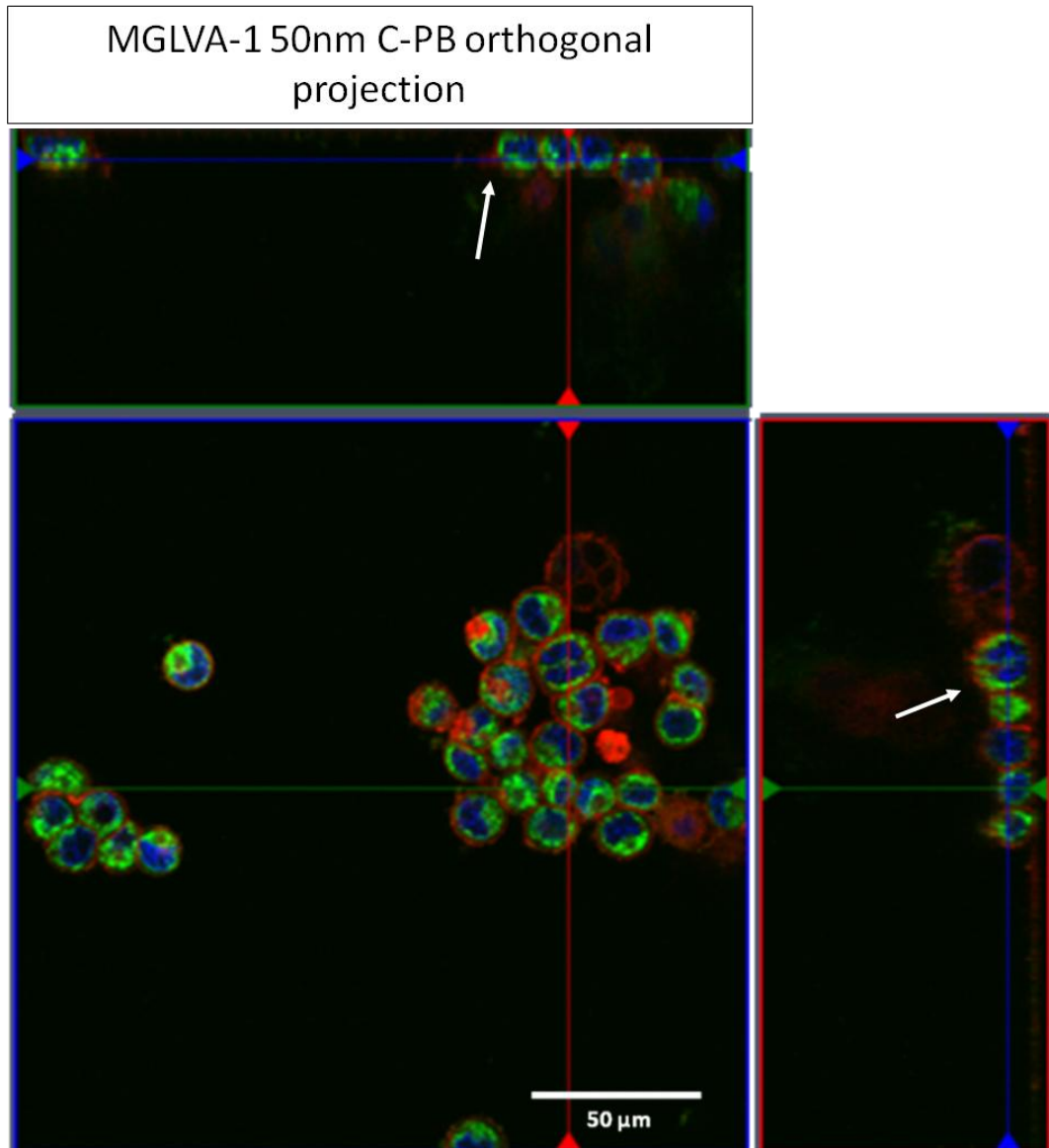


Figure 4-20 Orthogonal projection of a 3D image taken from MGLVA-1 cells treated with 50 $\mu\text{g/ml}$ 50 nm C-PB. The arrows show that the nanoparticles (green) are internalized by cells and are localized inside the membrane (red) periphery of cells. Blue: nuclei. Scale bar represents 50 μm .

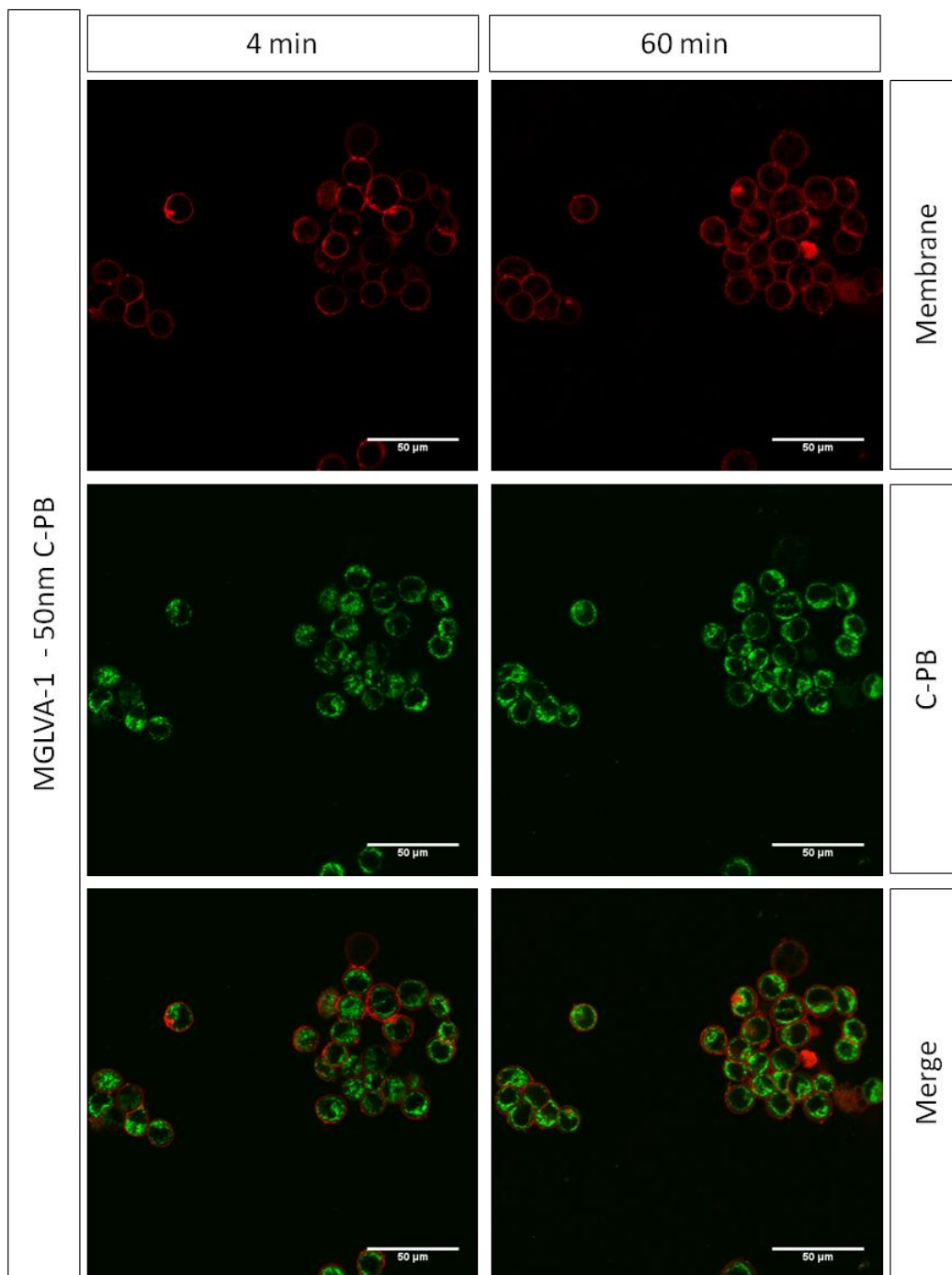


Figure 4-21 MGLVA-1 cells treated with 50 μg/ml 50 nm C-PB for 60 minutes. The images show the green channel of the C-PB at 4 and 60 minutes incubation with cells, the red channel for the CellMask deep membrane staining and a merge of the two. There is only little evidence of redistribution of the C-PB over time in different compartments of the cells as well as only little internalization of the CellMask over time. Scale bars represent 50 μm.

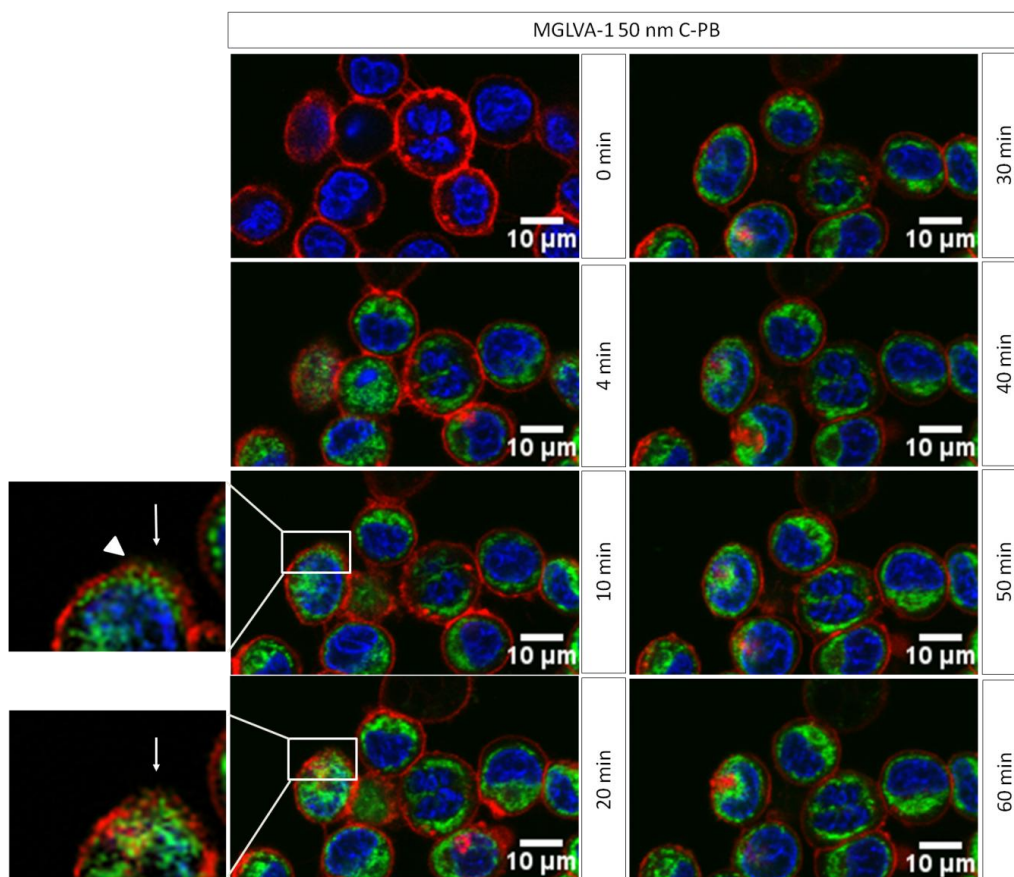


Figure 4-22 Details of the live images studies shown in Figures 4-19 – 4-21 of MGLVA-1 cells treated with 50 µg/ml 50 nm C-PB for a period of 60 minutes. The zoom at 10 and 20 minutes and the arrows give evidence for aggregates of nanoparticles trafficking the cytoplasmic membrane. The white arrow heads point to the membrane ruffles. Green: C-PB fluorescence, red: CellMask deep membrane staining and Blue: Hoechst dye are shown in these images. Scale bars represent 10 µm.

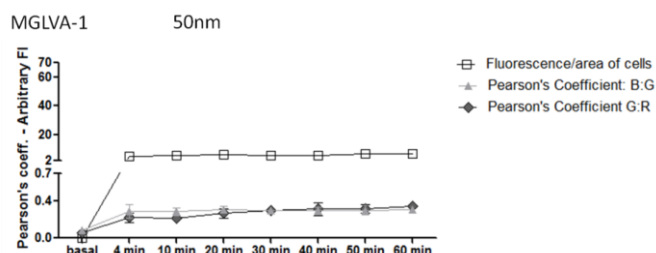


Figure 4-23 Analysis of the fluorescence of MGLVA-1 cells treated with 50 nm C-PB for 60 minutes. Quantification of the green fluorescence of the C-PB normalised by cell area and background (white squares and black connecting line). Co-localization quantification given by the Pearson's coefficient measured at different time-points with a JACoP plugin from ImageJ. Co-localization for the green fluorescence of C-PB and the red CellMask membrane dye (dark grey diamonds and black connecting line); C-PB and the Hoechst blue fluorescence colocalization is shown by the light grey triangles and connecting line. Error bars represent the standard deviation of the mean (n>20).

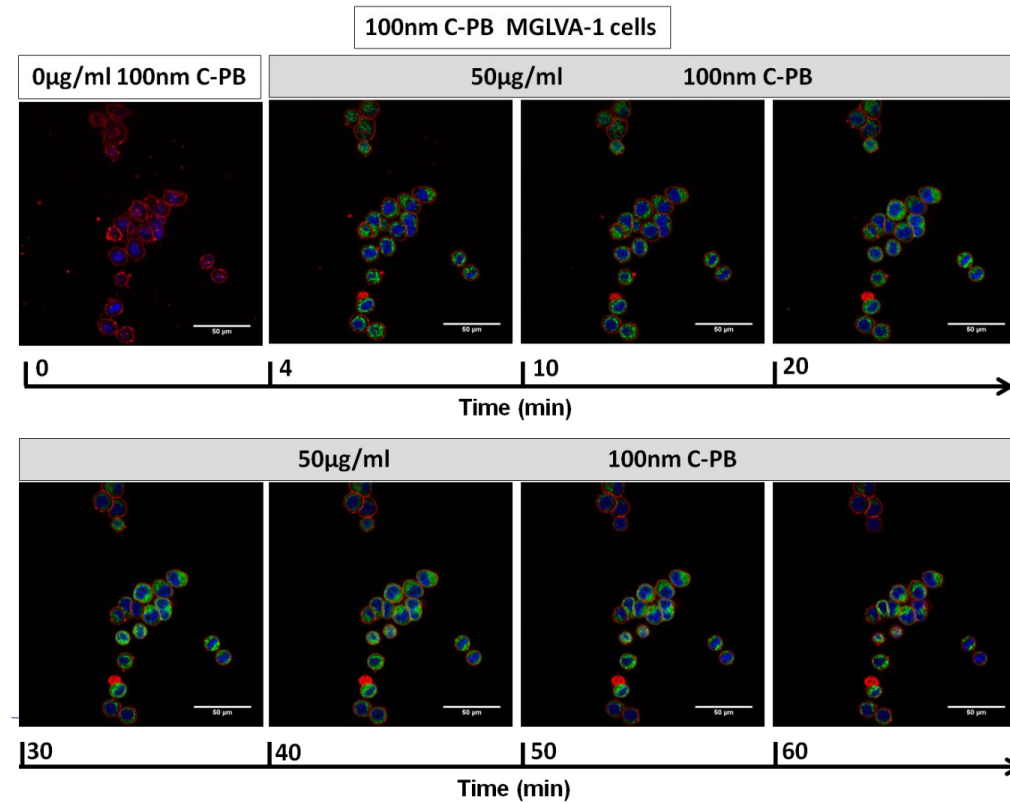


Figure 4-24 MGLVA-1 gastric cancer cells treated with 100 nm C-PB for a period of 60 minutes. Time 0 refers to cells before the treatment with nanoparticles. Pictures were subsequently taken at 4, 10, 20, 30, 40, 50 and 60 minutes from the application of the C-PB. Green fluorescence from the 100 nm C-PB is present in the cytoplasm of MGLVA-1 at 4 minutes from the application of the C-PB. Red fluorescence: CellMask membrane staining, Blue fluorescence: Hoechst nuclei dye. Scale bars represent 50 µm.

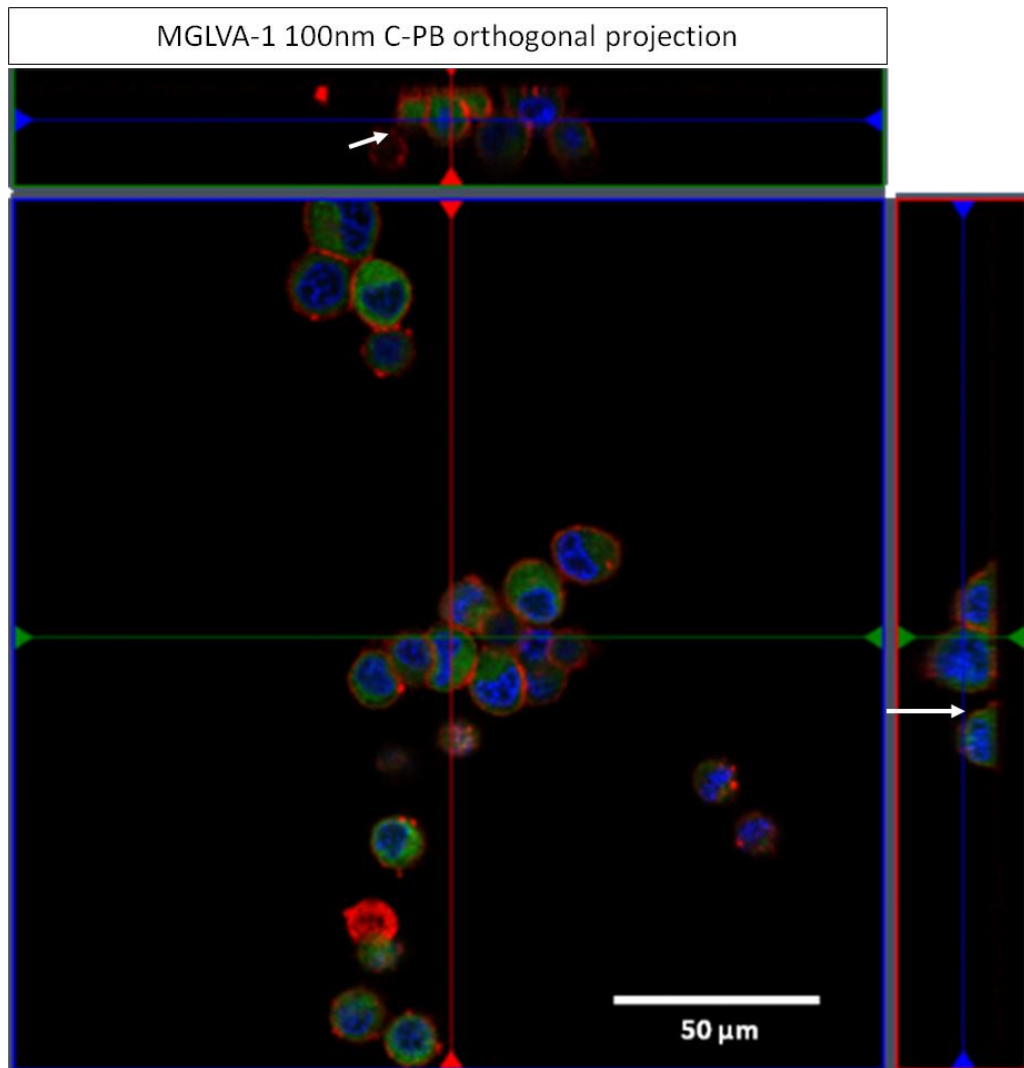


Figure 4-25 Orthogonal projection of a 3D image obtained from MGLVA-1 cells treated with 100 nm C-PB. Blue: Hoechst, Green: C-PB, Red: CellMask membrane staining. The arrows point to the regions that show that the nanoparticles are internalized and localize in a region between the nuclei and the membrane. Scale bar represents 50 μm .

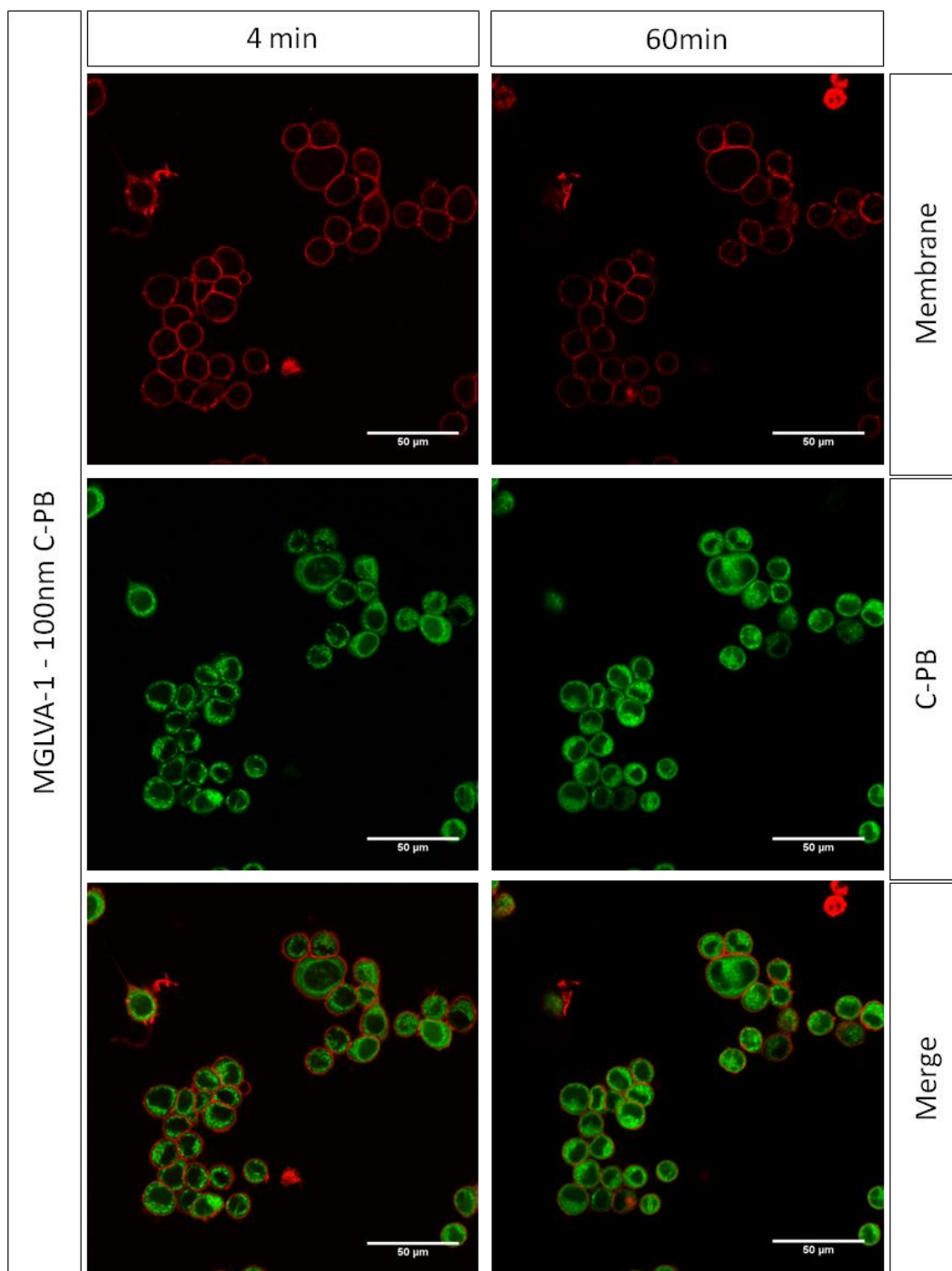


Figure 4-26 Redistribution of the C-PB (Green) and CellMask membrane staining (red) over time for MGLVA-1 cells treated with 50 $\mu\text{g}/\text{ml}$ of 50 nm C-PB (green). The Figures show 4 and 60 minutes images with single channels for C-PB and cell Mask and a merge of both. Scale bars represent 50 μm .

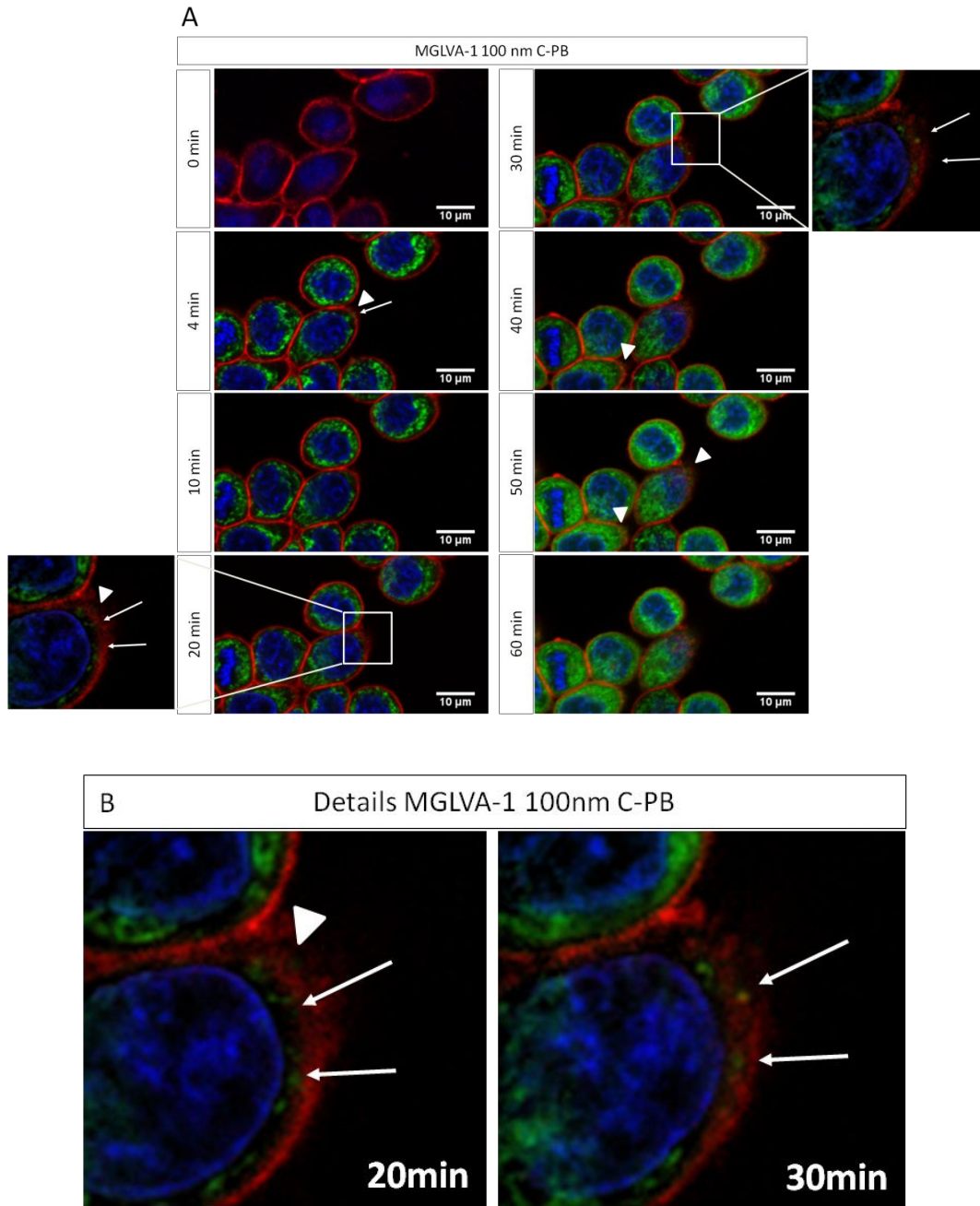


Figure 4-27. A. Details of live images shown in Figure 4-24 - 4-26 of the endocytosis and trafficking of 100 nm C-PB in MGLVA-1 cells for a period of 60 minutes. B. Magnification of the regions enclosed in the squares of Figure 28A. From the enlarged images it is possible to verify some degree of rearrangement of the CellMask membrane dye on the plasma membrane from time 0 and 4 minutes where the dye concentrates in a more compact fashion of the plasma membrane of the cells after the application of C-PB. Also C-PB appear to redistribute, and from 30 minutes it is possible to see a more diffuse and less discrete cytoplasmic fluorescence. From the magnification detail in Figure 28B at 20 and 30 minutes incubation it is possible to detect a movement of aggregates of nanoparticles towards the plasma membrane of cells and the extracytoplasmic compartment. (arrows). The arrow heads point to the membrane ruffling present on the membrane of MGLVA-1 cells. Scale bars represent 10 μm .

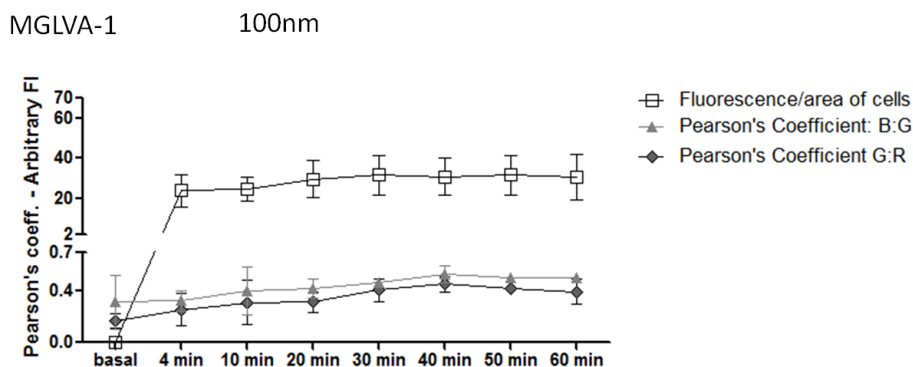


Figure 4-28 Analysis of the fluorescence of MGLVA-1 cells treated with 100 nm C-PB for 60 minutes. Quantification of the green fluorescence of 100 nm C-PB normalized by cells area and subtracted of the background fluorescence from regions adjacent the cells subtracted from the analysis (white squares and black connecting line). Pearson's coefficient quantification obtained with a JACoP plug-in of ImageJ of the co-localization of the C-PB with the red CellMask membrane staining (dark grey diamonds and black connecting line) and C-PB and Hoechst nuclei staining (light grey triangles and connecting line). Error bars represent the standard deviation of the mean (n>20).

4.4 Discussion

Initial experiments on the inhibition of clathrin-mediated endocytosis focused on the use of the dopamine antagonist CPZ (Table 4-2).

Chemical nomenclature	Chemical structure	Molecular weight
3-(2-chloro-10H-phenothiazin-10-yl)-N,N-dimethyl-propan-1-amine		355.33

Table 4-2 CPZ chemical structure, chemical nomenclature and molecular weight.

CPZ is an amphiphilic molecule that intercalates in the inner leaflet of the membrane of cells¹⁸. Its cationic portion interacts with the negative charge of phospholipids and, in particular, phosphoinositides¹⁹. This binding alters the properties of the membrane, causing redistribution of phospholipids between the inner and outer leaflet and

Results – Inhibition of Endocytosis and Microscopy Studies

clustering of membrane proteins^{19,20}. As a consequence it has been widely used as a CME inhibitor. However, its specificity has been often questioned in the literature. Its interference with other endocytic processes such as phagocytosis in neutrophils and macrophages has been repeatedly shown and it has been hypothesised that CPZ could interfere also with macropinocytosis in non specialised cells²¹. This conclusion has been justified by the similarity of the machinery of macropinocytosis and phagocytosis. However, recent findings suggest that clathrin might be also involved in phagocytosis processes partially restoring the credibility of the CPZ as a specific CME inhibitor^{22,23}.

Experiments described above showed that the inhibition of CME with CPZ was time- and cell-dependent and the duration of the incubation period of cells with specific pathway inhibitors was an important factor to take into consideration in these studies as effects were time-dependent.

As described in chapter 3, at the working concentrations used in the experiments reported in this chapter, CPZ inhibits endocytosis by binding to calmodulin, which regulates the recruitment of the myristoylated alanine-rich C-kinase substrate protein (MARCKS) that sequesters the phospholipid phosphatidylinositol 4,5-bisphosphate (PI(4,5)P2). This phospholipid is essential for the interaction of AP-2 adaptor protein with the plasma membrane in CME^{24,25}. These data from the literature suggested a first hypothesis in order to explain the unusual pattern of Htf inhibition of uptake with CPZ: that with increased CME activity in the cell and consequent expression of clathrin, the longer is the time taken by CPZ to inhibit CME. However, conversely to the expectations, HCT116 cells, for which the highest expression of CHC α was found by immunocytochemistry experiments (please see chapter 3), were more quickly inhibited by the drug, while for MGLVA-1 cells, which expressed relatively low levels

of clathrin and higher levels of caveolin-1 compared to HCT116 and 3T3 cells, Htf uptake was less easily inhibited by CPZ.

Two other hypotheses were then formulated:

- A disparity of expression of MARCKS in different cell lines might be the cause for the difference in CPZ action where, an increase in MARCKS would be expected to decrease the time needed to inhibit the Htf uptake pathway, or
- Calmodulin expression might be different in different cell lines and thus the higher the level of cells with increased calmodulin, the longer the time taken for CPZ to inhibit Htf uptake.

There are prior reports of differences in expression of MARCKS in different cell lines^{26,27} but there is very little literature on the different levels of expression of calmodulin depending on the cell line. Furthermore, Bickeboller *et al* specifically characterized HCT116 cells for the expression of MARCKS by immunoblotting showing that the expression of the protein is low with respect to other colon cancer cell lines²⁷. This experimental observation alone is not sufficient to rule out the above-mentioned hypothesis as the expression of MARCKS should be evaluated in conjunction with time of inhibition of endocytosis. At the moment it is not possible to draw definitive conclusions from the data available. Further studies are necessary to better characterise any connections between the expression of calmodulin/MARCKS and the length of time needed to inhibit endocytosis with CPZ.

The finding that CPZ was inactive in the inhibition of Htf uptake after the maximal inhibition time-point of the endocytosis of Htf has not been reported in the literature previously. It was hypothesized that the recovery of the endocytosis of Htf was due to membrane toxicity of CPZ and the theory that increased Htf internalization after a maximal inhibition of CME was a consequence of such toxicity was evaluated.

Results – Inhibition of Endocytosis and Microscopy Studies

The possibility of effects on cell activity by CPZ, additional to endocytic uptake inhibition, was investigated. CPZ has been also reported as a pore-forming molecule²⁸ and it is regularly used as a promoter of membrane fusion in experiments studying the dynamics of membrane reorganization in cells. However, this membrane-fusion property of CPZ is exerted only at concentrations that are near its critical micelle concentration (4 mM), i.e. well above the concentrations used in the pathway inhibition experiments of 80 μM ²⁹. Nevertheless, concentrations of CPZ above 50 μM have been reported to produce leakage of low molecular weight cytoplasmic materials in platelets (< 2000 Da) suggesting that CPZ is indeed able to produce small pores in the membrane of cells²⁰. On the other hand, Htf is a large protein with a molecular weight of 80kDa and dimensions of 5 x 5 x 1.6 nm³⁰, suggesting that Htf is unlikely to enter cells as a consequence of CPZ-induced membrane pore formation. In addition, from the experiments using CPZ at 40 and 60 μM , it was observed that the extent of the recovery of Htf uptake after inhibition was more significant at lower concentrations of CPZ, where any toxicity and pore-forming ability would be reduced. Further evidence that the recovery of the levels of Htf uptake was due to active transport of the protein inside cells was obtained from experiments in which media were used containing no Ca^{2+} and Mg^{2+} . By depleting the levels of these two ions, the cells became energy-depleted too, and recovery of Htf uptake stopped with a steady reduction of the Htf internalization over a period of 4 h in 3T3 cells³¹. These data together suggest that inhibition of Htf uptake by CPZ and subsequent recovery of Htf endocytosis was not likely have occurred via a general toxicity effect of CPZ on cells, but instead was due to temporary interruption by CPZ of an active and energy-dependent transport of Htf into cells. Although this mechanism might be attributed to off target effects of a non-specific and complex

Results – Inhibition of Endocytosis and Microscopy Studies

inhibitor of endocytosis such as CPZ, some speculations in other directions might also be worth some consideration.

The internalization of Htf by a non-transferrin receptor-mediated mechanism in hepatocytes was first reported in the 1980's³² with transferrin receptor 2 (TR2) being cloned some years later³³. The presence of TR2 in tissues other than the liver and erythroid precursor cells has been debated. However, some authors report the presence of TR2 in colon cancer and glioma cells and, more importantly, in HCT116 cells, which are part of the panel of cell lines used in these studies³⁴⁻³⁷.

TR2 is a type II transmembrane glycoprotein with at least two alternative splicing isoforms, TR2 α and β ³⁸. TR2 α has a transmembrane and short cytoplasmic domain while TR2 β has only the extracellular portion of the protein and lacks the transmembrane and cytoplasmic domains. TR2 also binds iron, although at a lower affinity ($K_d=30 \times 10^{-9}M$) with respect to transferrin receptor 1 (TR1, $K_d=7 \times 10^{-9}M$) also known as p90, CD71 and transferrin receptor³⁹. The endocytic process by which the transferrin is endocytosed together with TR2 is identical to the endocytosis of TR1. The complex is internalized, it is transported to an acidic compartment and then recycled back to the plasma membrane where the apo-transferrin is released³². TR2 presents a Yxx Φ motif that can bind an AP2 adaptor protein which suggests that it can be internalized by a clathrin receptor pathway. Chen and coworkers also showed that TR1 and TR2 can internalize through an AP2 pathway and compete for the pathway in the presence of holo-transferrin confirming support for a clathrin-mediated uptake pathway^{36,39}. Chen *et al* showed that the internalization of TR2 in the presence of holo-transferrin is directed towards a multivesicular body degradative pathway and this might explain the short half life of TR2 in the presence of holo-transferrin when TR1 is active. The presence in the media of transferrin and binding of the transferrin to the TR2 can extend the half life of the receptor and direct it

Results – Inhibition of Endocytosis and Microscopy Studies

towards a recycling pathway instead. The binding to the TR2 in physiological conditions has been reported to occur only when the TR1 was down-regulated in the liver which suggests that the receptor has a physiological role in the maintenance of the homeostasis of iron such as a sensor for transferrin levels in serum^{36,38,40}. From the data reported in this chapter and the literature it is possible to suggest that TR2 might be responsible for the uptake of Htf when TR1 is inhibited. There is prior evidence of the presence of the receptor at least for one cell line used in the experiments reported in this chapter (HCT116), and the mechanism by which the TR2 is activated and directed to a recycling pathway fits well with the results shown in this thesis^{34,35}. The mechanism hypothesized from these data is the following: when the TR1 is inhibited by CPZ, the TR2 starts binding Htf. This event triggers the switch from a degradative to a recycling pathway, which increases TR2 expression. The proposed increase in concentration of the receptor can be hypothesized in the experiments reported at 3 and 4 h in 3T3 cells and 2, 3 and 4 h in HCT116 cells. At 4 h the levels of endocytosis in these cell lines is comparable to the positive control, where the internalization of Htf occurs by a TR1-mediated route, which suggests that the TR2 can replace the activity of TR1 in the absence of functional TR1. However, there are a few points that still remain unclear.

Chen *et al* showed that both TR1 and 2 were active by clathrin-mediated endocytosis, but it is not clear why a TR2-mediated pathway would not be inhibited by the action of CPZ since the activity of CPZ is not due to specific TR1 or TR2 binding. A key question is whether the TR2 triggers a different endocytosis mechanism when it switches from a degradative to recycling pathway. It may be possible that TR2 induces clathrin-mediated endocytosis but employs a different connector protein (other than AP2) which does not rely on PI(4,5)P2 for anchoring the forming clathrin lattice to the plasma membrane. If this were to be the case, it must be a new and

uncharacterised protein given that all the known clathrin adaptor proteins rely on PI(4,5)P2⁴¹ at the moment⁴² (the presence of new and uncharacterised adaptor proteins has been already suggested in the literature)⁴³. Chen *et al* also reported that, in the absence of holo-transferrin, TR2 can internalize through a different pathway and Calzolari and coworkers also came to this conclusion³⁴. The latter group of researchers showed that TR2 is associated with the detergent resistant insoluble fraction of cells in lipid rafts (colocalising to some extent with caveolae and caveolin-1 and in a different region with respect to TR1) and they also suggested a more signalling relevant role of the receptor in these conditions given that there was high colocalization with a CD81 membrane protein involved in exosome formation and signalling^{39,44,45}. However, these studies were not carried out on the panel of cell lines used in the experiments presented in this thesis. A caveolin-dependent endocytosis mechanism for internalization of Htf after the TR1 is inhibited is unlikely as Htf uptake is universally recognized as a CME marker⁴⁶. Clathrin has been recently found to be involved in phagocytosis as described more in detail in §1.3.4.7 of this thesis. However also phagocytosis is known to necessitate PI(4,5)P2 for its function (although through a slightly different process) and seems an improbable alternative internalization process candidate at the present⁴⁷. However, there may still be uncharacterized mechanisms by which proteins such as transferrin can enter cells when highly potent amphiphiles such as CPZ are present, and/or cells are stressed by being in the artificial cell culture environment rather than in a tissue.

Another feature of the inhibition of CME by CPZ might be explained by the data from different passage numbers of the cell lines used in inhibition studies. It was found that the higher the passage number or ageing of cells, the lower the levels of endocytosis inhibition by CPZ. This finding was partly expected, since dynamin expression, which is implicated in both clathrin and caveolin endocytosis, has been reported to be

Results – Inhibition of Endocytosis and Microscopy Studies

susceptible to passage number and confluence of cells⁴⁸. Calmodulin expression has also been shown to change in relation to cell ageing and this might contribute to these results⁴⁹. As the density of cells in these experiments was deliberately kept constant to sub-confluent levels to control the expression of endocytic proteins, it seems likely that an important determinant factor in the variability of the inhibition of Htf uptake was the passage number and ageing of cells.

In order to investigate further the endocytic pathways involved in Htf uptake and therefore of relevance to nanoparticle and drug delivery system uptake, assays were carried out with the inhibitor Pitstop 2 (Table 4-3). Pitstop 2 is a small molecule that was originally selected from screening assays based on structure-activity relationship (SAR)^{14,50}.

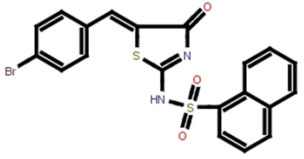
Chemical nomenclature	Chemical structure	Molecular weight
N-[5-(4-Bromobenzylidene)-4-oxo-4,5-dihydro-1,3-thiazol-2-yl]naphthalene-1-sulfonamide		473.36

Table 4-3 Pitstop 2 chemical structure, nomenclature and molecular weight.

Pitstop 2 is believed to bind specifically to the amino-terminal domain of clathrin which is essential for the interaction of the CHC with the endocytic machinery, which in turn assembles the clathrin lattice leading to vesicle formation. Pitstop 2 has been described as the first chemical inhibitor specific for CME, and is claimed to be non toxic in HeLa cells for up to 24 h. However, a number of papers have shown toxic effects of Pitstop 2, including reports of interactions with spindle formation in dividing HeLa cells, leading to cell death⁵¹. Also the specificity of Pitstop 2 has been

Results – Inhibition of Endocytosis and Microscopy Studies

questioned, as it has effects on processes specific to other pathways of endocytosis^{52,53}. However, the differences in structure of Pitstop 2 and CPZ were sufficient that investigation of the effects of Pitstop 2 on Htf uptake were considered of interest in comparison to those of CPZ. Strong inhibition of Htf uptake was obtained at 1 and 2 h incubation with Pitstop 2 in HCT116 cells, in contrast to experiments involving CPZ, where a partial recovery of Htf uptake was observed at 2 h. However, toxicity of Pitstop 2 was observed during inhibition experiments and thus the incubation time of Pitstop 2 with cells was reduced to 2 h instead of 4 h incubation as used in experiments with CPZ. Toxicity, as suggested by the experiments using HBSS depleted of Ca^{2+} and Mg^{2+} , can generate a failure in the recovery of the Htf uptake after inhibition.

CPZ was also used in LacCer inhibition studies as a further control of CPZ specificity towards CME. Here, CPZ did not show any inhibition of endocytosis of LacCer as expected and already reported in the literature^{15,21}. However, an increase of LacCer endocytosis was observed in the presence of the inhibitor and confirms results obtained by Vercauteren and coworkers¹⁵.

LacCer inhibition of endocytosis by MBCD was not complicated by the recovery of inhibition and cell passage number. Incubation times and cell line characteristics did not affect the ability of the inhibitor to function. The inhibition obtained was steady and maximal for a period of 4 h incubation and, as shown by viability studies in chapter 3 as well as experimental observations, it was not due to toxicity of the inhibitor on cells. Only a minimal dependence on cell lines was observed in MGLVA-1 cells. Here, although a good inhibition of LacCer uptake was obtained already at 1 h incubation of the inhibitor with cells, a maximal inhibition was obtained at 2 h. No dependence on passage number of cells was observed in these experiments and this gives evidence of the inherent non specificity of the drug towards a caveolin and

Results – Inhibition of Endocytosis and Microscopy Studies

dynamamin-mediated endocytosis where passage number of cells indeed affects the results of the inhibition. Furthermore, when MBCD was used as a control of its specificity towards CIE in Htf inhibition studies, the drug had a small but detectable inhibition of CME that was more evident at specific incubation times of the drug with cells. The latter result might be interpreted differently if the hypothesis that a caveolin-dependent pathway is involved in Htf uptake proves to be true.

Inhibition of C-PB uptake in the presence of CPZ and MBCD shows that the same material can be directed towards different endocytic machineries depending on the cell line tested and, significantly, without modification of the nanoparticles with specific targeting molecules. This result is not entirely unexpected as some other authors already showed different sensitivity to inhibitors of endocytosis depending on the cell line⁵⁴. 50 nm C-PB showed specificity towards CME, macropinocytosis or phagocytosis as demonstrated by the inhibition of their endocytosis in the presence of CPZ. Even if phagocytosis is considered not to be a highly represented process in non-specialized cells, it cannot be completely ruled out from these data. After inhibition of the uptake of 50 nm C-PB in HCT116 and MGLVA-1 cells with CPZ, no recovery of the uptake of 50 nm C-PB was observed. The nanoparticles that had not been targeted with any specific receptor binding molecules appeared to be selectively internalized by a CPZ-sensitive pathway. This might be due to the specificity of the uptake of these nanoparticles towards a CPZ-sensitive pathway. However, another possibility for these results might be due to a combination of CPZ and C-PB of 50 nm resulting in toxicity.

The same nanoparticles were endocytosed by 3T3 fibroblasts quite efficiently but the mechanism of internalization remains unknown. Both inhibitors used were ineffective in the inhibition of their endocytosis and suggests that 3T3 fibroblasts use non-CPZ non-MBCD sensitive machinery for the endocytosis of 50 nm C-PB. When cells

Results – Inhibition of Endocytosis and Microscopy Studies

actively engaged in endocytosis were exposed to endocytic inhibitors that were not active on the pathway involved in the endocytosis of materials, the uptake of these materials was boosted and this mechanism has already been shown in the literature¹⁵. These results suggest a more dynamic way of thinking of endocytosis where pathways communicate with each other and 'sense' the level of activity of one pathway and compensate for its failure. This compensation can be quite substantial with up-regulation of the pathway up to 3 times the positive control in which the level of endocytosis is not perturbed by inhibitors of endocytosis. 100 nm C-PB on the other hand, internalized through a less specific mechanism of endocytosis and its endocytosis was only marginally inhibited before other pathways of internalization intervened and endocytosis recovered quickly to positive control levels.

Microscopy live studies gave evidence that the nanoparticles studied accessed 3T3, HCT116 and MGLVA-1 cells and they were endocytosed in less than 4 minutes. This data is in line with the literature that suggests a time of internalization as quick as 1 minute for some synthetic materials⁵⁶. Microscopy data did not rule out the possibility that the process taking place for the internalization of 50 nm C-PB in MGLVA-1 and HCT116 cells is due to phagocytosis or macropinocytosis. Microscopy pictures in fact show intense membrane activity and ruffling compatible with exocytosis, macropinocytosis and phagocytosis. 50 nm C-PB endocytosis was proven to be sensitive to CPZ in HCT116 and MGLVA-1 cells by inhibition studies and these data alone were also compatible with macropinocytic or phagocytic processes together with a CME uptake. CPZ inhibition of endocytosis, in fact, is not limited to CME only but also to phagocytosis and macropinocytosis. Although recent evidence suggests a clathrin involvement in phagocytosis which partially restores CPZ credibility as a CME inhibitor, from the data obtained it is not possible to assert with certainty what is the

Results – Inhibition of Endocytosis and Microscopy Studies

endocytic process taking place for the uptake of 50 nm C-PB in HCT116 and MGLVA-1 cells.

As shown from analysis of C-PB treated cells over time, the level of fluorescence reaches a plateau which suggests that cells are able to counterbalance the presence of extracellular C-PB. From experimental evidence, it is possible to suggest, from 2 out of the 4 experiments described, that one of the ways used by cells to counterbalance the endocytosis of C-PB might be through active exocytosis of nanoparticles. The most evident drop of C-PB fluorescence after 20 minutes was observed in 3T3 cells with respect to the other cell lines tested as shown by analysis of the total cell fluorescence normalized by area of cell (Figure 4-13, 4-18B, 4-23 and 4-28). 3T3 cells showed an extracellular vesicle of about 1 μ m (zoom image at 30 minutes of Figure 4-12), loaded with C-PB as it is possible to extrapolate from the green fluorescence of the core of the vesicle, and it was enveloped by a membrane. However, even if the literature reports sizes of 0.1-1 μ m for exocytic vesicles, the size of the vesicles detected in the extracellular compartment of 3T3 cells is close to those of apoptotic bodies. It has been shown that the size of apoptotic bodies is in the range of 1-5 μ m, a factor which should be taken into account when suggesting exocytosis⁵⁷. In support of the hypothesis of exocytosis is the size of the aggregates of nanoparticles on the membrane of cells: these ranged between 0.5 and 0.8 μ m and thus were of sizes that fit well with those of exocytic vesicles reported in the literature. Furthermore, from the magnification pictures shown of the 3T3 and MGLVA-1 cells, it is possible to suggest directionality towards the extracellular compartment of the cells for these aggregates of nanoparticles, again supporting the hypothesis. Aggregates of 50 nm C-PB were also observed on the plasma membrane of HCT116 and MGLVA-1 cells. However, a clear direction was not detected for the nanoparticles in these latter experiments. At least for HCT116 cells, a possibility is

that cells were not able to release the C-PB into the extracellular compartment because of the strong interactions of the nanoparticles with plasma membrane proteins. This process can be observed in the higher magnification image at 60 minutes in Figure 4-17 where a layer of green nanoparticles can be clearly distinguished over the CellMask membrane staining dye at 60 minutes. As C-PB are predominantly hydrophobic nanoparticles with a surface shell of negatively charged carboxyl groups, in serum-free media they may interact avidly with hydrophobic and/or positively charged proteins^{54,58}. It is possible to suggest that the event reported might be due to the interaction of C-PB negative charge and positive membrane proteins or positive domain of membrane proteins that are present on the plasma membrane of HCT116 cells. Exocytosis is known to be affected by the experimental use of buffers instead of full media. However, the effects described change depending on the material and cell line taken into consideration and some authors suggest that the presence of serum-free media boosts exocytosis while some others report an opposite effect^{54,56}.

4.5 Conclusions

From the experiments reported in this chapter some novel data have emerged in regard to the inhibition of endocytosis with CPZ. The time and cell specificity of the inhibitor of endocytosis and the subsequent recovery of the endocytosis of Htf have not been reported before and explains the difficulty reported by scientists working on inhibition of endocytosis in the use of CPZ as an inhibitor of this process. The effect on the passage number and ageing of cells on the endocytosis process also is a significant piece of information that has not been reported in the literature before and that has been important in establishing appropriate conditions for effective use of the inhibitor in C-PB inhibition studies in the reported experiments. The effect of the

inhibitor on LacCer uptake was also another interesting result that has been reported only once in the literature. Both LacCer and C-PB endocytosis were boosted in the presence of inhibitors of endocytic pathways that were not actively involved in the pathway of internalization of the material investigated. This suggests that the inhibition of one pathway activates other pathways of internalization giving a more organic and interconnected picture of endocytosis. Finally, 50 nm C-PB appear to be endocytosed by a CPZ-sensitive pathway and their uptake does not recover over time. Although this effect could be due to the combined toxicity of C-PB and CPZ, another hypothesis might be that C-PB show some specificity towards a CPZ-sensitive pathway and further investigations are required in order to understand the mechanisms underlying such specificity. Microscopy studies confirm that the nanoparticles are internalized by cells and that the endocytic process is rapid and efficient with nanoparticles internalized by cells already after 4 minutes. A suggestion of exocytosis of 100 nm C-PB in 3T3 and MGLVA-1 is also provided by these studies together with evidence of a membrane specific binding ability of 50 nm C-PB in HCT116 cells but not on MGLVA-1 cells. This observation supports the idea that the same nanoparticles can interact with different cells in different ways.

References

- 1 Tian, T. *et al.* Exosome Uptake through Clathrin-mediated Endocytosis and Macropinocytosis and Mediating miR-21 Delivery. *J Biol Chem* (2014).
- 2 Schmid, E. M. & McMahon, H. T. Integrating molecular and network biology to decode endocytosis. *Nature* **448**, 883-888 (2007).
- 3 Kann, M., Schmitz, A. & Rabe, B. Intracellular transport of hepatitis B virus. *World J Gastroenterol* **13**, 39-47 (2007).
- 4 Moreno-Ruiz, E. *et al.* Candida albicans internalization by host cells is mediated by a clathrin-dependent mechanism. *Cell Microbiol* **11**, 1179-1189 (2009).
- 5 Mehrbod, P. *et al.* Simvastatin modulates cellular components in influenza A virus-infected cells. *Int J Mol Med* **34**, 61-73 (2014).

Results – Inhibition of Endocytosis and Microscopy Studies

- 6 Tchoupa, A. K., Schuhmacher, T. & Hauck, C. R. Signaling by epithelial members of the CEACAM family - mucosal docking sites for pathogenic bacteria. *Cell Commun Signal* **12**, 27 (2014).
- 7 Zhang, Y. & Whittaker, G. R. Influenza entry pathways in polarized MDCK cells. *Biochem Biophys Res Commun* (2014).
- 8 Alva-Murillo, N., Lopez-Meza, J. E. & Ochoa-Zarzosa, A. Nonprofessional phagocytic cell receptors involved in *Staphylococcus aureus* internalization. *Biomed Res Int* **2014**, 538546 (2014).
- 9 Minakshi, R. & Padhan, K. The YXXPhi motif within the severe acute respiratory syndrome coronavirus (SARS-CoV) 3a protein is crucial for its intracellular transport. *Virol J* **11**, 75 (2014).
- 10 Rejman, J., Oberle, V., Zuhorn, I. S. & Hoekstra, D. Size-dependent internalization of particles via the pathways of clathrin- and caveolae-mediated endocytosis. *Biochem J* **377**, 159-169 (2004).
- 11 Li, T. & Takeoka, S. Enhanced cellular uptake of maleimide-modified liposomes via thiol-mediated transport. *Int J Nanomedicine* **9**, 2849-2861 (2014).
- 12 Quader, S. *et al.* Selective intracellular delivery of proteasome inhibitors through pH-sensitive polymeric micelles directed to efficient antitumor therapy. *J Control Release* **188C**, 67-77 (2014).
- 13 Solarska-Ściuk, K. *et al.* Intracellular transport of nanodiamond particles in human endothelial and epithelial cells. *Chemico-Biological Interactions* **219**, 90-100 (2014).
- 14 Robertson, M. J. *et al.* Synthesis of the Pitstop family of clathrin inhibitors. *Nat. Protocols* **9**, 1592-1606 (2014).
- 15 Vercauteren, D. *et al.* The Use of Inhibitors to Study Endocytic Pathways of Gene Carriers: Optimization and Pitfalls. *Mol Ther* **18**, 561-569 (2010).
- 16 van Renswoude, J., Bridges, K. R., Harford, J. B. & Klausner, R. D. Receptor-mediated endocytosis of transferrin and the uptake of Fe in K562 cells: identification of a nonlysosomal acidic compartment. *Proceedings of the National Academy of Sciences* **79**, 6186-6190 (1982).
- 17 Pagano, O. C. M. a. R. E. Internalization and sorting of a fluorescent analogue of glucosylceramide to the Golgi apparatus of human skin fibroblasts: utilization of endocytic and nonendocytic transport mechanisms. *J Cell Biol* **125**, 769-781 (1994).
- 18 Ferrell, J. E., Jr., K.T., M. & Huestis, W. H. Membrane bilayer balance and platelet shape: morphological and biochemical responses to amphipathic compounds. *Biochim Biophys Acta* **939**, 223-237 (1988).
- 19 Chen, J. Y. *et al.* Selective amphipathic nature of chlorpromazine binding to plasma membrane bilayers. *Biochimica et Biophysica Acta (BBA) - Biomembranes* **1616**, 95-105 (2003).
- 20 Holmsen, H. & Rygh, T. Chlorpromazine makes the platelet plasma membrane permeable for low-molecular weight substances and reduces ATP production. *Biochemical Pharmacology* **40**, 373-376 (1990).
- 21 Ivanov, A. I. Pharmacological inhibition of endocytic pathways: is it specific enough to be useful? *Methods in molecular biology* **440**, 15-36 (2008).
- 22 Sullivan, C. S. *et al.* The adaptor protein GULP promotes Jedi-1-mediated phagocytosis through a clathrin-dependent mechanism. *Molecular Biology of the Cell* (2014).
- 23 Liu, C., Wang, J. & Zhang, X. The Involvement of MiR-1-Clathrin Pathway in the Regulation of Phagocytosis. *Plos One* **9**, e98747 (2014).

Results – Inhibition of Endocytosis and Microscopy Studies

- 24 Eisenberg, S., Giehl, K., Henis, Y. I. & Ehrlich, M. Differential Interference of Chlorpromazine with the Membrane Interactions of Oncogenic K-Ras and Its Effects on Cell Growth. *Journal of Biological Chemistry* **283**, 27279-27288 (2008).
- 25 Levin, R. M. & Weiss, B. Mechanism by Which Psychotropic Drugs Inhibit Adenosine Cyclic 3',5'-Monophosphate Phosphodiesterase of Brain. *Molecular Pharmacology* **12**, 581-589 (1976).
- 26 Rosé, S. D., Cook, H. W., Palmer, F. B. S. C., Ridgway, N. D. & Byers, D. M. Differential Expression of MARCKS and Other Calmodulin-Binding Protein Kinase C Substrates in Cultured Neuroblastoma and Glioma Cells. *Journal of Neurochemistry* **63**, 2314-2323 (1994).
- 27 Bickeboller, M. *et al.* Functional characterization of the tumor-suppressor MARCKS in colorectal cancer and its association with survival. *Oncogene* **0** (2014).
- 28 Kozlovsky, Y., Chernomordik, L. V. & Kozlov, M. M. Lipid Intermediates in Membrane Fusion: Formation, Structure, and Decay of Hemifusion Diaphragm. *Biophysical Journal* **83**, 2634-2651 (2002).
- 29 Mondal Roy, S. & Sarkar, M. Membrane fusion induced by small molecules and ions. *J Lipids* **2011**, 528784 (2011).
- 30 Kilar, F. & Simon, I. The effect of iron binding on the conformation of transferrin. A small angle x-ray scattering study. *Biophysics Journal* **48**, 799-802 (1985).
- 31 Tarasov, A. I., Griffiths, E. J. & Rutter, G. A. Regulation of ATP production by mitochondrial Ca(2+). *Cell Calcium* **52**, 28-35 (2012).
- 32 Graham, R. M., Chua, A. C., Herbison, C. E., Olynyk, J. K. & Trinder, D. Liver iron transport. *World J Gastroenterol* **13**, 4725-4736 (2007).
- 33 Kawabata, H. *et al.* Molecular cloning of transferrin receptor 2. A new member of the transferrin receptor-like family. *J Biol Chem* **274**, 20826-20832 (1999).
- 34 Calzolari, A. *et al.* Transferrin receptor 2 is frequently expressed in human cancer cell lines. *Blood Cells, Molecules, and Diseases* **39**, 82-91 (2007).
- 35 Calzolari, A. *et al.* Tfr2 expression in human colon carcinomas. *Blood Cells, Molecules, and Diseases* **43**, 243-249 (2009).
- 36 Chen, J., Wang, J., Meyers, K. R. & Enns, C. A. Transferrin-directed internalization and cycling of transferrin receptor 2. *Traffic* **10**, 1488-1501 (2009).
- 37 Calzolari, A. *et al.* Transferrin Receptor 2 Is Frequently and Highly Expressed in Glioblastomas. *Translational Oncology* **3**, 123-134 (2010).
- 38 Kawabata, H. *et al.* Expression of hepcidin is down-regulated in Tfr2 mutant mice manifesting a phenotype of hereditary hemochromatosis. *Blood* **105**, 376-381 (2005).
- 39 Silvestri, L., Nai, A., Pagani, A. & Camaschella, C. The extrahepatic role of TFR2 in iron homeostasis. *Front Pharmacol* **5**, 93 (2014).
- 40 Johnson, M. B., Chen, J., Murchison, N., Green, F. A. & Enns, C. A. Transferrin receptor 2: evidence for ligand-induced stabilization and redirection to a recycling pathway. *Molecular Biology of the Cell* **18**, 743-754 (2007).
- 41 Owen, D. J., Collins, B. M. & Evans, P. R. Adaptors for clathrin coats: structure and function. *Annu Rev Cell Dev Biol* **20**, 153-191 (2004).
- 42 Mishra, S. K. *et al.* Disabled-2 exhibits the properties of a cargo-selective endocytic clathrin adaptor. *The EMBO Journal* **21**, 4915-4926, doi:10.1093/emboj/cdf487 (2002).
- 43 Traub, L. M. Sorting it out: AP-2 and alternate clathrin adaptors in endocytic cargo selection. *J Cell Biol* **163**, 203-208, doi:10.1083/jcb.200309175 (2003).
- 44 Calzolari, A. *et al.* Tfr2 localizes in lipid raft domains and is released in exosomes to activate signal transduction along the MAPK pathway. *J Cell Sci* **119**, 4486-4498 (2006).

Results – Inhibition of Endocytosis and Microscopy Studies

- 45 Poli, M. *et al.* Transferrin receptor 2 and HFE regulate furin expression via mitogen-activated protein kinase/extracellular signal-regulated kinase (MAPK/Erk) signaling. Implications for transferrin-dependent hepcidin regulation. *Haematologica* **95**, 1832-1840 (2010).
- 46 Sahay, G., Alakhova, D. Y. & Kabanov, A. V. Endocytosis of nanomedicines. *Journal of Controlled Release* **145**, 182-195 (2010).
- 47 Scott, C. C. *et al.* Phosphatidylinositol-4,5-bisphosphate hydrolysis directs actin remodeling during phagocytosis. *J Cell Biol* **169**, 139-149 (2005).
- 48 Damke, H., Baba, T., van der Blik, A. M. & Schmid, S. L. Clathrin-independent pinocytosis is induced in cells overexpressing a temperature-sensitive mutant of dynamin. *The Journal of Cell Biology* **131**, 69-80 (1995).
- 49 Linskens, M. H. *et al.* Cataloging altered gene expression in young and senescent cells using enhanced differential display. *Nucleic Acids Res* **23**, 3244-3251 (1995).
- 50 Donner, A. Signaling: Clathrin pitstops. *Nat Chem Biol* **7**, 654-654 (2011).
- 51 Smith, C., Haucke, V., McCluskey, A., Robinson, P. & Chircop, M. Inhibition of clathrin by pitstop 2 activates the spindle assembly checkpoint and induces cell death in dividing HeLa cancer cells. *Molecular Cancer* **12**, 4 (2013).
- 52 Dutta, D., Williamson, C. D., Cole, N. B. & Donaldson, J. G. Pitstop 2 Is a Potent Inhibitor of Clathrin-Independent Endocytosis. *Plos One* **7** (2012).
- 53 Willox, A. K., Sahraoui, Y. M. E. & Royle, S. J. Non-specificity of Pitstop 2 in clathrin-mediated endocytosis. *bioRxiv* (2014).
- 54 Lesniak, A. *et al.* Effects of the Presence or Absence of a Protein Corona on Silica Nanoparticle Uptake and Impact on Cells. *J Am Chem Soc* **135**, 1438-1444 (2013).
- 55 Panyam, J. & Labhasetwar, V. Dynamics of endocytosis and exocytosis of poly(D,L-lactide-co-glycolide) nanoparticles in vascular smooth muscle cells. *Pharm Res* **20**, 212-220 (2003).
- 56 Gyorgy, B. *et al.* Membrane vesicles, current state-of-the-art: emerging role of extracellular vesicles. *Cell Mol Life Sci* **68**, 2667-2688 (2011).
- 57 Monopoli, M. P., Bombelli, F. B. & Dawson, K. A. Nanobiotechnology: Nanoparticle coronas take shape. *Nature Nanotechnology* **6**, 11-12 (2011).

5-Chapter 5

***In vitro* studies of thermoresponsive micelle-like
nanoparticles**

5.1 Introduction

One of the major problems in the development of new drugs is producing molecules that are not only effective, with specificity at the target cell, but which also have the required physico-chemical properties to ensure they accumulate, after administration, at the intended tissue. In many cases it is not possible to combine these features in one molecule and thus carriers or delivery systems are needed in order to take a drug with sub-optimal solubility or stability to a target in the body. Delivery systems can facilitate administration and biodistribution and can reduce unwanted off target toxicity of the drug. A large variety of materials have been developed which can encapsulate delicate, potent and/or poorly soluble drugs during transit in the body and then release the drug at a distal site. The specificity of delivery at the target cell, tissue or organ can be affected by a variety of methods, many of which take advantage of the specific characteristics of the inflammation site that often develops as a consequence of the medical condition and/or of the cell biology in the pathological tissues. The changed physiology at a disease site can lead to hyperthermia, a modified oxidative or reductive environment, and/or a changed pH. As a consequence, drug delivery systems which change their properties with temperature, redox state and pH are potential means of delivering drugs specifically at disease sites. Polymeric micelle-like nanoparticles are an example of such delivery systems, as their self-assembly into supramolecular structures is reversible and can be triggered in the forward or reverse direction by a variety of stimuli. Polymer micelle-like nanoparticles for biomedical applications are easily formed by preparing a hydrophobic core polymer block, which can accommodate hydrophobic compounds

(e.g. anticancer drugs) and coupling this block to a hydrophilic shield polymer that bestows water solubility to the carrier system.

In this chapter the results on biocompatibility and cell penetration of thermoresponsive micelle-like nanoparticles are studied and reported. The thermoresponsiveness of the system was designed in the long term to target specifically inflamed tissue, as found in a variety of diseases. Pathological conditions can produce an inflammation that has been reported to raise the local temperature up to 42°C in some cases (hyperthermia). Hyperthermia can also be administered by ultrasound probes and near infrared irradiation in conjunction with the treatment with thermoresponsive materials¹⁻⁴.

5.2 Materials used for the studies

The thermoresponsive materials studied were based on polymers synthesized previously in our group by Abulateefeh *et al* and subsequently synthesized by Lee Moir. They can be described by the following general formulas in Figure 5-1 and 5-2⁵:

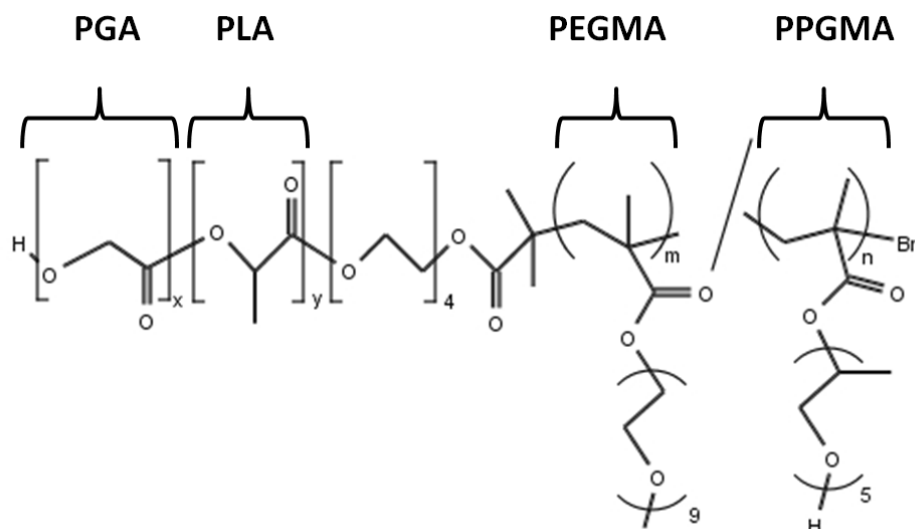


Figure 5-1 Poly(lactide-*co*-glycolide)-*block*-poly(poly(ethylene glycol methyl ether methacrylate)-*co*-poly(propylene glycol methacrylate)) (PLGA-*b*-(PPGMA-*co*-PEGMA)) thermoresponsive polymers. The different regions (or blocks) that constitute the polymer are labelled for easy detection. Some of the characteristics of these structures are summarised in the description in the text. X, y, m and n numbers are different in each polymer.

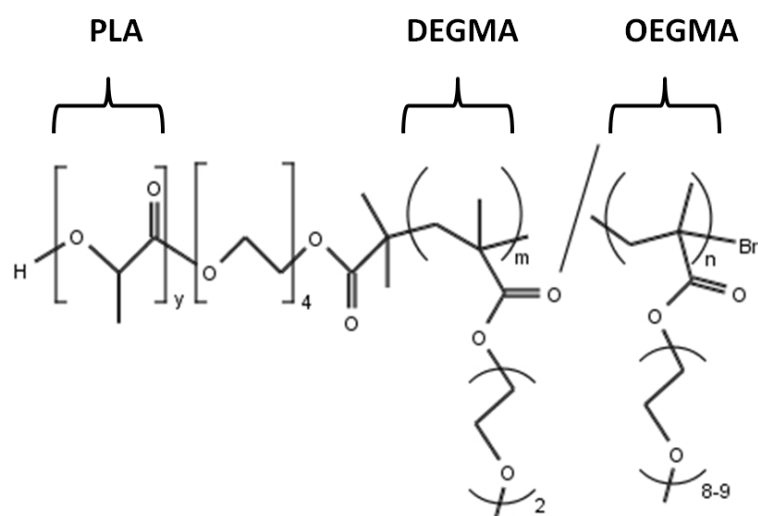


Figure 5-2 Polylactide- *block*- poly(poly(diethylene glycol methacrylate)-*co*-poly(oligoethylene glycol methacrylate)) (PLA-*b*-(DEGMA-*co*-OEGMA)) thermoresponsive polymers. The blocks that form the polymer are labelled for an easy detection. Both the hydrophobic and hydrophilic regions of these polymers have been modified in these second set of polymers with respect to polymers in Figure 5-1 and ⁵. Some of the characteristics of these structures are summarised in the description in the text. X, y, m and n numbers are different for each polymer.

Results – In vitro Studies of Thermoresponsive Polymers

The structures of poly(lactide-co-glycolide)-*block*-poly(poly(ethylene glycol methyl ether methacrylate)-*co*-poly(propylene glycol methacrylate)), (PLGA-*b*-(PPGMA-*co*-PEGMA)) is given in Figure 5-1. The polymer shown in Figure 5-2, which is slightly different to those prepared by Abulatefeh et al⁵ is poly(lactide- *block*-poly(poly(diethylene glycol methacrylate)-*co*-poly(oligoethylene glycol methacrylate)) (PLA-*b*-(DEGMA-*co*-OEGMA)). The PLGA/PLA region forms the hydrophobic, inner core of the micelle when these co-polymers are added to water. PLGA is a polyester block copolymer formed by poly-lactic acid (PLA) and poly-glycolic acid (PGA) (Figure 5-1). The PLA contains an asymmetric α carbon producing 2 enantiomeric structures referred as D and L or, R and S. The PLGA acronym refers to R and S poly lactic acids represented in equal ratio in the polymer⁶. PLGA is a biocompatible and biodegradable material that has been approved by the Food and Drug Administration (FDA)⁷. The susceptibility to degradation is affected by the molecular weight of the PLGA and by the ratio between PLA and PGA, where increasing the ratio of PLA reduces the rate of hydrolysis and acid-catalysed degradation⁸. The thermoresponsive properties of the polymer are given by PEGMA, PPGMA, DEGMA and OEGMA. These regions have the ability to change their structure from coil to globule with increasing temperature, changing their conformation from stretched and highly hydrated to collapsed and only partially hydrated⁹. This phenomenon occurs above a designed lower critical solution temperature (LCST) that in these polymers has been determined indirectly as the increase of turbidity of the polymer solution (cloud point) and it is referred to as the thermal transition temperature (TTT)¹⁰. The ratios between the PEGMA and PPGMA monomers in the chain can change the LCST of the polymer with higher quantities of PPGMA lowering the LCST of the individual polymer chains and the TTT of micelle-like nanoparticles and nanoparticles

Results – In vitro Studies of Thermoresponsive Polymers

formed from the co-polymers^{5,11}. Different ratios of PLA and PGA were used in these polymers to modify the size of the polymer and hence the size of the hydrophobic core of the micelle as well as different ratios of PEGMA (LCST \approx 90°C), PPGMA, DEGMA (LCST \approx 26°C) and OEGMA (LCST \approx 90°C) to study how these modifications affected the LCST and TTT¹²⁻¹⁵. Micelle-like nanoparticles were formed by nanoprecipitation¹⁶, adding an acetone solution, containing the solubilised polymer, to water either dropwise or with the aid of a syringe pump. These nanoparticles were of the size range (50-150 nm) similar to that of common virus particles, and thus were considered of interest as drug delivery systems.

The specific aim of this part of study was to produce polymers and micelle-like structures that were stable in suspension at normal physiological temperatures and resistant to cell uptake, but which were able to internalise into cells when above their TTT. Prior data from Abulatefeh *et al*, as well as numerous studies from the Chilkoti group, had shown that thermoresponsive polymers, polypeptides and nanoparticles were selectively internalised into some specific cell lines only when above their TTT^{16,17}. This study aimed to investigate if this phenomenon was cell-dependent, and if the polymer thermal response could be used for target specificity against cancer cells, as a first step towards organ or diseased issue specificity. Furthermore, it was intended to study the routes of internalization used by the polymer micelle-like nanoparticles to access cells as well as to compare and contrast the intracellular trafficking pathways of thermoresponsive polymers with those of C-PB reported earlier.

In this chapter are shown the results of tests of cell activity of micelle-like nanoparticles following incubation with the thermoresponsive polymers (formulated as kinetically trapped micelle-like nanoparticles), and microscopy studies to assess

Results – In vitro Studies of Thermoresponsive Polymers

the ability of the micelle-like nanoparticles polymers to access cells. The characteristics of the original polymers and the micelle-like nanoparticles formed by the assembly of these polymers are summarised in Table 5-1 and 5-2. The ζ potential for the nanoparticles tested was negative and close to neutrality (values ranging between -0.5 and -4 mV). ζ potential measurements were run in HEPES buffer 1 mM, pH 7.4 at 20°C.

Nanoparticle formulation number	Constituent polymers PLGA ratio PLA:PGA	Constituent polymers [PPGMA]: [PEGMA]	M _n (GPC)	M _w (GPC)	Đ (polydispersity)	TTT	Diameter of the micelles (nm)	Dye
1	65:35 (Mn~7000)	3:1	29333	36658	1.25	~40°C	53.6/210	Rhodamine B (non conjugated)
2	65:35 (Mn~7000)	1:1	24633	29352	1.19	~64°C	29.2/179.2	Rhodamine B (non conjugated)
3	75:25 (Mn 8260)	2:1	15118	17087	1.13	~50°C	31/198.6	Rhodamine B (non conjugated)
4	75:25 (Mn 8260)	3:2	14050	15736	1.12	~58°C	29.2/197.6	Rhodamine B (non conjugated)
5	65:35 (Mn 17708)	4:1	31143	41836	1.34	~41 °C	142.4	Fluorescein (conjugated to PEGMA)
6	75:25 (Mn 19586)	5:1	28329	50014	1.76	~24°C	118	Fluorescein (conjugated to PEGMA)
7	75:25 (Mn 19586)	5:1	28329	50014	1.76	~24°C	49/312	Fluorescein (conjugated to PEGMA)

Table 5-1 Summary of the characteristics of the PLGA-b-(PPGMA-co-PEGMA) thermoresponsive polymers and micelle-like nanoparticles used for the study. Molecular weights have been determined by Gel Permeation Chromatography (GPC). The diameter of the nanoparticles was measured by DLS and carried out at 20°C in HEPES 20 mM.

Results – In vitro Studies of Thermoresponsive Polymers

Nanoparticle formulation number	Constituent polymers PLGA ratio PLA:PGA	Constituent polymers [DEGMA]: [OEGMA]	Mn (GPC)	Mw (GPC)	Đ (polydispersity)	TTT	Diameter of the micelle (nm)	Dye
8	100:0 (Mn 13000)	95:5	47289	63840	1.35	29	56.4	Rodamine B + Fluorescein methacrylate*
9	100:0 (Mn 13000)	95:5	41948	60482	1.44	27	44.8	Rodamine B + Fluorescein methacrylate*

Table 5-2 Summary of the characteristics of PLA-b-(DEGMA-co-OEGMA) thermoresponsive micelle-like nanoparticles used in the study. Molecular weights have been determined by Gel Permeation Chromatography (GPC); the diameter of the micelles was measured by DLS at 20°C and HEPES 20 mM buffer. A double system of detection was used here consisting of Rhodamine and Fluorescein methacrylate covalently bound to the backbone of the polymer*.

* Rhodamine B and Fluorescein methacrylate were inserted randomly in the backbone of the hydrophilic region of the polymer and constituted 5% w/w of the reagents of the polymerization.

Results – In vitro Studies of Thermoresponsive Polymers

Polymer formulation	Experiments carried out	Cell lines	Techniques	Aggregation of micelles upon storage
1	Toxicity studies	3T3 HCT116 MGLVA-1	MTT	na
2	Toxicity studies	3T3 HCT116 MGLVA-1	MTT	na
3	Toxicity studies	3T3 HCT116 MGLVA-1	MTT	na
4	Toxicity studies	3T3 HCT116 MGLVA-1	MTT	na
5	Microscopy 37 - 42°C 8h	3T3 HCT116	Widefield microscopy	na
6	Toxicity studies	3T3 HCT116 MGLVA-1	MTT	Detected after one month storage at -20°C
	Microscopy live images studies of the kinetics of uptake at 37°C for up to 1h	3T3	Confocal microscopy	
	Microscopy with preincubation of the polymer at 37°C for 30 minutes and incubation of the polymer with cells for 2 and 17h			
7	Microscopy with preincubation of the polymer at 37°C for 30 minutes and incubation of the polymer with cells for 2h	3T3	Confocal microscopy	Already present in the formulation
8	Microscopy at 37°C after 24h incubation	3T3, HCT116, MGLVA-1	Widefield microscopy	Already present and increasing with time
	Microscopy at room temperature followed by overnight incubation at 37°C both with and without cells	HCT116	Widefield microscopy	
9	Microscopy with 1h preincubation at room temp., 1h preincubation at room temperature and overnight incubation at 37°C and 37°C overnight without preincubation step	3T3 HCT116	Confocal microscopy	Present only upon incubation with cells at room temperature

Table 5-3 Summary of experiments carried out for each polymer formulation.

5.3 Methods

For a schematics of all the experiments carried out with polymers formulations 1-9, cell lines used, and aggregation state please refer to Table 5-3.

5.3.1 Cell viability studies

Cell viability of thermoresponsive nanoparticles 1, 2, 3, 4 and 6 was assessed with an MTT test at 4 h incubation. The incubation time of the nanoparticles with cells for cell viability studies was decided on the basis of the inhibition studies timescale. The aim was to evaluate the effects of the polymers on metabolic activity when used with cells for the time-length needed for the inhibition studies. These tests were intended to verify that the synthesis and formulation process (in which potentially cytotoxic solvents and catalysts were used) did not lead to contamination of the final polymer formulations with toxic components. It was also intended to verify that the polymer structure was cell compatible. Cell viability of micelle-like nanoparticles from polymer 5, 7, 8 and 9 were not assessed because of lack of time.

Cells were counted and seeded in full media at a density of 31200 cells/cm² in a clear 96 well plate and allowed to attach to the bottom of the wells overnight. The day after, the medium was aspirated off and replaced with HBSS/HEPES 20 mM for the negative control, with PEI 500 µg/ml (positive control) and concentrations of polymer nanoparticles ranging from 31.25 to 1000 µg/ml in triplicate wells. Subsequently MTT (50 µl of 1 mg/ml solution) was applied. Upon completion of the MTT incubation time the absorbance readings were recorded at 550 nm and results were plotted in GraphPad Prism, subtracted of the reading of the blank measurements without cells and normalised against the untreated negative controls. As a further control of the reliability of the data obtained with MTT tests, statistical measurements of the Z factor

and Signal Window were measured according to equations in §2.2.5.4 of the general materials and methods section.

5.3.2 Cell uptake studies

Uptake of thermoresponsive polymers was assessed with two techniques: widefield and confocal microscopy. Widefield microscopy was used for a screening on the behavior of the polymer nanoparticles in the presence and in the absence of cells. However, for a thorough assessment of the uptake of the nanoparticles in cells, confocal microscopy was used as the latter technique is the most suitable for uptake studies given that the resolution allows for the distinction of the regions outside and inside cells¹⁸.

The micelle-like nanoparticles chosen for uptake studies were 5, 6, 7, 8 and 9. The reasons why polymer formulations 1-4 were excluded from uptake studies were many: they presented a Rhodamine dye that was only adsorbed to the micelle and was susceptible to leakage, the polymerization of polymer 3 and 4 was only partially successful producing rather small polymers that were not ideal for the formation of micelle-like nanoparticles. Also all these polymers, when formulated via the nanoprecipitation technique, presented a double distribution of sizes which was problematic for interpreting endocytosis inhibition studies. Finally, their transition temperature was rather high and ranging between 40 and 64°C and mostly not compatible with cell studies. As the polymer nanoparticles were predicted not to internalize when in a hydrated (and less protein interacting form) when below their TTT, the microscopy study of polymers 1-4 in cells was not taken further^{5,16}.

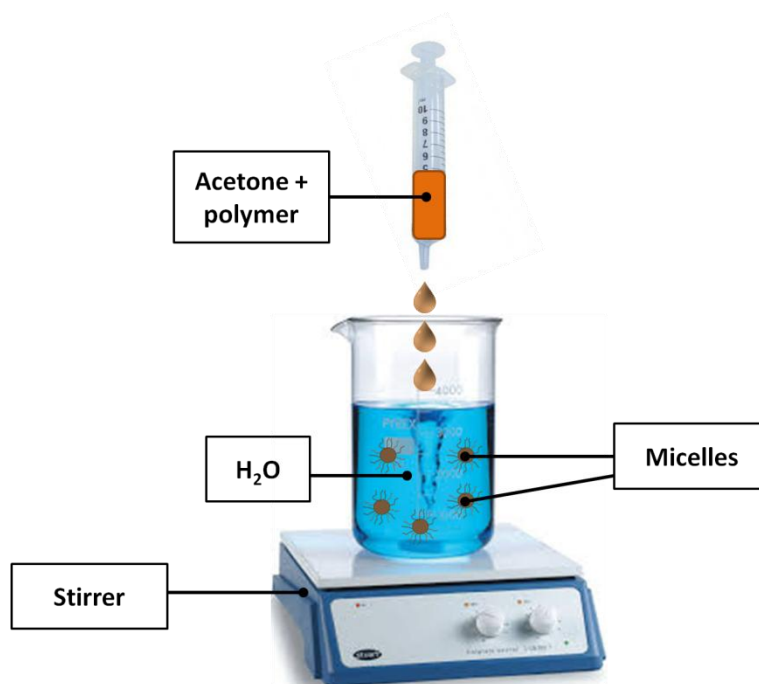


Figure 5-3 Manual method for the formation of micelle-like nanoparticles from amphiphilic polymers. This simple method consisted in dropwise addition of the acetone polymer-containing solution to an aqueous solution under constant stirring. The acetone/water solution obtained was left to evaporate overnight to remove the acetone from the solution. This method was used for the production of the polymer formulations 1-7.

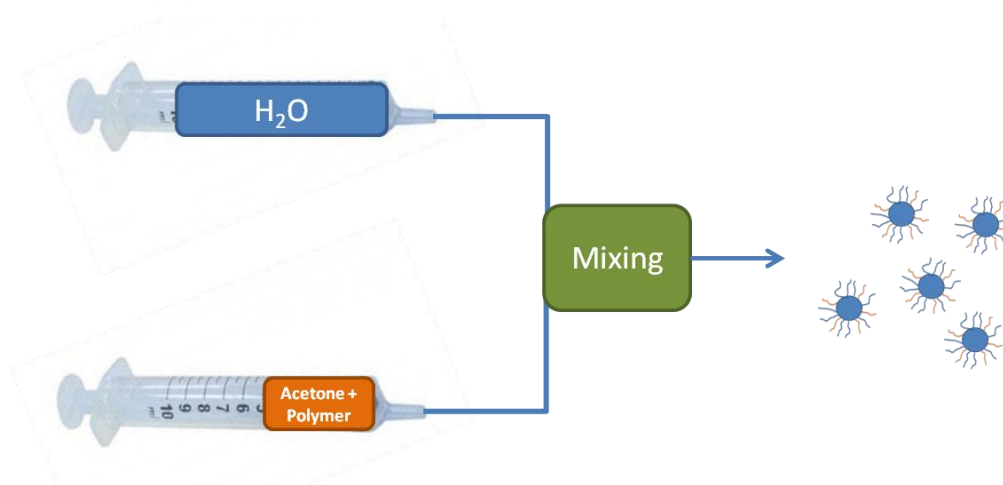


Figure 5-4 Schematic representation of the mixing apparatus used for the production of polymer formulation 8 and 9. The apparatus consisted of two chambers, one for the polymer dissolved in acetone and another for the water. The mixing was occurring gradually, controlling the flux of the two solutions that were coming to contact at a T junction of the apparatus.

5.3.3 Assessment of the uptake of polymer micelle-like nanoparticles 5

3T3 and HCT116 cells were counted and seeded at a density of 31200 cells/cm² in 6 well plates in duplicate and in full media and incubated at 37°C and 5% v/v CO₂ to allow cells to attach to the bottom of the plate overnight. The following day micelle 5 suspensions were thawed, vortexed and sonicated for 1 minute. Full media from cells was aspirated and replaced with 500 µl solution of 500 µg/ml of the micelle or HBSS/HEPES 20 mM for the negative control. Cells were incubated for further 8 h. Cells treated with the nanoparticles were incubated at 42°C. Two negative controls were used, one untreated control was incubated at 37°C and another incubated at 42°C. Standard tissue culture incubators were used for these experiments with a controlled atmosphere of 95%v/v humidity and 5% v/v CO₂. Upon completion of the incubation time cells were viewed on a Nikon Eclipse Ti widefield microscope, Kingston Upon Thames, UK, to detect any signs of toxicity due to the micelle or the treatment at 42°C as well as internalization of the nanoparticles in cells.

5.3.4 Assessment of the kinetics of endocytosis of formulation 6

3T3 cells were counted and seeded at a density of 31200 cells/cm² on round glass coverslips in 6 well plates and full media and incubated overnight to allow cells to attach to the glass coverslips. The following day, CellMask deep red plasma membrane staining 1 µg/ml was applied and incubated for 30 minutes. The media was subsequently aspirated, the coverslip applied on a mounting chamber and cells treated with HBSS/HEPES 20 mM. Micelle formulation 6 was previously thawed, equilibrated to room temperature, vortexed and sonicated for 1 minute and subsequently added to the buffer at final working concentration of 500 µg/ml. Live images were acquired on untreated cells in HBSS/HEPES 20 mM before the

application of the polymer nanoparticles and at 10, 20, 40, 50 and 60 minutes from their application on cells. Micelle-like nanoparticles 6 were labeled with a fluorescein methacrylate dye for confocal microscopy.

5.3.5 Uptake studies for nanoparticle formulations 6 and 7

3T3 cells were counted and seeded on glass coverslips as described above and allowed to attach to coverslips overnight. The following day, micelle 6 and 7 suspensions were thawed to room temperature, vortexed, sonicated for 1 minute and incubated at 37°C for 30 minutes before diluting an aliquot of the stock in HBSS/HEPES 20 mM to 500 µg/ml and applying them to cells. Cells were further incubated with nanoparticles 6 and 7 for 2 h while a further incubation time set at 17 h was attempted for micelle 6. Negative control cells and micelle-treated cells were imaged on a Zeiss 710 confocal microscope.

5.3.6 Uptake studies of the internalization of micelle 8

3T3 and HCT116 and MGLVA-1 cells were counted and seeded at a density of 31200 cells/cm² in clear 96 well plates in full media and allowed to attach to the bottom of the plate overnight. The following day, the micelle suspensions were thawed and left to equilibrate to room temperature, vortexed and sonicated for 1 minute. The media from cells was aspirated and different concentrations of the nanoparticles were applied to the wells in triplicates for concentrations ranging between 31.25 and 1000 µg/ml in HBSS/HEPES 20 mM. The negative control consisted of cells treated with HBSS/HEPES 20 mM. Treated cells were incubated for further 24 h. Upon completion of the incubation time cells were viewed on a Nikon Eclipse Ti widefield microscope to detect and signs of toxicity and internalization of the nanoparticles in cells.

HCT116 cells were counted and seeded in full media at a density of 31200 cells/cm² in a 25 cm² flasks and allowed to adhere to the bottom of the flask overnight. The day after, the media was aspirated and cells treated with 250 µg/ml of the nanoparticles in HBSS/HEPES 20 mM in which micelles had been previously thawed, vortexed and sonicated for 1 minute. Cells were incubated at room temperature for 1 h, viewed on a Nikon Eclipse Ti widefield microscope and subsequently incubated overnight at 37°C. A 25 cm² flask without cells was rinsed with full media and used as a control, incubated with the same solution of the micelle that was applied on cells, at room temperature for 1 h and subsequently incubated overnight at 37°C. Images were taken after 1 h incubation at room temperature in both cells treated with nanoparticles and flasks with nanoparticles but devoid of cells. Another set of images was taken after overnight incubation at 37°C before and after rinsing the nanoparticles suspension.

5.3.7 Uptake studies of the internalization of micelle-like nanoparticles 9

HCT116 and 3T3 cells were seeded at a density of 31200 cells/cm² on rounded glass coverslips in 6 well plates and allowed to attach to the glass coverslip overnight. Subsequently, cells were incubated with 250 µg/ml of polymer formulation 9 overnight with and without an additional incubation step carried out for 1 h at room temperature. Alternatively, cells were treated for 1 h at room temperature with 500 µg/ml of micelles formulation 9 before confocal microscopy. Cells were stained with Hoechst 33342 1 µg/ml and/or CellMask deep red plasma membrane staining 1 µg/ml for 30 minutes and the staining solution removed prior to confocal microscopy on a Zeiss Confocal microscope 710.

5.4 Results

5.4.1 Acute cell viability studies

MTT studies on polymer nanoparticle formulations 1, 2, 3, 4, are shown in Figure 5-5, and MTT assays of polymer 6 are shown in Figure 5-6. The graphs in Figure 5-5 represent the mean and standard deviation of triplicate experiments. Graph in Figure 5-6 represent the mean and standard deviation of duplicate experiments. Graphs illustrate that the nanoparticles were generally well tolerated in the cell lines tested and at the chosen experimental settings.

Results – In vitro Studies of Thermoresponsive Polymers

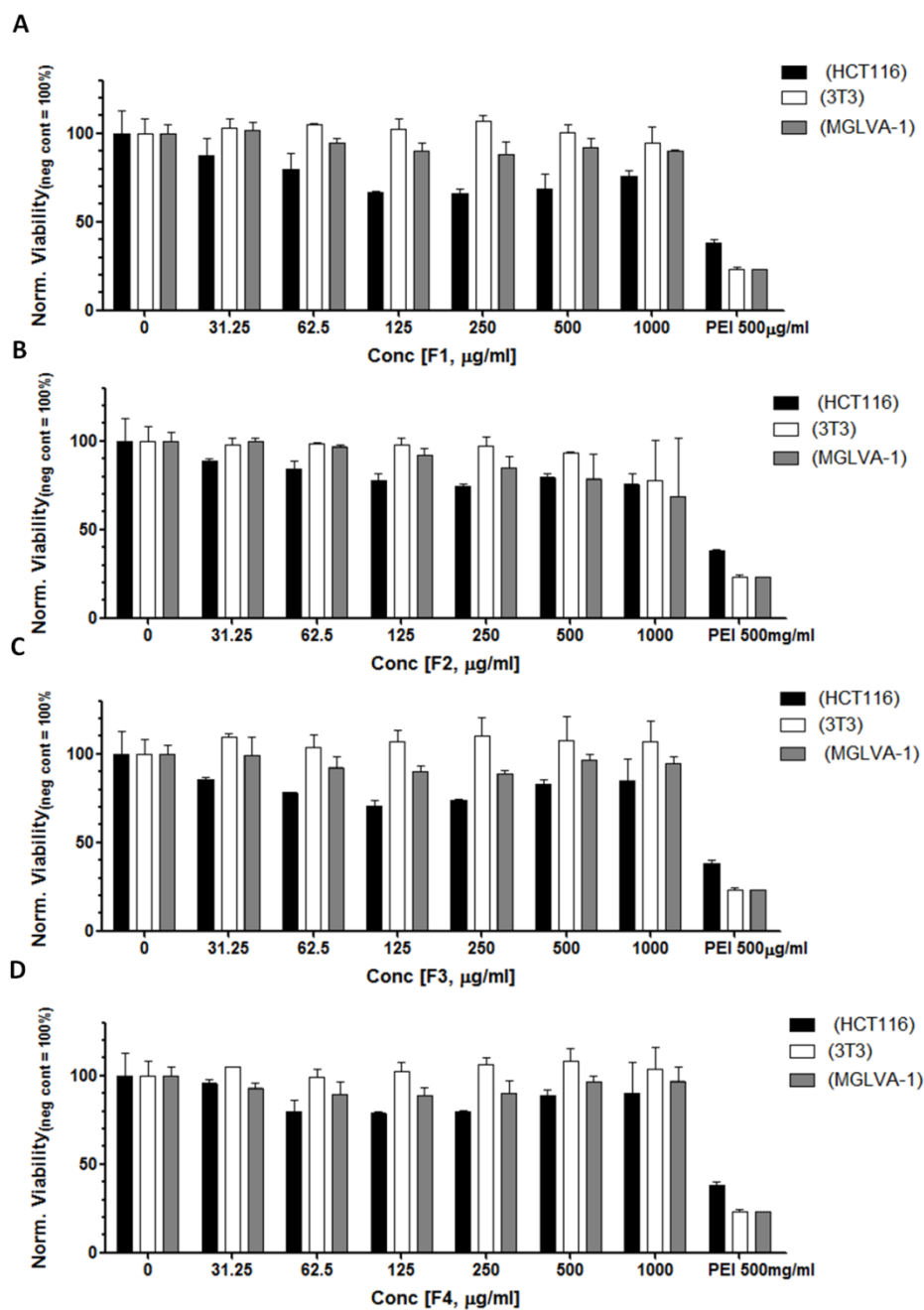


Figure 5-5 Assessment of cell activity interference of micelle-like formulation 1 (A), 2 (B), 3 (C) 4 (D) following incubation in 3T3, HCT116 and MGLVA-1 cells with an MTT acute test at 4 h. Cells were seeded in a clear 96 well plate and different dilutions of micelle applied in triplicate wells. Absorbance readings were recorded at 550 nm. PEI 500 µg/ml was used as a positive control. Results are normalised against the negative control and represent the mean and standard deviation of triplicate experiments (n=3).

Results – In vitro Studies of Thermoresponsive Polymers

For all the polymers tested there was little effect on cell metabolic activity and for this reason broad IC_{50} values and 95% confidence intervals were calculated. The Signal Window between the negative and positive control was calculated to investigate that there was enough separation between the positive and negative control absorbance for the MTT test, as this is an indication of the reliability of the assay¹⁹. In 3T3 fibroblasts the Signal Window was 5 which corresponds to a recommended value, in HCT116 it was 1.6 that corresponds to an acceptable value and in MGLVA-1 cells it was 7 and a recommended value according to Iversen et al¹⁹. Z factor values were equal to 0.5 for 3T3 cells (excellent separation between positive and negative control according to Zhang *et al*²⁰), for HCT116 it was equal to 0.2 which corresponds to a small separation between the positive and negative control, and Z factor for MGLVA-1 cells was equal to 0.7 corresponding to an excellent separation between positive and negative control.

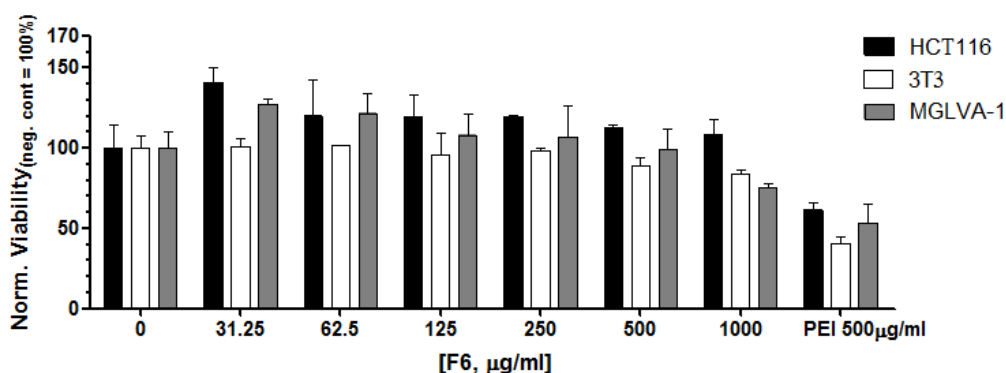


Figure 5-6 Assessment of cell activity of polymer micelles 6 on 3T3, HCT116 and MGLVA-1 cells with an MTT test. The data plotted here are the result of MTT readings at 550 nm of the viability of cells and are reported as the mean and standard deviation of duplicate experiments. Cells were seeded at a density of 31200 cells/cm² and allowed to attach to the bottom of a clear 96 well plate overnight. The following day cells were treated for 4 h with the formulated polymers (n=2).

Results – In vitro Studies of Thermoresponsive Polymers

Cell activity tests for micelle-like nanoparticles 6 are shown in Figure 5-6. The graph represents the mean and standard deviation of duplicate experiments and suggests that the polymers were well tolerated in the chosen cell lines and experimental settings. IC₅₀ values for polymer formulation 6 in 3T3 cells were equal to 5 mg/ml at a 95% confidence interval of 3.4-8 mg/ml; the obtained IC₅₀ value and confidence interval were not reliable in HCT116 cells (low toxicity) while in MGLVA-1 cells the polymers were essentially inactive. The Z factor and Signal Window for 3T3 cells were 0.2 and 1.7 respectively corresponding to a low separation between positive and negative control calculated by Z factor and an acceptable Signal Window; HCT116 cells presented a Z factor and Signal Window of -0.46 and -1.5 that are unacceptable while Z factor and Signal Window for MGLVA-1 cells were equal to 0.2 and 1.3 that correspond to poor separation between positive and negative control according to Z factor statistics but an acceptable Signal Window. The rather poor Z factor and Signal Window results obtained for polymer 6 were likely due to the unexpectedly low toxicity of the PEI positive control used in these studies.

5.4.2 Internalization studies of micelle-like structures from polymer 5

Polymer 5, formulated into nanoparticles with a single population of micellar diameters, and containing a Fluorescein dye covalently bound to the polymer backbone, were the first to be analyzed for internalization. The aim was to test the internalization of micelle-like nanoparticles of the polymer in 3T3, HCT116 and MGLVA-1 cells. As the TTT for the polymer was 41°C, the experiments were conducted at 37°C and 42°C (respectively below and above the TTT of the polymer). As the high transition temperature was a limiting step for confocal microscopy (which required special arrangements with the confocal microscopy unit), an initial screening

Results – In vitro Studies of Thermoresponsive Polymers

of the uptake of the micelle-like nanoparticles was carried out with a more accessible widefield microscope. As apparent from Figure 5-7, the micelle-like structures obtained from polymer 5 were not sufficiently fluorescent for further confocal microscopy. However, it was noted that the polymers appeared to have an unexpected protective action on cells undergoing treatment at 42°C for 8 h. As it can be seen from the images in Figure 5-7, 3T3 control cells treated at 42°C were rounded and unhealthy compared to the control cells treated at 37°C. The same cells incubated at 42°C in the presence of formulation 5 looked slightly more flattened and less rounded which suggested a higher resistance to the increase of temperature (arrows).

The density of HCT116 control cells treated at 42°C was reduced with cells detaching from wells and floating in the media as a consequence of the heat. The same cells treated at the same temperature in the presence of suspensions of nanoparticle formulation 5 presented a cell density that was similar to the untreated control at 37°C suggesting an acquired resistance to the increase of temperature. Although the HCT116 cell morphology is mainly rounded, some of the cells looked slightly elongated when in good health (see arrows in Figure 5-7 at 37°C). This morphology is not detected in cells treated with the micelle at 42°C and can be interpreted as an indicator of cell stress.

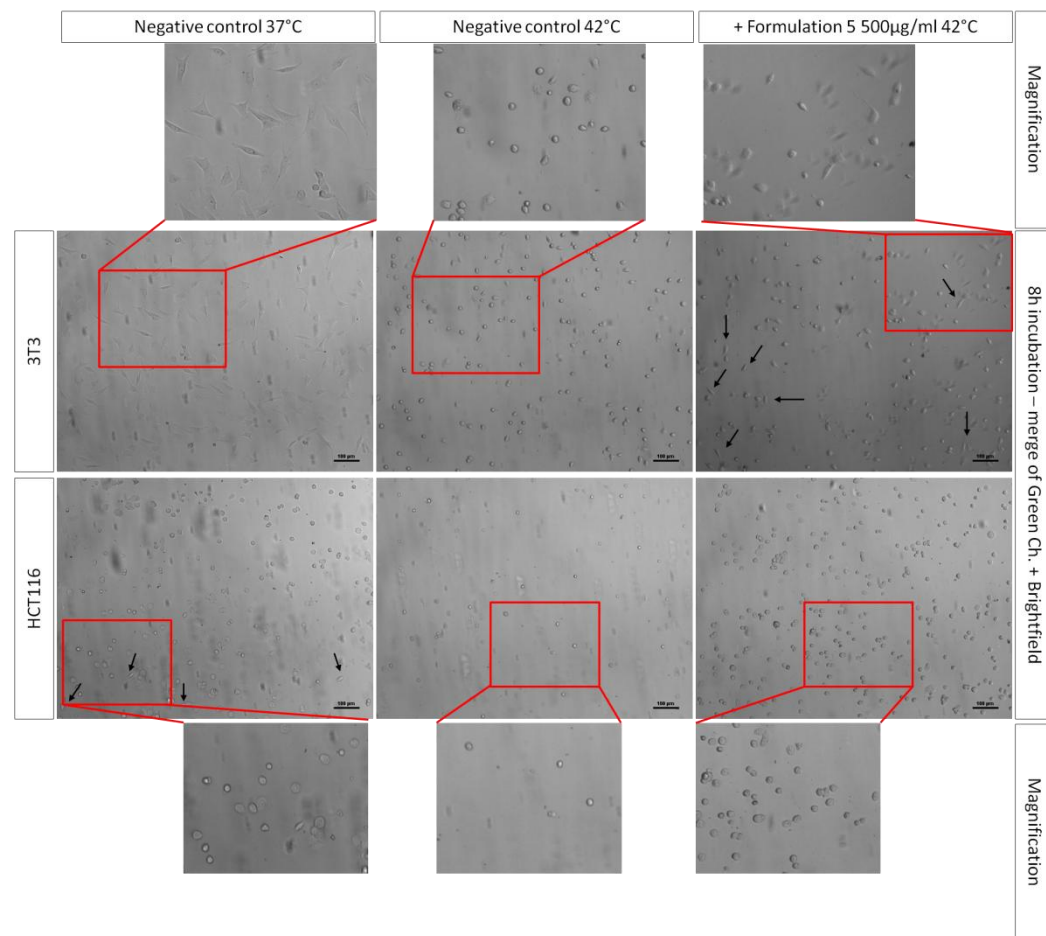


Figure 5-7 Micelle-like structures 5 incubated at 42°C (above TTT) for 8 h. The pictures shown above were taken on 3T3 and HCT116 cells incubated for 8 h in the presence and in the absence of the nanoparticles at 42°C. Another set of cells from the same experiments were incubated at 37°C and are inserted in the above picture as a further control. Pictures show a merge of the green channel and the brightfield. Arrows point at some of the features of the cells that suggest good health (see text for further information). Exposure time for the Green Fluorescent Protein (GFP) filter was set at 1 s. Scale bars represent 100 µm.

5.4.3 Micelle 6 and 7 live imaging studies

Micelle-like nanoparticle formulations 6 and 7 (produced from the same polymer in two different circumstances with the manual method illustrated in Figure 5-3), were the first polymers to be screened for internalization with confocal microscopy. The fluorescence of these materials in suspension was assessed by quickly exposing the Eppendorf tube containing the polymer to a GFP filter in a widefield microscope. As the suspension was strongly fluorescent, it was apparent that dye-labeling of the polymer had been successful. The polymer forming the micelle-like nanoparticles presented a TTT of 24°C, suggesting that, for internalization studies at 37°C, the polymers would present a hydrophobic surface. Prior DLS studies (Table 5-1), indicated that formulations 6 and 7, although made with the same technique (Figure 5-3) and from the same polymer, were not identical. Formulation 6 showed a low tendency towards aggregation, while micelle-like nanoparticles from the same polymer, but as formulation 7, were already aggregated before application on cells. Also the size distributions of the two micelle-like nanoparticles were different. Nanoparticles in formulation 6 were of 118 nm diameter while those in formulation 7 displayed two populations with diameters of the nanoparticles of 49 and 312 nm as measured by DLS (Table 5-1).

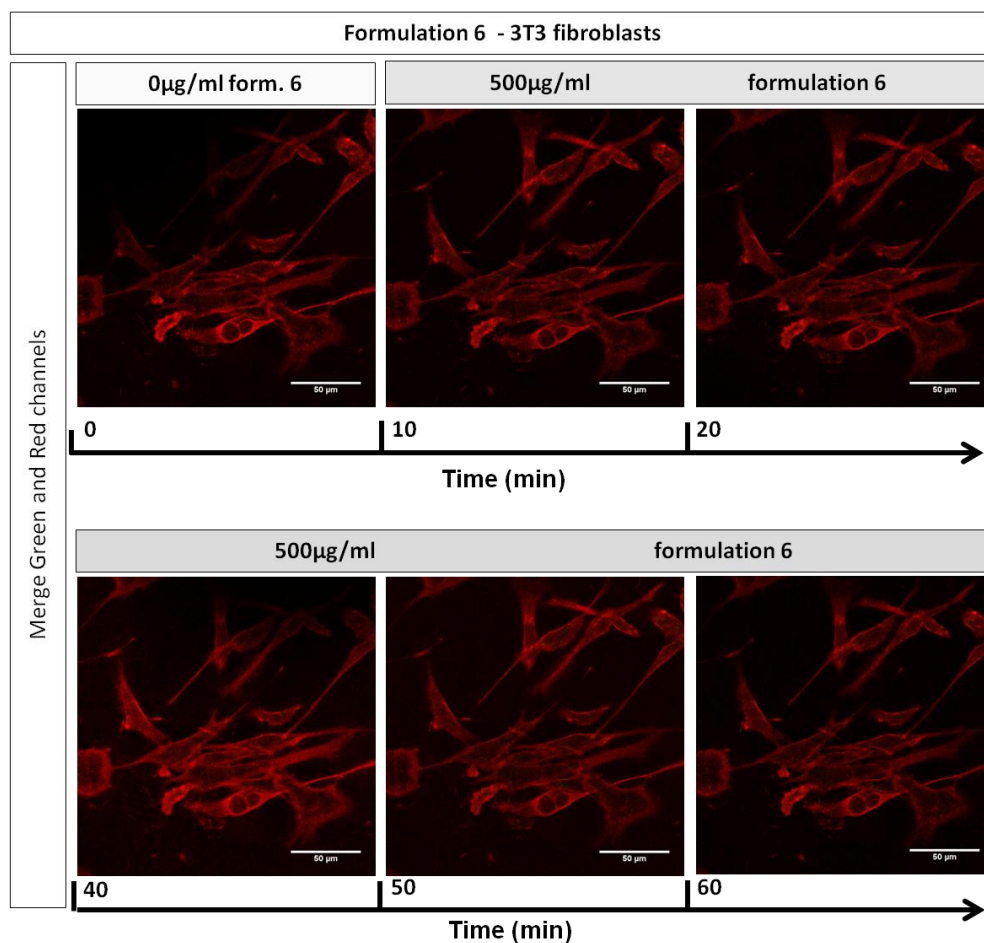


Figure 5-8 Confocal live studies of the kinetics of uptake of micelle-like formulation 6 on 3T3 cells. Images were acquired before applying the polymers (time 0) and after and at 10, 20, 40, 50 and 60 minutes from the application of the nanoparticles. The pictures above represent the merge of the green (micelles) and red (CellMask membrane staining) channels. Scale bars represent 50 µm.

A first set of experiments (Figures 5-8 and 5-9) was carried out using formulation 6 to investigate the uptake and to verify the time length of the uptake in 3T3 cells. The presence of the membrane dye was also introduced to investigate that, if uptake was occurring, as expected, the polymer formulation was localizing inside the membrane boundaries and not on the membrane or outside cells.

A timepoint experiment was carried out to understand the kinetics of internalization of micelle-like nanoparticles 6 and pictures of the cells treated with the nanoparticles

Results – In vitro Studies of Thermoresponsive Polymers

were acquired at 10, 20, 40, 50 and 60 minutes. The pictures showed in Figures 5-8 and 5-9 illustrate that nanoparticles were not internalized by 60 minutes from their application on cells.

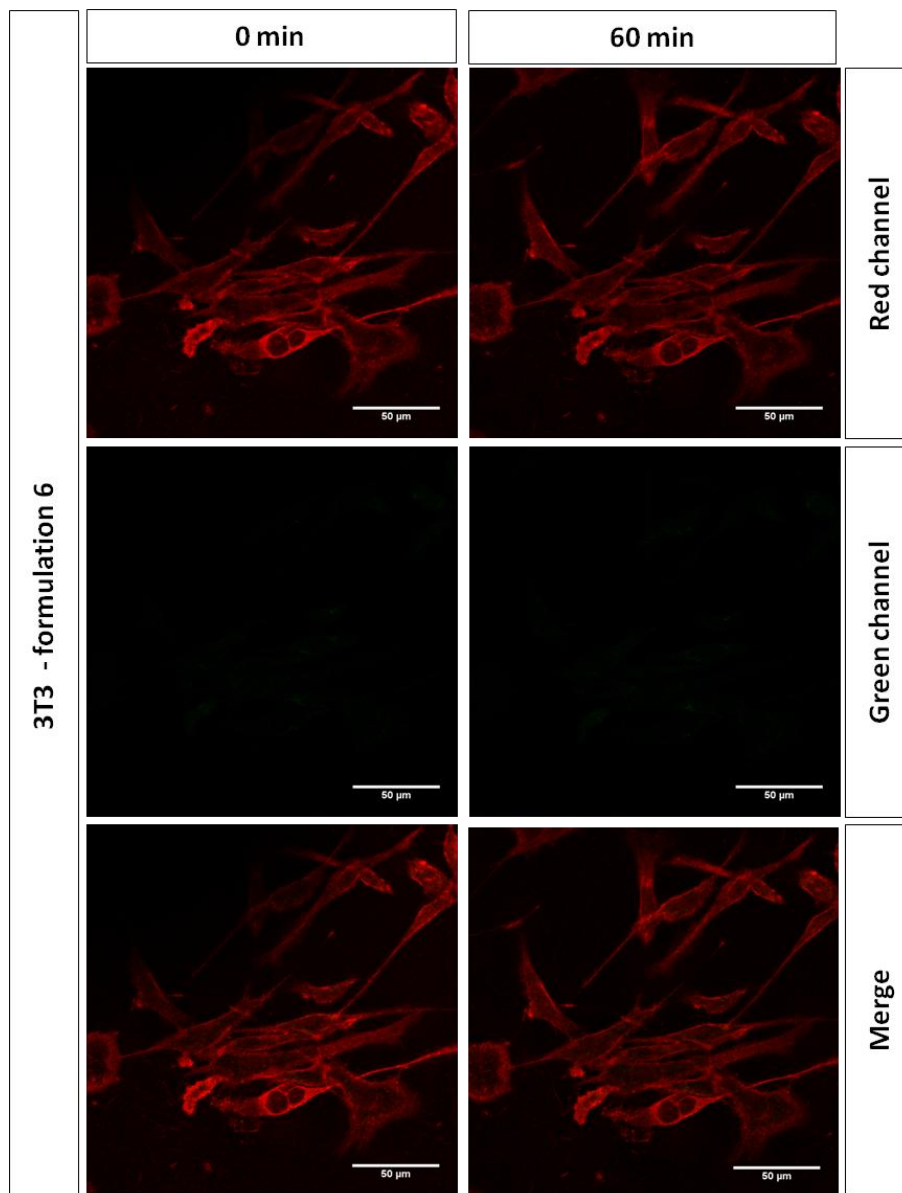


Figure 5-9 Comparison of the fluorescence intensity of 3T3 cells before and after 1 h treatment with micelle-like formulation 6. The pictures shown represent the single channels of emission for formulation 6 (Green channel) and CellMask deep red membrane staining (Red channel). Scale bars represent 50 μm.

Results – In vitro Studies of Thermoresponsive Polymers

To further investigate the reasons underlying this lack of internalization of formulation 6, another set of experiments was carried out, which consisted of preincubation of the micelle-like nanoparticles at 37°C before application on cells for increased times of incubation. These conditions were chosen taking into consideration the thermoresponsive properties of the polymer. For these polymers, formulated by nanoprecipitation into micelle-like nanoparticles, the surface in the hydrated state below the TTT (24°C) was considered less likely to promote internalization. By contrast, the change in conformation at the exterior around the thermal transition temperature (TTT) would produce a less hydrophilic surface to the particles, predicted to enhance uptake across lipid cell membranes. The extended incubation time with polymers pre-transitioned across their TTT was thus expected to lead to greater particle internalization. However, increases in the incubation time from 1 to 2 h did not result in 3T3 cells with fluorescent interiors, despite evidence (Figure 5-10) that the nanoparticles were strongly fluorescent when external to the cells. The formulation of micelle-like nanoparticles from formulation 6 also appeared to be well dispersed and non-aggregating, suggesting no changes in size over the temperature ranges compared to similar polymers which had been internalized by MCF-7 cells in previous studies^{5,16}. A second batch of the same polymer, nanoparticle formulation 7 (Table 5-1) was used and experiments carried out as explained above and in the materials and methods section. These micelle-like nanoparticles were applied to 3T3 cells after pre-incubation for 30 minutes at 37°C and were further incubated for 2 h on the cells. A higher tendency for aggregation was observed with this formulation, and large, self-associated structures were present as can be seen from Figures 5-11 and 5-12. The size of the aggregates ranged from a few microns to tens of microns making the internalization of such structures very unlikely. These data suggested

Results – In vitro Studies of Thermoresponsive Polymers

significant differences in the two formulations derived from the same precursor polymer. As polymer formulation 6 showed less tendency to aggregate, these nanoparticles were incubated with 3T3 cells for up to 17 h at 37°C, with a pre-incubation stage for the polymers of 30 minutes at 37°C before application to cells and imaging. Results, shown in Figure 5-13, illustrate that the nanoparticles formulation 6 were internalized (arrows) in 3T3 cells at 17 h. Absolute comparison of internalization was problematic as the negative control cells were accidentally contaminated by a sterilization product and exhibited toxicity-induced autofluorescence^{21,22}. Quantification and analysis with a Mann-Whitney t test of the fluorescence of each cell (subtracted from the background value of a region adjacent to the cell) reported a significantly increased fluorescence of cells treated with micelle-like nanoparticles 6 for a P value = 0.0038 (Figure 5-14). Fluorescence in cells treated with the micelle-like nanoparticles was not attributable to poor health of cells as the brightfield images showed no evidence of cell damage. However, further studies of the uptake of these polymer formulations were interrupted as the longer-term stability of nanoparticles 6 against aggregation was insufficient after one month incubation of the nanoparticles at -20°C. The study was suspended and the chemistry of the polymers as well as the method used for the constitution of the suspension of micelle-like nanoparticles rethought for further experiments.

Results – In vitro Studies of Thermoresponsive Polymers



Figure 5-10 3T3 cells treated with micelle-like formulation 6 for 2 h. Nanoparticles were thawed and pre-incubated at 37°C for 30 minutes before being diluted, applied to cells and further incubated at 37°C for 2 h. Images show the green channel, the brightfield channel and a merge of the two. Scale bars for the top row of pictures represent 50 µm; Scale bars for the bottom row of pictures represent 20 µm.

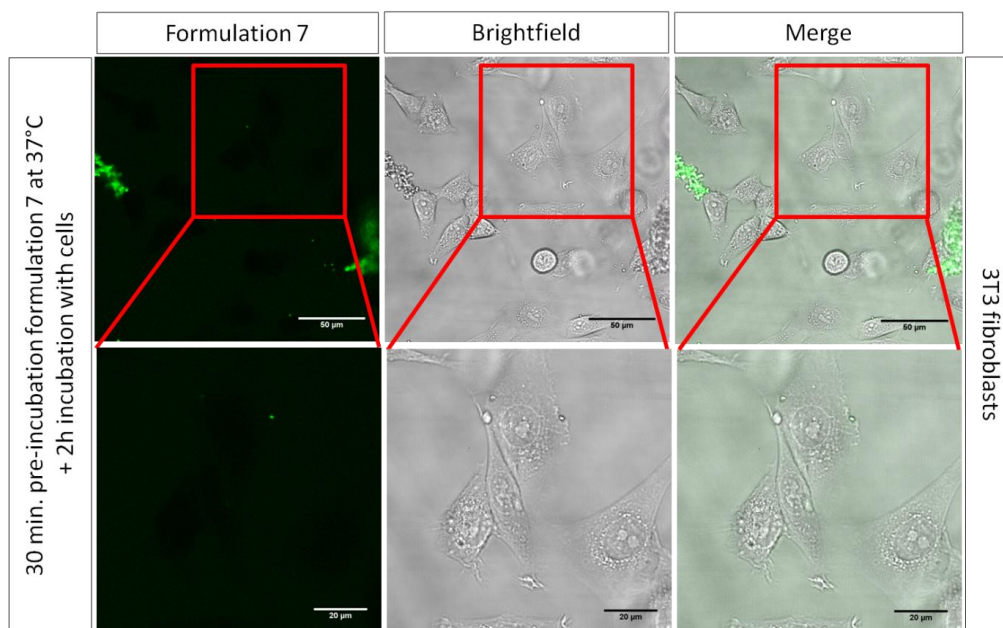


Figure 5-11 3T3 cells treated with micelle-like nanoparticles 7 preincubated for 30 minutes at 37°C before application on cells for 2 h. Scale bars for the top row represent 50 µm; Scale bars for the bottom row of Figures represent 20 µm.

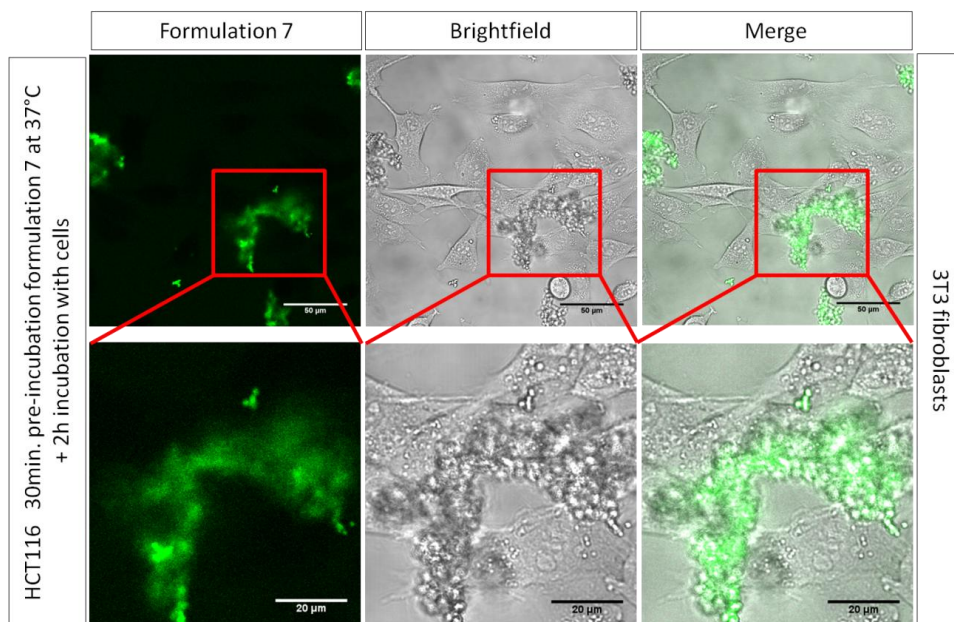


Figure 5-12 Micelle-like nanoparticles **7** preincubated at 37°C for 30 minutes prior to the application on 3T3 cells for 2 h. This set of images show the green channel, brightfield and a merge of both. Scale bars for the top row of pictures represent 50 μm; bottom row scale bars represent 20 μm.

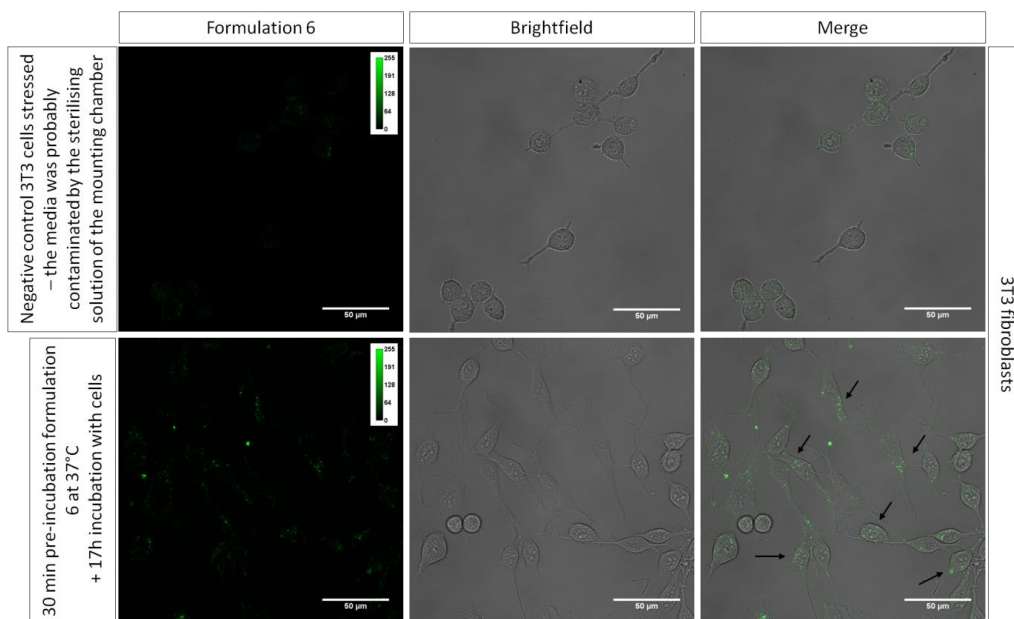


Figure 5-13 Micelle-like formulation **6** preincubated at 37°C for 30 minutes and subsequently applied to 3T3 cells for 17 h. This set of pictures shows the green channel, the brightfield and a merge of the two in 3T3 negative control (top row of pictures) and positive control of cells treated with nanoparticles 6 (bottom row of pictures). The negative control cells shown in this set of pictures look stressed, retracting their elongated features and rounding up. The reason for this behaviour is believed to be due to the accidental contamination of cells with the sterilising solution of the mounting chamber of the coverslips used for confocal microscopy. Arrows point to the green fluorescence of nanoparticles 6 internalised into 3T3 fibroblasts. Scale bars represent 50 μm.

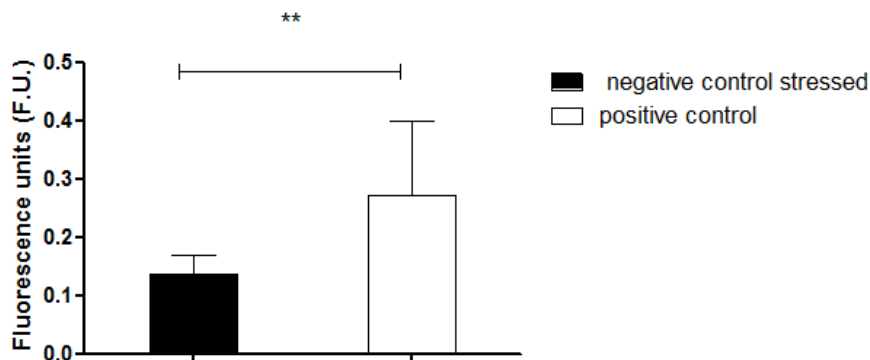


Figure 5-14 Mann-Whitney t test of the fluorescence for the negative untreated cells and positive control cells treated with formulation 6. The fluorescence was measured with ImageJ for each cell for both the negative and the positive controls, subtracted of the background measured from a region adjacent to the cell before analysing the measurements with a t test. Statistical analysis show a significance of the increase of fluorescence in cells treated with the nanoparticles for a P value of 0.0038. Error bars represent the standard deviation of the mean (n>15).

5.4.4 Live cell imaging of nanoparticles 8

Nanoparticles derived from polymer 8 (TTT = 29 °C) were based on very similar chemistries with respect to polymers 1-7, but formulation was carried out in a slightly different way. The polymer used for formulation 8 contained a hydrophobic PLA core and a thermoresponsive polyDEGMA/OEGMA outer block. The nanoparticles were prepared using nanoprecipitation, as before, but with a syringe-injection pump system for a more reproducible mixing of the acetone-polymer solution with water. The controlled fluid flow from the pumps allowed for a constant and reproducible flux of the two solvents when contacted at the T junction of the apparatus (Figure 5-4). Although good quality nanoparticles from polymer 8 were produced with the above mentioned technique (radius < 60 nm, narrow population distribution), after storage at -20°C and thawing, aggregated structures were present that required intense vortexing and sonication for dispersal. Experiments using widefield microscopy to assess uptake in 3T3, HCT116 and MGLVA-1 cells were carried out using nanoparticles 8 at a range of concentrations. The set of pictures in Figure 5-15, 5-16,

Results – In vitro Studies of Thermoresponsive Polymers

5-17, 5-18, 5-19 and 5-20 was also acquired to investigate that the two dyes used during the synthesis of the polymers and nanoparticles (Fluorescein methacrylate and Rhodamine B) were both visible. As apparent from Figures 5-15, 5-16, at the highest concentration of nanoparticles, (1000 $\mu\text{g/ml}$) large aggregates formed which produced a thick layer of material on cells. Furthermore, although this concentration was the highest of the ones tested and the exposure of the green channel was tested up to 3 times higher than the one used for the red channel in 3T3, and 10 times higher with respect to the exposure time used with HCT116 and MGLVA-1 cells, no fluorescence was detectable for the Fluorescein dye that was inserted in the backbone of the hydrophilic portion of the nanoparticles. Reducing the concentration from 1000 to 500 $\mu\text{g/ml}$ did not reduce sufficiently the thick layer of the aggregated polymer on cells, thus it was not possible to determine if any particles were internalized. Concentration of 500 $\mu\text{g/ml}$ of formulation 8 appeared to produce two different sorts of aggregations depending on the cell line tested (Figure 5-17). 'Worm-like' assemblies of nanoparticles 8 were found to be associated with 3T3 and HCT116 cells while MGLVA-1 cells were surrounded by shorter and thicker 'tubes' of associated particles together with sheet-layers of the polymer. At lower concentrations of nanoparticles (250 $\mu\text{g/ml}$) cells were more clearly discerned. HCT116 cell density was low enough to suggest that the polymer aggregates were preferentially interacting with cell surfaces rather than the underlying cellBIND coating of the 96 well plates substrate (Figure 5-18). The same association between nanoparticles and cell surfaces was also apparent, although less definitively, for 3T3 cells. The larger size of 3T3 cells makes them more confluent than HCT116 and thus the interactions between polymers and cells were less defined. Polymers incubated with MGLVA-1 cells did not appear to show a similar strong affinity for these cell

Results – In vitro Studies of Thermoresponsive Polymers

surfaces and aggregates of the polymers were distributed both on cells and on the bottom of the well. At polymer concentration of 31.25 µg/ml the association of the nanoparticles with 3T3 and HCT116 cells was evident (Figure 5-20). Polymer nanoparticles were preferentially found on the cells with respect to the cellBIND-treated plastic of the well. For all experiments, polymers were detected not only as associated nanoparticles but also as layers and sheets of agglomerated material. It was also notable that the polymers were associated with the 3 cell lines in different ways (Figure 5-19). For polymers attached to 3T3 cells, the nanoparticles were present in longer, thinner regions compared to those at HCT116 and MGLVA-1 cell surfaces. This suggested that the polymer nanoparticles were associated at the cell surface structures, which are known to differ for the 3 cell lines chosen, rather than being present in the cytosol in each case. It is known that 3T3 cells produce extracellular matrix components and it is possible that the nanoparticles were attached to these regions as well as to the rest of the 3T3 cell surface, accounting for the difference in the appearance of the nanoparticles aggregates on 3T3 cells compared to HCT116 and MGLVA-1 cells^{23,24}. Internalization of the polymer nanoparticles in the 3 cell lines was not clearly evident from the pictures at this magnification, suggesting either that no internalization had taken place or that any internalized nanoparticles were masked by the aggregated particles at the cell surfaces.

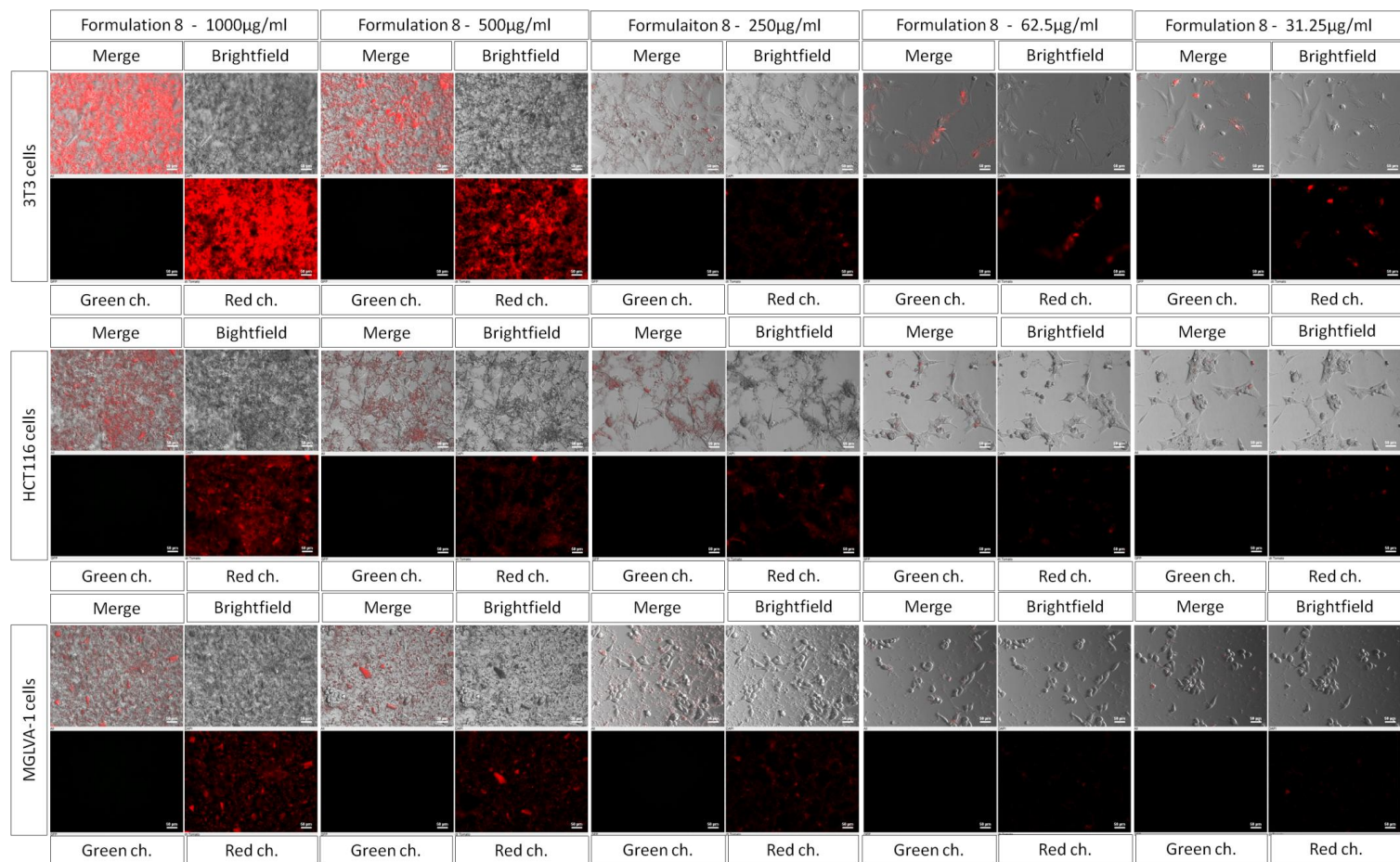


Figure 5-15 3T3, HCT116 and MGLVA-1 cells treated with different concentrations of formulation 8 for 24 h at 37°C. The Figure shows the Green and Red channels, brightfield and a merge of all. Cells were seeded at 31200cells/cm² in a 96 well plate and treated with formulation 8 previously thawed, vortexed and sonicated before application on cells. Images were acquired with a Nikon Eclipse Ti widefield microscope. The exposure time for the ds red tomato filter is 300 ms for 3T3 cells and 100 ms for HCT116 and MGLVA-1 cells. The exposure time for the GFP filter is 1s for all cell lines. The nanoparticles were expected to fluoresce in both the Green and the Red channels. Scale bars represent 50 µm.

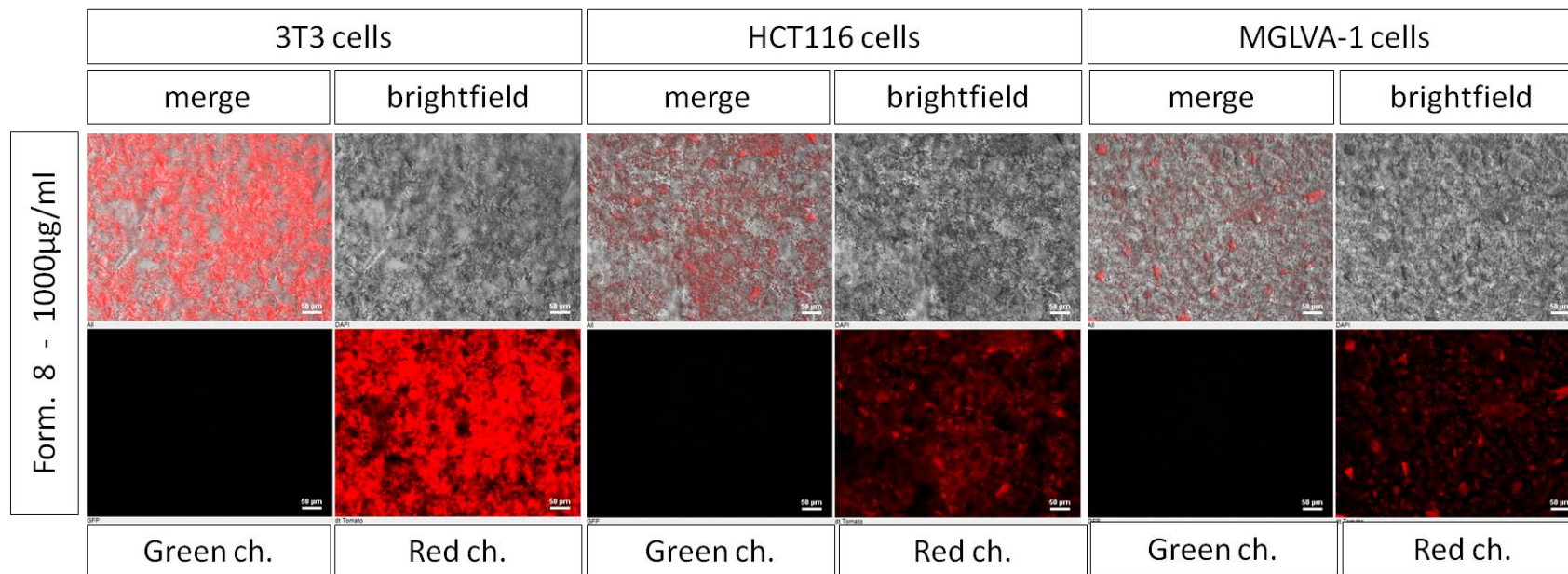


Figure 5-16 3T3, HCT116 and MGLVA-1 cells treated with 1000 µg/ml of formulation 8 for 24 h at 37°C. The Figure shows the Green and Red channels (bottom Figures), brightfield and a merge of all (top Figures). The nanoparticles were expected to fluoresce in both the Green and the Red channels. Scale bars represent 50 µm.

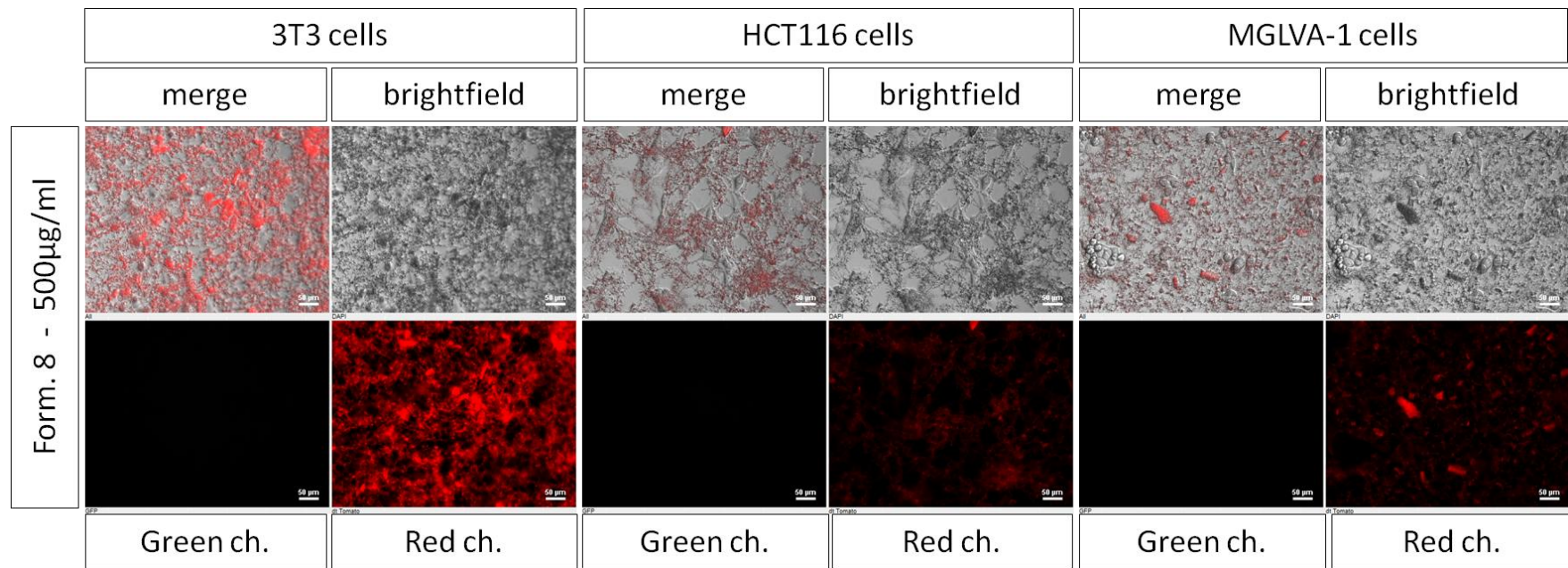


Figure 5-17 3T3, HCT116 and MGLVA-1 cells treated with 500 µg/ml of formulation 8 for 24 h at 37°C. The Figure shows the Green and Red channels (bottom Figures), brightfield and a merge of all (top Figures). The nanoparticles were expected to fluoresce in both the Green and the Red channels. Scale bars represent 50 µm.

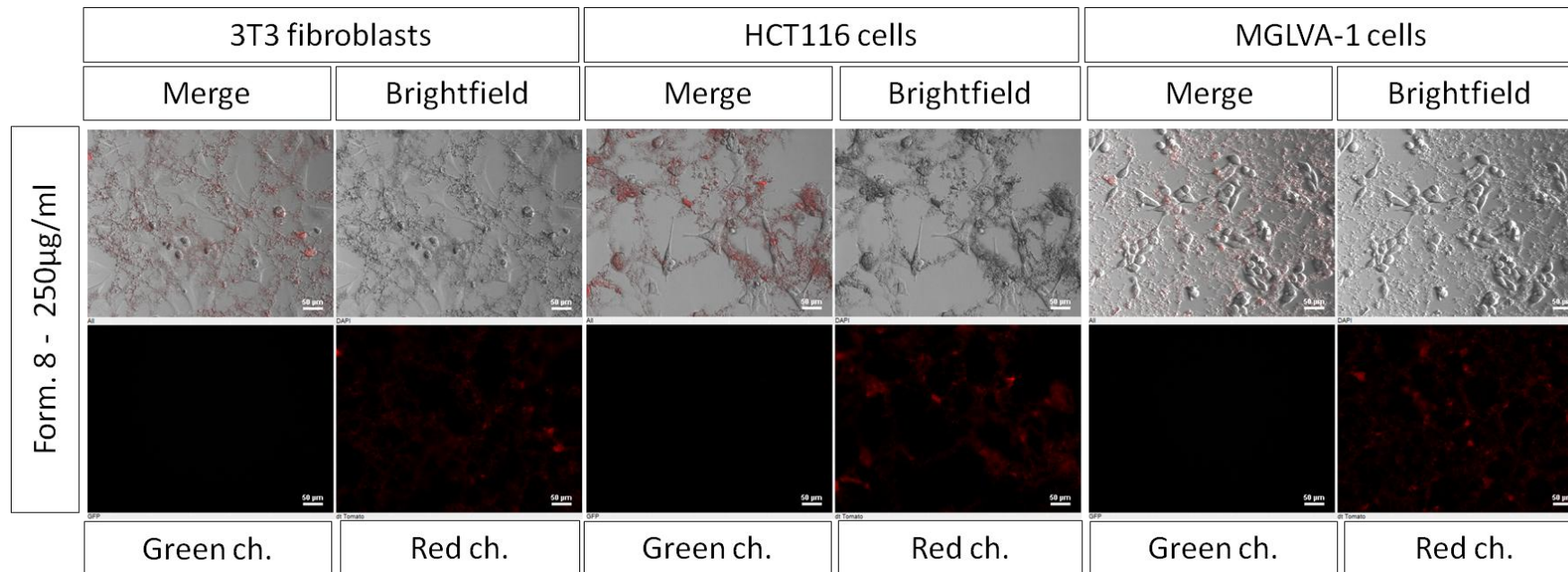


Figure 5-18 3T3, HCT116 and MGLVA-1 cells treated with 250 µg/ml of formulation 8 for 24 h at 37°C. The Figure shows the Green and Red channels, brightfield and a merge of all. The nanoparticles were expected to fluoresce in both the Green and the Red channels. Scale bars represent 50 µm.

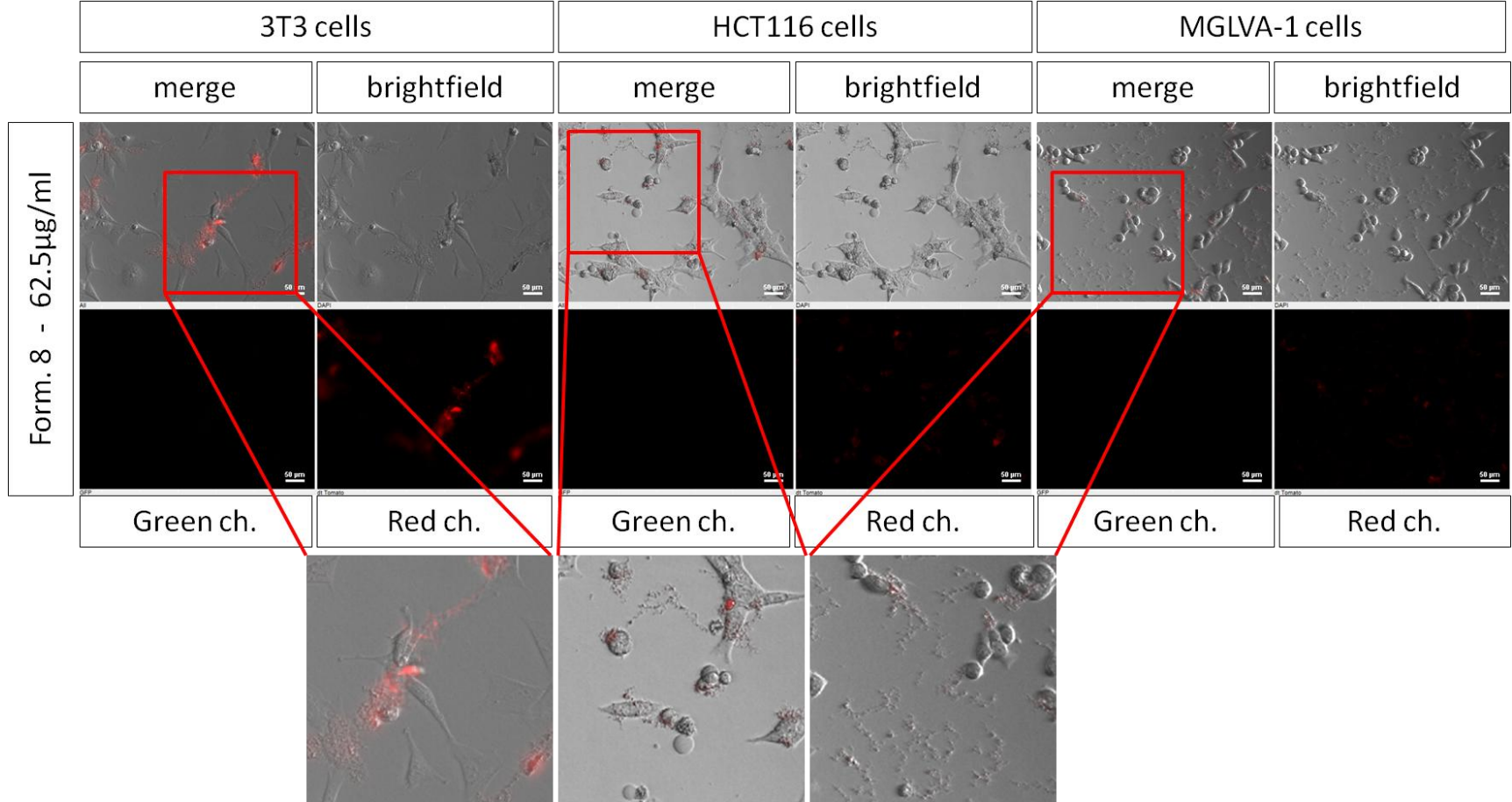


Figure 5-19 3T3, HCT116 and MGLVA-1 cells treated with 62.5 µg/ml of formulation 8 for 24 h at 37°C. The Figure shows the Green and Red channels, brightfield and a merge of all. The nanoparticles were expected to fluoresce in both the Green and the Red channels. Magnification images are provided at the bottom of the Figure and show some features of the aggregates. Scale bars represent 50 µm.

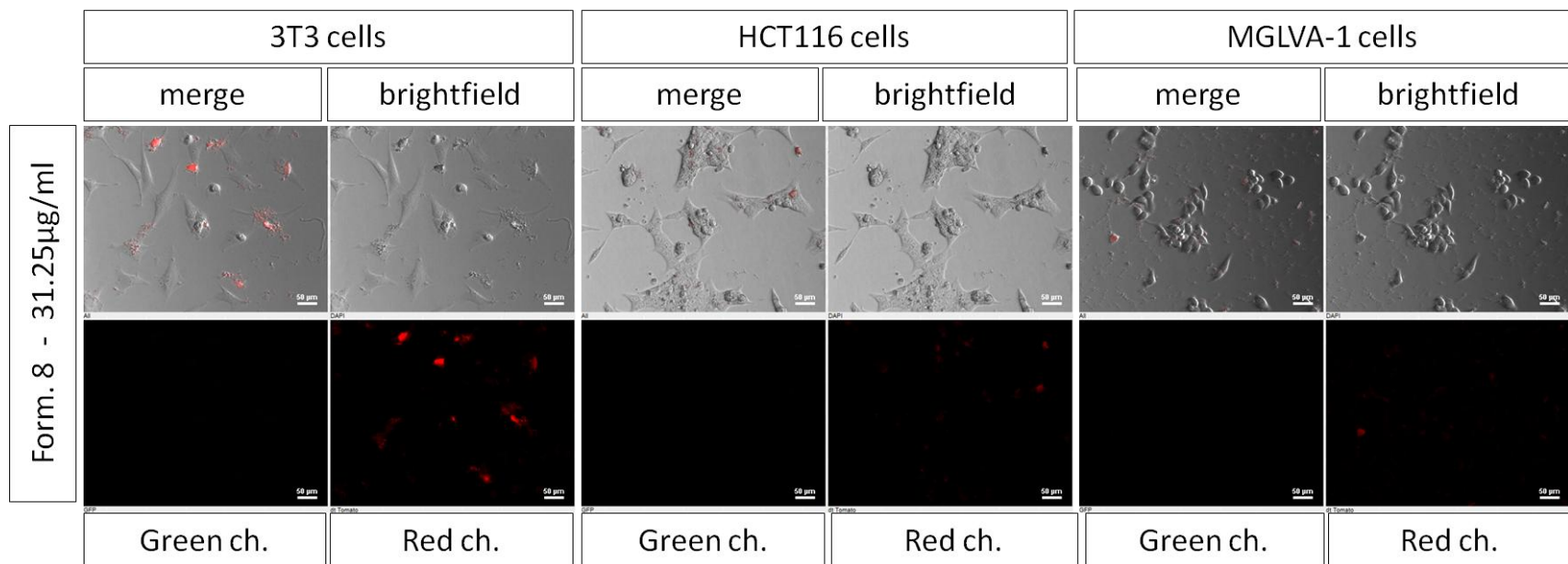


Figure 5-20 3T3, HCT116 and MGLVA-1 cells treated with 31.25 µg/ml of formulation 8 for 24 h at 37°C. The Figure shows the Green and Red channels (bottom Figures), brightfield and a merge of all (top Figures). The nanoparticles were expected to fluoresce in both the Green and the Red channels. Scale bars represent 50 µm.

Results – In vitro Studies of Thermoresponsive Polymers

As this polymer formulation was found to aggregate rapidly under the tested experimental conditions and did not appear to internalize, the polymers from this batch were not brought further to confocal microscopy studies.

However, from these initial results two hypotheses were formulated:

1. The aggregation was a consequence of the incubation of the micelle with cells; i.e. that components in the cell culture media were interacting with the nanoparticles causing aggregation and precipitation.
2. The aggregation was a consequence of the change of conformation of the thermoresponsive part of the micelle at 29°C and inherent instability of the resultant hydrophobic micelle surfaces in the aqueous suspension.

Following these hypotheses a second set of widefield microscopy experiments was run to enquire of the nature of the aggregates.

HCT116 cells were treated with the micelles at room temperature for 1 h (<21°C and below the TTT of the micelle = 29°C). In this conformation the micelles were predicted to stay in a more hydrated and less interacting and expectedly less aggregated conformation. This anticipated conformation was left to stabilize for 1 h before imaging. Cells treated at room temperature were then incubated at 37°C overnight and imaged again before and after rinsing the micelles from the flasks. Furthermore, to investigate that the aggregation of the micelle was not due to the presence of cells, a control without cells was also introduced in the experimental design.

After the thawing, the micelles looked more aggregated than previously noticed (Figure 5-21A). However, after vortexing and sonicating the nanoparticles, the

Results – In vitro Studies of Thermoresponsive Polymers

aggregates disappeared and the experiment was carried out as scheduled. Results showed that the treatment at room temperature did not reduce the formation of the aggregates that were still present and forming sheets of micelles in the range of a few micrometers. The following incubation at 37°C did not change the aggregation state of the micelles and pictures taken after the rinse of the micelles showed that some of the nanoparticles bound quite readily with the cellBIND treated polystyrene plastic of the flask. The presence of cells did not appear to change the aggregation state of the micelles. However, when comparing the conformation of the micelles from the images of the previous experiment where the micelles were incubated at 37°C without additional incubation steps (Figures from 5-15 to 5-20), some differences could be noticed. The presence of aggregated micelles in pseudo-filamentous filamentous and fibrous structures in the previous experiments was not apparent in the second set of experiments (Figure 5-22). In contrast, in the second experiment, micelles of formulation 8 were observed in wide sheet-like layers. After removing the polymer solution from cells and rinsing once with PBS, the aggregates appeared to be retained more in the presence of cells (Figure 5-22). The micelles were thawed a second time to repeat the experiment reported above on 3T3 and MGLVA-1 cells. However, this time the nanoparticles appeared heavily aggregated (Figure 5-21B and C) and vortexing and intense sonication did not disperse the aggregates. The experiment was interrupted.

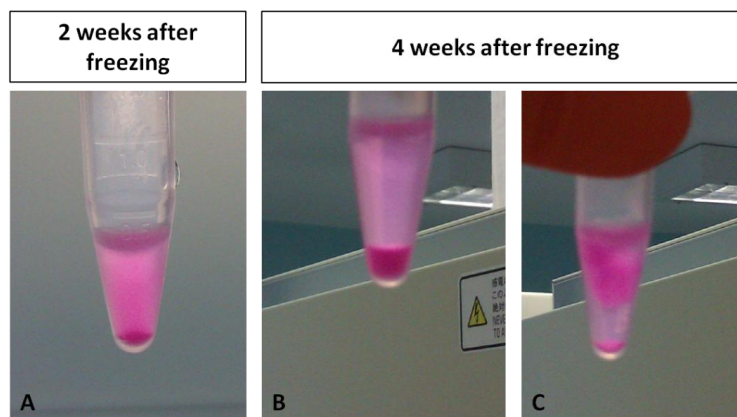


Figure 5-21 Evidence of aggregation over time of formulation 8 upon storage at -20°C. Figure A shows the aggregates of the micelles upon thawing after 2 weeks of storage of the micelle in a -20°C freezer. The aggregates, in that occasion were eliminated by the routine procedures of vortexing and sonication before the use of the micelles on cells. Figure B and C show two different Eppendorf tubes of the same micelles thawed after 4 weeks of storage of the nanoparticles in a -20°C freezer. The aggregates pictured in Figure B and C were only reduced upon vortexing and sonication and structures were prone to re-aggregation after a few minutes of settling of the polymer at the bottom of the Eppendorf tubes.

Results – In vitro Studies of Thermoresponsive Polymers

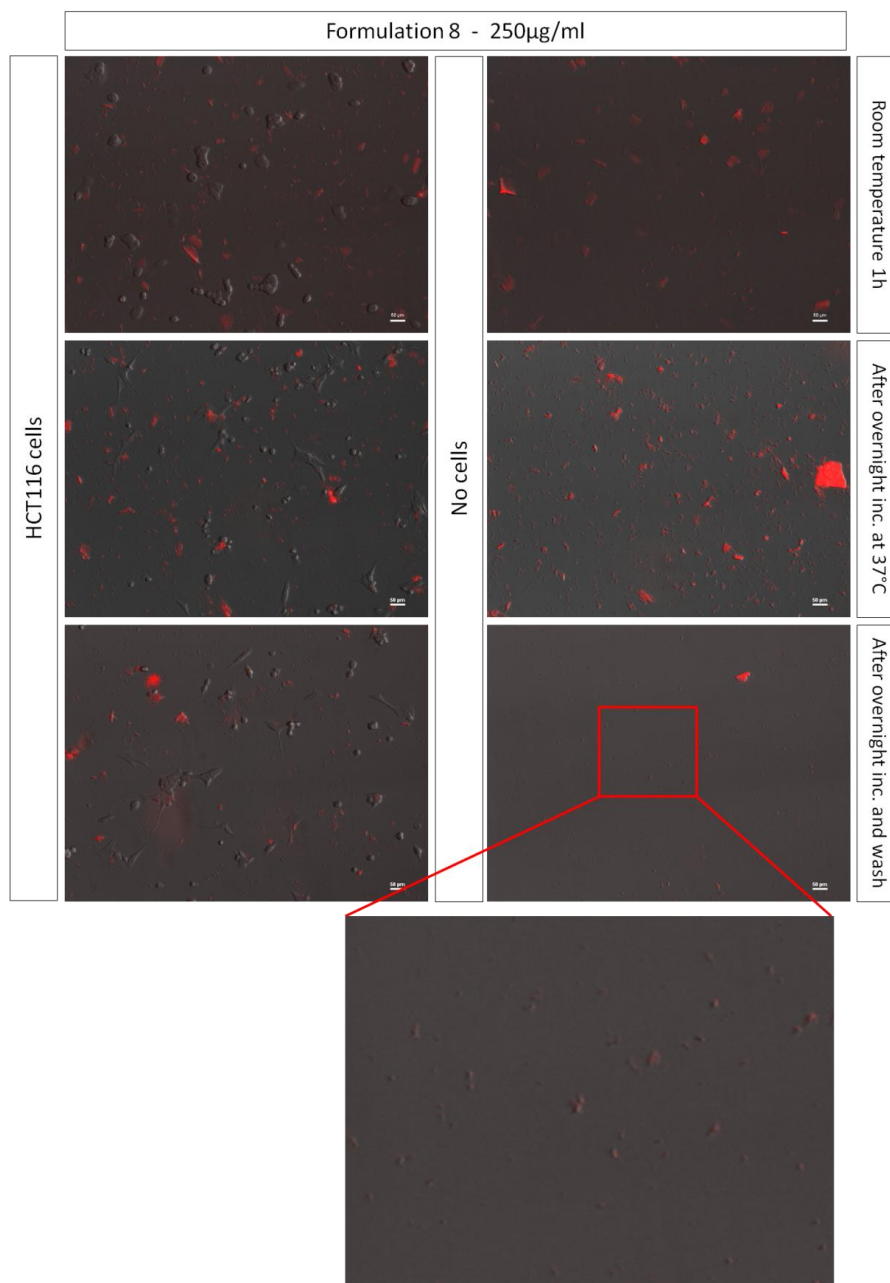


Figure 5-22 Flasks with or without HCT116 cells treated with formulation 8 at room temperature for 1 h, at 37°C overnight and before and after rinse. This set of pictures show the behaviour of formulation 8 (red channel) in the presence and in the absence of cells. Different settings were applied in these experiments. Flasks with or without cells were treated with micelle 8 for 1 h at room temperature**. Flasks were then moved to an incubator overnight at 37°C. The following day images were acquired prior and after rinsing the micelle from the flasks. Pictures shown in this Figure are the merge of the ds Red channel and the brightfield. Scale bars represent 50 µm.

** The flask without cells was rinsed with full media before the experiment to better resemble the conditions of the flask with cells.

5.4.5 Micelles 9 live imaging

The last polymer studied for cell internalization was polymer formulation 9. The chemistry of the polymer was very similar to formulation 8. The molar mass of the polymer, the diameter of the nanoparticles formed and the TTT closely resembled polymer 8 (Table 5-2). Because of the complications caused by the aggregation of the nanoparticle formulations upon freezing, the polymer was synthesized two days before the confocal microscopy experiment and the micelles produced by the syringe pump method described in Figure 5-4. The polymer was tested fresh without any freezing steps in between the synthesis and the application on cells. The internalization in HCT116 cells, assessed by confocal microscopy, was tested at room temperature and also below the TTT of the polymer (27°C). The polymer was also tested at a lower concentration of 250 µg/ml and incubated overnight at 37°C in HCT116 and 3T3 cells. As a further control of the aggregation stability, the polymer was also preincubated at room temperature for 1 h before the overnight incubation at 37°C in HCT116 cells.

The pictures of cells incubated with and without the polymer are shown in Figure 5-23, 5-24 and 5-25. Upon incubation at room temperature for 1 h and 500 µg/ml, some aggregation of the polymer in solution was visible. However, the aggregation was reduced when the polymer was used at 250 µg/ml and after overnight incubation. All cells treated with the polymer showed some extent of internalization, although the fluorescence was low. Internalization was apparent also when the polymer was incubated at room temperature and below the TTT. This suggests that the rearrangement of the polymer corona upon hydrophilic chain collapse above the TTT observed in buffer solutions either did not take place in the same way in the presence of cells, or that a change from a hydrophilic corona to a hydrophobic outer surface did

Results – In vitro Studies of Thermoresponsive Polymers

not significantly alter the internalization into cells. The distribution of the fluorescence resulting from polymer nanoparticles internalization was also different from that observed in C-PB. The fluorescence was more uniformly distributed in the cytoplasm and nuclei of cells and did not show the usual punctate structures that were detected for both C-PB nanoparticles and formulation of polymer 6. It should also be noted that z stack images (Figure 5-25) showed a tendency for the dye to undergo photo-bleaching and the internal fluorescence of the micelle was reduced upon repeated exposure to the laser beam.

Results – In vitro Studies of Thermoresponsive Polymers

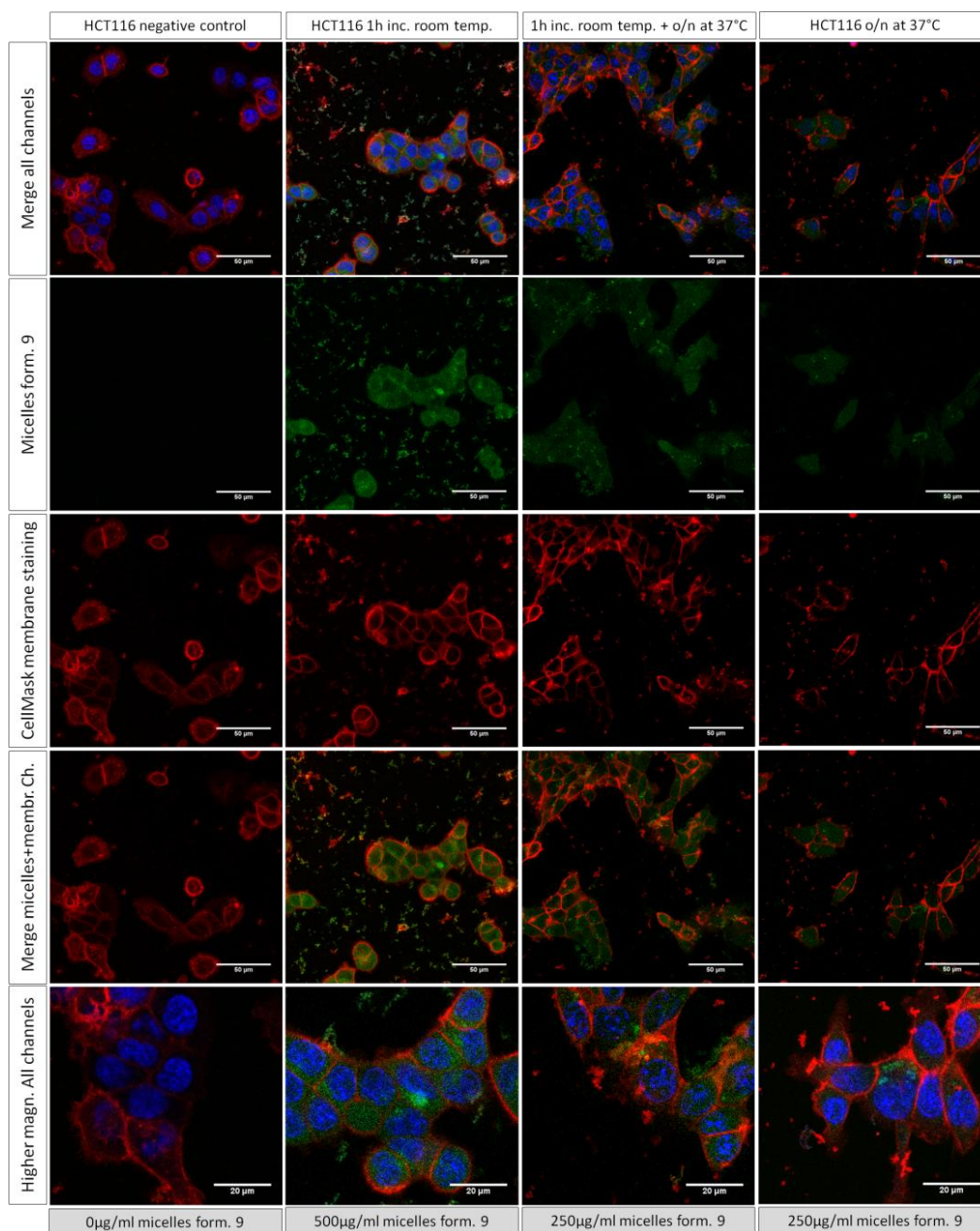


Figure 5-23 Formulation 9 incubated with HCT116 cells in different conditions. HCT116 cells were incubated with polymer formulation 9 for 1 h at room temperature, or overnight at 37°C, with or without a preincubation step of 1 h at room temperature. The concentration of formulation 9 is 500 μg/ml in room temperature experiments and 250 μg/ml in overnight experiments. Green: micelles; Blue: Hoechst staining of the nuclei; Red: CellMask deep red membrane staining. Polymers were labelled with Rhodamine B which is detected in a red channel. For an easy distinction of the micelles from the Deep Red CellMask dye, the micelles are shown in Green. The last row of images is given by a magnification of the most significant features of the internalization of formulation 9 in HCT116 cells. Scale bars for the first 4 rows represent 50 μm. Scale bars for the bottom row represent 20 μm.

Results – In vitro Studies of Thermoresponsive Polymers

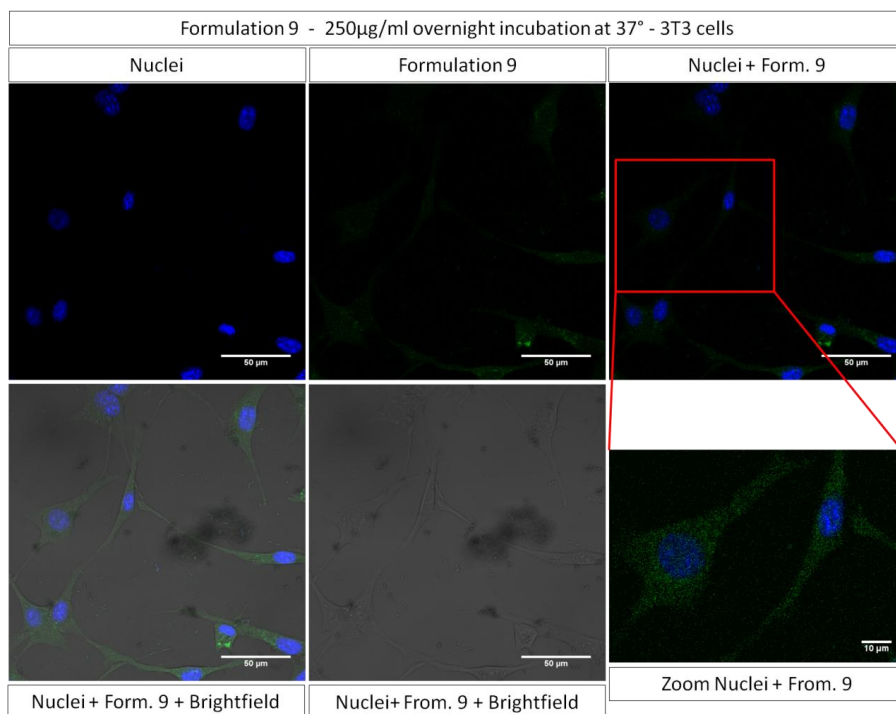


Figure 5-24 Internalization of 250 µg/ml of micelle suspension 9 after overnight incubation at 37°C. Images were acquired on a Zeiss 710 confocal microscope after staining the cells with Hoechst 33342 1 µg/ml (Blue). Green: Formulation 9 stained with a red Rhodamine B dye. The magnification picture in this Figure has been modified enhancing the fluorescence signal from the micelles to help the reader to detect the key features of the internalization of formulation 9 in 3T3 cells. Scale bars represent 50 µm for the full images and 10 µm for the zoomed image.

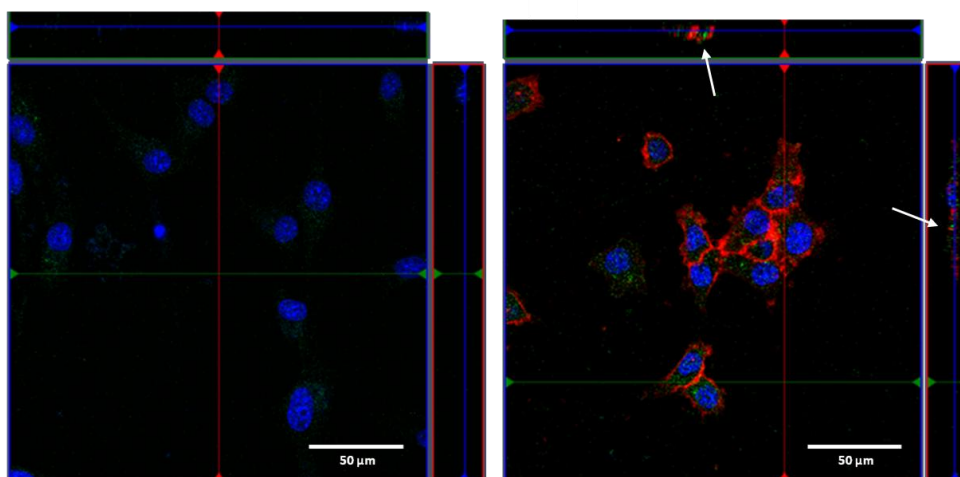


Figure 5-25 Orthogonal projection of a 3D image acquired on 3T3 (left) HCT116 cells (right) treated with 250 µg/ml of micelle suspension 9 overnight at 37°C. The arrows point at the internalization of the nanoparticles (Green) where its fluorescence can be localised within the boundaries of the red membrane. Nuclei: Blue. Scale bars represent 50 µm.

5.5 Discussion

Cell activity studies on micelles 1, 2, 3 and 4 showed that the materials were generally well tolerated in the tested cell lines. HCT116 cells were the most sensitive to polymer micelle-like nanoparticles 1-4 with a minimum cell activity observed at 250 µg/ml polymer. The drop in viability reached a minimum of about 70% viable cells in HCT116 with micelle 1-4 which implied a good overall biocompatibility of the micelles. The U shaped viability profile might have been due to different aggregation states of the polymers with the higher concentrations producing aggregates that reduced association and internalization of the polymers with/in the cells and hence interfering less with the cells activity.

Cell activity was also not affected adversely by polymer formulation 6. 3T3 fibroblasts were the most sensitive cell line of the panel of cells used. However, the PEI positive control in these experiments did not sufficiently reduce the viability of cells. This unexpected result must be taken into consideration when extrapolating from this set of data that micelle formulation 6 was well tolerated from cells.

Widefield microscopy studies at 37°C and 42°C for micelles 5 produced some inconclusive results on the ability of the micelle-like structures to access cells, given that the polymer did not present any detectable fluorescence. The reason for this absence of fluorescence was due to the insufficient concentration of the Fluorescein methacrylate dye used for the labelling of the polymer. However, the pictures obtained at 42°C showed that cells incubated with the micelles acquired some resistance to the increase of the temperature with respect to the negative control. This unexpected event has not been reported in the literature before and it should be further investigated in order to confirm that this phenomenon is consistently and

reproducibly happening as the data shown are based on one experiment only. One hypothesis can be attempted to justify this observation. Micelles 5 were brought from 37°C to 42°C upon initiation of the experiment. The solution that contained the polymer gradually increased its temperature from 37°C up to 42°C. While the temperature of the plates was increasing, at temperatures near 41°C that is the TTT of the polymer, the change in conformation of the nanoparticles started occurring, subtracting energy from the system, which in other terms means that, for some reasons the transition in conformation started happening in an endoergonic way while the ΔG of the transition was still positive, subtracting energy from the solution. This process might have slowed down the escalation of the temperature of the solution in contact with the cells delaying the increase of the temperature to up to 42°C for a time sufficient to produce this apparent protective effect of the nanoparticles on cells.

Confocal live imaging of polymer formulation 6 thawed and applied to 3T3 cells for 1 h at 37°C did not show any internalization of the micelles. Nanoparticles from formulation 6, with a transition temperature of 24°C, were anticipated to display a hydrophobic, more amphiphilic and more cell-interacting conformation upon incubation at 37°C. Based on prior data with similar nanoparticles, the collapsed structure of the PLGA-*b*-(PEGMA-co-PPGMA) above its TTT was expected to have interacted more promptly with the phospholipids bilayer and membrane proteins at the cell surfaces and promote an internalization process for the material. The internalization process is believed to occur in two steps:

1. The polymer chains at the nanoparticle surface interact with the cell and bind to its membrane/membrane bound proteins;

2. The nanoparticles are subsequently internalised via the triggering of a receptor-mediated process or through fluid phase endocytosis.

As no evidence of internalization was provided by confocal microscopy studies for micelle-like structures 6, it is possible to hypothesise that one of the two processes described above must have failed to occur. In other terms, the polymer might have failed the binding on the cell surface or the polymer was binding on the cell surface but was not internalised. However, if it was the internalization process to be failing, the membrane of cells might have been fluorescent because of the polymer-aggregates binding to the cell membrane; experimental evidence does not support this hypothesis. As a consequence, it is possible to suggest that a low interaction with the membrane of cells of the micelles was reducing its internalization. The pre-incubation step at 37°C and the extension of the incubation time to 2 hours did not produce any detectable internalization. This time-length of internalization was proven sufficient for the similar nanoparticles in other studies¹⁶. Nevertheless preincubation at 37°C and extension of the incubation time to 2 h showed that the micelles were not prone to aggregation and stable in their conformation and size. The internalization of the micelle-like nanoparticles occurred only when the micelles were incubated with cells for 17 h and this timescale of internalization was not compatible with the intended endocytosis pathway studies. This brings into question as to why the internalization of this formulation of polymer 6 was so slow. It might be possible that polymer 6 formulation had high affinity towards only a few proteins on the plasma membrane and this reduced its interaction with the membrane and consequently its internalization. Another hypothesis is that the polymer did not have any affinity for the plasma membrane of 3T3 cells but the prolonged incubation with 3T3 cells allowed for the cells to secrete enough proteins to condition the media. It has been reported in

the literature that such processes can enhance binding of the secreted protein to the polymer and hence its affinity for the cells' membrane and internalization²⁵. It is also important to stress that the lack of fluorescence inside cells upon incubation of the micelle-like polymer 6 might be due to a lack of detection of the polymer inside cells. It is known in the literature that Fluorescein methacrylate is a pH sensitive dye. It bears a carboxylic group that is protonated and hence switches the chemistry of the dye towards a less fluorescent form upon acidification of the solution in which resides. As many intracellular compartments to which the micelles can be directed upon internalization are acidic and with pH ranging between 6.5 and 4.5, it might be possible that the micelles were not poorly internalised but were not detectable as a result to traffic to acidic compartments. A reasonable question at this point might be on why the micelles were detected upon incubation at 17 h. One possible explanation might be that the polymer had moved to a less acidic compartment during the extended incubation. However, if the lack of cellular fluorescence was due to a failed internalization instead of a lack of fluorescence another consideration might be due. Previous work on polymers of very similar constituents and formation parameters showed internalization on MCF-7 epithelial cancer cell lines. Hence, it is possible to consider factors which might account for differences in the present study compared to the prior work: the 3T3 cells used for the studies were fibroblastic cell lines from mouse embryos and were not originating from a cancer line, thus suggesting some specificity of the PLGA-*b*-(PEGMA-*co*-PPGMA) micelles towards epithelial cancer cell lines.

Confocal microscopy on micelle formulation 7 showed that the formulation of the micelles with a manual nanoprecipitation method was not giving reproducible sizes of the micelles and it was confirmed by DLS studies (Table 5-1). The polymer used for

the formulation of these nanoparticles was the same as for formulation 6. However, upon incubation with cells, it produced large aggregates of tens of microns in size. The evidence that formulation 7 was more aggregated than micelle-like structures 6, that were originated from the same polymer, was already provided by DLS studies carried out straight after the formulation of the micelles where DLS was showing a double peak at 49 and 312 nm. It might be possible that the presence of bigger aggregates already in the original formulation of the polymer might have speeded up the process of nucleation that is essential for the formation of larger aggregates. Although formulation 6 showed a much slower tendency to aggregation, upon prolonged storage at -20°C (about one month) the polymer presented large aggregates that were not dissolving with intense vortexing or sonication. These results suggest a more general instability upon storage of PLGA-*b*-(PEGMA-co-PPGMA) nanoparticles produced by the manual nanoprecipitation route.

From the above evidence of colloidal instability of PLGA-*b*-(PEGMA-co-PPGMA) formulation 6 and 7, nanoparticles 8 and 9 were synthesised. They were constituted from subtly different co-monomers and were formulated into nanoparticles by an automated system in order to increase the reproducibility of the size and surface characteristics of the nanoparticles. Also, in the attempt to produce a more reliable probe to detect the polymer in any cell compartment, the materials were synthesised in the presence of 2 dyes: Rhodamine B for a clear detection of the polymer at acidic pH²⁶, and Fluorescein metachrylate for a convenient detection in non acidic compartments^{27,28}. However, when nanoparticles from formulation 8 were tested at different concentrations for 24 h at 37°C, aggregates nevertheless formed. While self-association and colloidal instability at 37°C might be expected for polymer nanoparticles with a TTT of 24°C, it was not expected when initial incubations were

Results – In vitro Studies of Thermoresponsive Polymers

carried out at room temperature ($< 21^{\circ}\text{C}$). Indeed, DLS measurements of the formulation 8 nanoparticles reported a size of 56.4 nm at 20°C , clearly indicating an initial non-aggregated formulation of the nanoparticles in HEPES 20 mM. The micelles aggregated at 37°C , which although not entirely unexpected owing to predicted loss of colloidal stability above the TTT, was problematic for cell assays as the self-association occurred rapidly. Literature reports of phase transitions of polymers have shown that aggregation depends on many variables: temperature, ionic strength of the solution, concentration of the polymer in solution, as well as geometry of the hydrophilic to hydrophobic block of the micelles. However, these considerations have been made on relatively small aggregates that are usually detected with TEM techniques. The aggregates reported in the experiments in this thesis were of several microns in size and this suggests that the rod-like structures and worms so easily detectable might be given by complex interactions of the micelles with each other producing layers and layers of particles thick enough to become detectable in a widefield microscope with a low power objective. The presence of such bulky aggregates suggests that the materials were exceptionally more stable when aggregating with respect to the single micelles in solution. Also, reducing the concentration to $31.25\ \mu\text{g/ml}$ did not prevent aggregation suggesting that the polymer nanoparticles were not stable in solution above their TTT and that aggregation was not intrinsically a consequence of a too high concentration of micelles in solution. Polymer formulation 8 appeared to show affinity for 3T3 and HCT116 cell surfaces. It is not clear if the presence of aggregates associated with 3T3 and HCT116 cells was due to an entrapment in the extracellular matrix proteins produced by 3T3 cells or to a more general affinity to the membrane composition of the cells as suggested by HCT116-aggregates interactions.

Results – In vitro Studies of Thermoresponsive Polymers

Furthermore, given that the fluorescence of aggregates was quite strong and the magnification used for the experiments was quite low, it is not possible to rule out some extent of internalization in cells of the modest portion of the nanoparticles that were non-aggregating. If some internalization occurred, it is possible that the lack of Fluorescein signal might have been due to internalization in acidic compartments as Fluorescein is well known for its pH dependent loss of fluorescence. However, most of the polymer was present outside cells and Fluorescein remained undetected in the GFP channel. The loss of fluorescence emission of Fluorescein methacrylate was most likely due to poor incorporation of the Fluorescein-based monomer during synthesis, as Fluorescein was used in low monomer feed ratios.

This double system of detection based on two dyes consisting in Fluorescein methacrylate and Rhodamine B is not new in literature and is has been already reported²⁹. This probe-system was chosen to give extra information on the pH of the compartment that the material was accessing upon endocytosis and also probing that the lack of fluorescence obtained with previous fluorescein labelled polymers was not due to the acidic compartmentalization of the materials upon internalization. It was disappointing not to be able to observe the dual signal in these experiments.

A hypothesis to explain the reasons for the strong tendency to aggregation of polymer nanoparticles 8 is that it might have been due to the chemistry of the PLA-*b*-(DEGMA-*co*-OEGMA). The portion of the DEGMA block, in fact, is highly represented in these polymers and constitutes 95% of the hydrophilic portion of the block copolymer. Although this ratio of the DEGMA portion is justified to lower the TTT of the polymer from about 90°C of the OEGMA to more physiologically relevant transition temperatures, literature reports that the more the thermoresponsive chains are short (and DEGMA is formed by only 2 repetitions of ethyl ether), the more the

adhesion properties of the micelles above the LCST. Hence the high proportions of the DEGMA were probably undermining the colloidal stability of the polymer when incubating at 37°C^{9,30}. It is also possible to speculate that this effect might have been reduced if the distribution of the OEGMA chains could have been controlled during the synthesis of the block copolymer. However, the statistical method used to synthesise these polymers does not allow this control. Another phenomenon that promoted aggregation and interfered with the stability of polymer 8 was the tendency for aggregation upon storage. This may have been due to too high concentration of the stock suspension of polymer in storage (7.5 mg/ml) and possible phase segregation in the buffer (HEPES 20 mM) leading to polymer-rich regions in suspension, chain entanglement and kinetic trapping of aggregates.

As a recent publication from Albanese *et al* showed that cells secretions can alter the properties of nanoparticles in relation to their tendency to aggregate, the polymer formulation 8 was tested both in the presence and in absence of HCT116 cells³¹. To further investigate the nature of the aggregation, the nanoparticles were incubated at room temperature and below the TTT of nanoparticle formulation 8 (29°C). Results showed that the filamentous network of aggregated particles in these settings did not occur, either in the presence or in the absence of cells. From these data it is not entirely possible to rule out the involvement of HCT116 cells surface proteins and secretions in the formation of polymer nanoparticle-complex filaments aggregates obtained at 37°C as it might be possible that cells at room temperature can expose different proteins on their surface, since the endocytosis is still active but the trans-Golgi network cargo sorting on the plasma membrane and exocytosis are inhibited and potentially changing the protein expression at the plasma membrane and secreted in the media³². However, the aggregation in fact happened in both cell and

Results – In vitro Studies of Thermoresponsive Polymers

cell-free conditions suggesting that cellular secretions alone were not responsible for the formation of the layers of aggregates of micelles in these settings. It is probable that the poly-DEGMA corona might be already sticky and prone to aggregation at room temperature and the pre-treatment at 20°C after thawing the micelles was stabilising the aggregation. This pretreatment was giving time to the micelles to rearrange to a more complex and a reduced entropy sheet conformation. This conformation might have been occurring less at higher temperatures because of thermal agitation of the solution in which the micelles reside, or the presence of cells at 37°C might have stabilised the formation of the worm-like aggregates instead. The evidence of aggregation below the TTT of the polymer suggests that the chemistry of these polymers was not optimised against the aggregation of the micelles upon storage. After rinsing, the majority of large aggregates were removed. However, small sheet-like structures were still present to the bottom of the plate after rinsing. This show that the nanoparticles had some moderate affinity for the cellBIND treated surface of the flask.

The last set of experiments was with polymer formulation 9 with a TTT of 27°C and a monomer composition closely resembling formulation 8. As it was evident from previous experiments that the nanoparticles were not stable upon storage, they were synthesized and micelles produced immediately before confocal live experiments. In this way the freeze-thawing step was avoided and fresh nanoparticles, with a DLS reported size (at 20°C) of about 45 nm applied on cells. The temperature was not altered and experiments with HCT116 at room temperature and uptake studies run after incubation of the polymer with cells for 1 h. Despite the numerous efforts to reduce the aggregation, the nanoparticles showed some extent of self association, although the aggregation state did not interfere with the internalization of the

nanoparticles. However, in these experiments the nanoparticles were internalising below the TTT in HCT116 cells. Experiments with polymer formulation 9 carried out overnight, with and without preincubation step of 1 h at room temperature showed internalization as well. As the concentration of polymer in the experiments at room temperature and the ones with the overnight incubation were different, it is not possible to verify if the extent of internalization differed with the two settings. One explanation can be attempted for the internalization of the micelle-like aggregates 9 irrespective of the TTT and consistent with the earlier data on polymer self-association below the TTT. It is known from the literature that PEG chains can interact to some level with proteins³³. Their antifouling characteristics are given by the length of the PEG chain and its ability to produce a thick layer of flexible brushes that reduces the interactions of the PEG chain with the proteins³⁴. PEG chains around 400 Da of Mw are believed to be the less protein-interacting³³. However, the OEGMA, with Mw of 375Da, is represented for only 5% in the PLA-*b*-(DEGMA-*co*-OEGMA) polymers. This might mean that the 'PEG component' was too small to effectively produce a brush to reduce the interaction with proteins. As a result, given that in the chosen experimental settings the media was formed by HBSS that contains only a few aminoacids, the bulk of the proteins exposed to the polymer were derived from the membranes of cells. This might explain why, although below the TTT, the polymer was sufficiently interacting with cell proteins to allow a rather fast internalization of the polymer that was observed within 1 h from the application of the polymer on cells. The signal obtained by the internalised micelles was weak both above and below the TTT. Upon overnight incubation, the presence of the aggregates in the media was less evident. However, also the concentration used for the overnight experiments was halved with respect to the experiments with cells run at room temperature which

Results – In vitro Studies of Thermoresponsive Polymers

might reduce aggregation. Consequently, it is not possible to determine the reasons for the loss of aggregates in the media of cells upon overnight incubation. Furthermore, as pointed out in the results section for polymer formulation 9, the fluorescence of the internalised nanoparticles was different with respect to formulation 6 and C-PB. The latter nanoparticles appeared as discrete dots of different sizes in the cytoplasm and perinuclear accumulation that were also evident in immunofluorescence staining of clathrin heavy chain α and caveolin-1. To some extent, for the overnight incubation of the micelles, some increase of polymer fluorescence in the perinuclear region was observed. However, it is important to point out that there is evidence that Hela cells lysosomes change their distribution towards a conformation resembling the diffused fluorescence observed in HCT116 and 3T3 cells when incubated with toxic drugs that induce apoptosis such as the anticancer etoposide³⁵. However, even though this specific polymer was not tested for toxicity, other polymers with similar characteristics did not interfere with cell activity according to an MTT assay. It is nevertheless true that one test alone does not give the full picture of the toxicity of novel materials. If toxicity was occurring, the cells might result fluorescent as a consequence of the toxicity instead of the uptake of the material if they produce ROS. ROS oxidise proteins making them fluorescent and emitting in the green and red channels (the same mechanism underlying the phototoxicity events in microscopy that cause auto-fluorescence as a consequence of a too long exposure to the high power laser beam). In this experiment, the Green channel did not show fluorescence. However, it is known that an oxidised form of riboflavin (vitamin B₂) produces autofluorescence, emitting around 550 nm which was the region of detection of the Rhodamine B dye in the confocal settings for these experiments^{36,37}. If toxicity and consequent autofluorescence was occurring that might be the reason for

fluorescence detection both above and below the TTT. Literature reports that ROS production is increased as the surface area of the material increases³⁸. Although the morphology of the cells did not suggest toxicity, the CellMask dye also stained some extracellular membrane features. These features might be apoptotic bodies as there are no macrophages to scavenge for these products and remove from the environment (although also non-specialised cells can clear from apoptotic bodies), or necrotic remains of cells. The toxicity overnight might also have been triggered by the prolonged incubation of cells in HBSS/HEPES media, where the absence of FBS might cause the cells to undergo stress and death. The last result for this set of experiments suggest that the micelles were undergoing photo-bleaching as the fluorescence obtained in the equatorial region of 3D images present a lower fluorescence with respect to the single plane images. This effect is reported in the literature for Fluorescein but Rhodamine B is considered a rather resistant dye, and the reasons underlying this effect are not clear. The next steps are to design the synthesis of improved materials and consequent experiments to rule out as much as possible any misinterpretation of the experimental results.

5.1 Conclusions

These experiments have revealed an unexpected difficulty for these synthetic polymers to produce micelles with reproducible characteristics. Polymer presented a high tendency to aggregation and inherent instability and little tendency to access cells. Although some progress has been made in regards to the manufacture of micelles with an automated system that can produce micelles from the same polymer that have similar characteristics of size, some improvements must still be addressed. One of the main problems for these polymers was their strong tendency to produce

bulky aggregates. The aggregation tendency was variable in different polymers. Polymer 6 with a PLGA-*b*-(PEGMA-*co*-PPGMA) chemistry was the most resistant to aggregation and produced stable micelles sizes for a period of two weeks. However, upon longer periods of storage the polymer presented extensive aggregation that was not compatible with the intended *in vitro* studies. This tendency became even more evident in the last two PLA-*b*-(DEGMA-*co*-OEGMA) polymers. Another issue that makes the control of aggregation more challenging is the statistical method used to synthesise these polymers. This way of producing polymers does not allow for a control of the distribution of the OEGMA in the hydrophilic chain of the polymer rendering the polymer tendency to agglomerate difficult to manage especially for polymers at low percentages of OEGMA. If this problem is not resolved by an optimization of the OEGMA ratio that is also compatible with a physiologically relevant TTT, other methods that allow for a more controlled synthesis of polymers for physiological applications might be worth some consideration³⁹⁻⁴³.

References

- 1 Arthur, R. M., Straube, W. L., Trobaugh, J. W. & Moros, E. G. Non-invasive estimation of hyperthermia temperatures with ultrasound. *Int J Hyperthermia* **21**, 589-600 (2005).
- 2 Chatterjee, D. K., Diagaradjane, P. & Krishnan, S. Nanoparticle-mediated hyperthermia in cancer therapy. *Ther Deliv* **2**, 1001-1014 (2011).
- 3 Dickerson, E. B. *et al.* Gold nanorod assisted near-infrared plasmonic photothermal therapy (PPTT) of squamous cell carcinoma in mice. *Cancer Letters* **269**, 57-66 (2008).
- 4 Svaasand, L. O., Boerslid, T. & Oeveraasen, M. Thermal and optical properties of living tissue: Application to laser-induced hyperthermia. *Lasers in Surgery and Medicine* **5**, 589-602, doi:10.1002/lsm.1900050607 (1985).
- 5 Abulateefeh, S. R. *et al.* Facile synthesis of responsive nanoparticles with reversible, tunable and rapid thermal transitions from biocompatible constituents. *Chemical Communications*, 6068-6070 (2009).
- 6 Makadia, H. K. & Siegel, S. J. Poly Lactic-*co*-Glycolic Acid (PLGA) as Biodegradable Controlled Drug Delivery Carrier. *Polymers (Basel)* **3**, 1377-1397 (2011).
- 7 Lu, J. M. *et al.* Current advances in research and clinical applications of PLGA-based nanotechnology. *Expert Rev Mol Diagn* **9**, 325-341 (2009).

Results – In vitro Studies of Thermoresponsive Polymers

- 8 Wu, X. S. & Wang, N. Synthesis, characterization, biodegradation, and drug delivery application of biodegradable lactic/glycolic acid polymers. Part II: biodegradation. *J Biomater Sci Polym Ed* **12**, 21-34 (2001).
- 9 Vancoillie, G., Frank, D. & Hoogenboom, R. Thermoresponsive poly(oligo ethylene glycol acrylates). *Progress in Polymer Science* **39**, 1074-1095 (2014).
- 10 Boutris, C., Chatzi, E. G. & Kiparissides, C. Characterization of the LCST behaviour of aqueous poly(N-isopropylacrylamide) solutions by thermal and cloud point techniques. *Polymer* **38**, 2567-2570 (1997).
- 11 Anghelache, A., Teodorescu, M., Stănescu, P., Drăghici, C. & Vuluga, D. Novel crosslinked thermoresponsive hydrogels with controlled poly(ethylene glycol)—poly(propylene glycol) multiblock copolymer structure. *Colloid Polym Sci* **292**, 829-838 (2014).
- 12 Hu, Z., Cai, T. & Chi, C. Thermoresponsive oligo(ethylene glycol)-methacrylate- based polymers and microgels. *Soft Matter* **6**, 2115-2123 (2010).
- 13 Luzon, M. *et al.* Water-soluble, thermoresponsive, hyperbranched copolymers based on PEG-methacrylates: Synthesis, characterization, and LCST behavior. *Journal of Polymer Science Part A: Polymer Chemistry* **48**, 2783-2792 (2010).
- 14 Lutz, J.-F. & Hoth, A. Preparation of Ideal PEG Analogues with a Tunable Thermosensitivity by Controlled Radical Copolymerization of 2-(2-Methoxyethoxy)ethyl Methacrylate and Oligo(ethylene glycol) Methacrylate. *Macromolecules* **39**, 893-896 (2005).
- 15 Ramírez-Jiménez, A., Alvarez-Lorenzo, C., Concheiro, A. & Bucio, E. Temperature-responsiveness and biocompatibility of DEGMA/OEGMA radiation-grafted onto PP and LDPE films. *Radiation Physics and Chemistry* **99**, 53-61 (2014).
- 16 Abulateefeh, S. R. *et al.* Enhanced uptake of nanoparticle drug carriers via a thermoresponsive shell enhances cytotoxicity in a cancer cell line. *Biomaterials Science* **1**, 434-442 (2013).
- 17 MacEwan, S. R. & Chilkoti, A. Controlled Apoptosis by a Thermally Toggled Nanoscale Amplifier of Cellular Uptake. *Nano Letters* **14**, 2058-2064 (2014).
- 18 Kirchhausen, T. Imaging endocytic clathrin structures in living cells. *Trends Cell Biol* **19**, 596-605 (2009).
- 19 Iversen, P. W., B.J., E., Sittampalam, G. S. & Cox, K. L. A comparison of assay performance measures in screening assays: signal window, Z' factor, and assay variability ratio. *Journal of Biomolecular Screening* **11**, 247-252 (2006).
- 20 Zhang, J. H., Chung, T. D. F. A. U. O. & Oldenburg, K. R. A Simple Statistical Parameter for Use in Evaluation and Validation of High Throughput Screening Assays. *Journal of Biomolecular Screening* **4**, 67-73 (1999).
- 21 Aubin, J. E. Autofluorescence of viable cultured mammalian cells. *Journal of Histochemistry & Cytochemistry* **27**, 36-43 (1979).
- 22 Goldman, R. D., Swedlow, J. R. & Spector, D. L. Vol. 1 (ed Cold Spring Harb Laboratory Press) (John Inglis, New York, USA, 2010).
- 23 Fabbro, C. *et al.* Cell type-specific transcription of the alpha1(VI) collagen gene. Role of the AP1 binding site and of the core promoter. *J Biol Chem* **274**, 1759-1766 (1999).
- 24 Goldberg, B. Collagen synthesis as a marker for cell type in mouse 3T3 lines. *Cell* **11**, 169-172 (1977).
- 25 Albanese, A. *et al.* Secreted Biomolecules Alter the Biological Identity and Cellular Interactions of Nanoparticles. *ACS Nano* **8**, 5515-5526, doi:10.1021/nn4061012 (2014).

Results – In vitro Studies of Thermoresponsive Polymers

- 26 Ramette, R. W. & Sandell, E. B. Rhodamine B Equilibria. *Journal of the American Chemical Society* **78**, 4872-4878 (1956).
- 27 Martin, M. M. & Lindqvist, L. The pH dependence of fluorescein fluorescence. *Journal of Luminescence* **10**, 381-390 (1975).
- 28 Geisow, M. J. Fluorescein conjugates as indicators of subcellular pH: A critical evaluation. *Experimental Cell Research* **150**, 29-35 (1984).
- 29 Hu, J. *et al.* Ultrasensitive ratiometric fluorescent pH and temperature probes constructed from dye-labeled thermoresponsive double hydrophilic block copolymers. *Journal of Materials Chemistry* **21**, 19030-19038 (2011).
- 30 Synytska, A. *et al.* Biocompatible polymeric materials with switchable adhesion properties. *Soft Matter* **6**, 5907-5914 (2010).
- 31 Albanese, A. & Chan, W. Effect of Gold Nanoparticle Aggregation on Cell Uptake and Toxicity. *ACS Nano* **5**, 5478 - 5489 (2011).
- 32 Manolea, F. *et al.* Arf3 is activated uniquely at the trans-Golgi network by brefeldin A-inhibited guanine nucleotide exchange factors. *Mol Biol Cell* **21**, 1836-1849 (2010).
- 33 Wu, J. *et al.* Binding characteristics between polyethylene glycol (PEG) and proteins in aqueous solution. *Journal of Materials Chemistry B* **2**, 2983-2992 (2014).
- 34 Roosjen, A., van der Mei, H. C., Busscher, H. J. & Norde, W. Microbial Adhesion to Poly(ethylene oxide) Brushes: Influence of Polymer Chain Length and Temperature. *Langmuir* **20**, 10949-10955 (2004).
- 35 Bottone, M. G. *et al.* Morphological Features of Organelles during Apoptosis: An Overview. *Cells* **2**, 294-305 (2013).
- 36 Rost, F. W. D. Vol. II (Cambridge University press Cambridge, USA, 1995).
- 37 Pawley, J. (ed Springer) (New York, USA, 2010).
- 38 Brown, D. M., Wilson, M. R., MacNee, W., Stone, V. & Donaldson, K. Size-dependent proinflammatory effects of ultrafine polystyrene particles: a role for surface area and oxidative stress in the enhanced activity of ultrafines. *Toxicol Appl Pharmacol* **175**, 191-199 (2001).
- 39 Furgeson, D. Y., Dreher, M. R. & Chilkoti, A. Structural optimization of a "smart" doxorubicin-polypeptide conjugate for thermally targeted delivery to solid tumors. *Journal of Controlled Release* **110**, 362-369 (2006).
- 40 Ghoorchian, A., Chilkoti, A. & López, G. P. Simple Assay for Proteases Based on Aggregation of Stimulus-Responsive Polypeptides. *Analytical Chemistry* **86**, 6103-6110 (2014).
- 41 Mastria, E. & Chilkoti, A. Genetically encoded "smart" peptide polymers for biomedicine. *MRS Bulletin* **39**, 35-43 (2014).
- 42 MacEwan, S. R. & Chilkoti, A. Applications of elastin-like polypeptides in drug delivery. *Journal of Controlled Release* **190**, 314-330 (2014).
- 43 Li, N. K., Garcia Quiroz, F., Hall, C. K., Chilkoti, A. & Yingling, Y. G. Molecular description of the LCST behavior of an elastin-like polypeptide. *Biomacromolecules* (2014).

6-Chapter 6

General discussion and future perspectives

Polymer-therapeutics are a stimulating field for the pharmaceutical industry. They have been intensely investigated for their new approach to treatments and for their clinical potential. Many polymer-drug conjugates have now reached the market and have succeeded in their promise to improve the array of choices for medicinal remedies, reducing toxicity, increasing specificity and consequently patients' overall quality of life¹. However, recent progress in polymer chemistry has fuelled the polymers therapeutics field with new and inspiring 'smart' materials that can respond to environmental changes providing potentially elegant and sophisticated ways to deliver drugs²⁻⁵. Evidence in the literature indicates that responsive materials can increase selectivity of drug targeting and reduce toxicity and *in vivo* studies are gradually changing the perception of the field^{6,7}. One of the most important possibilities for these (nano)materials is that they can enhance delivery of drugs at the cellular and subcellular level. However, the understanding of endocytic processes underlying the uptake of many nanomaterials is limited at the moment and approaches to direct the nanocarriers of drugs towards one specific endocytic pathway have not yet led to improved results in clinical trials. This has created a renewed interest in the understanding of the mechanisms that lead to endocytosis of nanocarriers. Deciphering these mechanisms would allow controlled intracellular delivery and could open new and unexplored perspectives for the pharmaceutical industry in areas such as gene delivery and, more importantly, provide a therapeutic approach for many untreatable diseases.

The aim of this thesis was to investigate the uptake of synthetic nanoparticles *in vitro* using inhibitors of endocytosis and to recognize any similarities in the uptake of carboxylated polystyrene bead nanoparticles (C-PB) and thermoresponsive block copolymer core-shell nanoparticles. As the polymers used for the study presented a

PEGMA brush that reduced their interactions with proteins and hence with a surface chemistry that was only marginally affected by the presence of FBS, C-PB studies were carried out in a buffer in the absence of FBS to better mimic the surface chemistry of the thermoresponsive polymers. Although thermoresponsive core-shell micelle-like nanoparticles with a similar chemistry had already been synthesized in our group in the past and showed good internalization rates in a specific cancer cell line, the newly synthesized thermoresponsive nanoparticles demonstrated a high tendency to aggregate above their thermal transition temperature (TTT) and an overall colloidal instability that hampered further endocytosis studies^{8,9}. The colloidal instability of PLGA-*b*-(PEGMA-*co*-PPGMA) and PLA-*b*-(DEGMA-*co*-OEGMA) nanoparticles, while not unexpected over prolonged time periods above the TTT, had not been reported before upon storage well below the TTT of the nanoparticles. Some ways to address this issue have been suggested in chapter 5; however, if not resolved, the colloidal instability might undermine any possibility of clinical applications of these nanocarriers. For this reason the aim of the experiments reported here remains unmet overall. Nevertheless, the study gave some information on aspects of endocytosis and C-PB uptake.

The first finding regarding the choice of cell viability tests for materials that interfere with endocytosis and/or are endocytosed confirms results shown in the literature. The choice of cell activity tests should be tailored to the material used, as nanomaterials can interfere with the test adopted and alter the concentration of the dye used as indicator of the viability of cells making difficult the interpretation of the results¹⁰. Many assays for cell viability rely on the endocytosis and exocytosis of viability markers¹¹⁻¹³. Results in this thesis show that this sort of activity test might overestimate the toxicity of some materials and should be used in conjunction with

other tests that do not rely on endocytosis/exocytosis. Also, viability tests that rely on enzymes to report cell activity interference should be used with caution when testing nanoparticles as some of these materials may interact with proteins and hence the enzymes of the assay compromising their activity¹⁴⁻¹⁶.

Some ground rules were also established on the inhibition of endocytosis of Htf (a CME marker) with CPZ. CPZ inhibition of Htf endocytosis was revealed to be time-dependent and its internalization was only transiently inhibited by CPZ. Furthermore, the inhibition reached a maximum that was cell- and time-dependent and after that timepoint the uptake of Htf recovered despite the presence of CPZ suggesting that Htf can internalize through an alternative way that is not CPZ sensitive. Also, the study revealed that the CPZ inhibition was dependent upon the passage number and ageing of cells. Many laboratories that work on endocytosis consider CPZ inhibition 'temperamental' and many cell lines 'resistant' to its inhibition. The results shown in this thesis attempt an interpretation of the reasons for the unpredictable ability of CPZ to inhibit internalization of Htf. This study reveals that two factors can affect the supposed 'resistance' to inhibition of Htf uptake with CPZ: the time of incubation, which should be tailored for the specific cell line, and the cell lines used for the study, which should be at low passage number in order to observe the inhibitory effect of CPZ. Previous literature has reported that dynamin expression is reduced in ageing cells and this could explain the reduced inhibitory action of CPZ in the same cell lines¹⁷.

Further steps on this first set of results would be to complement the flow cytometry experiments presented in this thesis with confocal microscopy studies to confirm the reduction in the internalization of the Htf and to add on any relevant information such as redistribution of the Htf-labeled endosomes in the presence of CPZ. Furthermore,

General Discussion and Future Perspectives

exploring the hypothesis of the involvement of TR2 in the recovery of the endocytosis of Htf in the presence of CPZ would aid the scientific relevance of these studies. Experiments should be done to evaluate the level of expression of TR2 in the cell lines used in this thesis to confirm the expression of the receptor as indirectly suggested by the current results and the literature. Easy methods to quantify the level of expression of the TR2 would be through Western blot and real time RT-PCR as these two methods allow for quantification of expression both at the protein and at the transcription level. These techniques could be complemented with immunofluorescence followed by flow cytometry and confocal microscopy for quantitative and qualitative evaluation of the expression of the two receptors¹⁸. To confirm that the recovery of inhibition of Htf is not an artifact produced by a non-specific inhibitor of endocytosis such as CPZ, the inhibition of Htf uptake should be explored by other means and a good starting point would be by siRNA silencing of the AP2 gene^{19,20}. These investigations would confirm that the inhibition observed with CPZ is mediated by the AP2 protein as reported in the literature. If this is the case, as expected, the uptake of Htf should recover after a temporary inhibition while the AP2 protein expression is knocked-down by the siRNA. As siRNA is a temporary way of silencing the expression of proteins, a good way to avoid misinterpretation in these experiments would involve a timepoint quantification of the levels of AP-2 protein and mRNA during the knockdown in relation to the levels of TR1 and 2. Moreover, it would be interesting to investigate the involvement of the caveolin or other lipid raft pathways that might be involved in the internalization of TR2. A first screening could easily be done with siRNAs against caveolin-1 and dynamin and with pharmacological inhibition of dynamin by Dynasore or the recent and more powerful version: Dingo-4a^{20,21}. As flotillins have been suggested to provide an alternative

General Discussion and Future Perspectives

endocytosis machinery when clathrin-mediated endocytosis is inhibited and they also localize in lipid rafts (as shown by Calzolari and coworkers which detected the TR2 in lipid rafts²²), they could constitute an alternative candidate for the endocytosis of Htf when cells are treated with CPZ^{22,23}. Flotillin involvement could be investigated with a flotillin-1 and 2 dominant negative mutants, such as Y160F and Y163F that perturbs the endocytosis through this pathway²⁴. Less immediate but fascinating experiments would involve the expression of a fluorescent or luminescent reporter for transferrin receptor 1 and 2 to further study the dynamics of expression upon inhibition of the CME pathway.

Data in this thesis and the literature suggest that dynamin might have a role in the loss of inhibition of CME in ageing cells. Hence, the quantification of dynamin levels in cells at low and high passage numbers would give interesting data to compare to the results with CPZ inhibition studies²⁵. Finally, to attempt an explanation of the reasons underlying different sensitivity to CPZ in different cell lines, the level of expression of calmodulin and MARCKS might be quantified^{26,27}.

Results on C-PB studies revealed that 50 nm C-PB access epithelial colon HCT116 and gastric MGLVA-1 cancer cells through a CPZ sensitive pathway which suggests the involvement of a CME or a macrophagic/macropinocytic uptake. The inhibition of endocytosis with CPZ did not appear to recover over time for these nanoparticles at the time points investigated suggesting a specific interaction of 50 nm C-PB with some membrane components (i.e. receptors) that are internalized by a CME or macropinocytic/phagocytic pathway. This suggests that some non-functionalized nanoparticles with properties similar to the carboxylated polystyrene nanoparticles, can also be internalized by a specific pathway implying that it might be possible to direct endocytosis towards one specific pathway without the use of targeting ligands.

General Discussion and Future Perspectives

To add information on this observed effect, 50 nm negatively charged nanoparticles other than C-PB might be a useful comparison. In addition, expanding the panel of cells for the studies, introducing other colon and gastric cancer cells as well as other fibroblasts, would add information confirming and defining the specificity of endocytosis of 50 nm C-PB which are negatively-charged, but still slightly hydrophobic. Finally, comparing the susceptibility to CPZ of 50 nm C-PB in the presence and in the absence of FBS could give useful information on the translation of these results in a more *in vivo* relevant environment.

Results on 100 nm C-PB showed that they are internalized by a CPZ sensitive pathway in 3T3 cells and by a MBCD sensitive pathway in MGLVA-1 cells. However, the internalization of 100 nm C-PB was only transiently inhibited by these endocytosis inhibitors and the uptake recovered over time suggesting a non specific mechanism of internalization for 100 nm C-PB. Consistent with this hypothesis, it was observed that, when the inhibitor of endocytosis was not effective in inhibiting the internalization of C-PB, it often caused an increase in the endocytosis of the nanoparticles. This finding mirrored the effects of CPZ in LacCer (a CIE marker) inhibition studies. When CPZ was used to verify that the drug was not interfering with CIE, a strong increment of CIE was observed that was increasing the internalization of LacCer up to 3 times more than the positive control. All together, these findings suggest a more dynamic and interconnected way of looking at endocytosis with activity of certain pathways being intensified and providing alternative machinery for endocytosis in response to the failure of other endocytosis mechanisms. This result suggests an additional complexity relating to the endocytosis of nanoparticles for drug delivery. However, it is possible to speculate that not all the possible pathways for the endocytosis of nanomaterials are interchangeable and a thorough investigation aimed to dissect all

General Discussion and Future Perspectives

the possible molecular mechanisms involved in the internalization of these nanoparticles when other pathways of uptake are inhibited could give more definitive answers to that hypothesis.

Microscopy studies with 50 and 100 nm C-PB showed that the nanoparticles triggered a rapid and efficient endocytosis. Also, for 100 nm C-PB in 3T3 and MGLVA-1 cells, an exocytic process was suggested which might explain how the cells reached a plateau in their fluorescence as a result of a maximal internalization of fluorescent C-PB. Although the data described in this thesis such as the size of the vesicles and the directionality of the movement point in the direction of exocytosis, further experiments should be run to confirm that the compartment that is observed trafficking to the membrane of cells with confocal microscopy is an exocytic vesicle. Labeling of the extracellular compartment with an exocytic marker (e.g. desmoyokin-Ahnak, d/A) as well as the use of exocytic inhibitors such as Exo I and II could confirm the nature of the compartment²⁸. Furthermore, literature reports that 3T3 cells can trigger exocytosis by a Ca^{2+} -mediated mechanism²⁹. Intercellular free Ca^{2+} is a known signalling pathway used by cells and it would be interesting to find out if the exocytic process triggered by 100 nm C-PB might be mediated by this way. Fluorescent indicators of free intracellular Ca^{2+} are available and a starting point might be monitoring their levels by flow cytometry or confocal microscopy²⁹. However, TEM studies, with a better resolution, would add information on the compartmentalization of the C-PB upon internalization as well as giving more details on the membrane trafficking observed in confocal microscopy.

Some considerations on the possibility for an *in vivo* translation of the results in this thesis are due at this point given that the aim of these studies was for a pharmaceutical application. The studies carried out in this thesis were intended as an

General Discussion and Future Perspectives

in vitro preliminary screening of the endocytosis of thermoresponsive nanomaterials. As such they were limited by the absence of FBS in the experimental settings, a 3D organization that is displayed in tissues, the cellular heterogeneity that is present in a whole organ, the absence of immune cells and blood stream. Furthermore, cells in an *in vivo* environment are 100% confluent and hence the expression of receptors and proteins on the plasma membrane may be very different to those in culture³⁰. Finally, the cells generally employed in *in vitro* studies are immortalized which means that they have undergone a spontaneous or induced process of genetic modification to survive in an artificial environment and that often makes them to behave in a less *in vivo* relevant way.

A first step to improve on these limitations could involve the investigation of endocytosis in primary cells. Furthermore, 3D studies might help to translate the present results towards an experimental setting more relevant to *in vivo* studies. Indeed, 3D culture might give some more information on how the tridimensional organization of cells affects endocytosis when cells are simultaneously involved in signalling processes, that share the same machinery of endocytic pathways, and if the signalling activity can cause switching of the internalization pathways of nanomaterials. Signalling in fact is believed to be reduced to a minimum in 2D monocultures where the architectural complexity of *in vivo* studies is less represented. A further advancement towards more *in vivo* relevant experiments might be through the use of co-cultures of epithelial and fibroblastic cells that *in vivo* cohabit and interact in the same tissue. Given that fibroblasts have already been investigated in the present studies, co-cultures of 3T3 and HCT116 or 3T3 and MGLVA-1 would represent an easy choice. However, it is important to stress that much of the research field of endocytosis in mammalian cells at the moment is limited to more or less

General Discussion and Future Perspectives

sophisticated 2D *in vitro* studies. The reason for such limitations is that 3D culture approaches are challenged by the level of perfusion of the more internal compartments of the 3D scaffolds. Another important limitation is provided by the level of detection of optical fluorescence techniques currently available and the level of penetration in thick specimens for the detection of fluorophores. Two-photon or multi-photon microscopy is one of the most promising approaches for *in vivo* endocytosis research available at the moment. However, studies of endocytosis in functioning organs with a spatial resolution at the cellular and subcellular level in mammals, is limited by the level of perfusion of the organs intended for the study of endocytosis and kidney and liver, with a high perfusion rate and, hence, more exposed than other organs to blood loaded markers of endocytosis, are the target of choice of these investigations^{31,32}. The limit of detection and tissue penetration with fluorophores and microscopic techniques could be solved in the near future by the optimization of research materials tagged with detection labels other than organic fluorophores. Gold nanorods, for example, with a plasmon band resonance in the so called 'water window' (800-1200 nm) are being evaluated for biological purposes³³. Their absorption wavelength is useful as water and many other body components do not absorb at those wavelengths enhancing the potential of penetration of light. Imaging by these means is claimed to give a spatial resolution of 100 nm in two photon luminescence microscopy and might well constitute a first step forward to the identification of subcellular endocytic processes in a tridimensional organization of cells³⁴. However, their irradiation also produces heat and this might potentially alter the tissue physiology and a careful evaluation of the level of interference that this phenomenon might cause is also a key question to answer.

A last challenge can be recognized in the study of the internalization of nanomaterials and translation to an *in vivo* situation. Many pathologies are associated with an altered expression of endocytic proteins. Pathologic environments can produce hypoxic niches and oxidative stress that can trigger autophagy and alter transiently the expression of membrane receptors and endocytic proteins, changing the way cells respond to endocytosis of nanoparticles³⁵. Furthermore, these alterations have been detected as a permanent hallmark in many pathological conditions. It is known in the literature that caveolin-1 overexpression or knockdown is associated with different form of cancers and many drug-resistant pathologies rely on a compromised endocytosis. It was shown that EGF-mediated gefitinib resistance in cancer is mediated by a compromised CME of the EGF receptor upon internalization that fails to be directed to degradation in a lysosome compartment³⁶. Other examples of known pathologies with an altered expression of endocytic proteins and an altered endocytosis are diabetes, Alzheimer's disease and Down's syndrome³⁷. These aspects of endocytosis make the translation from *in vitro* studies to the clinic probably more challenging but also open to new perspectives and applications. It seems possible from results in this thesis and the literature that when one pathway is compromised other pathways can be activated and the exploitation of this effect in pathologic situations for drug delivery purposes could be worth some investigation.

References

- 1 Yeo, Y. *Nanoparticulate Drug Delivery : Systems Strategies, Technologies, and Applications*. (John Wiley & Sons, 2013).
- 2 Koyamatsu, Y. *et al.* pH-responsive release of proteins from biocompatible and biodegradable reverse polymer micelles. *Journal of Controlled Release* **173**, 89-95 (2014).
- 3 Kempe, K., Ng, S. L., Gunawan, S. T., Noi, K. F. & Caruso, F. Intracellularly Degradable Hydrogen-Bonded Polymer Capsules. *Advanced Functional Materials*, n/a-n/a (2014).

General Discussion and Future Perspectives

- 4 Sakai, N., Jin, M., Sato, S.-i., Satoh, T. & Kakuchi, T. Synthesis of water-soluble polyisocyanates with the oligo(ethylene glycol) side-chain as new thermoresponsive polymers. *Polymer Chemistry* **5**, 1057-1062 (2014).
- 5 Themistou, E., Battaglia, G. & Armes, S. P. Facile synthesis of thiol-functionalized amphiphilic polylactide-methacrylic diblock copolymers. *Polymer Chemistry* **5**, 1405-1417 (2014).
- 6 Chan, N., An, S. Y., Yee, N. & Oh, J. K. Dual Redox and Thermoresponsive Double Hydrophilic Block Copolymers with Tunable Thermoresponsive Properties and Self-Assembly Behavior. *Macromol. Rapid Commun.* **35**, 752-757 (2014).
- 7 Khan, A. R. *et al.* Camptothecin prodrug block copolymer micelles with high drug loading and target specificity. *Polymer Chemistry* **5**, 5320-5329 (2014).
- 8 Abulateefeh, S. R. *et al.* Facile synthesis of responsive nanoparticles with reversible, tunable and rapid thermal transitions from biocompatible constituents. *Chemical Communications*, 6068-6070 (2009).
- 9 Abulateefeh, S. R. *et al.* Enhanced uptake of nanoparticle drug carriers via a thermoresponsive shell enhances cytotoxicity in a cancer cell line. *Biomaterials Science* **1**, 434-442 (2013).
- 10 Fisichella, M. *et al.* Mesoporous silica nanoparticles enhance MTT formazan exocytosis in HeLa cells and astrocytes. *Toxicology in Vitro* **23**, 697-703 (2009).
- 11 Vistica, D. T. *et al.* Tetrazolium-based assays for cellular viability: a critical examination of selected parameters affecting formazan production. *Cancer Res* **51**, 2515-2520 (1991).
- 12 Liu, Y. & Schubert, D. Cytotoxic Amyloid Peptides Inhibit Cellular 3-(4,5-Dimethylthiazol-2-yl)-2,5-Diphenyltetrazolium Bromide (MTT) Reduction by Enhancing MTT Formazan Exocytosis. *Journal of Neurochemistry* **69**, 2285-2293 (1997).
- 13 Abe, K. & Saito, H. Amyloid beta protein inhibits cellular MTT reduction not by suppression of mitochondrial succinate dehydrogenase but by acceleration of MTT formazan exocytosis in cultured rat cortical astrocytes. *Neurosci Res* **31**, 295-305 (1998).
- 14 Holder, A. L., Goth-Goldstein, R., Lucas, D. & Koshland, C. P. Particle-induced artifacts in the MTT and LDH viability assays. *Chem Res Toxicol* **25**, 1885-1892 (2012).
- 15 Monteiro-Riviere, N. A., Inman, A. O. & Zhang, L. W. Limitations and relative utility of screening assays to assess engineered nanoparticle toxicity in a human cell line. *Toxicol Appl Pharmacol* **234**, 222-235 (2009).
- 16 Saptarshi, S., Duschl, A. & Lopata, A. Interaction of nanoparticles with proteins: relation to bio-reactivity of the nanoparticle. *Journal of Nanobiotechnology* **11**, 26 (2013).
- 17 Linskens, M. H. *et al.* Cataloging altered gene expression in young and senescent cells using enhanced differential display. *Nucleic Acids Res* **23**, 3244-3251 (1995).
- 18 Calzolari, A. *et al.* Transferrin receptor 2 is frequently expressed in human cancer cell lines. *Blood Cells, Molecules, and Diseases* **39**, 82-91 (2007).
- 19 Motley, A., Bright, N. A., Seaman, M. N. & Robinson, M. S. Clathrin-mediated endocytosis in AP-2-depleted cells. *Journal of Cell Biology* **162**, 909-918 (2003).
- 20 Al Soraj, M. *et al.* siRNA and pharmacological inhibition of endocytic pathways to characterize the differential role of macropinocytosis and the actin cytoskeleton on cellular uptake of dextran and cationic cell penetrating peptides octaarginine (R8) and HIV-Tat. *Journal of Controlled Release* **161**, 132-141 (2012).
- 21 McCluskey, A. *et al.* Building a better dynasore: the dyngo compounds potently inhibit dynamin and endocytosis. *Traffic* **14**, 1272-1289 (2013).

General Discussion and Future Perspectives

- 22 Calzolari, A. *et al.* TfR2 localizes in lipid raft domains and is released in exosomes to activate signal transduction along the MAPK pathway. *J Cell Sci* **119**, 4486-4498 (2006).
- 23 Otto, G. P. & Nichols, B. J. The roles of flotillin microdomains--endocytosis and beyond. *J Cell Sci* **124**, 3933-3940 (2011).
- 24 Riento, K., Frick, M., Schafer, I. & Nichols, B. J. Endocytosis of flotillin-1 and flotillin-2 is regulated by Fyn kinase. *Journal of Cell Science* **122**, 912-918 (2009).
- 25 Hinshaw, J. in *Annual Reviews Collection* (Bethesda (MD), 2002).
- 26 Bickeboller, M. *et al.* Functional characterization of the tumor-suppressor MARCKS in colorectal cancer and its association with survival. *Oncogene* **0** (2014).
- 27 Damke, H., Baba, T., van der Bliek, A. M. & Schmid, S. L. Clathrin-independent pinocytosis is induced in cells overexpressing a temperature-sensitive mutant of dynamin. *The Journal of Cell Biology* **131**, 69-80 (1995).
- 28 Cocucci, E., Racchetti, G., Podini, P., Rupnik, M. & Meldolesi, J. Enlargeosome, an exocytic vesicle resistant to nonionic detergents, undergoes endocytosis via a nonacidic route. *Mol Biol Cell* **15**, 5356-5368 (2004).
- 29 Olofsson, M. H., Havelka, A. M., Brnjic, S., Shoshan, M. C. & Linder, S. Charting calcium-regulated apoptosis pathways using chemical biology: role of calmodulin kinase II. *BMC Chem Biol* **8**, 2 (2008).
- 30 Wang, J., Chen, G. & Pantopoulos, K. Inhibition of transferrin receptor 1 transcription by a cell density response element. *Biochem J* **392**, 383-388 (2005).
- 31 Sandoval, R. M. & Molitoris, B. A. Quantifying endocytosis in vivo using intravital two-photon microscopy. *Methods Mol Biol* **440**, 389-402 (2008).
- 32 Gopalakrishnan, S. & Harris, E. N. In vivo liver endocytosis followed by purification of liver cells by liver perfusion. *J Vis Exp* (2011).
- 33 Alkilany, A. M. & Murphy, C. J. Toxicity and cellular uptake of gold nanoparticles: what we have learned so far? *J Nanopart Res* **12**, 2313-2333 (2010).
- 34 Murphy, C. J. *et al.* Gold nanoparticles in biology: beyond toxicity to cellular imaging. *Acc Chem Res* **41**, 1721-1730 (2008).
- 35 Jasmin, J.-F., Frank, P. G. & Lisanti, M. P. in *Advances in experimental medicine and biology* (ed Landes Bioscience) (Springer, New York, USA, 2012).
- 36 Verrite, E. G. *Cancer Etiology, Diagnosis and Treatments : Drug Resistant Neoplasms*. (Nova Science Publishers, Inc., 2009).
- 37 Wu, F. & Yao, P. J. Clathrin-mediated endocytosis and Alzheimer's disease: An update. *Ageing Research Reviews* **8**, 147-149 (2009).

7-Appendix I

ICOS 3D prediction software results for *human cav-1*. The first table shows the 2D and 3D rearrangements of adjacent aa and their exposure to the solvent. The second table shows the analysis for their exposure to the solvent only. The regions highlighted in yellow refer to the epitope of the mAb clone 2297. The 'All.con' bottom row gives a final score for all the parameter taken into account by the analysis.

DT.Q5	30330033033300300333003003300303030004
DT.con	30330033013300300133003003300303030003
GG.Q2	111111111110111011111111111011110000
GG.Q3	22221122122202220222122212200212120000
GG.Q5	43442244244413432243244324311324231000
GG.con	43442244244403430343244324310324230000
MST.Q2	111111111111111111111111111111111111
MST.Q3	11111111111111111111112221111111111111
MST.Q5	11110111111111111111112231111111111111
MST.con	2222222222222222222222333222222222222
RCH.Q2	1011001101110110011101101100101000000
RCH.Q3	1111111101110111011111110111011110000
RCH.Q5	33332233133313331333233313311323331100
RCH.con	31331133033303310333133303300313110000
RNG.Q2	1111111111101110111111111100111110000
RNG.Q3	21221122122201210122122112110212110000
RNG.Q5	32332233233312321233233323221323221100
RNG.con	32332233233302320233233323210323220000
SA.Q2	00001100100010000000100010001010101111
SA.Q3	01001100100010001000100010012010112222
SA.Q5	01003301300030013000300020033030313444
SA.con	00003300300030001000300020013030303444
All.con	32331133133302321333133313310323220000

8-Appendix II

ICOS 3D prediction software results for *murine cav-1*. The first table shows the analysis for the 2D and 3D rearrangements of adjacent aa and their exposure to the solvent. The second table takes into consideration their exposure to the solvent only. The regions highlighted in yellow refer to the epitope of the mAb clone 2297. The 'All.con' bottom row gives a final score for all the parameters taken into account by the analysis.

DT.Q5	30330033003303330033003003300303030004
DT.con	30330033003301330033003003300303030003
GG.Q2	1111111111111111111111111111111100111110000
GG.Q3	21221122122212221222122212200212120000
GG.Q5	42442244244423442343234324311424231100
GG.con	42442244244423442343234324300424230000
MST.Q2	111
MST.Q3	11111111111111111111111122111111111111111
MST.Q5	11110111111011111110223111111111111111111
MST.con	222222222222222222222233222222222222222
RCH.Q2	10110011001101110111011101100101010000
RCH.Q3	11111111011111211111011101100111110000
RCH.Q5	31332233233323333333133333300333331100
RCH.con	30331133013313331333033303300313130000
RNG.Q2	111111111111111111111111111111110111111000
RNG.Q3	21221122122212221222122112110212111000
RNG.Q5	32332233233323332333233223221323222110
RNG.con	32332233233323332333233223220323222000
SA.Q2	01001100100010000000100010011010101111
SA.Q3	01001100100010001000200010021010101222
SA.Q5	03003200300030003000300020133030203344
SA.con	03003200300030001000300020033030203344
All.con	31331133123313331333133313311323231001

9-Appendix III

ICOS 3D prediction software results for *human* CHC α . The region highlighted in yellow refers to the epitope of the mAb clone X22. The 'All.con' bottom row gives a final score for all the parameters taken into account by the analysis. The first table gives the results for the rearrangements of the aa in 2D and 3D, their point of contact and their exposure to the solvent. The second table gives the score for their exposure to the solvent only.

0 - 69	0	1	2	3	4	5	6																																																															
seq	A	Q	I	L	P	I	R	F	Q	E	H	L	Q	L	Q	N	L	G	I	N	P	A	N	I	G	F	S	T	L	T	M	E	S	D	K	F	I	C	I	R	E	K	V	G	E	Q	A	Q	V	V	I	I	D	M	N	D	P	S	N	P	I	R	R	P	I	S	A	D	S	A
cCN.Q2	0001111111110100101000110101111110111111000001111111000011110101111																																																																					
cCN.Q3	0012221212221211120001212112221211222221100111222221011121111212222																																																																					
cCN.Q5	1133443434342311313111341433444343344443412001334444441113133333314444																																																																					
cCN.con	0013443434341300303000340413444341344443401000334444440001033331304444																																																																					
dCN.Q2	001111111110100101000110100111110111111000001111111000010110101111																																																																					
dCN.Q3	001222121222121121201012121121211222221100111222221011121121212222																																																																					
dCN.Q5	11134434344413113131113131143411134444311111334444441111132131314444																																																																					
dCN.con	002344343444030030300023030043423034444430000033444444000031230304444																																																																					
DT.Q2	1111111111111101011111111111011111110001000111111111111111110111																																																																					
DT.Q3	11																																																																					
DT.Q5	4333333333333330304343333433333343333330004003333333303333333340433																																																																					
DT.con	3333333333333330303333333333313333333000400133333323333333330333																																																																					
GG.Q2	00011101111010010100011010111110011111000000111111000010000101011																																																																					
GG.Q3	00022212102202001020000201002120001222200000012222200000010201012																																																																					
GG.Q5	0013342421331311203110131211324111234343211001124444341101111121313123																																																																					
GG.con	000334142133030020300013020132411013434320000024444340000010010303023																																																																					
MST.Q2	0111111111111111110111																																																																					
MST.Q3	0111111111111111110111																																																																					
MST.Q5	011111111111111111120111																																																																					
MST.con	02222222222222222202223																																																																					
RCH.Q2	000111101110100101000110101111100111111000000111111000011110101111																																																																					
RCH.Q3	000222212221222101010121222222222222221010001122222001122212202222																																																																					
RCH.Q5	0014444344443443430003314444444444444431300033344443003333333404444																																																																					
RCH.con	0004444414441322313000330424444422444444101000133444430011133332404444																																																																					
RNG.Q2	000111111110100101000010100111110011111000000111111000010000101011																																																																					
RNG.Q3	0001221211101001010001101002121100222210000001222211000010000101012																																																																					
RNG.Q5	00123323222121120201022121232322113333321100122333221111121111212123																																																																					
RNG.con	0002332322202002020001202003222003333320000023333220000020000202023																																																																					
SA.Q2	1110001010001011010110010100001011000000111111000000111101111010000																																																																					
SA.Q3	222000101100202212022102021010122100001121222110000002112211111020110																																																																					
SA.Q5	4441013031113034141344313143030344310001233444230000103344333323131300																																																																					
SA.con	4440003030003034040344103041010324300000133444230000003334313323030100																																																																					
All.con	0013332323331311212010231312333221233333201000123333331011121221313233																																																																					
70 - 139	0	1	2	3	4	5	6																																																															
seq	I	M	N	P	A	S	K	V	I	A	L	K	A	G	K	T	L	Q	I	F	N	I	E	M	K	S	K	M	K	A	H	T	M	T	D	D	V	T	F	W	K	W	I	S	L	N	T	V	A	L	V	T	D	N	A	V	H	W	S	M	E	G	E	S	Q	P	V	K	M	
cCN.Q2	111100111111011111110000111110100111111100011111111111111000001111																																																																					
cCN.Q3	22221112222111122221201101211212111222222111222222112222212100112122																																																																					
cCN.Q5	444421344443313243443311112333423132444444322344444334444434100013334																																																																					
cCN.con	44441034444330324344330000233341301244444411134444433444443400003334																																																																					

RCH.con	244444444403302443443210434444443144444442444444242300033324444412330
RNG.Q2	01111111010110111111100011111111001010011011111101010001111111110010
RNG.Q3	1122122101011012212210001112211220011100110121111010100012112211210010
RNG.Q5	1233233212022123323321102223322332122211221232122120211123223322321221
RNG.con	0233233202022023323320002223322330021200220232222020200023223322320020
SA.Q2	1000000010100110000001110010000001100001001000100101011100110010011101
SA.Q3	1000100121200110010002110110010001211112101000100211012210110011012101
SA.Q5	2000100231410330021014330231031003312143113001201433134310230032034313
SA.con	2000000130400330010004330130010003301013003000200413034300230031034303
All.con	1333333212033013323331103223322331122221331333233131310033123323311131
840 - 909	0 1 2 3 4 5 6
seq	TDELVAEVEKRNRLKLLLPWLEARIHEGCCEEPATHNALAKIYIDSNNNPERFLRENPYYDSRVVGKYCEK
cCN.Q2	1001100100001101111110001001000101100110111000001001100101100011101100
cCN.Q3	2002101200101212210221011000101111211221222010002001200102211112112200
cCN.Q5	3113302310212313331331022001101333332343333110113113311313313233213311
cCN.con	3003301300102303331330012001000313311341333000003003300303301133203300
dCN.Q2	1001100100000101110110001000000101100110111000001001100101100011001100
dCN.Q3	2002101200101212210220011000100112211221222010002001200102221112102201
dCN.Q5	3113301310111313321331112001111113311431333111113113311313311223113311
dCN.con	3003300300000303320330002000000203300430333000003003300303310123003300
DT.Q2	11111101111111111111111110011111111111111101011011111111111111111111
DT.Q3	11
DT.Q5	33333303333333333333330333400333333333333333303033033334333333333333
DT.con	33333303333333333333332333300333333333333333303033033333333333333333
GG.Q2	1001101110001111111111110000001111111111000001011100101100011101100
GG.Q3	2002211210102212221221112000000102221221222000002012210201201022202200
GG.Q5	4114422421212424432342233112111213332442434110113124421202311124313311
GG.con	4004412420103424432342233000000113332442434000003024410302300034303300
MST.Q2	10111011111111111011111111101111111111111111111101111110111111111111
MST.Q3	101110111111111110111111111011111111211111111111111101111111211211
MST.Q5	101110111111111110111111111011111111211111111101110110111111211211
MST.con	20222022222222220222222220222222232222222202222220222220222222322322
RCH.Q2	100110010000110111111000100000011111011111000001001100101110011101100
RCH.Q3	200110121011121222221111000101222222222211100201220010222122112211
RCH.Q5	301330333033334444443433300030333444444443413113033310303443334333333
RCH.con	3003301310113314444431113000101334442444443101003013300303442134313311
RNG.Q2	101111111000111111111110000000111111111000001011100101100011001100
RNG.Q3	101221121010121121122111100000002211221211000001011210101100011001100
RNG.Q5	2123322321112322322332222111111112322332322110112123321202211122112211
RNG.con	202332232000232232233222200000003322332322000002023310202200022002200
SA.Q2	011001101111001000100010011111110001100100011110110011010011100110011

SA.Q3	0220021012121010011002210221121110011001000211220210022121011110120022
SA.Q5	1330133033332030023103321444343330023003010334431331034142133310131143
SA.con	0330033033331030013002310443343310023003000333430330034041033300230043
All.con	3013301310112313331331122000101223322332333110003013310203311123213311
910 - 979	0 1 2 3 4 5 6
seq	RDPHLACVAYERGQCDLELINVCNENSLFKSLSRYLVRKDPBLWGSVLLSNPYRRPLIDQVVQTALSE
cCN.Q2	0111111110010100011011101110011011100000110011000001100110111011100
cCN.Q3	112222222011010111202221212211221121011010220122000101101220122122200
cCN.Q5	234444443113131113313333443321331233011131331233000013311331343233301
cCN.con	134444443003030003303331433310330233000010330133000003300330343133300
dCN.Q2	11111111100001000110101011110011011100000110011000001100110111011100
dCN.Q3	1122222220010100012021212221122112101101022012200001101220122122200
dCN.Q5	1111444431211311133131313311331333011121331133001113211331343133311
dCN.con	22334444300003000330303033330330333000010330033000003200330343033300
DT.Q2	10111111111011111111111111111111111100111111111111111111111111111111
DT.Q3	11
DT.Q5	3333333333304334
DT.con	31333333333033
GG.Q2	01001111111000100011010101111111111110000101111110000110011111111100
GG.Q3	000022222010010002200010222112222200001022112200001100221222122200
GG.Q5	111143344312112111341212133442244334411121442344100102211442344233311
GG.con	010043344311002000340202033442244334400002044234400002200442344233300
MST.Q2	11111111101111111111111111111111110111111011111111111111111111111111
MST.Q3	1111111121111110111111112111121110111011011111111101110111112111
MST.Q5	111111121011111011111112111121111011111101111111111110111112111
MST.con	22222223202222122222223222232222022212202222222221222122223222
RCH.Q2	1111111110000100011011011110111110000011001100001100110111011100
RCH.Q3	2222222222101211220222222222222201101022112200010120122122222220
RCH.Q5	34444444433031133314444444434434430331303333300030330344444444430
RCH.con	34444444422103101330444244442443443011010331133000103301441444244420
RNG.Q2	000011111100010001101010111111111000001111110000001011111111100
RNG.Q3	00001112211000100011010101112111211210000022112100000000221122112100
RNG.Q5	111122233211121112212121222322322321111133223210010111133233223211
RNG.con	0000223332000200022020222322322320000033223200000101332233223200
SA.Q2	100000000111101110010101000011000000111101001100111010011001000100011
SA.Q3	11110000021121121021111010011001000211112001100222121121002100100022
SA.Q5	3343001001333413331031313100133102101433323003201344332243003100310134
SA.con	31110000033340333003030300033001000433313003200344131143003000300034
All.con	1222333333111021113303131333322332333011010331233000102201331333233310
980 - 1049	0 1 2 3 4 5 6
seq	TQDPPEEVSVTVKAFMTADLPNELIELLEKIVLDNSVSEHRNLQNLILLITAIKADRTRVMEYINRLDNYD

GG.Q2	0011111110100100100110110000010011111111100000101111111111100100110110
GG.Q3	0122122220100100211221220000020122122122101000002121222221200201211220
GG.Q5	1244234422012113214423411101312442442342121111142324434432311312422441
GG.con	0144234402002003104413400000301442442342010001042324434432300301421440
MST.Q2	011101111111111111011011110110111111111111111111111101110111
MST.Q3	01210111121111111110120111110111011111111111111111111212111101111111
MST.Q5	01210111121111111110120111110111011011111111111111111212111101111111
MST.con	0232022223222222222023022222022202202222222222222222323222202220222
RCH.Q2	0011011101001001001101100000100110110010000011111111111100100100110
RCH.Q3	01221222220020021021011001001012102211110110021222222222200100110110
RCH.Q5	033344443303301331331331030130333133333303301334444444444301301331330
RCH.con	013314442300300310330330010030133033113101100334444444444300300310330
RNG.Q2	011111110100100111111110000101111111111100001111111110100101111110
RNG.Q3	012211210100100101221221000001221221121111000011112212220100101211210
RNG.Q5	12332332120121121233233212011123323322322211112223323331201212322321
RNG.con	023323320200200212332332000010233233223222000022223323330200202322320
SA.Q2	110010001011010100100100111110110010010011111010000000001011011001001
SA.Q3	2100200020211210120021022121121002002101211221101010000002021021022002
SA.Q5	3300311031431431330032034343133013103303433433301030000103143133033014
SA.con	3300300030430430130031034343033003003103433431300010000003043033023004
All.con	0133133313002003113302300100201331331231111002133323333331300301311330
1190 - 1259	0 1 2 3 4 5 6
seq	GPNNAHIQQVGDRCYDEKMYDAAKLLYNNVSNFGRLASTLVHIGEYQAAVDGARKANSTRTWKEVCFACV
cCN.Q2	0011101001100110000101111110010010111011101001001101100100101100110111
cCN.Q3	1122201002101210001102212221120021122122212002002102211101102211221121
cCN.Q5	1343313113201320001314423431230131144344323013114314311301313321332233
cCN.con	0143303003200320000304423430130030244144313003004304300300303310331233
dCN.Q2	0111101001000100000101111110010010011011101001001101100100101100110111
dCN.Q3	0121201002101210001202211221110021122122212002002102201101202210221121
dCN.Q5	1113313113202320111313332331131131144144313113113313311311313311331232
dCN.con	0233303003101310000303332330030030044044303003003303300300303300330232
DT.Q2	0111111101011111100111111111111111111111111111111011111111011111111111
DT.Q3	11
DT.Q5	033330330303333440333333333333433333333333333303330333340333333333333
DT.con	03333233030333333013333333333333333333333333333333330333233333033333333333
GG.Q2	00101010011011100001011111100100101111111111111111011110100101111111111
GG.Q3	000010201221222000020222220120020122122212112112212210200102211221222
GG.Q5	111121312432342101131333444223113124424442422424423421311213422432333
GG.con	0010203014313430000303334440130030244244424224224413420300203422432333
MST.Q2	11111101111011011111111111
MST.Q3	11112110122101111111112111111111111111111111111111121112111110111111221

cCN.Q3	111111012101201211211202201200102212112222211100201220221000110122022
cCN.Q5	32122302310333013213333133113101033132234434411201311331331021331243134
cCN.con	310113013003300310313303300300033031134434400100300330330000330143034
dCN.Q2	1000010010011001001011011001000011010011111100000100110110000110011011
dCN.Q3	1011110121012002112111022011001022121122212211100201220221000110122022
dCN.Q5	3111130131133013113113133113101133131134434311111311331331011331143134
dCN.con	300003003003300300302303300300003303003443430000300330330000330043034
DT.Q2	11111110111011111111111111111101111111111111111001111111111111111111
DT.Q3	11111111111111111111111111111121111111111111111111111111111111111111
DT.Q5	33333130333033333333333333333404333333333333330333333333343333333333
DT.con	333332303330333333333333333330433333333333330133333333333333333333
GG.Q2	1111110111011001001011011011000011011111111110000100111111000110111111
GG.Q3	211112112112200200101202211200002212212222211000201221221000120122122
GG.Q5	42212322422341131131231442241111332432433344221131144243211231244234
GG.con	4222231242134003003023044124000033143243334421000300442432000230244234
MST.Q2	111111011101111111111111101101011111111111111110111011111110111011
MST.Q3	111111011101111111111112011111011111122111111110121011111110121012
MST.Q5	1111110111111111111111201111101111112211111110121011111110121012
MST.con	2222202220222222222223022022022222332222222023202222220232023
RCH.Q2	10000100100110011111101100100001101101111111000100110110000110011011
RCH.Q3	22111101210220022222112111001022222222211100201220221021120122122
RCH.Q5	333333033303300334444333313300303333344444433301303331333033330344344
RCH.con	321113013103300334444313301300103323324444433100301330331021330144144
RNG.Q2	111111111111001001001111110000111111111111010010111111000110111111
RNG.Q3	211112112112200100100112211200001121122212110100101221221000110122122
RNG.Q5	222232232233112112112233223111022232233323321211212332332111221233233
RNG.con	322232232233002002002233223000022232233323320200202332332000220233233
SA.Q2	0101001101100110110100100110110100100100000011011011001001101001100100
SA.Q3	0112102101200220120110200210221201101100010011121021002001212102100200
SA.Q5	0333313303300431431321300330443301302300020133343133003103443113300310
SA.con	0313103303300430330310300330441300301300010033143033003003413003300300
All.con	312123013113300311312313311300103313223333321100301331331011230133133
1540 - 1609	0 1 2 3 4 5 6
seq	SESKDTELAEE LLQWFLQEEKRECFGACLF TCDLLRPDVVLETAWRHNIMDFAMPYFIQVMKEYLTKVD
cCN.Q2	10100001100110111000000111111111011010111011111010011111111110110010
cCN.Q3	1110010121122012101001122222222122121121112211021122222211210210120
cCN.Q5	21310203321331343010124444444444243243332333331334444443323320330230
cCN.con	2030010331033034300001144444444441431413321333330311444443323320330130
dCN.Q2	00000001100110111000000111111111011010111011010011111101110110010
dCN.Q3	1110010121122012100001122222222122121222112211021122222211210210110
dCN.Q5	1111111331133133301111144444444441431413331233231311444443313221331131

GG.Q3	12111111110000000000100000222201101110101111101111111100120100
GG.Q5	24222222221111101012101113332122121211112212121212222211221200
GG.con	2411121112000000000120000033331221222120222212222222200230100
MST.Q2	11
MST.Q3	111111111111111111111111111111111122111111111121211111121111222211
MST.Q5	111111111111111111111111111111112111111111121211111121111222121
MST.con	22222222222222222222222222222222332222222223232222223222233322
RCH.Q2	01000000000000000011
RCH.Q3	011000000000000000022200
RCH.Q5	131111011111000000333440
RCH.con	030000000000000000033444444444444444444444444444444444444444311
RNG.Q2	1111111111111000000100000111101011010101111111111111100111000
RNG.Q3	12111111111110000001000001111110111101010111111111111100111000
RNG.Q5	232222222222111000121111122222222221212222222222222211222110
RNG.con	232222222222000000200000222120221202022222222222222200222000
SA.Q2	10111111111111111101111000000000000000000000000000000000011
SA.Q3	2022212222222222221112211000010000101011000001000001011000022
SA.Q5	30333333434444444443334343100110011111311101011110111131011144
SA.con	3033333343444444444313433100000000000100000000000010000044
All.con	1311010111001000000231112233332333332323333333333333322333211

seq	LLDQGQLNKYESLELCRFVLQQGRKQLLEKWLKEDKLECSSEELGDLVKSVDPPTLALSIVYLRANVFNKVIQ						
SA.Q2	0011010111000000100001111100110011110100110010011000100000001010011001						
SA.Q3	0022220121100100110012211200110022221101120020012110100010012021121001						
SA.Q5	0143331332100300200034422300331044431411330131034231300020023142233003						
SA.con	0043230332000100200014422300330044430300330030034110300010013041133003						
All.con	4300103101344244134420011044113400003033104303410223144424420302201441						
490 - 559	0	1	2	3	4	5	6
seq	CFAETGQVQKIVLYAKKVGYPDWIFLLRNVMRISPDQGGQFAQMLVQDEEPLADITQIVDVFMEYNLIQ						
SA.Q2	0001111011001001111011000000100010001100100110011110101001001000101001						
SA.Q3	0002111021012002112112101100110011102101200110122221101011001001212111						
SA.Q5	0003333133013104334134311300330032114301300211144444313033003101424223						
SA.con	0003333033003004334034100100310031004300300220044441303013003000414113						
All.con	4440111301430340110310233244124412330143044113300002131421441343020221						
560 - 629	0	1	2	3	4	5	6
seq	QCTAFLLDALKNNRPSEGPLQTRLLEMNLMHAPQVADAILGNQMFTHYDRAHIAQLCEKAGLLQRALEHF						
SA.Q2	000100010011111111000100000011111001000111000001011001101111001101100						
SA.Q3	1002000200221222221000100100111112002100212101111112002102212012101200						
SA.Q5	3003001310433344433001300300133343013101334213323133003203433113203411						
SA.con	1003000300433344433000300100033333003000334101113033003203433003203400						
All.con	2440443034001000001443144244311100430343010232221310440140010330141033						
630 - 699	0	1	2	3	4	5	6
seq	TDLYDIKRAVVHHTHLLNPEWLVNYFGSLSVEDSLECLRAMLSANIRQLQICVQVASKYHEQLSTQSLIE						
SA.Q2	1101101000010110111000100110111100100110010000100100010001001100011001						
SA.Q3	2211101100010110212001200121212110200111021111100110020011002201011002						
SA.Q5	4413303200031431334001310341334321310330033313300300030023114313133003						
SA.con	4403303100030330334000300340334310300330031101300300030013004301033003						
All.con	0031141244413013010443034103010123034113402232144134404421330032311440						
700 - 769	0	1	2	3	4	5	6
seq	LFESFKSFEGLFYFLGSIVNFSQDPPDVHFYKIQAAACKTGQIKEVERICRESNCYDPERVKNFLKEAKLTD						
SA.Q2	0011010010000001100101111100010010001111011001001111001011001111011						
SA.Q3	1022121120001001101211211201010010002121121011001222011121012001222121						
SA.Q5	1034141230012103312424433300130030004243133033003444123143033103434133						
SA.con	0034040130001003301413433300030030004243033013003444013043033003434033						
All.con	3400303204432341132020011043314414440101301421441000321301410341000301						
770 - 839	0	1	2	3	4	5	6
seq	QLPLIIVCDRFDVHDLVLYLYRNNLQKYIEIYVQKVNPSRLPVVIGLLDVCSEDEVKLNLIIVVRGQF						
SA.Q2	0100000001010011000000111001000000110000100100010010101110011001001110						
SA.Q3	1100010012120011001000211011001000121111210100010021101221011001101210						
SA.Q5	3200010023141033002101433023103100331214311300020143313431023003203431						
SA.con	1200000013040033001000433013001000330101300300020041303430023003103430						
All.con	2144434420303411442343011421342344103232033144414302131003411441241013						

840 - 909	0	1	2	3	4	5	6
seq	STDELVAEVEKRNRLKLLLPWLEARIHEGCEEPATHNALAKIYIDSNNNPERFLRENPYYDSRVVGKYCE						
SA.Q2	101100110111100100010001001111110001100100011111011001101001110011001						
SA.Q3	1022002101212101001100221022112111001100100021122021002212101111012002						
SA.Q5	31330133033320300231033214443433002300301033443133103414213331013114						
SA.con	3033003303333103001300231044334331002300300033343033003404103330023004						
All.con	1300430141010241442134102300010112441144143401000301340030231113410330						
910 - 979	0	1	2	3	4	5	6
seq	KRDPHLACVAYERGQCDELINVCNENSLFKSLSRYLVRKDPPELWGSVLLESNPYRRPLIDQVQTALS						
SA.Q2	11000000001111011100101010000110000011110100110011101001100100010001						
SA.Q3	211110000021121122102111111001100100021111200110022212112100200010002						
SA.Q5	3334300100133341333203131310113310210143332300330134433123300310031003						
SA.con	3311100000033340333103030300003300100043331300330034413013300300030003						
All.con	0122244344301103100240313133331134234301112044114300020320144034413440						
980 - 1049	0	1	2	3	4	5	6
seq	ETQDPEEVSVTVKAFMTADLPNELIELLEKIVLDNSVSEHRNLQNLILLTAIKADRTRVMEYINRLDNY						
SA.Q2	11111110010010001010110001001100011110110110000000001111100100110110						
SA.Q3	2121121011001101212012100200210112122122111011000001021112101200210220						
SA.Q5	4343243013003101434133301300330134343144223033000000133324302310331441						
SA.con	4343243003003000414033100300330014343044123011000000033324301300330440						
All.con	0101101431441343020310243044014320100300211422444443301110142034013003						
1050 - 1119	0	1	2	3	4	5	6
seq	DAPDIANIAISNELFEEFAFIRKFDVNTSAVQVLIETHIGNLDRAYEFAERCNPEAVW SCLAKAQLQKG						
SA.Q2	1011001000111001000100110111110010001101101000100110111100 010010001111						
SA.Q3	1121002001212102100100221211120020002111102101200210211200 110010102221						
SA.Q5	3143003101434114301301331433330031013313314202310331433300 320031114443						
SA.con	304300300043400410030033043333003000330304101300330433300 120030004443						
All.con	1301440343010330243143003011104403430131130242034013011044 214413330001						
1120 - 1189	0	1	2	3	4	5	6
seq	VKEAIDS YIKADDPSSYMEVVQAANTSGNWEELVKYLQMARKKARES YVETELIFALAKTNRLAELEEFI						
SA.Q2	01100100 01011011011001001111101100100100111111010001000000101101100100						
SA.Q3	02100200 02121121012002102212112100200110221222110101000000102102102200						
SA.Q5	03300310 03143243133013203434313300300330343343130103000000314313303301						
SA.con	03300300 03043143033003103434303300300310343343030003000000304303302300						
All.con	40144034 40301201310430240010130144044124001000314341444444130130141043						
1190 - 1259	0	1	2	3	4	5	6
seq	NGFNNAHIQQVGDRCYDEKMYDAAKLLYNNVSNFGRLASTLVHLGEYQAAVDGARKANSTRTWKEVCFAC						
SA.Q2	1110001011001100111101001000110110110000000011011001001101101001100000						
SA.Q3	2111111022002101222102001100210220110010001021012002001112102001100110						
SA.Q5	4334313133003302444313102100331441330030003033033013003314313003300310						
SA.con	4331103033003301444303002000330440330010001033033003003304303003300100						

All.con	0112231300440142000130341344013003114424442401410430441130130441144234						
1260 - 1329	0	1	2	3	4	5	6
seq	VDGKEFRLAQMCGLHIVVHADELEELINYYQDRGYFEEELITMLEAALGLERAHMGMFTELAAILYSKFKPQ						
SA.Q2	01111010000001001101101100100111100100010010001011110000000000010111						
SA.Q3	0212101001100020011011012001112211102100200110021222111000100000021212						
SA.Q5	1433313103200141133133033003123334113300300330142444423000300001031324						
SA.con	0433303001100040033033033003013333003100300310041444311000100000030324						
All.con	3010131342244303311311410441320010330244044124302000022444244443403010						
1330 - 1399	0	1	2	3	4	5	6
seq	KMREHLELFWSRVNIPKVLRAAEQAHLWAEELVFLYDKYEEYDNAITMNMHPTDAWKEGQFKDIITKVAN						
SA.Q2	1001001100110101100100110000100000011011011001000100110010100010001000						
SA.Q3	1012102100210102100210111100210000011122021001000211221121210120002011						
SA.Q5	3023103201431313300320332301330010133243143002101433441243420230013133						
SA.con	3013003200430303300310331100310000033143043002000411440141410130003011						
All.con	1420340143013130144024112243024434311200301441343022003202024204430322						
1400 - 1469	0	1	2	3	4	5	6
seq	VELYYRAIQFYLEFKPLLLNDLLMVLSPLRDHTRAVNYFSKVKQLPLVKPYLRVSVQNHNNKSVNESLNNL						
SA.Q2	0100010000001110100010010011101000001001101101001100110010001000100010						
SA.Q3	1110020010002111210010010012201111002102212201001200110021012101200020						
SA.Q5	2320130031104331310130030034313112003203434313103310230032013301300030						
SA.con	1310030010004330300030030034303001003103414303003300230031003100300030						
All.con	2124304423340113034314414410031332440240020031341034114402430243044404						
1470 - 1539	0	1	2	3	4	5	6
seq	FITTEEDYQALRTSIDAYDNFDNISLAQRLEKHELIEFRRIAAYLFKGNRQKQSVELCKKDSLYKDAMQY						
SA.Q2	0010100110110011011010010011011010010010000001101101100100110100110010						
SA.Q3	0011210210120022012011020021022120110110001001112102100200121210210020						
SA.Q5	0033331330330043143132130033044330130230002013334313300310344311330031						
SA.con	0031310330330043033031030033044130030130001003314303300300341300330030						
All.con	4412023014104400300312304401400204314214442431120130144034102033014403						
1540 - 1609	0	1	2	3	4	5	6
seq	ASESKDTELAEEELLQWFLQEEKRECFGACLFQCYDLLRFDVVLETAWRHNIMDFAMPYFIQVMKEYLTKV						
SA.Q2	0010111100010010001111100000000001001000000000010010000001000100110						
SA.Q3	0121211200110021002122120000000100200101000110011201200100101011200210						
SA.Q5	0132433410330031014343341000001101311313001300021413310100203102311330						
SA.con	0031433400130030004343320000000000300301000100010401300000103001300330						
All.con	4302011034214403430100113444443343033132443234423032034344241332033014						
1610 - 1675	0	1	2	3	4	5	6
seq	DKLDASESLRKEEEQATETQPIVYGQPQLMLTAGPSVAVPPQAPFGYGYTAPPYGGPQPGFGYSM						
SA.Q2	110111111111111111110111100011						
SA.Q3	220222121222222222221122110000100001010110000001000101011000022						
SA.Q5	3303333343444444444433343431001100111111311101011111111131011144						

SA.con	3303333334344444444431343310000000000001000000000000010000044
All.con	0040001010000000000001210002344334433333323334343333333323433300

10-Appendix IV

ICOS 3D prediction software results for *murine* CHC α . The first table shows the analysis of the 2D and 3D rearrangements, point of contact of adjacent aa and their exposure to the solvent. In the second analysis, only the exposure to the solvent is taken into account. The region highlighted in yellow refers to the epitope of the mAb clone X22. The 'All.con' bottom row gives a final score for all the parameters taken into account by the analysis.

0 - 69	0	1	2	3	4	5	6																																																															
seq	A	Q	I	L	P	I	R	F	Q	E	H	L	Q	L	Q	N	L	G	I	N	P	A	N	I	G	F	S	T	L	T	M	E	S	D	K	F	I	C	I	R	E	K	V	G	E	Q	A	Q	V	V	I	I	D	M	N	D	P	S	N	P	I	R	R	P	I	S	A	D	S	A
cCN.Q2	0001111111110100101000110101111110111111000001111111000011110101111																																																																					
cCN.Q3	0012221212221211120001212112221211222221100112222221011121111212122																																																																					
cCN.Q5	1133443434342311313111341433444343344443412001334444441113133333314444																																																																					
cCN.con	0013443434341300303000340413444341344443401000334444440001033331304344																																																																					
dCN.Q2	001111111110100101000110100111110111111000001111111000010110101011																																																																					
dCN.Q3	001222121222121121201012121121211222221100111222221011121121212222																																																																					
dCN.Q5	111344343444131131311131311434111344444311111334444441111132131314144																																																																					
dCN.con	002344343444030030300023030043423034444430000033444444000031230304144																																																																					
DT.Q2	1111111111111101011111111111011111110001001111111111111111110111																																																																					
DT.Q3	11																																																																					
DT.Q5	4333333333333330304343333433333343333330004003333333303333333340433																																																																					
DT.con	33333333333333303033333333333133333330004003333333323333333330333																																																																					
GG.Q2	00011101111010010100011010111110011111000000111111000010000101011																																																																					
GG.Q3	00022212102202001020000201002120001222200000012222200000010201012																																																																					
GG.Q5	0013342421331311203110131211324111234343211001124444341101111121313123																																																																					
GG.con	00033414213303002030001302013241101343432000002444434000010010303023																																																																					
MST.Q2	01111111111111111011																																																																					
MST.Q3	0111111111111111101112																																																																					
MST.Q5	0111111111111111120112																																																																					
MST.con	022222222222222202223																																																																					
RCH.Q2	000111101110100101000110101111100111111000000111111000011110101111																																																																					
RCH.Q3	000222212221222101010121222222222222221010001122222001122212202222																																																																					
RCH.Q5	0014444344443443430003314444444444444431300033344443003333333404444																																																																					
RCH.con	0004444414441322313000330424444422444444101000133444430011133332404444																																																																					
RNG.Q2	0001111111101001010000101001111100111111000000111111000010000101011																																																																					
RNG.Q3	0001221211101001010001101002121100222210000001222211000010000101012																																																																					
RNG.Q5	001233232221211202010221212323221133333211001223333221111121111212123																																																																					
RNG.con	000233232220200202000120200322200333332000002333322000020000202023																																																																					
SA.Q2	11100010100010110101100101000010110000001111110000001111101111010000																																																																					
SA.Q3	222000101100202212022102021010122100001121222110000002112211111020110																																																																					
SA.Q5	4441013031113034141344313143030344310001233444220000103344333323131310																																																																					
SA.con	444000303000303404034410304101032430000013344422000003334313323030100																																																																					
All.con	0013332323331311212010231312333221233333201000123333331011121221313233																																																																					
70 - 139	0	1	2	3	4	5	6																																																															
seq	I	M	N	P	A	S	K	V	I	A	L	K	A	G	K	T	L	Q	I	F	N	I	E	M	K	S	K	M	K	A	H	T	M	T	D	D	V	T	F	W	K	W	I	S	L	N	T	V	A	L	V	T	D	N	A	V	H	W	S	M	E	G	E	S	Q	P	V	K	M	
cCN.Q2	11110011111101111111000011110100111111100011111111111111000001111																																																																					
cCN.Q3	22221112222111122221201101211212111222222111222222112222212100112122																																																																					
cCN.Q5	444421344443313243443311112333423132444444322344444334444434100013334																																																																					
cCN.con	44441034444330324344330000233341301244444411134444433444443400003334																																																																					

SA.Q2	111110100010001000100111101100100010111000111001101101111011100000000
SA.Q3	2111101101110111012002111021001000202121011120021012122121211000100110
SA.Q5	333331330331023303301333314300300041434312334003303424434443300210310
SA.con	3333303101300131013003333043003000404341013340033034144341433000100100
All.con	1111031232123322321331110301331333120102311103312331020011101133333223
420 - 489	0 1 2 3 4 5 6
seq	LDQGQLNKYESLELCRFLVQQGRKQLLEKWLKEDKLECSSEELGDLVKSVDPTLALSVYLRANVPNKVIQC
cCN.Q2	100001001111111011100000110011000010110011011001110111111001011001101
cCN.Q3	1000120012221221222100110220121000110220121022001221222122112011012212
cCN.Q5	3010131133343443443201120331233001131331133033103441443334213133134334
cCN.con	3000030033343441443100010330133000030330033033003440443334103033014314
dCN.Q2	100001001111011011100000110011000010110011011001010111011001011001101
dCN.Q3	1000020011221221222100010220121000120221021022001120222122102012012212
dCN.Q5	3011131122331441333111121331133001131331132133112131444133113121114314
dCN.con	3000030022330440333000010330033000030330032033002030444033003023004304
DT.Q2	11100111111111111111111111111011111111111011111011111111110111111111
DT.Q3	11
DT.Q5	33300333333333333333330333330333443343333033333033333333330303333333
DT.con	33300333333333333333332333330333333333333033333033333333330323333333
GG.Q2	10000100111111111100001011111100001010001101100001011111101010011111
GG.Q3	20000100122212222200001022112200002011002202200102022222202000012212
GG.Q5	3111131123343443334111121442244111131321143143112131444344313012124424
GG.con	3000030023343443334000020442244000030310043043001030444344303010024424
MST.Q2	111111111111111111111110111111111101110110111111111111111110111111
MST.Q3	1111111111111111111111101111111111011211111111121111112111011111
MST.Q5	1111111111111011111111101111111111011201101111121111121111111111
MST.con	222222222222222222222022222222202230220222223222223222022222
RCH.Q2	1000010011111111110000011011100001111001101100111111111101001011111
RCH.Q3	20001111222222222110110221121001110220021022002222222212012122222
RCH.Q5	3013130134444444433303303433330013333333303310343444444443333134444
RCH.con	300003003444444443110110341333000132330033033003434444444413013034444
RNG.Q2	1000010001111111111000011111100001010001111100001011111101010011111
RNG.Q3	1000010001121221121100000221122000010110022121000010222122101010012212
RNG.Q5	21111211122323322322101113322331112121113223211121333233213121123323
RNG.con	2000020002232332232200000332233000020200033232000020333233203020023323
SA.Q2	0110101110000001000011111001100111101001100110001000000010100110010
SA.Q3	0222201211001001100122112001100222211011200200121101000100120211210010
SA.Q5	1433313321003002000344223003310444313113301310342313000200231422330030
SA.con	043230332000100200014422300330044430300330030341103000100130411330030
All.con	3000031123332332333110110331133001131320132033002231333233213022023323
490 - 559	0 1 2 3 4 5 6

RCH.con	244444444403302443443210434444443144444442444444242300033324444412330
RNG.Q2	0111111101011011111111000111111111001010010011111101010001111111110010
RNG.Q3	1122122101011012212210001112211221011100100121111010100012112211210010
RNG.Q5	1233233212022123323321102223322332122211221232122120211123223322321221
RNG.con	023323320202202332332000222332233102120020023222020200023223322320020
SA.Q2	1000000010100110000001110010000001100001001000100101011100110010011101
SA.Q3	1000100121200110010002110110010001211112101000100211012210110011012101
SA.Q5	2000100231410330021014330231031003312143113000201433134310230032034313
SA.con	2000000130400330010004330130010003301013003000200413034300230031034303
All.con	1333333212033013323331103223323331122221331333233131310033123323311131
840 - 909	0 1 2 3 4 5 6
seq	TDELVAEVEKRNRLKLLLPWLEARIHEGCSEEPATHNALAKIYIDSNNNPERFLRENPYYDSRVVGKYCEK
cCN.Q2	1001100100001101111110001001000111100110111000001001100101100011101100
cCN.Q3	2002101200101212210221011000101122211221222010002001200102211112112200
cCN.Q5	3113302310212313331331023011101333302343333110113113311313313233213311
cCN.con	3003301300102303331330013001000333301341333000003003300303301133203300
dCN.Q2	1001100100000101110110001001000101100110111000001001100101100011001100
dCN.Q3	2002101200101212210220011000100122211221222010002001200102221112102201
dCN.Q5	3113301310111313321331113003111113311341333111113113311313311223113311
dCN.con	3003300300000303320330003002000213300340333000003003300303310123003300
DT.Q2	11111101111111111111111110011111111111111101011011111111111111111111
DT.Q3	11
DT.Q5	33333303333333333333330333400333333333333333303033033334333333333333
DT.con	33333303333333333333332333300333333333333333303033033333333333333333
GG.Q2	1001101110001111111111110000001111111111000001011100101100011101100
GG.Q3	2002211210102212221221112000000102221221222000002012210201201022202200
GG.Q5	4114422421212424432342233112111213332442434110113124421202311124313311
GG.con	4004412420103424432342233000000113332442434000003024410302300034303300
MST.Q2	10111011111111111011111111101111111111111111111110111111011111111111
MST.Q3	101110111111111110111111111011111111111111111111101111110111111211211
MST.Q5	10111011111111111011111111101111111211111111101110110111111211211
MST.con	20220222222222220222222222022222222222222222222220222220222222322322
RCH.Q2	100110010000110111111000100000011111011111000001001100101110011101100
RCH.Q3	200110121011121222222111000101222222222211100211220010222122112210
RCH.Q5	3013303330333344444434333000303344444443444310013333310303343334333333
RCH.con	300330131011331444443211300010134444244344410003113300303342134313310
RNG.Q2	1011111110001111111111100000001111111111000001011100101100011001100
RNG.Q3	101221121010121121122111100000012211221212000001011210101100011001100
RNG.Q5	2123322321112322322332222111111122322332323110112123321202211122112211
RNG.con	202332232000232232233222200000023322332323000002023310202200022002200
SA.Q2	011001101111001000100010011111110001100100011110110011010011100110011

GG.Q2	00111111	10100000	11011011	000001	00111111	11100000	10111111	11111111	001001	101110			
GG.Q3	0022122	201001	002112	221220	000020	122122	122101	000002	121222	221200	201211	220	
GG.Q5	1134234	312012	113224	423411	101312	442423	421211	112424	443443	2311	3124	22441	
GG.con	0034234	302001	003214	41340000	301442	442342	010001	0424	2443	4432	300301	421440	
MST.Q2	0111011	111111	111111	101101	111101	111011	111111	111111	111111	111111	101110	11111	
MST.Q3	0121011	112111	111111	110120	111110	111011	011111	111111	111111	111111	121211	111011	
MST.Q5	0121011	112111	111111	110120	111110	111011	011011	111111	111111	111111	121211	111011	
MST.con	0232022	223222	222222	2023	022222	202202	202222	222222	222222	222222	2323	222202	210222
RCH.Q2	0011011	101001	001001	10110000	100110	110010	000001	111111	111111	111111	001001	00110	
RCH.Q3	0122022	222001	002102	101100	100101	121022	111101	1002	122222	222222	001001	10110	
RCH.Q5	0133144	403033	013313	331030	130333	133333	303301	3144	444444	444430	1301	330330	
RCH.con	0033044	413003	003103	303300	100301	330331	131011	0032	444444	444443	003003	10330	
RNG.Q2	0111111	101001	001111	111110	000010	111111	111100	0001	111111	111010	001011	11110	
RNG.Q3	0122112	101001	001012	212210	000001	221221	121110	0000	111122	122201	001012	11210	
RNG.Q5	1233222	212012	012123	323212	011123	323223	222111	1122	2332	333120	121232	2321	
RNG.con	0233222	202002	0123	323320	000102	332332	322200	0022	2233	233302	002023	22320	
SA.Q2	1100100	010110	101001	001111	101100	100100	111110	1000	000000	0101	101100	1001	
SA.Q3	2200200	021211	210120	021022	121100	200210	121222	1101	010000	0202	102101	2002	
SA.Q5	3300311	141431	431330	032034	343133	013103	3034	3343	2301	030000	1031	431330	33014
SA.con	3300300	040430	430130	031034	343033	003103	4334	3100	010000	0304	303301	3004	
All.con	0133123	312002	003213	302300	100201	331331	231111	0021	3332	333333	130030	1311330	
1190 - 1259	0	1	2	3	4	5	6						
seq	GPNNAHIQVGDRCYDEKMYDAAKLLYNNVSNFGRRLASTLVHIGEYQAAVDGARKANSTRTWKEVCFACV												
cCN.Q2	0011101	0011001	100001	011111	100100	101110	110100	100101	101100	100101	100100	101100	110011
cCN.Q3	1121201	002101	210001	102212	221120	021122	122212	002002	102211	101102	221122	1121	
cCN.Q5	134331	311320	132000	131442	343123	013114	443443	2301	3114	3143	113013	133213	32233
cCN.con	014330	300320	032000	304423	430130	302441	443130	3004	3043	003003	033103	331133	
dcCN.Q2	0110101	001000	100000	101111	100100	100110	111010	001001	101100	100101	100100	110011	
dcCN.Q3	0121201	002101	210001	102212	221120	021122	122212	002002	102211	101102	221122	1121	
dcCN.Q5	111131	311320	232011	131333	233113	113114	443131	1311	331331	111131	331133	1232	
dcCN.con	023030	300310	131000	303332	330030	300440	443030	3003	3033	002003	033003	30132	
DT.Q2	0111111	101111	111110	011111	111111	111111	111111	111111	101111	111111	111111	11111	
DT.Q3	1111111	111111	111111	111111	111111	111111	111111	111111	111111	111111	111111	11111	
DT.Q5	033030	330303	333440	333333	333333	433333	333333	3330	3330	4033	3333	33333	
DT.con	033232	330323	333330	133333	333333	333333	333333	3330	3332	3330	3033	333333	
GG.Q2	0010101	001101	111000	101111	100100	101111	111011	111011	101001	011111	111111	11111	
GG.Q3	000010	201221	220000	202222	201200	201221	221211	2122	122100	002211	221222	222	
GG.Q5	111121	312432	332101	131333	442231	131244	244424	2242	2442	3321	101213	422432	333
GG.con	001020	301431	333000	303334	440130	302442	444242	1422	4413	3320	100203	422432	333
MST.Q2	111111	101110	111111	111111	111111	111111	111111	111111	111111	111111	101111	11111	
MST.Q3	111121	101221	011111	111121	111111	111111	111111	111111	111121	112111	111101	111112	21

cCN.Q3	100111012101201211211202201200102212112222211100201220221000110122022
cCN.Q5	3002230231033113233333133113101033132234434411201311331331021331243134
cCN.con	3001130130033003113133033003000033032134434400100300330330000330143034
dCN.Q2	1000010010011001001011011001000011010011111100000100110110000110011011
dCN.Q3	1001110121012002112111022011001022121122212211100201220221000110122022
dCN.Q5	3111130131133013113113133113101133131134434311111311331331011331143134
dCN.con	300003003003300300302303300300003303003443430000300330330000330043034
DT.Q2	11111010111011111111111111111011111111111111110011111111111111111111
DT.Q3	1111111111111111111111111111112111111111111111111111111111111111111111
DT.Q5	33333130333033333333333333333404333333333333330333333333343333333333
DT.con	333330303330333333333333333330433333333333333013333333333333333333
GG.Q2	11111011101100100101101101100001101111111110000100111111000110111111
GG.Q3	211112112212200200101202211200002212212222211000201221221000120122122
GG.Q5	4222322422341131131231442241111332432433344221131144243211231244234
GG.con	422231243134003003023044124000033143243334421000300442432000230244234
MST.Q2	11111011101111111111111101101011111111111111110111011111110111011
MST.Q3	11111011101111111111112011111011111122111111110121011111110121012
MST.Q5	1111101111111111111111201111101111112211111110121011111110121012
MST.con	22222022202222222222230220220222223322222220232022222220232023
RCH.Q2	10000100100110011111101100100001101101111111000100110110000110011011
RCH.Q3	2211101210221022222112111001022222222211100201220221021120122122
RCH.Q5	33333033303300344444333313300303333344444433301303331333033330344344
RCH.con	3211130131033003444443133013001033233244444433100301330331021330144144
RNG.Q2	1111111111110010010011111110000111111111111010010111111000110111111
RNG.Q3	1111121121112001001001122112000011121122212110100101221221000110122122
RNG.Q5	322222232233112112112233223111022232233323321211212332332111221233233
RNG.con	322232232233002002002233223000022232233323320200202332332000220233233
SA.Q2	0111101101100110110100100110110100100100000011011011001001101001100100
SA.Q3	0221102101200220120110200210221201101100010011121021002001212102100200
SA.Q5	1333313303310331431321300330443301302300020133343133003103443113300310
SA.con	0333303303300330330310300330441300301300010033143033003003413003300300
All.con	311112013212300311312313311300103313223333321100301331331011230133133
1540 - 1609	0 1 2 3 4 5 6
seq	SESKDTELAEE LLQWFLQEEKRECFGACLF TCYDLLRPDVVLETAWRHNIMDFAMPYFIQVMKEYLTKVD
cCN.Q2	10100001100110111000000111111111011010111011111010011111111110110010
cCN.Q3	1110010121122012101001122222222122121121112211021122222211210210120
cCN.Q5	21310203321331343010124444444444243243332333331334444443323320330230
cCN.con	2030010331033034300001144444444441431413321333330311444443323320330130
dCN.Q2	00000001100110111000000111111111011010111011010011111101110110010
dCN.Q3	1110010121122012100001122222222122121222112211021122222211210210110
dCN.Q5	1111111331133133301111144444444441431413331233231311444443313221331131

seq	LLDQGQLNKYESLELCRFVLQQGRKQLLEKWLKEDKLECSSEELGDLVKSVDPTLALSIVYLRANVFNKVIQ
SA.Q2	001111011010000010001111100110011110100110000011000100010001010011000
SA.Q3	0022220121110200100022211200210022210200210010012110200010012020111001
SA.Q5	0143431342340300300034432400331144431410330020033211300030123141133002
SA.con	0043430341310200300034432400330044430400330010033100300030013040033001
All.con	4300003102124144144400011044013300013034014424410233044414320303311442
490 - 559	0 1 2 3 4 5 6
seq	CFAETGQVQKIVLYAKKVGYPDWIFLLRNVMRISPDQGQQAQMLVQDEEPLADITQIVDVFMEYNLIQ
SA.Q2	000110101100100110101110000000010001100100100011110001001001000100001
SA.Q3	0002111011002002212111100100110011102101200110022211001011001001212102
SA.Q5	0004213133013103314133311100330021114301300310144444113033003101323213
SA.con	0004203033003003304033300000110020004300300300044431003013003000312103
All.con	4440131311430340030311133344224413330143044134300002331421441343021230
560 - 629	0 1 2 3 4 5 6
seq	QCTAFLLDALKNNRPSEGPLQTRLLEMNLMHAPQVADAILGNQMFTHYDRAHIAQLCEKAGLLQRALEHF
SA.Q2	000100010011111111000100000010011001100110010010010010001000100
SA.Q3	1002001200221222222011100101111112002100222101112111002002211001100200
SA.Q5	3003101300433344443131300303233344003301434313213333003103313013201411
SA.con	1003000300433344443010300101131134003300434103103113003003301003100400
All.con	2440343044001000000323144242212200440143000231230221440340032431243033
630 - 699	0 1 2 3 4 5 6
seq	TDLYDIKRAVVHHTHLNPEWLVNYFGSLSVEDSLECLRAMLSANIRQNLQICVQVASKYHEQLSTQSLIE
SA.Q2	11010000000101101010001001101110010011001000100000000001001100011001
SA.Q3	2201101100120110212001200220112100200110021011100100010012002201021002
SA.Q5	4313302200031331313001310441334301300330032013300200030023004313133003
SA.con	4303101100030330303000300440334300300330031003100100010013004301033003
All.con	0031242244303113030443034003110143044114402431244244424420440032301440
700 - 769	0 1 2 3 4 5 6
seq	LFESFKSFEGLFYFLGSIVNFSQDPPDVHFYKIQAAACKTGQIKEVERICRESNCYDPERVKNFLKEAKLTD
SA.Q2	0011010010000001100101111100010010001111011011001111001011001001101011
SA.Q3	0022121120001001100211211200010020002121021011002222111021012002212121
SA.Q5	0133241130001003311314433300130030014343133033003344113143033103434143
SA.con	0033140030000003300303433300030030004343033033003344003043013003414043
All.con	4300203304443441133030011044314404430101301411440000331301420340020301
770 - 839	0 1 2 3 4 5 6
seq	QLPLIIVCDRFDVHDLVLYLYRNNLQKYIEIYVQKVNPSRLPVVIGLLDVCSEDEVIKNLILVVRGQF
SA.Q2	1000000000010011000000101001001000110101100100000000101110011000001110
SA.Q3	1100000011120021001000212011002000221112201100000010202220011001002110
SA.Q5	3300000033131133002101333023003010331314311300000131413441033003103431
SA.con	3100000011030033001000313013003000330304300300000010403440033001003330
All.con	1244444422303301442343020421440434003130033144444323030003411442340013

840 - 909	0	1	2	3	4	5	6
seq	STDELVAEVEKRNRLKLLLPWLEARIHEGCEEPATHNALAKIYIDSNNNPERFLRENPYYDSRVVGKYCE						
SA.Q2	10110010011010010001000100111011110000000000011011001101000110001001						
SA.Q3	1022002101212102001100221022112111001000100011112102200221211111002002						
SA.Q5	3033003203323213112300332044434333011000201033443133103424213332003103						
SA.con	3033003103313103001300231044314333000000100011143033003414101331003003						
All.con	1400440241020230332144102400020111433444243422201300340020232112440340						
910 - 979	0	1	2	3	4	5	6
seq	KRDPHLACVAYERGQCDELELINVCNENSLFKSLSRYLVRKDPPELWGSVLLESNPYRRPLIDQVVTALS						
SA.Q2	11001000000111100110010001010011001000111111001100111100110010000000						
SA.Q3	2111100000022120111002001212101110110022111200110022212112200110010012						
SA.Q5	4334300100143431233003101434113320310033332400330134434223300310031013						
SA.con	4311300000043330133003000414003310300033332400330034434113300300010002						
All.con	0122144344300003211440343020331124134400111044114300010220044134423431						
980 - 1049	0	1	2	3	4	5	6
seq	ETQDPEEVSVTVKAFMTADLPNELIELLEKIVLDNSVSEHRNLQNLILLTAIKADRTRVMEYINRLDNY						
SA.Q2	111111100000100011101110010011000111101101100000000010011100100110110						
SA.Q3	212112201110100022211210020011001222122111011000000021112101200210221						
SA.Q5	4443143011003001444134301300330124433144233033000000031324302310330441						
SA.con	4343243000003000444034300300330014433044133011000000030124301300330440						
All.con	0001100433341443000310143044114320000300211422444444403210142034014003						
1050 - 1119	0	1	2	3	4	5	6
seq	DAPDIANIAISNELFEEFAIFRKFDVNTSAVQVLIETHIGNLDRAYEFAERCNPEAVW SCLAKAQLQKG						
SA.Q2	1011001000101001000100110110110010001101101100100110111100 010010001111						
SA.Q3	1121002001212002100100221211120020002112102101200220221200 110020002211						
SA.Q5	3143013102423113300301331422230031013323314202300331433300 320031114342						
SA.con	3043003001413003100300330421230030003313304201300330433300 120030004332						
All.con	1301430342020330244143003012104403430120130142044003001044 214403330001						
1120 - 1189	0	1	2	3	4	5	6
seq	VKEAIDS YIKADDPSSYMEVVQAANASGNWHEELVKYLQMARKKARES YVETELIFALAKTNRLAELEEFI						
SA.Q2	01100100 010110110110011011110110010011001111101000000000101101100100						
SA.Q3	02100200 01121121012002102212112100200110121222110101000000212102102200						
SA.Q5	03300311 13343343133003203434313301310330243343130303000001313313303301						
SA.con	03300300 03143143033003203434303300300330143343030101000000303303302300						
All.con	40144033 31201201310440140010130143034114201000314242444443030130141043						
1190 - 1259	0	1	2	3	4	5	6
seq	NGFNNAHIQQVGDRCYDEKMYDAAKLLYNVSNFGRLASTLVHLGEYQAAVDGARKANSTRTWKEVCFAC						
SA.Q2	110010101100110011100100100001011001000001011011001001101101001100000						
SA.Q3	2111111012002101222102101000210221110010001021022002001112212101100110						
SA.Q5	4334313133003312444213302100331341030010103033033013003314314012300310						
SA.con	4311303033003301444103102000230340030000003033033003003304304002300100						

All.con	012213131044013200230241344113003314434341401400430441130030331144234						
1260 - 1329	0	1	2	3	4	5	6
seq	VDGKEFRLAQMCGLHIVVHADELEELINYYQDRGYFEEELITMLEAALGLERAHMGMFTLAILYSKFKPQ						
SA.Q2	0111101000101010001011011001001111011001001100101100000000000010111						
SA.Q3	0212102101101010001121012002102212102100200210021221101000100000021212						
SA.Q5	1333313003213130013143033013104434213300300330141444310000300001041334						
SA.con	033330300120303000304303300300443420330030033004044110000100000040334						
All.con	3010130342131314431301410430340010130144044014303002233444244443403010						
1330 - 1399	0	1	2	3	4	5	6
seq	KMREHLELFWSRVNIPKVLRAAEQAHLWAEELVFLYDKYEEYDNAITMNMHPTDAWKEGQFKDIITKVAN						
SA.Q2	100100110011010110011011000010000001101101100100011111001100110001011						
SA.Q3	1012102101210201200210111100110100011122011001000212221122210120012021						
SA.Q5	3023103201431303310330332201330010123143133002001433441133410230023143						
SA.con	3013003200430303300330331100310000023043033002000433440033400230013043						
All.con	1420340143013041034014112243124334311300311441443010003300034104420301						
1400 - 1469	0	1	2	3	4	5	6
seq	VELYYKAIQFYLEFKPLLLNDLLMVLSPLRDHTRAVNYFSKVKQLPLVKPYLRVSVQNHNNKSVNESLNNL						
SA.Q2	0100010010001111100010000011100000001001101101001100110011001100100010						
SA.Q3	1200110010002111110010010011201111002101212102001200110121012100200120						
SA.Q5	1400130031104322310130020033313132003103434313103300330333013301300231						
SA.con	0400030030004322300030010033301011003003414303003300330133003300300130						
All.con	3044314413340111134314424411032322440341020130341044114201430143044203						
1470 - 1539	0	1	2	3	4	5	6
seq	FITTEEDYQALRTSIDAYDNFDNISLAQRLEKHELIEFRRIAAYLFKGNRQKQSVLCKKDSLYKDAMQY						
SA.Q2	0011100100110011011010010011011010010000001101101100100111100100010						
SA.Q3	0022210210120022022021020011022010110110001001212102100200122210210020						
SA.Q5	1133321330330033143133030033033130130330002013334313300310344311330031						
SA.con	0033310310330033043031030033033030030130001003314303300300344300310030						
All.con	3300023024104400300302404411400314314214442431020130144034100033024403						
1540 - 1609	0	1	2	3	4	5	6
seq	ASESKDTELAEEELLQWFLQEEKRECFGACLFYCYDLLRFDVVLETAWRHNIMDFAMPYFIQVMKEYLTKV						
SA.Q2	0010111100110010001111110000000001001010000000010110000001000100110						
SA.Q3	0121221200210020002122120000000100200102000110011201210100001001200210						
SA.Q5	0134333310330031014343340000001301411314000320123413410100003002311330						
SA.con	0031333300330030004343340000000100400304000110011403400000003001300330						
All.con	4302001034014403430100104444443243033130444224322031034344441442033014						
1610 - 1675	0	1	2	3	4	5	6
seq	DKLDASESLRKEEEQATETQPIVYGQPQLMLTAGPSVAVPPQAPFGYGYTAPPYGPQPGFGYSM						
SA.Q2	11011111111111111111001111000000001000000000000000000000000000000011						
SA.Q3	2201221221222222222111121210101100112011111010001000011011000122						
SA.Q5	33034334334444444444333343431000311114111311101011111143131111144						

SA.con	330343343344444444433114343000010000400010000000000011010000044
All.con	00410010010000000000112201013343233330333233333433333322323333300